SAND2016-9610R

Advances in Geologic Disposal System Modeling and Application to Crystalline Rock

Fuel Cycle Research & Development

Prepared for
U.S. Department of Energy
Used Fuel Disposition

P.E. Mariner, E.R. Stein, J.M. Frederick, S.D. Sevougian, G.E. Hammond, and D.G. Fascitelli
Sandia National Laboratories

September 22, 2016

FCRD-UFD-2016-000440
SAND2016- xxxxx R

Sandia National Laboratories is a multi-mission laboratory managed and operated by Sandia Corporation, a wholly owned subsidiary of Lockheed Martin Corporation, for the U.S. Department of Energy's National Nuclear Security Administration under contract DE-AC04-94AL85000.

ACKNOWLEDGEMENTS

The authors greatly appreciate the contributions of Sandia technical staff Ayman Alzraiee, Brad Day, Teklu Hadgu, Sungtae Kim, Kris Kuhlman, Heeho Park, Matthew Thomas, and Todd Zeitler to the development and testing of PFLOTRAN and the support of three-dimensional discrete fracture network modeling through dfnWorks by Los Alamos researchers Jeffrey Hyman, Satish Karra, Nataliia Makedonska and Hari Viswanathan.

EXECUTIVE SUMMARY

The Used Fuel Disposition Campaign (UFDC) of the U.S. Department of Energy (DOE) Office of Nuclear Energy (NE), Office of Fuel Cycle Technology (OFCT) is conducting research and development (R&D) on geologic disposal of used nuclear fuel (UNF) and high level nuclear waste (HLW). Two of the high priorities for UFDC disposal R&D are design concept development and disposal system modeling (DOE 2011, Table 6). These priorities are directly addressed in the UFDC Generic Disposal Systems Analysis (GDSA) work package, which is charged with developing a disposal system modeling and analysis capability for evaluating disposal system performance for nuclear waste in geologic media (e.g., salt, granite, clay, and deep borehole disposal).

This report describes specific GDSA activities in fiscal year 2016 (FY 2016) toward the development of the enhanced disposal system modeling and analysis capability for geologic disposal of nuclear waste. The GDSA framework employs the PFLOTRAN thermal-hydrologic-chemical multi-physics code (Hammond et al. 2011a; Lichtner and Hammond 2012) and the Dakota uncertainty sampling and propagation code (Adams et al. 2012; Adams et al. 2013). Each code is designed for massively-parallel processing in a high-performance computing (HPC) environment. Multi-physics representations in PFLOTRAN are used to simulate various coupled processes including heat flow, fluid flow, waste dissolution, radionuclide release, radionuclide decay and ingrowth, precipitation and dissolution of secondary phases, and radionuclide transport through engineered barriers and natural geologic barriers to the biosphere. Dakota is used to generate sets of representative realizations and to analyze parameter sensitivity.

In FY 2016, advances in the GDSA modeling capability include:

- A new canister degradation model and model framework;
- An improved waste form process model fully integrated with canister degradation, decay and ingrowth, instantaneous release, waste form degradation, waste form mass and surface area, and radionuclide release;
- An improved selection of fully integrated waste form degradation models: the Fuel Matrix Degradation Model (FMDM), a HLW glass degradation model, an instantaneous degradation model, and a custom model that allows the user to specify a constant fractional dissolution rate that is either mass-specific or surface-area-specific;
- A 3-generation analytical solution for decay and ingrowth of isotopes in all phases in the transport domain (also implemented for the waste form);
- An isotope partitioning model that simulates element-specific, solubility-limited precipitation and dissolution and equilibrium isotope partitioning across all phases (aqueous, adsorbed, and precipitate); and
- A preprocessor for mapping fracture networks into porous media meshes to simulate characteristic flow and transport processes of mapped fractures.

As these process models and capabilities were being implemented and improved, integration with other UFDC work continued at a strong pace. The primary focus of direct integration this year was simulation of flow and transport in fractured rock. In the crystalline work package, fracture continuum modeling (FCM) and discrete fracture network (DFN) modeling were developed and compared for potential use in GDSA performance assessment (PA) (Wang et al. 2016). FCM was performed using a specialized mapping routine (Wang et al. 2016), and DFN modeling was performed using dfnWorks (Hyman et al.

2015a). For GDSA modeling, dfnWorks was used to generate each DFN, and mapDFN, a new mapping tool developed under the GDSA work package, was used to create an equivalent continuous porous medium (ECPM) representation of each DFN.

As in previous years, the GDSA group queried other UFD work packages to identify additional capabilities that need to be added to the GDSA modeling capability. In addition, other needed models were identified by performing an informal gap analysis using a features, events, and processes (FEPs) list. Identified models were added to the GDSA process model integration table established in FY 2015 (Mariner et al. 2015, Table 3-1). Information in the table was updated and refined, and the models were qualitatively assessed by level of effort, level of readiness, and integration time frame. The revised integration table and the presentation slides of proposed models for GDSA model integration are included in this report.

The crowning achievement this year was the establishment of a new crystalline rock reference case that utilizes the code development and integration work summarized above. The new reference case contains a crystalline host rock simulated using stochastically generated DFNs mapped into an unstructured grid. Because DFNs are highly heterogeneous, the modeling domain is fully simulated in three dimensions without symmetry planes. The new/improved process models for canister degradation, waste form degradation, and radionuclide release, decay, and partitioning are all included in this application. The crystalline repository reference case is based on the reference case described in Wang et al. (2014, Section 2). Realizations of the developed reference case indicate that maximum concentrations of ^{129}I and ^{237}Np at monitored locations in the model domain are sensitive to waste package degradation rates, waste form dissolution rates, and sorption coefficients and are particularly sensitive to fracture distribution. It should be noted that the fractured host rock simulated in this report is biased toward greater connectivity than is likely to exist in a sparsely fractured rock selected for nuclear waste disposal. A large fracture density was necessary for this iteration to create a system in which flow and transport occurs in the fractures. For applications to an actual site, it will be necessary to model identified fracture features and to quantify probabilities of percolating networks at the scales of interest.

Progress in the development of the GDSA framework continues to affirm that HPC-capable codes can be used to simulate important multi-physics couplings directly in a total system performance assessment of a geologic repository. The generic repository applications modeled to date indicate that the developing capability can simulate complex coupled processes in a multi-kilometer domain while simultaneously simulating the coupled behavior of meter-scale features, including every waste package within the domain.

Over the past several years the modeling capabilities of the GDSA framework have greatly advanced. Additional development is needed, however, for a mature PA framework. The challenge is to address the remaining needs using available resources. Meeting this challenge will require close integration with technical teams across the UFDC.

This report fulfills the Generic Disposal System Analysis Work Package Level 3 Milestone – *Advances in Geologic Disposal System Modeling and Application to Crystalline Rock* (M3FT-16SN080304011).

CONTENTS

Page

FIGURES

Page

TABLES

Page

ACRONYMS

BWR	boiling water reactor
CFM	Colloids Formation and Migration
CSNF	commercial SNF
DBH	Deep borehole
DFN	discrete fracture network
DOE	U.S. Department of Energy
DR	disposal research
DRZ	disturbed rock zone
DSNF	DOE spent nuclear fuel
EBS	engineered barrier system
ECPM	equivalent continuous porous medium
EDZ	excavation disturbed zone
FCM	fracture continuum model
FEP	feature, event, and process
FMDM	Fuel Matrix Degradation Model
FY	fiscal year
Ga	billion years
GC	general corrosion
GDSA	generic disposal system analysis
GWd	gigawatt-day
HC	hydride cracking
HDF5	hierarchical data format, version 5
HLW	high-level radioactive waste
HPC	high-performance computing
IAEA	International Atomic Energy Agency
L	liter (or length in generic units expressions)
LANL	Los Alamos National Laboratory
LBNL	Lawrence Berkeley National Laboratory
LC	localized corrosion
LHS	latin hypercube sampling
LOE	level of effort
M	moles per liter (or mass in generic units expressions)
Ma	million years
mbsl	meters below sea level
MIC	microbiologically-influenced corrosion
mol	moles
MPI	message passing interface
MTHM	metric tons heavy metal
MTIHM	metric tons initial heavy metal
MWd	megawatt-day

ACRONYMS (CONT.)

NA	not applicable
NBS	natural barrier system
NE	Office of Nuclear Energy
OFCT	Office of Fuel Cycle Technology
OoR	(age) out-of-reactor
ORNL	Oak Ridge National Laboratory
PA	performance assessment
PETSc	Portable Extensible Toolkit for Scientific Computation
PMC	process model coupler
PWR	pressurized water reactor
QA	quality assurance
R&D	research and development
RBSN	Rigid-Body-Spring-Network
RN	radionuclide
SA	sensitivity analysis
SCC	stress corrosion cracking
SNF	spent nuclear fuel
SNL	Sandia National Laboratories
T	time units
T	temperature
TBD	to be determined
TH	thermal-hydrologic
THC	thermal-hydrologic-chemical
THM	thermal-hydrologic-mechanical
THMC	thermal-hydrologic-mechanical-chemical
TST	transition state theory
UA	uncertainty analysis
UFDC	Used Fuel Disposition Campaign
UNF	used nuclear fuel
URL	underground research laboratory
V&V	verification and validation
W	watt
WF	waste form
WIPP	Waste Isolation Pilot Plant
WP	waste package
wt%	percentage by weight

1. INTRODUCTION

The Used Fuel Disposition Campaign (UFDC) of the U.S. Department of Energy (DOE) Office of Nuclear Energy (NE), Office of Fuel Cycle Technology (OFCT) is conducting research and development (R&D) on geologic disposal of used nuclear fuel (UNF) and high level nuclear waste (HLW). Two of the highest priorities for UFDC disposal R&D are design concept development and disposal system modeling (DOE 2011, Table 6). These priorities are directly addressed in the UFDC Generic Disposal Systems Analysis (GDSA) work package, which is charged with developing a disposal system modeling and analysis capability for evaluating disposal system performance for nuclear waste in geologic media. Disposal options for UNF and HLW include mined repository concepts in salt, argillite, and crystalline rock and deep borehole disposal in crystalline rock (Arnold et al. 2011; Hardin et al. 2012).

In 2013, GDSA transitioned to a framework based on PFLOTRAN and Dakota, a framework that GDSA continues to develop today. PFLOTRAN is a multiphase flow and reactive transport model for describing surface and subsurface processes (Hammond et al. 2011a; Lichtner and Hammond 2012), and Dakota is an uncertainty quantification and sensitivity analysis code (Adams et al. 2012; Adams et al. 2013). These codes were chosen to provide the primary GDSA framework because they are open source, massively parallel, and together have the potential to simulate a total integrated geologic repository system and its surroundings probabilistically and in three dimensions. The developing modeling capability is called the GDSA model framework or the GDSA capability in this report.

This report describes GDSA accomplishments for fiscal year 2016 (FY 2016). Recent prior development and accomplishments are documented in Mariner et al. (2015); Sevougian et al. (2013); Sevougian et al. (2014); Freeze et al. (2013b); Clayton et al. (2011); Freeze and Vaughn (2012); and Vaughn et al. (2013).

The overall objective of the GDSA work package is to develop a disposal system modeling and analysis capability that supports the prioritization of Disposal Research (DR) R&D and the evaluation of disposal system performance, including uncertainty, for a range of disposal options (e.g., salt, argillite, crystalline, deep borehole). The purpose is to develop a GDSA capability that:

- integrates updated conceptual models of subsystem processes and couplings developed under this and other DR work packages;
- is used to evaluate DR R&D priorities;
- leverages existing computational capabilities (e.g., meshing, visualization, high-performance computing (HPC)) where appropriate; and
- is developed and distributed in an open-source environment.

Three major tasks were identified for FY 2016:

- Upgrade models for baseline isotope behavior (e.g., phase-partitioning, decay, release);
- Integrate subsystem conceptual models, developed under this and other DR work packages, into the GDSA-PA system model architecture (e.g., colloid transport, non-Darcy flow, discrete fracture model, waste package degradation); and
- Perform simulations of selected reference case demonstration problems and conduct sensitivity analyses to inform R&D planning.

This report fulfills the GDSA Work Package Level 3 Milestone – *Advances in Geologic Disposal System Modeling and Application to Crystalline Rock* (M3FT-16SN080304011). It incorporates information from the following supporting milestones: M2FT-16SN080303082 (Wang et al. 2016); M3FT-16LA080504031 (Reimus et al. 2016); M2FT-15SN0807071 (Wang et al. 2015); M2FT-14SN0807051

(Wang et al. 2014); M2FT-15SN0808011 (Mariner et al. 2015); M3FT-14SN0808032 (Sevougian et al. 2014); and M3FT-13SN0808062 (Freeze et al. 2013a).

Section 2 discusses the GDSA performance assessment (PA) vision and summarizes the conceptual model framework and the PFLOTRAN-based computational framework of the GDSA modeling capability. Section 3 reports progress on process model development and specific integration activities that facilitated process model development. Section 4 provides an application of the GDSA capability to a generic commercial repository in crystalline rock. Conclusions are summarized in Section 5.

2. GDSA PERFORMANCE ASSESSMENT

A performance assessment (PA) for underground disposal of nuclear waste requires a comprehensive analysis of features, events, and processes (FEPs) that could potentially affect the release of radionuclides from emplaced waste packages and the transport of released radionuclides to the biosphere. The foundation of a PA is the computational framework. Section 2.1 discusses the GDSA long-term vision for the computational framework. The present computational framework and conceptual model framework are summarized in Section 2.2.

2.1 GDSA PA Vision

A license application for a new UNF and HLW repository will not be submitted for many years. For example, the 2013 DOE timeline, which assumed supportive action by Congress, projected selection of multiple candidate sites by 2022, selection of a single site by 2026, and submittal of a license application by 2037 (DOE 2013). A timeline for a potential repository for defense and DOE-managed waste has not been established. With continued advances in general computational capabilities over time, GDSA PA software will need to keep up. The long-term vision for the GDSA effort is therefore to develop a geologic repository modeling capability that can adapt to, and take advantage of, future advances in computational software and hardware and future advances in process modeling. In line with this vision, the near term mission is to develop a robust suite of fully functional generic repository reference case applications (1) for application to candidate sites by the time they are selected and (2) for evaluation of the effects of FEPs and input parameters on repository performance to inform R&D planning.

In consideration of the long-term vision for GDSA, two open-source, HPC codes will serve as the core of the modeling capability: PFLOTRAN and Dakota. PFLOTRAN is a massively-parallel thermal-hydrologic-chemical (THC) flow and transport code, and Dakota is a versatile probabilistic code (Section 2.2.2). The PFLOTRAN code will be developed over time by GDSA to accommodate new geologic disposal process models and capabilities through additional code development or coupling with external process models. The HPC capabilities of PFLOTRAN and Dakota will allow for ever higher fidelity in GDSA total system performance assessments as more powerful HPC resources become available.

As the GDSA model framework evolves, the GDSA group will continue to generate and refine three-dimensional models of disposal repository concepts complete with surrounding geospheres and connected biospheres. Sensitivity analyses will be performed on these models to distinguish the importance of features, processes, and parameters on model results. These analyses will help to prioritize future disposal R&D.

2.2 GDSA PA Framework

A PA model is an important component of a comprehensive PA for a nuclear waste repository. In a comprehensive PA all plausible scenarios and processes that may affect repository performance are addressed. FEPs and scenarios are evaluated and screened. Potentially pertinent FEPs are identified for simulation in the PA model. Probabilistic simulations are performed, and results are evaluated against performance metrics. Uncertainty and sensitivity analyses may also be performed to inform prioritization of additional research and model development. An overview of PA methodology and terminology is presented in Sevougian et al. (2014, Section 2.2) and Meacham et al. (2011, Section 1).

The PA model framework consists of a conceptual model framework and a computational framework. The conceptual model framework (Section 2.2.1) is the assemblage of FEPs and their interactions pertinent to repository system performance. The computational framework (Section 2.2.2) is the integration of software codes and mathematical models for quantitatively simulating the conceptual model and probabilistically assessing repository performance.

2.2.1 Conceptual Model Framework

A conceptual model framework requires a coherent representation of pertinent FEPs. Figure 2-1 schematically illustrates the conceptual model framework for a repository system. To calculate a dose to a receptor in the biosphere, radionuclides released from the waste form must pass through the repository engineered barrier system (EBS) and the surrounding natural barrier system (NBS).

A FEPs database like the one developed and described in Freeze et al. (2011) can be used to help identify a full set of potentially important FEPs for a specific conceptual repository model. Many of the FEPs in a FEPs database may be directly simulated in the PA model. In a comprehensive PA, excluded FEPs (i.e., FEPs not simulated in the PA model) must be addressed in separate analyses and arguments.

The two general concepts for deep geologic disposal of nuclear waste are mined repository disposal and deep borehole (DBH) disposal. These concepts have markedly different EBS and NBS features. For a mined repository, waste is generally placed along horizontal drifts at a depth of several hundred meters (Hardin et al. 2011). For deep borehole disposal concepts, waste is emplaced vertically at depths of approximately 3,000 to 5,000 meters (Arnold et al. 2011).

Important processes and events in the conceptual model are those that could significantly affect the movement of radionuclides in the EBS and NBS. Such processes and events include waste package corrosion, waste form dissolution, radionuclide release, radioactive decay, heat transfer, aqueous transport, advection, diffusion, sorption, aqueous chemical reactions, precipitation, buffer chemical reactions, gas generation, colloidal transport, earthquakes, and inadvertent human intrusion of the repository.

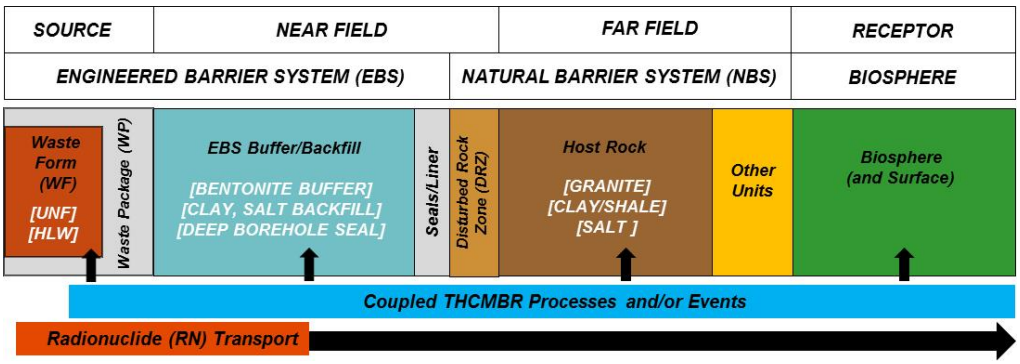

Figure 2-1. Schematic diagram of the conceptual model framework of a generic geologic disposal system.

2.2.2 Computational Framework

PA model simulations require a large number of realizations. For this reason, the GDSA PA computational framework is designed for massively-parallel processing in a high-performance computing (HPC) environment. The GDSA computational framework consists of the following components:

- Input parameter database
- Software for sampling, sensitivity analysis, and uncertainty quantification (Dakota)
- Petascale multiphase flow and reactive transport code (PFLOTRAN), working in concert with coupled process model codes (e.g., FMDM)
- Computational support software and scripts for meshing, processing, and visualizing results (e.g., CUBIT, Python, ParaView, VisIt).

The flow of data and calculations through these components is illustrated in Figure 2-2. In a probabilistic simulation, Dakota generates stochastic input for each GDSA PA realization based on parameter uncertainty distributions defined in the input set. The sampled inputs are used by PFLOTRAN and its coupled process models to simulate source term release, EBS evolution, flow and transport through the EBS and NBS, and uptake in the biosphere. After the simulation, various software may be used to reduce and illustrate the output calculations of parameters and performance metrics. Dakota may also be used to evaluate the effects of parameter uncertainty on specific outputs.

Dakota and PFLOTRAN are the core simulation codes of the GDSA PA computational framework. These components are described in more detail in Sections 2.2.2.1 and 2.2.2.2.

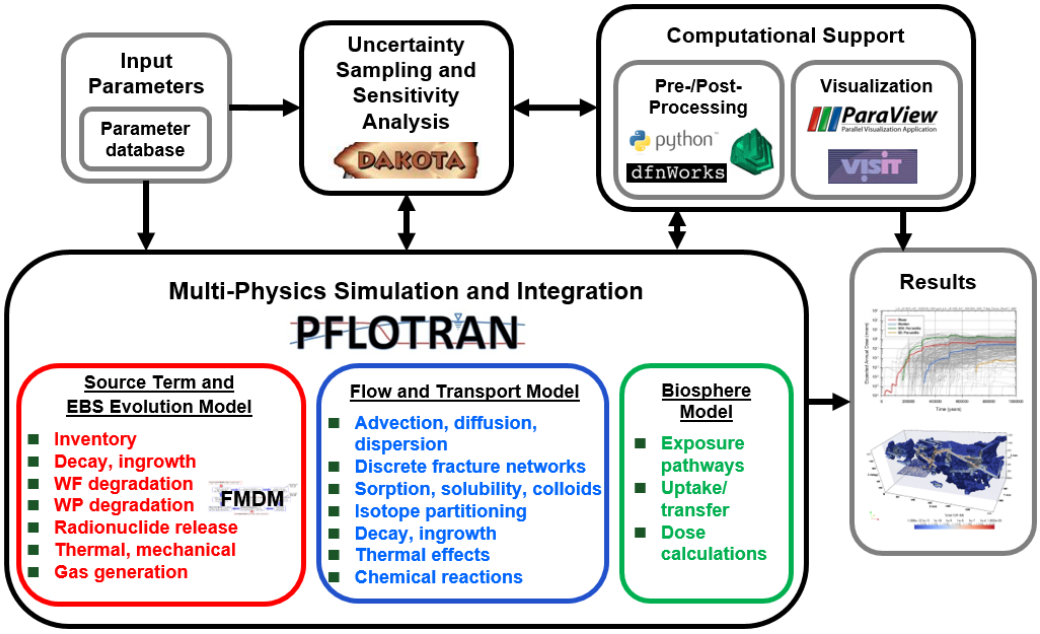

Figure 2-2. GDSA PA computational framework.

2.2.2.1 Dakota

The Dakota software toolkit is open source software developed and supported at Sandia National Laboratories (Adams et al. 2012; Adams et al. 2013). GDSA modeling uses Dakota as the interface between input parameters and PFLOTRAN. Dakota is also used to analyze the effects of uncertainty in GDSA parameter values on repository performance.

Dakota can be used to manage uncertainty quantification, sensitivity analyses, optimization, and calibration. Specific Dakota capabilities important to GDSA include (Figure 2-3):

- Generic interface to simulations
- Mixed deterministic / probabilistic analysis
- Uncertainty quantification with sampling and epistemic methods
- Supports scalable parallel computations on clusters.

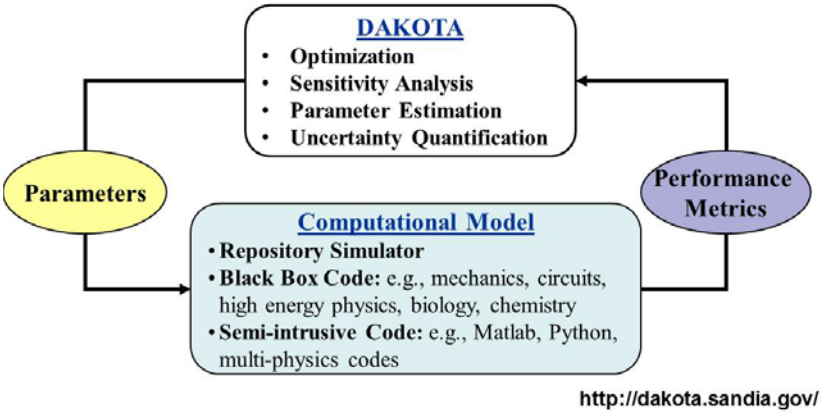

Figure 2-3. Dakota software workflow and capabilities.

2.2.2.2 PFLOTRAN

PFLOTRAN (Hammond et al. 2011a; Lichtner and Hammond 2012) is an open source, reactive multi-phase flow and transport simulator designed to leverage massively-parallel high-performance computing to simulate subsurface earth system processes. PFLOTRAN has been employed on petascale leadership-class DOE computing resources (e.g., Jaguar [at Oak Ridge National Laboratory (ORNL)] and Franklin/Hopper [at Lawrence Berkeley National Laboratory (LBNL)]) to simulate THC processes at the Nevada Test Site (Mills et al. 2007), multi-phase CO_2-H_2O for carbon sequestration (Lu and Lichtner 2007), CO_2 leakage within shallow aquifers (Navarre-Sitchler et al. 2013), and uranium fate and transport at the Hanford 300 Area (Hammond et al. 2007; Hammond et al. 2008; Hammond and Lichtner 2010; Hammond et al. 2011b; Chen et al. 2012; Chen et al. 2013).

PFLOTRAN solves the non-linear partial differential equations describing non-isothermal multi-phase flow, reactive transport, and geomechanics in porous media. Parallelization is achieved through domain decomposition using the Portable Extensible Toolkit for Scientific Computation (PETSc) (Balay et al. 2013). PETSc provides a flexible interface to data structures and solvers that facilitate the use of parallel computing. PFLOTRAN is written in Fortran 2003/2008 and leverages state of the art Fortran programming (i.e. Fortran classes, pointers to procedures, etc.) to support its object-oriented design. The code provides "factories" within which the developer can integrate a custom set of process models and time integrators for simulating surface and subsurface multi-physics processes. PFLOTRAN employs a single, unified framework for simulating multi-physics processes on both structured and unstructured grid discretizations (i.e. there is no duplication of the code that calculates multi-physics process model functionals in support of structured and unstructured discretizations). The code requires a small, select set of third-party libraries (e.g., MPI, PETSc, BLAS/LAPACK, HDF5, Metis/Parmetis). Both the unified structured/unstructured framework and the limited number of third-party libraries greatly facilitate usability for the end user.

Specific PFLOTRAN capabilities for the simulation of generic disposal systems include:

- Multi-physics
  - Multi-phase flow
  - Multi-component transport
  - Biogeochemical processes
  - Thermal and heat transfer processes
- High-Performance Computing (HPC)

  - Built on PETSc – parallel solver library
  - Massively Parallel
  - Structured and Unstructured Grids
  - Scalable from Laptop to Supercomputer
- Modular design based on object-oriented Fortran 2003/2008 for easy integration of new capabilities

Flow and transport processes simulated by PFLOTRAN are illustrated schematically in Figure 2-4 for the near field and in Figure 2-5 for the far field. These figures also illustrate where process model feeds or abstractions may be used to represent some of the more complex multi-physics couplings in specific disposal concepts.

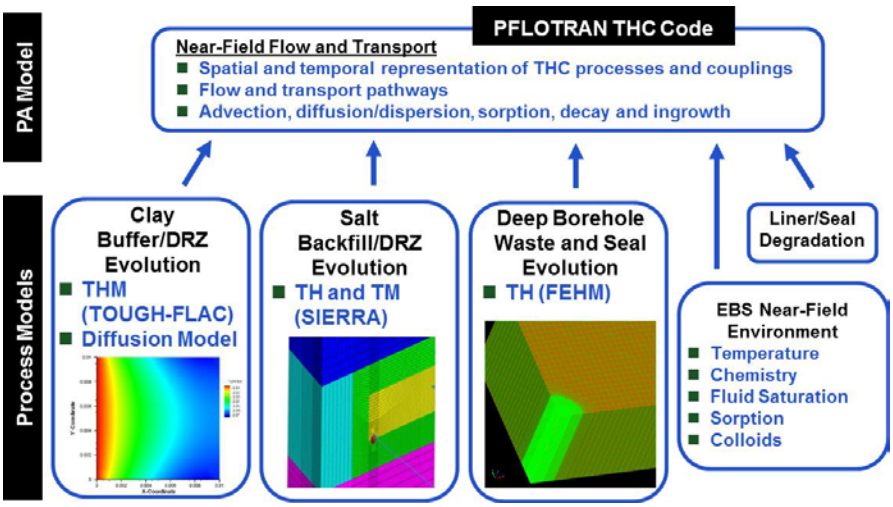

Figure 2-4. Implementation of PFLOTRAN for near-field flow and transport.

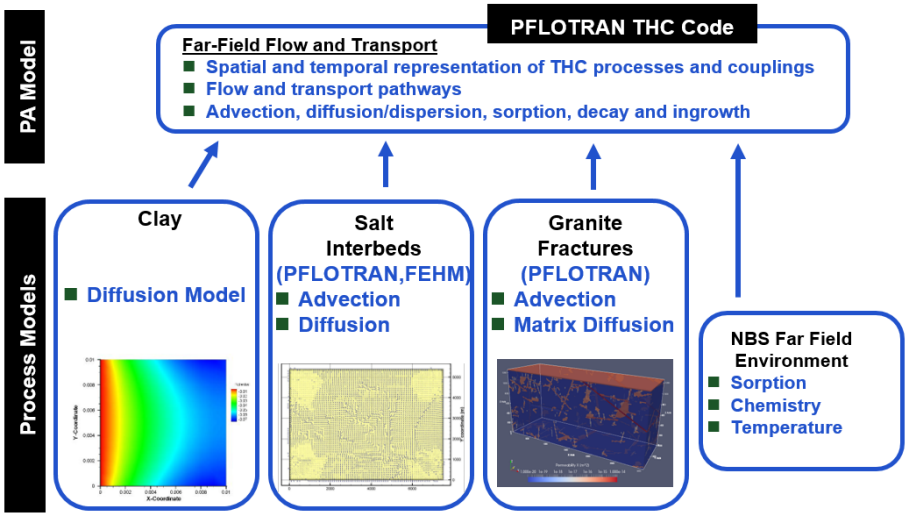

Figure 2-5. Implementation of PFLOTRAN for far-field flow and transport.

3. GDSA Process Model Development

Incorporating process models into the GDSA framework greatly facilitates evaluation of the importance of FEPs in PA applications. The approach of using detailed models directly in a PA is a continuation of the successful modeling approach adopted for the Waste Isolation Pilot Plant (WIPP) PAs (Rechard R.P. 1995; Rechard 2002; Rechard and Tierney 2005) and differs from the modeling approach adopted for past PAs for disposal of UNF and HLW in volcanic tuff (Rechard and Stockman 2014). Section 3.1 describes the integration activities GDSA performed this year to incorporate process models developed by other UFDC work packages into the GDSA computational framework. Section 3.2 discusses additional process models that were added or advanced this year.

3.1 Process Model Integration

Figure 3-1 is a schematic timeline showing the major stages in U.S. HLW/UNF repository development, indicating the current stage: concept evaluation and technology R&D, prior to the selection of an actual repository site. During this timeframe, repository performance assessment progresses from generic modeling to site-specific modeling, but maintains three primary, ongoing functions throughout the several-decade period:

1. Evaluate potential disposal concepts and sites in various host rock media
2. Help prioritize R&D activities
3. Support the development of a repository safety case

All three of these functions require a strong integration effort among the various modeling and testing programs in the UFDC. This section describes some of the current integration efforts between process modeling and performance assessment modeling.

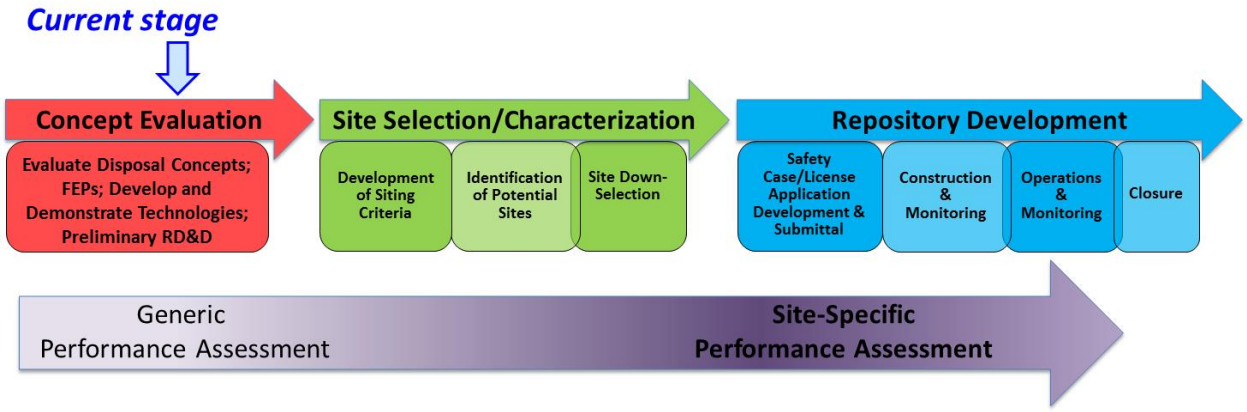

Figure 3-1. Evolution of performance assessment through various phases of repository development.

3.1.1 Planning and Outreach

To ensure an efficient representation of physical-chemical processes in the system performance assessment model, subject to ever-present computational hardware and software constraints, an ongoing dialog is necessary between PA scientists who focus on an efficient total system model and domain scientists who concentrate on a detailed representation of a specific domain and associated process(es). This “integration” dialog was re-emphasized in FY 2015 (Mariner et al. 2015) and has been furthered during FY 2016. As described in Mariner et al. (2015, Table 3-1), the intent for the current fiscal year, FY

2016, was to apply resources toward those models that were ranked with a "1" or "2" in the categories "Process Models to be Implemented Collaboratively" and "Process Models to be Implemented by GDSA." Some of process models had their implementation completed in FY 2016; some are ongoing; some were deferred; and some were deemed infeasible (non-Darcy flow). Table 3-1 below is an updated and more complete version of the original Model Integration table presented in Mariner et al. (2015), indicating the status of GDSA model development and integration as of the completion of FY 2016. Eight different categories of models and code development activities are distinguished in this table:

1. Basic GDSA-PFLOTRAN framework/code capabilities
2. GDSA Code Efficiency
3. Generic reference-case model enhancement/development and PA analyses for other work packages
4. GDSA model/code verification and validation (V&V) and documentation (including benchmarking)
5. Collaborative process model implementation – shorter term (process models are assumed to be developed under non-GDSA work packages)
6. Collaborative process model implementation – longer term (process models are assumed to be developed under non-GDSA work packages)
7. Collaborative process model implementation – not currently scoped/funded in UFDC DR
8. Models Added or Improved in FY 2016

Most of the GDSA/Process Model collaborative integration work (i.e., across UFDC work packages), introduced in Mariner et al. (2015), falls under categories 5, 6, and 7 of Table 3-1. Those items marked as "Ongoing" (i.e., Tasks 24 and 27) were the major focus of integration efforts in FY 2016. In addition, the category "Models Added or Improved in FY 2016," all of which have an indicated status of "Complete," was also a major focus of GDSA activity in FY 2016. These submodels were completed within the GDSA work package (Tasks 40 to 46).

Much of the groundwork for success with model integration activities was established during the 2015 UFDC Annual Working Group Meeting (held June 9-11, 2015 in Las Vegas, Nevada), as discussed in Mariner et al. (2015). Ten "lightning" talks (i.e., limited to five minutes each) were given by process modelers, with two objectives for each talk: (1) why the given process model is important to PA, and (2) how it can be coupled to the GDSA Framework in the next year or two. This 2015 integration session, combined with a decision to develop and focus on the granite/crystalline repository reference case in FY 2016 (see Section 4), has led to a major effort and concomitant success in integrating the dfnWorks process model (see Task 27 in Table 3-1) with PFLOTRAN, as discussed below in Section 3.1.3.1.

Following up on the success of the Integration Session in FY 2015, another integration session was held during the 2016 UFDC Working Group Meeting, June 7-9, 2016 in Las Vegas, NV. This session focused on fifteen proposals for future GDSA/process model integration, which are documented in Appendix A as the set of PowerPoint presentations made during this integration session. This set of presentations has been evaluated and distilled by GDSA scientists during the update of the Model Integration table (Table 3-1). Additional information was distilled from Appendix A of Mariner et al. (2015), which documents the Model Integration Templates for many of the models proposed in the presentations in Appendix A of this deliverable. On the basis of various considerations, one of the primary planned integration efforts for FY 2017 is in the area of colloid-facilitated radionuclide transport (Task #25), as discussed below in Section 3.1.3.2.

Within the Model Integration Table there are three main evaluation columns to prioritize activities for further development of the GDSA Framework:

- Column 6: Integration Time Frame ("Priority Order and Urgency"), i.e., how soon should we integrate?
- Column 7: Current Status ("Level of Readiness/Technical Maturity"), i.e., how soon could we integrate?
- Column 8: Level of Effort Required (for Integration with PA/PFLOTRAN), i.e., how long will it take once we start?

The urgency ratings for Column 6 are "N = near term" (or FY17), "M = medium term" (or FY17-FY19), and "F = far term" (FY19 and beyond). The urgency rating given to each process model in this column represent a judgment call by GDSA scientists regarding how important each of these models are to total system performance. The ratings in Column 8 regarding Level of Effort Required have not yet been formulated in terms of full-time employees, but this is planned for the future.

3.1.2 Work Package Leveraging

A special category of activities in Table 3-1 is labeled "Generic reference-case model enhancement/ development and PA analyses for other work packages." Many of the tasks in this category involve leveraging other work packages with the GDSA work package, i.e., combining GDSA resources with other work-package resources (or relying mostly on the personnel and funding in other work packages) to complete some of the integration and analysis items necessary for a complete performance assessment model. Of note here are Tasks 14, 15, and 16, which represent work on the primary repository concepts and host rock media being considered in the UFDC. Much of the work needed to develop and finalize generic reference cases, as well as to run performance assessment analyses, for these repository concepts (i.e., crystalline, argillite, deep borehole, DOE-managed waste) will be conducted under the corresponding work packages, in consultation with GDSA personnel.

3.1.3 Collaborative Process Model Implementation

This section describes two examples of integration between GDSA and process modelers. The first section, 3.1.3.1, describes the effort to combine a discrete fracture network into the PA modeling system. It is one of the major GDSA activities conducted during FY 2015, and was continued in FY 2016. The second section, 3.1.3.2, briefly introduces a major planned integration activity for FY 2017, which is the incorporation of a more complete colloid-facilitated transport model into PFLOTRAN. This capability is explained in more detail in Reimus et al. (2016), deliverable M3FT-16LA080504031.

3.1.3.1 Discrete Fracture Networks

Numerical simulation of the crystalline reference case requires a method for simulating coupled heat and fluid flow and radionuclide transport in both porous media (bentonite buffer, surface sediments) and fractured rock (the repository host rock). Discrete fracture networks (DFNs), networks of two-dimensional planes distributed in a three-dimensional domain, are commonly used to simulate isothermal fluid flow and particle transport in fractured rock, and have been used to assess the performance of proposed radioactive waste repositories in crystalline rock at Aspo (Selroos et al. 2002) and Forsmark, Sweden (Hartley and Joyce 2013).

DFNs are limited by their inability to simulate heat conduction through the rock matrix (and resulting inability to capture the effects of thermally driven fluid fluxes or to couple chemical processes to thermal processes), and by the availability of computational resources necessary to simulate problems involving high fracture density, large domain size, or multiple unknowns such as, for instance, multiple chemical

species. When DFNs become large, simplifications are commonly made, such as modeling flow only in fracture intersections (pipe model); using equivalent continuous porous medium (ECPM) representations in all or part of the model domain; breaking the problem into smaller pieces; simulating only steady state flow regimes; and relying on particle tracking instead of solving the set of fully coupled reactive flow and transport equations.

Of the simplifications listed above, the ECPM best fits the needs of performance assessment simulations of heat-generating waste. When properly defined, the ECPM maintains the flow and transport characteristics of a DFN, allows for uncomplicated placement of porous materials within the model domain, simulates heat conduction (and solute diffusion) through the matrix of the fractured rock, and allows for fully coupled, transient simulation of reactive transport.

Integration of DFNs with PA is a collaborative effort with Los Alamos National Laboratory (LANL). DFNs are generated with LANL's dfnWorks (Hyman et al. 2015a; Hyman et al. 2015b) and mapped to ECPM with a Python script called mapDFN.

dfnWorks takes as input statistical distributions describing fracture orientation and fracture radii, fracture density (fractures per km^3), parameters relating fracture transmissivity (m^2/s) to fracture radius, and the dimensions of the three-dimensional model domain. It distributes fractures randomly within the space of the model domain and keeps only those fractures that belong to a cluster connecting at least two faces of the domain. For each fracture in a connected cluster, it returns the coordinates of the fracture center, the unit vector defining the pole normal to the plane of the fracture, and the fracture radius, permeability, and aperture (which is calculated as a function of the fracture transmissivity according to the cubic law).

mapDFN takes as input the output from dfnWorks and parameters describing the desired ECPM model domain and discretization, including the origin and extent of the domain and the size (length) of the grid cells, which are constrained to be cubic. It determines which fractures intersect which grid cells, and calculates grid cell permeability and porosity on the basis of fracture permeability and aperture.

Anisotropic grid cell permeability is calculated by summing the contributions of all the fractures intersecting the cell. For each fracture, intrinsic transmissivity (T_f in m^3) is calculated from permeability (k_f) and aperture (b_f) as

$$T_f = k_f b_f \tag{3-1}$$

and described as a tensor, whose coordinates are then rotated into the coordinates of the grid. The resulting tensor, with diagonal and off-diagonal terms, is a complete description of the transmissivity ellipse of the fracture in the coordinates of the ECPM grid. The off-diagonal terms are neglected, and the diagonal tensor describing cell permeability is calculated as

$$\begin{bmatrix} k_{xx} & & \\ & k_{yy} & \\ & & k_{zz} \end{bmatrix} = \frac{1}{d} \sum \begin{bmatrix} T_{xx} & & \\ & T_{yy} & \\ & & T_{zz} \end{bmatrix}_f \tag{3-2}$$

where d is the length of the cell side, and the sum is over all fractures intersecting the cell. PFLOTRAN simulates only the diagonal portion of the permeability tensor, due to the oscillatory, non-monotonic solutions that can result from its numerical methods for discretization (i.e. first- and second-order finite volume) when the full tensor is used.

In the calculation of porosity, the simplifying assumption is made that each fracture intersecting the cell does so parallel to a face of the cell. Then the porosity (ϕ) of the cell is

$$\phi = \frac{1}{d}\sum b_f \tag{3-3}$$

where d is the length of the cell side, and b_f is the aperture of fracture f. This value is the fracture porosity, which is a very small fraction of the total porosity in a fractured crystalline rock. Applying it to all cells intersected by fractures is critical to correct simulation of transient transport in the fracture network.

mapDFN assigns all cells in the domain not intersected by fractures user-specified values for matrix permeability and porosity.

3.1.3.2 Colloid-Facilitated Transport

As described in Reimus et al. (2016), the most important processes affecting colloid-facilitated radionuclide transport over the long time and distance scales relevant to nuclear waste repository risk assessments are radionuclide desorption (or any other type of dissociation) from colloids and irreversible filtration of colloids. Specifically, the rates of radionuclide desorption or dissociation and the rates of irreversible colloid filtration must *both* be slow relative to transport time scales for colloid-facilitated radionuclide transport to contribute significantly to radionuclide fluxes at a compliance boundary. Furthermore, there must be a *joint* occurrence of these two slow processes for significant colloid-facilitated radionuclide transport to occur. If radionuclides remain strongly associated with colloids that do not migrate, or if colloids that transport efficiently do not have a strong association with radionuclides, then colloid-facilitated transport to the biosphere is likely to be of low risk during the regulatory period.

The foregoing case of kinetically limited desorption from colloids (effectively, irreversible sorption) is the most likely colloid-enhanced risk contributor to total dose in the biosphere. However, another situation that can enhance radionuclide transport from the repository, is a local equilibrium condition of fast radionuclide adsorption/desorption rates onto both colloids and immobile surfaces (relative to transport time scales). If the product of the effective radionuclide partition coefficient on colloids and the steady-state colloid concentration (i.e., $K_c C_c$, in the terminology of this report) exceeds 1.0 by more than a few percent, then this situation could result in enhanced radionuclide transport. Colloid filtration rates in this case do not matter; it is steady-state colloid concentrations that govern the magnitude of colloid-facilitated transport. This condition is considered to be unlikely, as it generally requires larger concentrations of colloids than are typically observed in nature. However, if it does occur, it will result in a relatively large fraction of radionuclide mass being transported with a smaller effective retardation factor than the radionuclide in the absence of colloids. Both this enhanced equilibrium transport condition, and the previous irreversible sorption case, are primarily a concern with respect to the plutonium inventory.

A generalized mathematical model for the above two forms of colloid-facilitated radionuclide transport, written for flow in parallel-plate fractures with diffusion into a surrounding matrix (y-direction), which represents non-flowing or secondary porosity, is described by Reimus et al. (2016) and will be considered for integration into PFLOTRAN, as a way to model colloid-facilitated transport in GDSA. The model equations also apply equally well to a porous medium if the matrix or secondary porosity is set equal to zero and the fracture properties are taken to be the porous medium properties (in this case, all equations for transport in the matrix can be ignored). The model is based on work presented in two recent Used Fuel Disposition reports (Wang et al. 2013, Chapter 2; Wang et al. 2014, Chapter 7) and, in particular, on work conducted as part of the Colloids Formation and Migration (CFM) international partnership project (Noseck et al. 2016). This model can be applied to identify and evaluate the conditions under which colloid-facilitated radionuclide transport is likely to contribute to nuclear waste repository risk assessment calculations.

Table 3-1. GDSA model integration and development table.

Task #	Task Name	Task Description	Code	Personnel	INTEGRATION TIME FRAME ("Priority Order/ and Urgency") N = Near term (FY17) M = Medium term (FY17 – FY19) F = Far term (FY19 +) How soon should we?	CURRENT STATUS Level of Readiness/ Technical Maturity How soon could we start?	LEVEL OF EFFORT (LOE) required for Integration with PA/PFLOTRAN L = 1 month M = 6 months H = 1 year or more How long once we start?	NOTES
Basic GDSA-PFLOTRAN framework/code capabilities:								
1	Grid refinement	• Octree-grid adaptive mesh refinement using p4est • Block grid refinement	PFLOTRAN; p4est	Hammond, Alzraiee SNL	**M**	**1 year**	**H**	• Octree capability is still being developed by the originators
2	Operator splitting for reactive transport	• Add operator-splitting numerical method for reactive transport	PFLOTRAN	Hammond SNL	**N**	**Now**	**L - M**	• Enables larger simulations as the system of equations is smaller
3	UA/SA	• Standardized set of UA/SA, including rank regression • Stability of mean, including control variates	Dakota, etc.	Stein, MacKinnon, Kuhlman SNL	**N**	**Now**	**M**	• We already have the Dakota capability (e.g., PRCCs) • Not clear that we have a stepwise linear regression capability
4	Solution density	• Liquid density dependence on salinity	PFLOTRAN	Hammond SNL	**N**	**Now**	**L**	• Need to implement salinity dependence in PFLOTRAN TH mode
5	Pitzer model	• Implement Pitzer activity coefficients (Wolery version)	PFLOTRAN	Hammond, Jove-Colon SNL	**M**	**Now**	**M**	• We prefer the Wolery, rather than the Felmy, implementation • Important for repositories in salt and for deep borehole

Table 3-1. GDSA model integration and development table.

Task #	Task Name	Task Description	Code	Personnel	INTEGRATION TIME FRAME ("Priority Order/ and Urgency") N = Near term (FY17) M = Medium term (FY17 – FY19) F = Far term (FY19 +) How soon should we?	CURRENT STATUS Level of Readiness/ Technical Maturity How soon could we start?	LEVEL OF EFFORT (LOE) required for Integration with PA/PFLOTRAN L = 1 month M = 6 months H = 1 year or more How long once we start?	NOTES
6	Species and element properties	• Solute-specific diffusivities • Temperature-dependent solubilities	PFLOTRAN	Hammond, Mariner SNL	**M**	**6 months**	**L**	• Probably only a second order effect.
7	Basic biosphere model	• Aquifer; overlying sediments; infiltration; withdrawal well(s); IAEA ERB-1A dose calculation (GDSA)	GDSA	Mariner SNL	**N (but see notes)**	**Now**	**L**	• Instead use drinking water standards from YMP, i.e., a concentration metric instead of a dose metric?
9	Mechanical processes	• ROMs for creep closure General representation of "M" in PFLOTRAN?	PFLOTRAN	Park, Hammond SNL Kara LANL	**M**	**1 to 2 years?**	**H**	• Important for salt at early times, but how important for directly including this process in a long-term PA?
10	Solid solution model	• Precipitation and dissolution of solid solutions	PFLOTRAN	Lichtner, Hammond SNL	**F**	**2 years**	**H**	• A simpler version (ignoring molar volumes) may be implemented sooner
11	Miscellaneous	• Checkpoint/restart capability for UFDC process models • Gridded dataset support for initial solute concentrations	PFLOTRAN	Hammond SNL	**N**	**Now**	**L**	
GDSA Code Efficiency								
12	Numerical solution methods	• Improve GENERAL multiphase convergence (analytical derivatives)	PFLOTRAN	Hammond SNL	**N**	**Now**	**M**	

Table 3-1. GDSA model integration and development table.

Task #	Task Name	Task Description	Code	Personnel	INTEGRATION TIME FRAME ("Priority Order/ and Urgency") N = Near term (FY17) M = Medium term (FY17 – FY19) F = Far term (FY19 +) How soon should we?	CURRENT STATUS Level of Readiness/ Technical Maturity How soon could we start?	LEVEL OF EFFORT (LOE) required for Integration with PA/PFLOTRAN L = 1 month M = 6 months H = 1 year or more How long once we start?	NOTES
13a	Implicit solution for decay and ingrowth	• Use implicit solution instead of operator splitting for PFLOTRAN "sandbox" capability	PFLOTRAN	Hammond SNL	**M**	**Now**	**M**	
13b	Implicit solution for decay and ingrowth	• Use implicit solution instead of operator splitting for PFLOTRAN reactive transport equations	PFLOTRAN	Hammond SNL	**M**	**Now**	**H**	
Generic reference-case model enhancement/development and PA analyses for other work packages:								
14	CSNF repository reference cases (argillite; crystalline; salt)	• Revise properties, EBS/repository design, conceptual models, geometry, etc., as necessary • Refine spatial heterogeneity in salt, clay, etc., as necessary • Include multiphase flow (e.g., buffer resaturation) • Need for mechanical processes • Dual/multi-continuum for transport in granite	GDSA	SNL	**N**	**Ongoing**	**Funding dependent**	
15	Defense repository reference cases	• Modification of any models or code capabilities to accommodate a repository for DOE-managed HLW/SNF	GDSA	SNL	**N**	**Ongoing**	**Funding dependent**	

Table 3-1. GDSA model integration and development table.

Task #	Task Name	Task Description	Code	Personnel	INTEGRATION TIME FRAME ("Priority Order/ and Urgency") N = Near term (FY17) M = Medium term (FY17 – FY19) F = Far term (FY19 +) How soon should we?	CURRENT STATUS Level of Readiness/ Technical Maturity How soon could we start?	LEVEL OF EFFORT (LOE) required for Integration with PA/PFLOTRAN L = 1 month M = 6 months H = 1 year or more How long once we start?	NOTES
16	Deep borehole reference case	• Modification of any models or code capabilities to model a deep borehole concept	GDSA	SNL	**N**	**Ongoing**	**Funding dependent**	
17	Performance metrics	• Develop a "standardized" set of performance metrics for each reference case (e.g., a grid of wells for granite)	GDSA	Sevougian, Stein, Mariner SNL	**N**	**Now**	**M**	• This issue arose for the granite repository where the granite and fractures were effectively outcropping
18	More complete UA/SA	• "Full" suite of UA/SA, similar to YMP analyses • Template for site-screening decisions	GDSA	SNL	**N**	**TBD**	**M**	
19	Chemical processes	• Effect of chemistry on near-field degradation and transport • Possibly a separate, "nested" model	PFLOTRAN	Hammond, Jove-Colon, Mariner et al. SNL	**M**	**Now**	**H**	
20	Disruptive events	• PA processes initiated or dependent upon external events, such as human intrusion, glaciation, and seismicity. Also, include early WP failures.	PFLOTRAN	Mariner, Sevougian, Hammond, et al. SNL et al.	**F**	**TBD**	**H+**	• Requires stylized scenarios and regulations for generic repositories and for site-screening activities • Should remain on hold until there are candidate sites
21	Surface processes and features	• Develop model parameters for infiltration & surface discharge	GDSA	Mariner, et al SNL	**M**	**1 years**	**M**	• Consider processes such as precipitation, evapotranspiration,

Table 3-1. GDSA model integration and development table.

Task #	Task Name	Task Description	Code	Personnel	INTEGRATION TIME FRAME ("Priority Order/ and Urgency") N = Near term (FY17) M = Medium term (FY17 – FY19) F = Far term (FY19 +) How soon should we?	CURRENT STATUS Level of Readiness/ Technical Maturity How soon could we start?	LEVEL OF EFFORT (LOE) required for Integration with PA/PFLOTRAN L = 1 month M = 6 months H = 1 year or more How long once we start?	NOTES
								surface runoff, streams, lakes, etc
22	Other missing FEPs (processes)	• Gas generation and movement • Ongoing climatic effects • Neutron generation	GDSA	Mariner, et al. SNL	**M - F**	**1 year**	**H**	• Gas generation/ movement might be important with regard to corrosion processes and buffer stability
GDSA model/code V&V and documentation (including benchmarking):								
23	QA	• V&V, benchmarking, and documentation of codes, including pre- and post-processors	GDSA	Frederick, Stein, Mariner, etc. SNL	**N**	**Now**	**Ongoing**	• PFLOTRAN wiki already has significant regression testing, but documentation could be improved.
Collaborative process model implementation – shorter term (process models are assumed to be developed under non-GDSA work packages):								
24	SNF Degradation	• Mixed potential model of spent fuel matrix degradation (including possible effect of Fe corrosion) • Radiolysis	PFLOTRAN/ FMDM	Frederick, Hammond SNL Jerden, ANL	**N**	**Ongoing**	**M**	• Direct implementation in PFLOTRAN already complete and now at the testing stage. • Additional development and more efficient coding suggested
25	(Pseudo) Colloid-Facilitated	• Formation, stability, and transport of pseudocolloids in the near field and far field	PFLOTRAN	Hammond SNL Reimus	**N**	**Now**	**M**	• Direct implementation in PFLOTRAN suggested, with perhaps some

Table 3-1. GDSA model integration and development table.

Task #	Task Name	Task Description	Code	Personnel	INTEGRATION TIME FRAME ("Priority Order/ and Urgency") N = Near term (FY17) M = Medium term (FY17 – FY19) F = Far term (FY19 +) How soon should we?	CURRENT STATUS Level of Readiness/ Technical Maturity How soon could we start?	LEVEL OF EFFORT (LOE) required for Integration with PA/PFLOTRAN L = 1 month M = 6 months H = 1 year or more How long once we start?	NOTES
	Transport Model			LANL Zavarin LLNL				simplification of the conceptual model.
26	Intrinsic Colloids	• Intrinsic Pu colloid formation, stability, and transport in the near and the far fields, as a function of T	PFLOTRAN	Hammond SNL Reimus LANL Zavarin LLNL	**M**	**TBD**	**M**	• Direct implementation in PFLOTRAN, with perhaps some simplification of the conceptual model.
27	Discrete Fracture Network (DFN) Model	• Fluid flow & transport in fracture networks • Mapping tools (dfnWorks to PFLOTRAN) • Dual continuum; matrix diffusion	dfnWorks, PFLOTRAN, Python	Stein, Hammond SNL Viswanathan Makedonska LANL	**N**	**Ongoing**	**M**	• potential FY17 enhancements: heat transport; fracture intersects borehole • Dual continuum/matrix diffusion ready now
28	HLW WF degradation (process model)	• Glass waste degradation • Radiolysis • Transition state theory	PFLOTRAN	Rieke, PNNL Ebert, ANL	**N - M**	**Now**	**H**	• Needed for Defense Waste Repository • Integration with Waste Form Campaign
29	Waste Package Degradation Model (mechanistic)	• Degradation of waste packages and canisters • Carbon steel; stainless steel; copper waste packages • Include various degradation processes (SCC, GC, LC, MIC, early failure)	PFLOTRAN et al.	Jove Colon SNL	**M**	**1 to 3 years?**	**H**	• Direct implementation in PFLOTRAN suggested, similar to SNF degradation

Table 3-1. GDSA model integration and development table.

Task #	Task Name	Task Description	Code	Personnel	INTEGRATION TIME FRAME ("Priority Order/ and Urgency") N = Near term (FY17) M = Medium term (FY17 – FY19) F = Far term (FY19 +) How soon should we?	CURRENT STATUS Level of Readiness/ Technical Maturity How soon could we start?	LEVEL OF EFFORT (LOE) required for Integration with PA/PFLOTRAN L = 1 month M = 6 months H = 1 year or more How long once we start?	NOTES
Collaborative process model implementation – longer term (process models are assumed to be developed under non-GDSA work packages):								
30	Salt Coupled THM processes	• Coupled thermal-hydrological-mechanical processes in salt EBS and EDZ	TOUGH-FLAC	Rutqvist. Martin LBNL	**N - M**	**Now for 2-D Several years for 3-D**	**H**	• Response surface suggested (permeability and porosity fields)
31	Coupled THC processes in Salt	• Coupled thermal-hydrologic-chemical processes in a salt repository	PFLOTRAN	Stauffer LANL Hammond SNL	**N - M**	**Now**	**M**	• Hammond indicates that chemical components can be added to gas phase in PFLOTRAN formulation.
32	Two-Part Hooke's Model (saturated)	• Clay deformation	TPHM-FLAC3D	Zheng LBNL	**M - F**	**TBD**	**TBD**	• Abstraction suggested (permeability, porosity, stress).
33	THMC processes in EBS	• THMC (includes clay illitization)	TOUGH REACT/FLAC3D	Rutqvist, Zheng LBNL	**M - F**	**M, C indicated to need "work"**	**TBD**	• Response surface suggested (permeability, porosity, cation exchange capacity, swelling stress). • Chemical processes still under development
34	THM model of buffer materials (unsaturated)	• Coupled thermal-hydrological-mechanical processes in compacted clays	BBM+TOUGHREACT+FLAC	Rutqvist LBNL	**M - F**	**Now for 2-D Several years for 3-D**	**H**	• Response surface suggested (permeability and porosity fields)

Table 3-1. GDSA model integration and development table.

Task #	Task Name	Task Description	Code	Personnel	INTEGRATION TIME FRAME ("Priority Order/ and Urgency") N = Near term (FY17) M = Medium term (FY17 – FY19) F = Far term (FY19 +) How soon should we?	CURRENT STATUS Level of Readiness/ Technical Maturity How soon could we start?	LEVEL OF EFFORT (LOE) required for Integration with PA/PFLOTRAN L = 1 month M = 6 months H = 1 year or more How long once we start?	NOTES
35	Rigid-Body-Spring-Network (RBSN)	• Discrete Fracture Network (DFN) with THM (argillite/clay)	TOUGH2-RBSN	Kim, Rutqvist LBNL	**M - F**	**??**	**M - H**	• Abstraction suggested (fracture property response surface). A coupled version of RBSN requires dynamic input (T, p, σ).
Collaborative process model implementation – not currently scoped/funded in UFD DR:								
36	Biosphere pathways	• Detailed biosphere pathways, processes, and FEPs	GDSA	Mariner, et al SNL Others?	**F**	**3 years?**	**H**	• This should probably wait until there are actual candidate sites • Needs to consider the various biosphere FEPs in the UFDC list (3.3.XX.YY)
37	Cladding Degradation	• Cladding degradation processes (e.g., HC)	PFLOTRAN ?		**F**	**1 year**	**M**	
38	In-Package Flow	• Modeling of flow and transport inside waste packages/canisters • Evolution of corrosion products	PFLOTRAN		**F**	**2 years**	**H**	• Requires development of a tractable conceptual model

Table 3-1. GDSA model integration and development table.

Task #	Task Name	Task Description	Code	Personnel	INTEGRATION TIME FRAME ("Priority Order/ and Urgency") N = Near term (FY17) M = Medium term (FY17 – FY19) F = Far term (FY19 +) How soon should we?	CURRENT STATUS Level of Readiness/ Technical Maturity How soon could we start?	LEVEL OF EFFORT (LOE) required for Integration with PA/PFLOTRAN L = 1 month M = 6 months H = 1 year or more How long once we start?	NOTES
39	In-Package Chemistry	• Fully coupled in-package chemistry model, as it impacts degradation, mobilization, and transport inside the WP	PFLOTRAN	Mariner?	**F**	**2 to 3 years**	**H**	
Models Added or Improved in FY 2016:								
40	HLW WF degradation (simplified)	• Glass waste degradation	PFLOTRAN	Frederick, Mariner SNL	**Complete**	**Complete**		• Simple temperature-dependent rate equation
41	WP Degradation Model Framework (non-mechanistic)	• Degradation of WP outer barrier over time	PFLOTRAN	Mariner, Frederick SNL	**Complete**	**Complete**		• Default model samples rates • Breach times may also be entered • Mechanistic models may be coupled to this framework
42	Decay in Precipitate Phase	• Decay/ingrowth of radionuclides in mineral phases and release of decay products	PFLOTRAN	Mariner, Hammond SNL	**Complete**	**Complete**		• Direct coupling in PFLOTRAN.
43	Waste Form Radioactive Decay Model	• Decay and ingrowth of isotopes within WF over time	PFLOTRAN	Frederick, Mariner, Hammond SNL	**Complete**	**Complete**		

Table 3-1. GDSA model integration and development table.

Task #	Task Name	Task Description	Code	Personnel	INTEGRATION TIME FRAME ("Priority Order/ and Urgency") N = Near term (FY17) M = Medium term (FY17 – FY19) F = Far term (FY19 +) How soon should we?	CURRENT STATUS Level of Readiness/ Technical Maturity How soon could we start?	LEVEL OF EFFORT (LOE) required for Integration with PA/PFLOTRAN L = 1 month M = 6 months H = 1 year or more How long once we start?	NOTES
44	Radionuclide Release Model	• Congruent release of radionuclides in WF due to WF dissolution • Instant release fractions	PFLOTRAN	Frederick, Mariner, Hammond SNL	**Complete**	**Complete**		• Tracks isotope masses remaining in WF due to dissolution, decay, ingrowth, and instant release
45	Effective Solubility Model for Isotopes	• Precipitation and dissolution of isotopes as a function of elemental concentrations	PFLOTRAN	Mariner, Hammond SNL	**Complete**	**Complete**		• Direct coupling in PFLOTRAN.
46	Equilibrium Isotope Partitioning Model	• Ensures isotopes of each element are distributed among aqueous, sorbed, and precipitate phases to maximize entropy	PFLOTRAN	Mariner, Hammond SNL	**Complete**	**Complete**		
47	Equivalent Continuous Porous Medium	• Map discrete fracture network to porous medium domain for PA simulations	mapDFN.py	Stein, Hammond SNL LANL DFN team	**Complete**	**Complete**		• Preprocessor

3.2 GDSA Process Model Development

In addition to the collaborative development of discrete fracture networks and colloid modeling (Section 3.1.3), the GDSA group in FY 2016 implemented or improved process models and/or process model frameworks for waste package degradation and radionuclide behavior. Figure 3-2 identifies key source-term processes and radionuclide processes that can significantly affect the release, partitioning, and transport of radionuclides in the GDSA reference cases. Processes and/or process model frameworks that were improved or implemented this year are highlighted in red in the figure. They include:

- Section 3.2.1 – Canister degradation and breach modeling framework (added) with an empirical breach model (added) and a simple canister degradation model (added)
- Section 3.2.2 – Four waste form degradation process models (added or improved) and instantaneous release (added)
- Section 3.2.3 – Decay and ingrowth for the waste form (added) and for the transport domain (improved)
- Section 3.2.4 – Solubility-controlled precipitation and dissolution (improved)
- Section 3.2.4 – Equilibrium isotope partitioning (added)

Progress made on these process models and process model frameworks in FY 2016 is described in the subsections indicated. Additional potentially-important processes of this type, not represented in Figure 3-2 but identified for future work in Table 3-1, include gas generation, intrinsic colloid formation, and neutron activation.

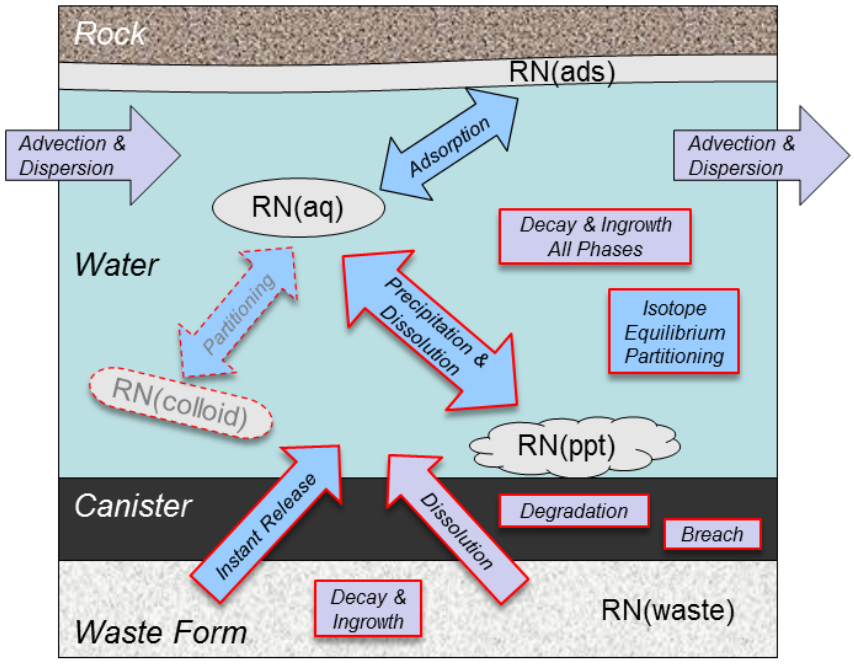

Figure 3-2. Schematic diagram of included processes affecting radionuclide (RN) concentrations in aqueous, adsorbed, colloid, and precipitate phases.

3.2.1 Canister Degradation

In FY 2015, the conceptual model for simulating waste package canister degradation in the GDSA framework was significantly advanced. The conceptual model addresses (1) the timing of canister breach and (2) the performance of the canister after breach. In this conceptual model, the status of the canister is defined by two abstract terms, canister vitality (V) and canister performance (P). Canister vitality is a normalized measure of remaining time or remaining canister wall thickness before canister breach, and canister performance is a normalized measure of the physical ability of the canister to contain the source. Initially, both terms have a value of 1. Before canister breach, while corrosion reduces the time remaining or canister wall thickness remaining before canister breach, the canister vitality decreases. When it reaches zero, the canister is breached and canister performance begins to decrease. See Mariner et al. (2015, 3.2.4) for details.

This year, implementation of the canister degradation model in PFLOTRAN was initiated. For this initial stage of implementation, a framework was completed for simulating canister vitality, the first of the two parameters in the conceptual model, and canister breach. The canister vitality is initialized to 1, and is reduced at each time step by the effective canister vitality degradation rate R_{eff}, according to

$$R_{eff} = R \cdot e^{C\left(\frac{1}{333.15} - \frac{1}{T(t,\vec{x})}\right)} \tag{3-4}$$

where R is the base canister vitality degradation rate at 60ºC, T is the local temperature (in Kelvin), and C is the canister material constant. This equation assumes that reaction rates are a function of temperature as described by the Arrhenius equation. For general corrosion, R represents the normalized general corrosion rate at 60ºC in units of 1/T (i.e., units of L/T normalized by the thickness of the canister wall), and the associated canister vitality is then a normalized measure of the remaining canister thickness before breach. Once canister vitality drops below zero, the canister is considered breached, and a Boolean flag is turned on for the waste form object inside of it.

The user may alternatively specify the canister breach time for each waste package. This functionality was included to allow for early breach times, or to guarantee a breach time if the effect of temperature cannot be estimated to calculate a degradation rate.

The canister vitality degradation rate as it has been initially implemented this year provides a framework upon which more mechanistic processes can interface. Coupling and interfacing the canister degradation model with more mechanistic processes (such as general corrosion, stress corrosion cracking (SCC), pitting corrosion, microbiologically-influenced corrosion (MIC), rock fall, etc.) is planned to start in the next fiscal year.

3.2.2 Waste Form Process Model

This year, significant restructuring within the existing Waste Form Process Model accommodated several new capabilities. The existing waste form process model did not allow for more than one type of waste form. For each new type of waste form, an entire new process model had to be created, requiring significant investment in code development. Moreover, simulations had been limited to a single type of waste form because multiple waste form process models were not allowed to run simultaneously. After recognizing the commonalities that existed between each waste form, the Waste Form Process Model was refactored to allow modularity in the code infrastructure and multiple waste form types in a single simulation. The process model, shown schematically in Figure 3-3, now consists of three main components: (1) the waste form canister, (2) the waste form object, and (3) the waste form mechanism. The following subsections describe each component in detail.

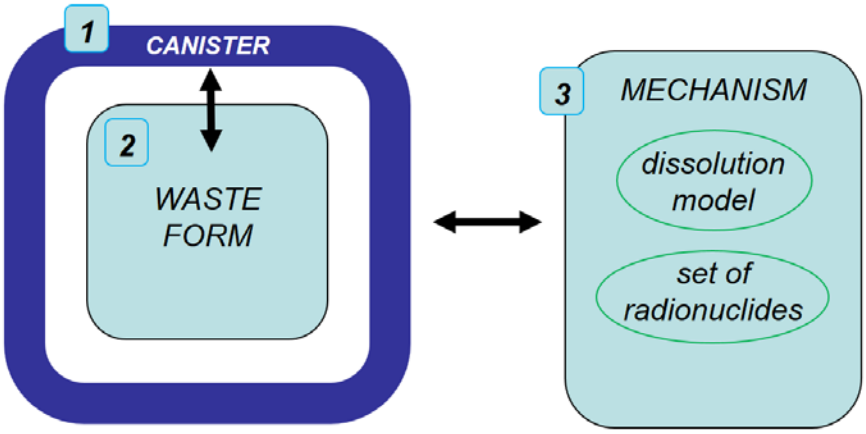

Figure 3-3. The three main components of PFLOTRAN's Waste Form Process Model consist of the waste form canister, the waste form object, and the waste form mechanism.

3.2.2.1 Coupling to the Canister Degradation Model

The first component of the Waste Form Process Model is the waste form canister. It represents a coupling to the canister degradation model as illustrated in Figure 3-3. Once the canister vitality drops to zero, a Boolean flag is turned on for the waste form object inside of it. The coupling remains abstract, so that it does not matter what kind of waste form the canister contains, only that the waste form inside has a Boolean flag indicating canister breach. The abstraction allows modularity, so that the canister degradation model can be applied to any type of waste form object through standardization. It also allows for variable breach times, with dependence on the local conditions, so that not all waste forms in the simulation breach at the same time.

3.2.2.2 Waste Form Object

The second component of the Waste Form Process Model is the waste form object. This object is very generic and contains only the information that is common between any waste form types. The user defines each waste form object's location in the domain, as well as its initial volume, and exposure factor (a surface area multiplying factor to the waste form's effective dissolution rate). Within the waste form object, the value of its effective dissolution rate is stored. Each waste form object has a pointer to the waste form mechanism (the third component of the process model) that describes waste form type-specific information. The dissolution equation that defines the effective dissolution rate is obtained from the waste form mechanism. The waste form object also stores the concentrations of the set of radionuclides it contains. The initial set of radionuclides is obtained from the waste form mechanism.

Radionuclide decay and ingrowth is now internally calculated for the set of radionuclides in each waste form according to a 3-generation analytical solution derived for multiple parents and grandparents and non-zero initial daughter concentrations (Section 3.2.3). The solution is obtained explicitly in time. This represents a vast improvement over last year's capability, where external text files provided look-up tables for several radionuclide concentrations over time. As part of the process model refactoring, PFLOTRAN now internally calculates isotope concentrations. This reduces input-output routines, improving numerical efficiency. Internal calculation of radionuclide decay and ingrowth also allows the ability to account for instantaneous release fractions for certain radionuclides upon canister breach, a process that was excluded in the look-up table approach.

Upon canister breach, the waste form object begins to dissolve according to the dissolution model that is defined by the waste form mechanism to which the waste form object points. Waste form volume

decreases accordingly. The effective dissolution rate along with the radionuclide concentrations, determines the source term (radionuclide release rate) for each waste form.

3.2.2.3 Waste Form Mechanism

The third component of the Waste Form Process Model is the waste form mechanism. In contrast to the other two components, this object is specific to the type of waste form being simulated and contains information which defines the behavior of each specific waste form type. The mechanism contains the value of the waste form bulk density, the set of initial radionuclides (initial mass fractions, molecular weights, decay rates, daughter species, and instantaneous release fractions), and a pointer to the waste form dissolution model. In some cases, it also stores the waste form specific surface area.

Since a performance analysis simulation typically contains hundreds or thousands of waste form objects but only a few waste form "types," separating the waste form type-specific information into the waste form mechanism improves modularity and numerical efficiency. An additional benefit of the modularity is that new waste form types can easily be created in PFLOTRAN by simply creating new waste form mechanisms. In the previous version, accommodating a new waste form type meant writing an entirely new waste form process model. Moreover, coupling to external dissolution models (such as FMDM) is easily accomplished through the modularity provided with the waste form mechanism.

Currently, four types of waste form mechanisms have been implemented. Details of each mechanism are described below. For three of the waste form mechanisms, a series of three figures are included to demonstrate the capability of the Waste Form Process Model. The figures portray the evolution of a single waste form inside a cube of 27 (3×3×3) 1-m^3 grid cells. The simulation assumes no fluid flow, no diffusive flux across the domain boundaries, and a constant temperature of 25ºC. The simulations were run for 100 million years (10^8 years). Each are identical except for the waste form mechanism used. A schematic of the computational domain is shown in Figure 3-4.

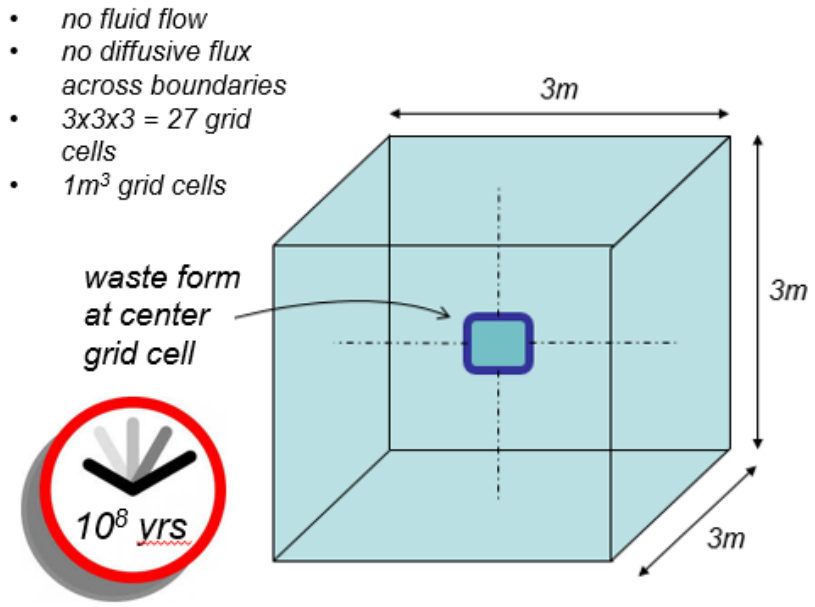

Figure 3-4. Schematic of computational domain for waste form dissolution demonstrations.

The GLASS Mechanism

High level waste in the form of glass logs are simulated using the GLASS mechanism. The glass dissolution model used in this mechanism is according to Kienzler et al. (2012)

$$r(T) = 560e^{\frac{-7397}{T(t,\bar{x})}} \tag{3-5}$$

where *r(T)* is the effective dissolution rate (kg-glass m^{-2} s^{-1}) and *T* is the temperature (Kelvin) at the current time (*t*) and location ($\bar{x}$) of the waste form. A more versatile form of this equation comes from transition state theory (TST), e.g., the Aagaard-Helgeson equation shown on page A-52 of Appendix A. Adding a generic TST equation to the Waste Form Process Model is planned for the future. The effective dissolution rate is converted to a fractional dissolution rate by multiplying *r(T)* by the specific surface area (in units of L^2/M), which is provided by the user. Figure 3-5, Figure 3-7, and Figure 3-6 demonstrate a Savannah River glass waste form using this mechanism, and Figure 3-8, Figure 3-9, and Figure 3-10 demonstrate a Hanford glass waste form using this mechanism.

The Instantaneous Mechanism

For the Instantaneous mechanism (currently called DSNF mechanism in PFLOTRAN), at the time step when breach occurs the entire radionuclide inventory of the waste form is released over the length of the time step. Concurrently, the volume of the waste form is reduced to zero. DOE spent nuclear fuel (DSNF) is simulated using this mechanism.

Figure 3-11, Figure 3-12, and Figure 3-13 demonstrate a waste form composed of DOE spent nuclear fuel in the 300W – 500W bin using this mechanism. Effects of solubility, adsorption, and diffusion can be seen for neptunium in Figure 3-13. Upon canister breach, enough neptunium is released from the waste form to reach the aqueous solubility limit, thus neptunium precipitate is formed locally, and neptunium is also adsorbed locally. As neptunium decays across all phases, the total aqueous neptunium concentration remains constant at the solubility limit as the precipitated neptunium buffers the aqueous phase. At ~10^7 years, the buffering behavior eventually exhausts the precipitated phase, and the aqueous concentration begins to fall below the solubility limit. The aqueous drop in concentration is initially very fast as neptunium dissolves and becomes adsorbed in neighboring grid cells, which maintains a steep concentration gradient. This continues for some time until equilibrium is reached within the entire domain, and further drops in neptunium concentration depend only on the decay rate, rather than a combination of decay rate and diffusion.

The FMDM Mechanism

Used nuclear fuel (composed of uranium dioxide) is simulated using the Fuel Matrix Degradation Model (FMDM) mechanism. This mechanism also demonstrates how external dissolution models can be coupled to PFLOTRAN. The dissolution model used in this mechanism is obtained via coupling to the FMDM by calling a single external subroutine developed by Jerden et al. (2015) called AMP_Step. Details regarding the FMDM conceptual model and algorithmic design (e.g. code executed within the call to AMP_Step) are provided by Jerden et al. (2015). While PFLOTRAN-FMDM coupling has been successfully established, it is not yet optimized. Optimization is needed to speed up FMDM simulation. FMDM run time has a major impact on the overall run time of a repository simulation when there are a large number of waste packages. Figure 3-14, Figure 3-15, and Figure 3-16 demonstrate a waste form composed of used nuclear fuel using this mechanism.

The CUSTOM Mechanism

To allow additional flexibility, the CUSTOM mechanism was created so that a user can specify a fractional dissolution rate (in units of 1/T), or a waste form dissolution rate that is based on specific

surface area (in units of $M/L^2/T$). If the user specifies a surface area dependent dissolution rate, a specific surface area (in units of L^2/M) must also be provided.

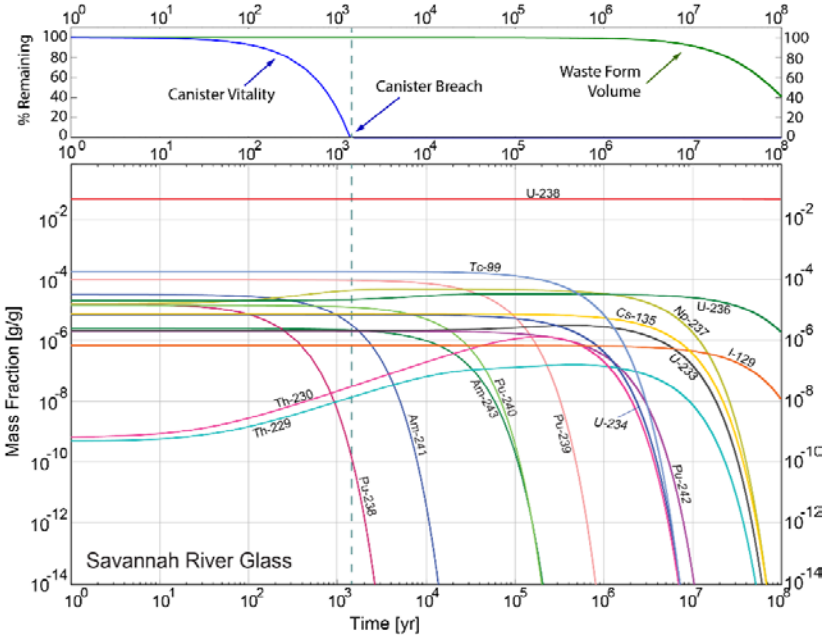

Figure 3-5. Canister vitality, waste form volume, and radionuclide mass fraction in a HLW Savannah River Glass waste form using the GLASS mechanism. Initial inventory of selected radionuclides based on year 2038.

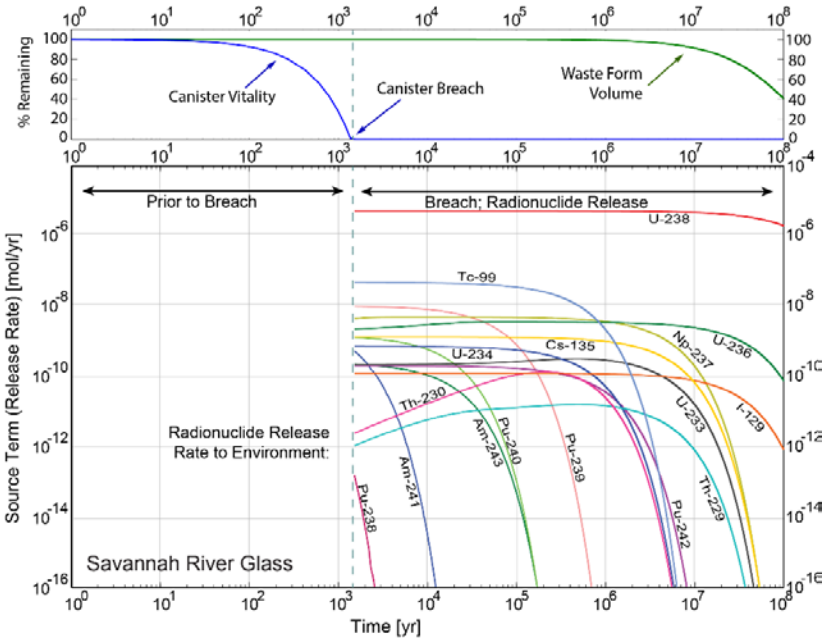

Figure 3-6. Canister vitality, waste form volume, and radionuclide release rate (source term) for a HLW Savannah River Glass waste form using the GLASS mechanism. Initial inventory of selected radionuclides based on year 2038.

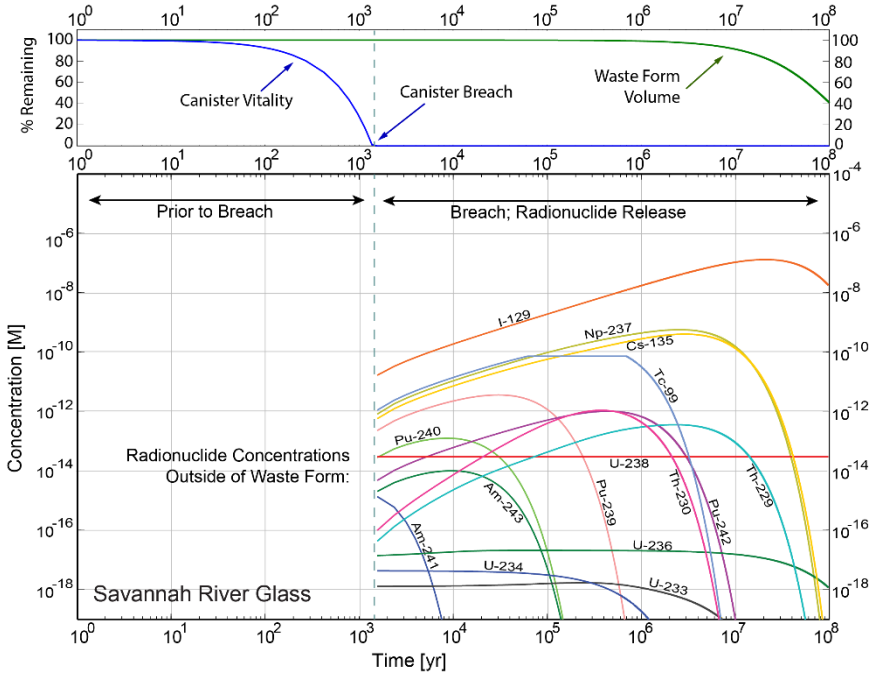

Figure 3-7. Canister vitality, waste form volume, and aqueous radionuclide concentration outside of a HLW Savannah River Glass waste form using the GLASS mechanism. Initial inventory of selected radionuclides based on year 2038.

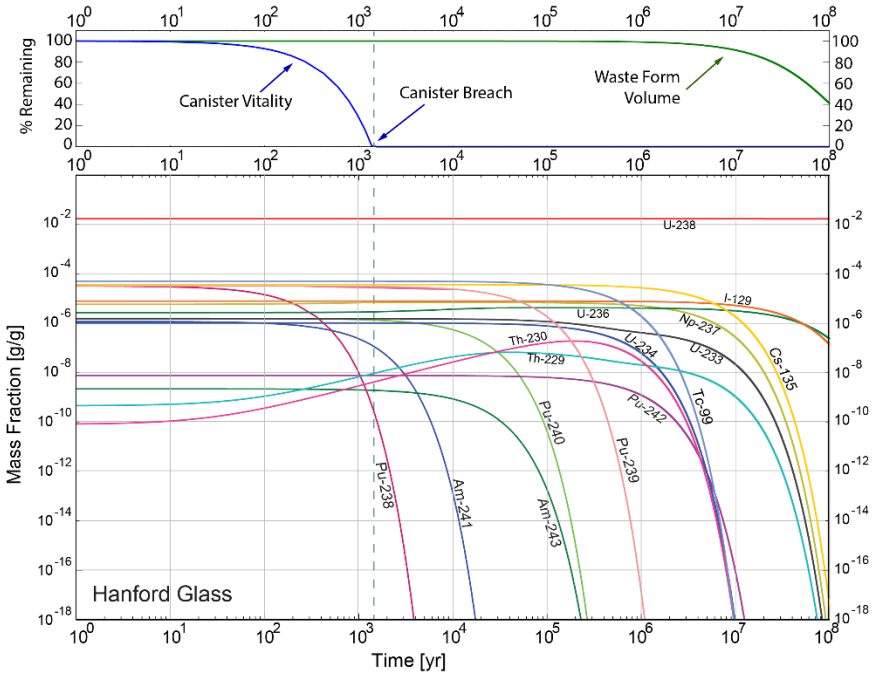

Figure 3-8. Canister vitality, waste form volume, and radionuclide mass fraction in a HLW Hanford Glass waste form using the GLASS mechanism. Initial inventory of selected radionuclides based on year 2038.

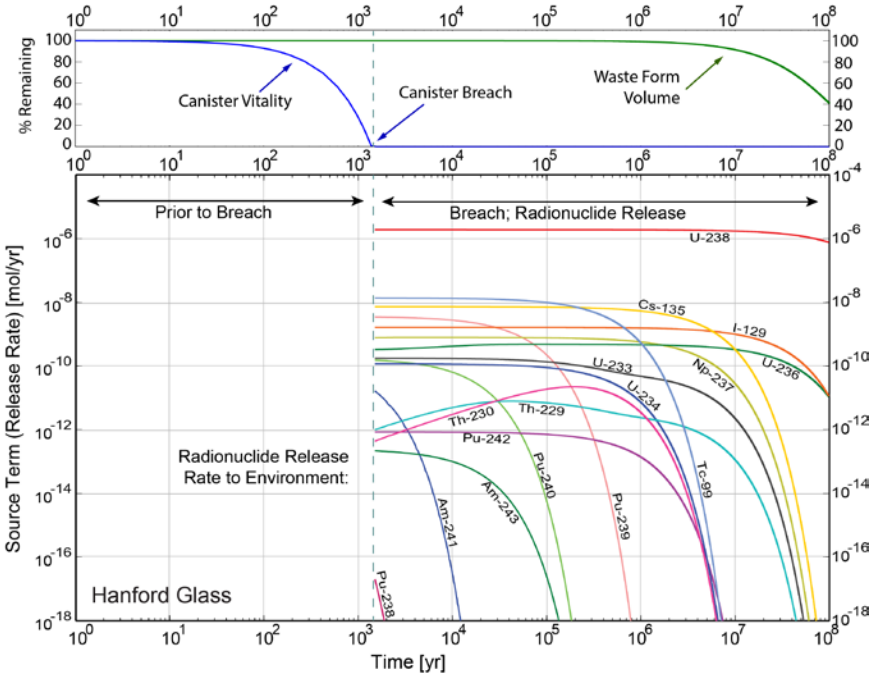

Figure 3-9. Canister vitality, waste form volume, and radionuclide release rate (source term) for a HLW Hanford Glass waste form using the GLASS mechanism. Initial inventory of selected radionuclides based on year 2038.

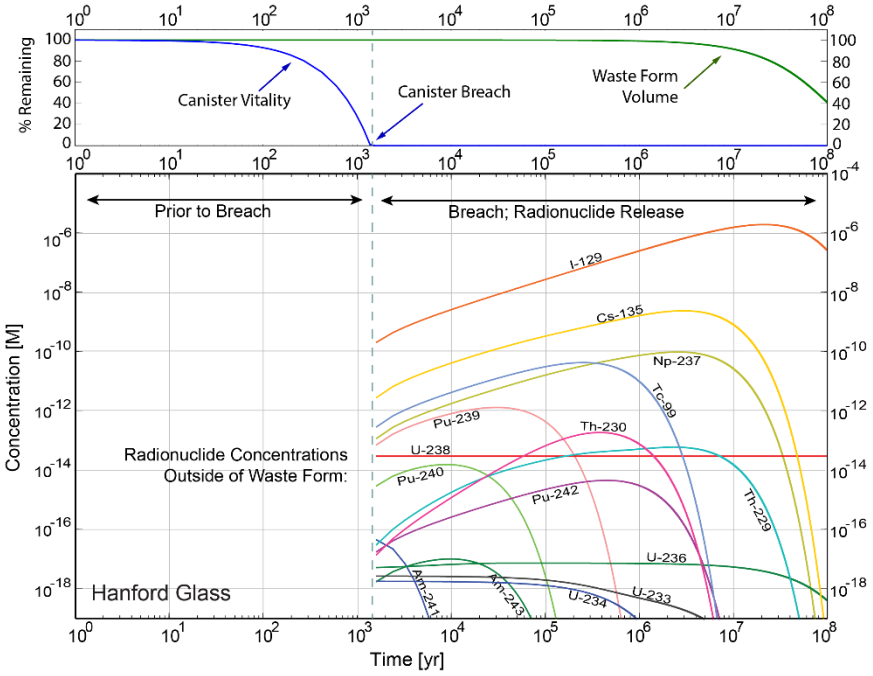

Figure 3-10. Canister vitality, waste form volume, and aqueous radionuclide concentration outside of a HLW Hanford Glass waste form using the GLASS mechanism. Initial inventory of selected radionuclides based on year 2038.

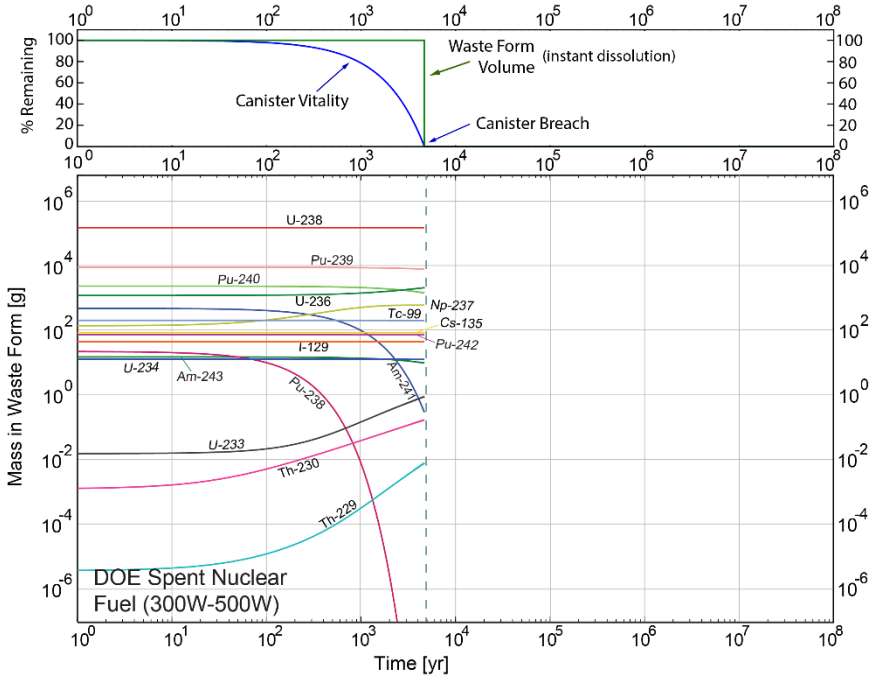

Figure 3-11. Canister vitality, waste form volume, and radionuclide mass fraction in a DOE spent nuclear fuel (300W – 500W bin) waste form using the Instantaneous mechanism. Initial inventory of selected radionuclides based on year 2038.

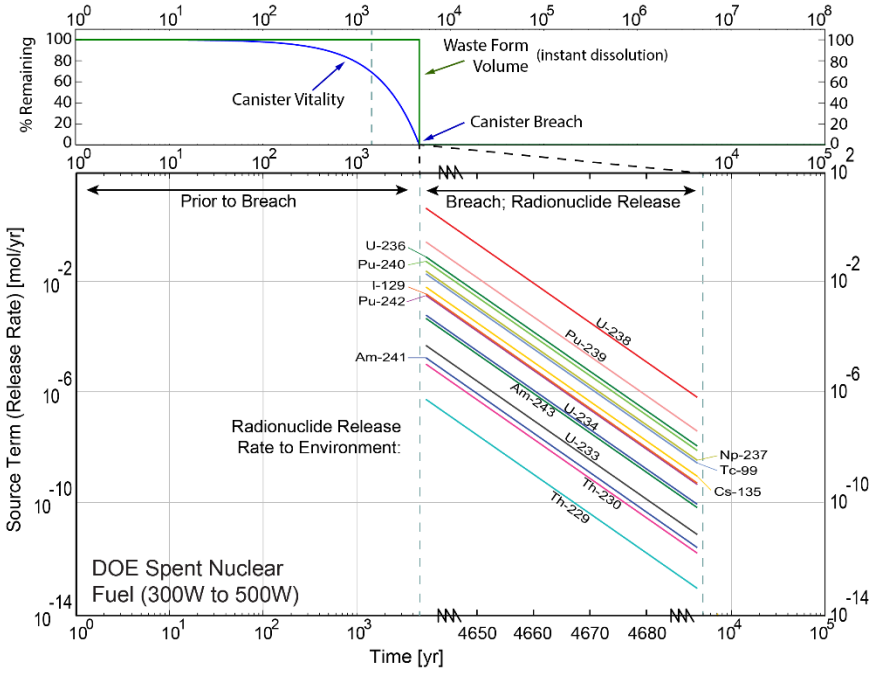

Figure 3-12. Canister vitality, waste form volume, and radionuclide release rate from a DOE spent nuclear fuel (300W – 500W bin) waste form using the Instantaneous mechanism. Initial inventory of selected radionuclides based on year 2038.

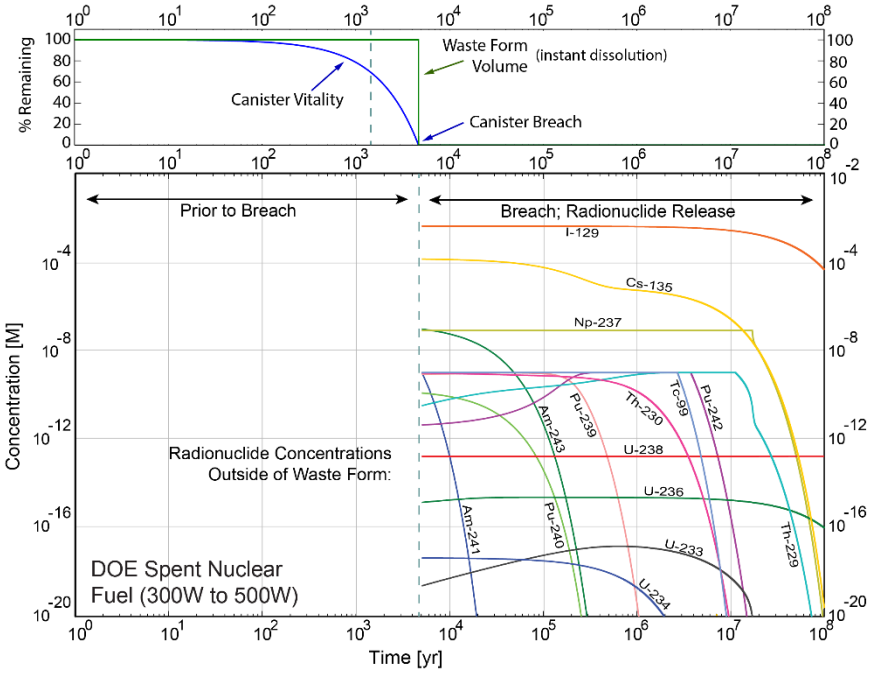

Figure 3-13. Canister vitality, waste form volume, and aqueous radionuclide concentration outside a DOE spent nuclear fuel (300W – 500W bin) waste form using the Instantaneous mechanism. Initial inventory of selected radionuclides based on year 2038.

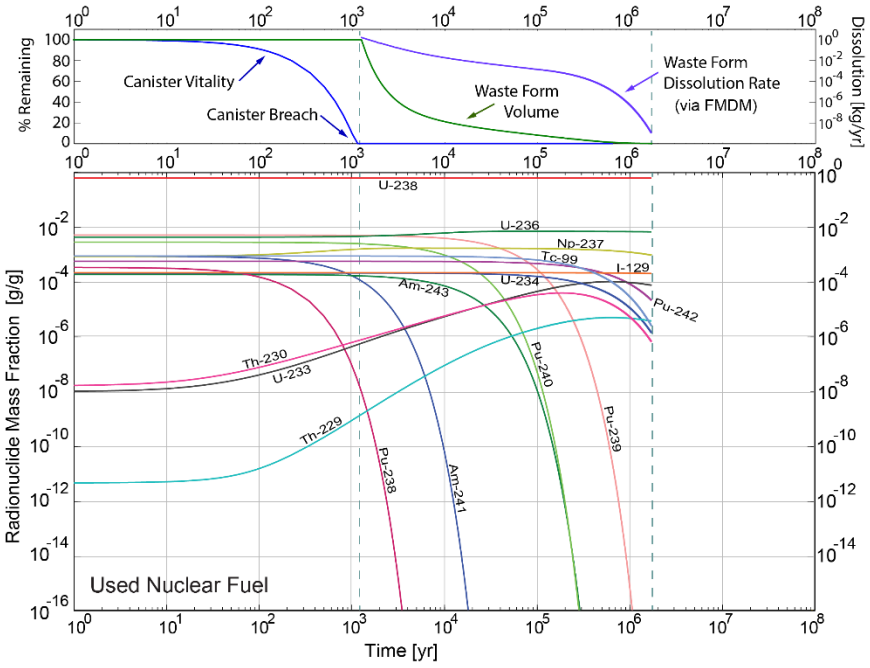

Figure 3-14. Canister vitality, waste form volume, waste form dissolution rate, and radionuclide mass fraction in a used nuclear fuel waste form using the FMDM mechanism. Initial inventory of selected radionuclides based on 30-year decay time, commercial PWR assemblies, 60,000 MWd/MTHM burn-up, and 4.73% enrichment.

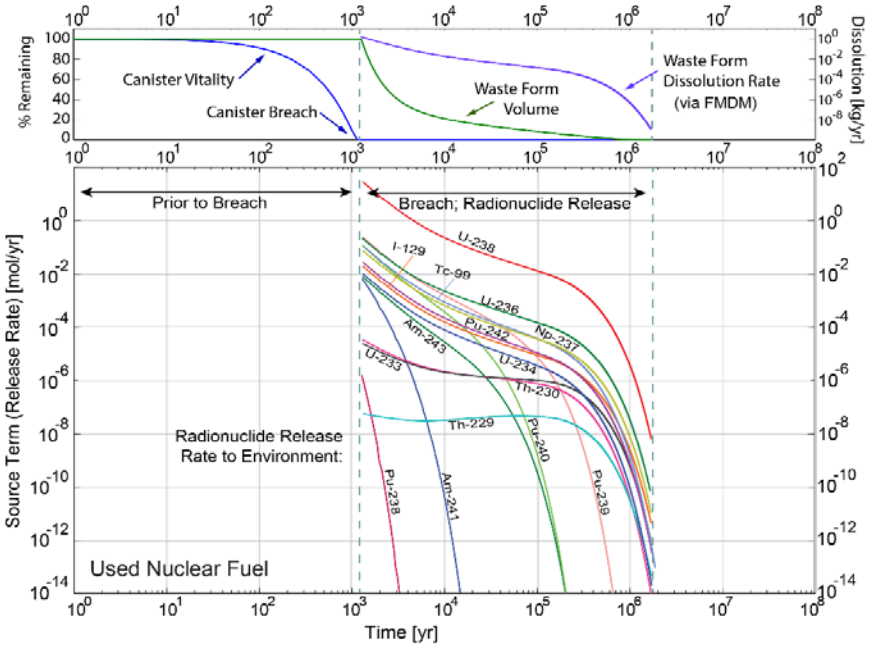

Figure 3-15. Canister vitality, waste form volume, waste form dissolution rate, and radionuclide release rate from a used nuclear fuel (300W – 500W bin) waste form using the FMDM mechanism. Initial inventory of selected radionuclides based on 30-year decay time, commercial PWR assemblies, 60,000 MWd/MTHM burn-up, and 4.73% enrichment.

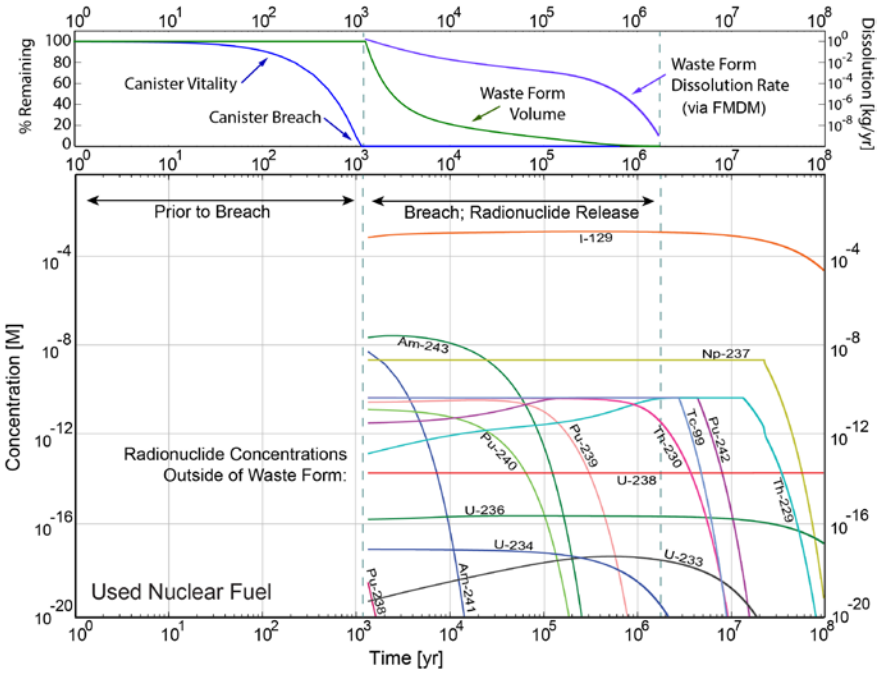

Figure 3-16. Canister vitality, waste form volume, waste form dissolution rate, and aqueous radionuclide concentration outside a used nuclear fuel (300W – 500W bin) waste form using the FMDM mechanism. Initial inventory of selected radionuclides based on 30-year decay time, commercial PWR assemblies, 60,000 MWd/MTHM burn-up, and 4.73% enrichment.

3.2.3 Isotope Decay Model

In FY 2016 a new Isotope Decay Model was developed for PFLOTRAN. Previously, decay and ingrowth could only be simulated by the chemistry process model of PFLOTRAN via the reactive transport solver. That approach is not sufficient for repository system modeling because it cannot be applied to precipitated isotopes. To include precipitated mineral phases in the chemistry process model would require a significant effort and a substantial increase in simulation time. Therefore, a new approach outside of the chemistry process model was developed. An analytical solution was implemented to calculate decay and ingrowth of total isotope concentrations in each cell at each time step prior to isotope partitioning (Section 3.2.4). This model was also included in the Waste Form Process Model to calculate decay and ingrowth of isotopes in the waste form. In this section, details of the new Isotope Decay Model are provided along with important assumptions and an example.

A limited 3-generation analytical solution for isotope decay and ingrowth was derived and implemented. The solution calculates $D(t)$, the total cell concentration of an isotope at time *t*, from the initial total cell concentration of the isotope (D^o), the initial total cell concentrations of its parent(s) (P_p^o), and the initial total cell concentrations of its grandparent(s) (G_g^o) as

$$D(t) = \left(D^o - \sum_p \frac{\lambda_p P_p^o}{\lambda_D - \lambda_p} - \sum_p \sum_g \frac{\lambda_p \lambda_g G_g^o}{(\lambda_p - \lambda_g)(\lambda_D - \lambda_g)} + \sum_p \sum_g \frac{\lambda_p \lambda_g G_g^o}{(\lambda_p - \lambda_g)(\lambda_D - \lambda_p)} \right) e^{-\lambda_D t} + \sum_p \frac{\lambda_p P_p^o}{\lambda_D - \lambda_p} e^{-\lambda_p t} - \sum_p \sum_g \frac{\lambda_p \lambda_g G_g^o}{(\lambda_p - \lambda_g)(\lambda_D - \lambda_p)} e^{-\lambda_p t} + \sum_p \sum_g \frac{\lambda_p \lambda_g G_g^o}{(\lambda_p - \lambda_g)(\lambda_D - \lambda_g)} e^{-\lambda_g t} \quad (3\text{-}6)$$

Subcripts D, p, and g identify the isotope, parent(s), and grandparent(s), respectively. The λ values are the corresponding decay constants (1/T).

The limitation of this analytical solution is that there must be insignificant ingrowth of grandparent(s) during the time step. This is true in GDSA applications for many of the isotopes but not all. Deriving a 4- or 5-generation analytical solution would yield a highly unwieldy equation and would still not address the needs of longer chains. Therefore, a numerical solution is planned for development and implementation in the near future. For a new numerical solver, the 3-generation analytical solution may be used to provide smart guesses for faster convergence. In addition, the 3-generation analytical solution may be used to test a developed numerical solver against an analytical solution for simulations in which there is no ingrowth of grandparents.

The Isotope Decay Model is called in PFLOTRAN for each cell in the transport domain at each time step. An identical version is also implemented in the Waste Form Process Model so that decay and ingrowth of isotopes in each waste form in each waste package is simulated at each time step. This is one of the important improvements in the Waste Form Process Model this year. By tracking the decay and ingrowth of each waste form in each waste package, accurate calculations for instantaneous radionuclide releases and evolving radionuclide concentrations remaining within the waste form can be made. Examples of decay and ingrowth in the waste form are shown in Figure 3-5, Figure 3-8, Figure 3-11, and Figure 3-14.

To test the 3-generation analytical solution implemented in the Isotope Decay Model, a calculation was performed on a waste form whose evolving radionuclide inventory over time was calculated using the numerical code ORIGEN-S (Anttila 2005, pp. 152-158). The waste in this calculation is BWR Atrium. It has a 4.2% enrichment, 50 MWd/kgU burnup, and includes the following 7-generation decay chain from the neptunium series:

$$^{245}\text{Cm} \rightarrow {}^{241}\text{Pu} \rightarrow {}^{241}\text{Am} \rightarrow {}^{237}\text{Np} \rightarrow {}^{233}\text{Pa} \rightarrow {}^{233}\text{U} \rightarrow {}^{229}\text{Th}$$

For the 3-generation analytical solution to be valid for ^{233}U and ^{229}Th in this chain, i.e., insignificant ingrowth of grandparent(s), the short-lived isotope ^{233}Pa (half-life of 27 days) had to be removed from the calculation. Removing ^{233}Pa does not hinder the calculation because ^{233}Pa is short-lived and does not affect the calculation of its daughter. If the concentration of ^{233}Pa were needed in the simulation, it could be calculated separately assuming secular equilibrium with ^{237}Np.

The results of the two calculations are plotted in Figure 3-17. The plot shows that the 3-generation solution is highly accurate in the 6-generation simulation. However, concentrations of ^{233}U and ^{229}Th are notably low for the first 100 years. ^{241}Pu and ^{241}Am are the grandparents of ^{233}U and ^{229}Th, respectively. ^{241}Pu has ingrowth from ^{245}Cm, and ^{241}Am has ingrowth from ^{241}Pu. Thus, the requirement of the 3-generation solution, i.e., insignificant ingrowth of grandparent(s), may not be adequately met during the first 100 years in this simulation for ^{233}U and ^{229}Th.

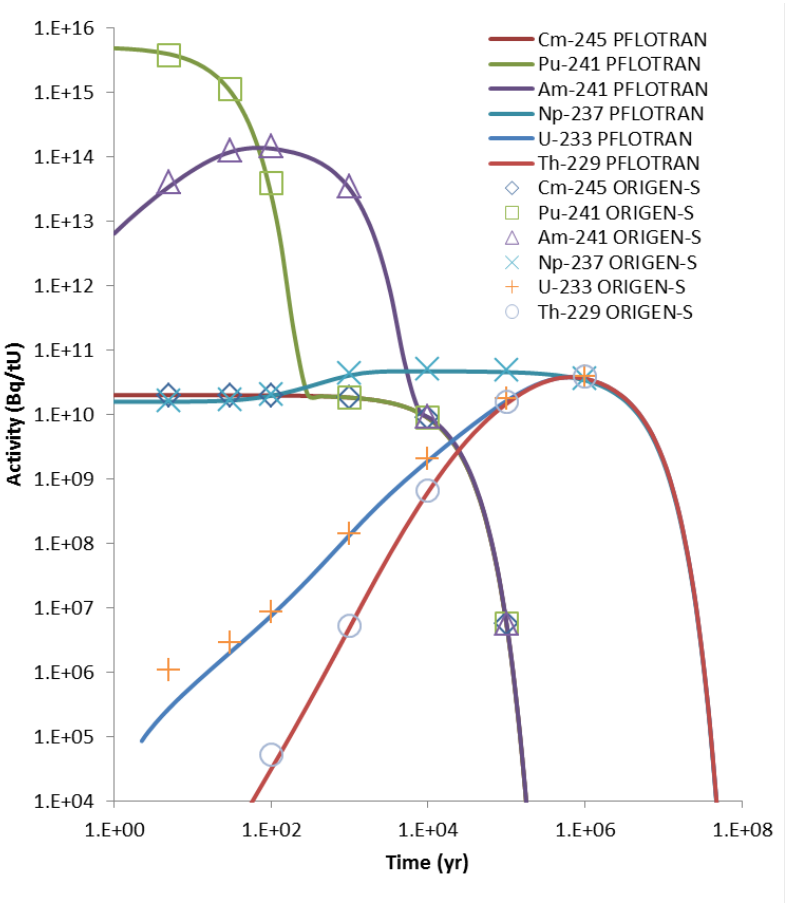

Figure 3-17. Comparison of 3-generation decay and ingrowth analytical solution implemented in the Isotope Decay Model with the results of ORIGEN-S for BWR Atrium waste, 4.2% enrichment, 50 MWd/kgU burnup.

3.2.4 Isotope Partitioning Model

The Isotope Partitioning Model implemented in PFLOTRAN this year provides a new aqueous solubility process model and a new equilibrium isotope partitioning process model. This new model provides an alternative to the PFLOTRAN chemistry process model for simulating equilibrium precipitation, dissolution, and adsorption. While the PFLOTRAN chemistry process model is well-established for

simulating chemical reactive transport (Lichtner et al. 2015), important limitations are that it requires (1) significant effort to ensure that all desired reactions are included and correct and (2) precious computer time when performing hundreds of probabilistic realizations on million-cell meshes. In addition, because the PFLOTRAN chemistry process model and its database were developed for elemental reactions, they are not easily adapted for isotopes.

The Isotope Partitioning Model distributes isotopes and elements among aqueous, adsorbed, and precipitate phases based on element-specific adsorption coefficients (e.g., K_d values) and element-specific solubility limits. For solubility, instead of identifying and simulating specific minerals and chemical reactions, the user defines redox-specific elemental solubility limits or their probability distributions. Solubility is modeled as a function of the element (or redox state of an element) because (1) isotopes of the same element will behave similarly and (2) differences in solubility between isotopes of the same element are generally much smaller than the uncertainty in environmental conditions. In addition, the Isotope Partitioning Model distributes isotopes of the same element across the phases such that the isotope mole fractions for a given element are the same in each phase. Distributing isotopes in this way maximizes entropy and ensures that important isotopes are not disproportionally trapped within a precipitate phase.

A flow diagram of the Isotope Partitioning Model is shown in Figure 3-18. After the transport step in each model grid cell, the total concentrations of each isotope are calculated and sent to the Isotope Decay Model for decay and ingrowth. The resulting isotope concentrations are then summed by element and partitioned among aqueous, adsorbed, and precipitated phases in accordance with adsorption coefficients, solubility limits, and amounts of mineral sorbents and water in the cell. In the final step, the elemental concentrations in each phase are divided into isotopic concentrations in the same proportions as the overall isotopic mole fractions in the cell. All calculations within the Isotope Partitioning Model are exact and require no iteration.

To simulate solubility limits accurately, the model requires that all isotopes that could potentially have a significant contribution to the aqueous elemental concentration be included in the simulation. Thus, if an element's aqueous concentration may be limited by solubility and its concentration may be significantly affected by concentrations of stable and/or unstable isotopes in the natural groundwater and/or by isotopes introduced from the degradation of waste forms and/or EBS materials (e.g., ^{238}U), then these additional isotopes need to be included in the model. Excluding potentially significant isotopes from the simulation will effectively inflate the elemental solubility and result in increased mobility for the included isotopes in the simulations. In addition, excluding an isotope from the model based on low isotopic mole fractions in the source term may not be justified because in a transport model the isotope in question could be a descendant of a highly mobile ancestor that allowed it to separate from the other isotopes of its element.

An additional limitation of the Isotope Partitioning Model is that it is highly conditional. It requires the user to predetermine redox-specific elemental solubility limits and equilibrium adsorption coefficients. Nonetheless, this model is expected to be highly useful in performance assessment and GDSA applications in which conditions are expected to be sufficiently stable. When reactions are likely to occur that cause significant chemical changes (e.g., to pH), a full reactive transport calculation using a chemical speciation model should be performed. In the future, additional functionality may be built into the solubility limits and adsorption coefficients of the Isotope Partitioning Model so that they may be a function of other evolving parameters such as temperature and pH.

Effects of the solubility process model of the Isotope Partitioning Model can be seen in some of the figures in Section 3.2.2.3. In Figure 3-7, Figure 3-10, Figure 3-13, and Figure 3-16, total aqueous concentrations of uranium, neptunium, and plutonium do not exceed solubility limits, which are set at ~10^{-13} M, ~10^{-7} M, and ~10^{-10} M, respectively. Figure 3-10 shows how important ^{238}U is to the solubility-limited concentrations of shorter-lived uranium isotopes. When an element reaches its solubility limit, the

excess is precipitated and tracked and the persistence of the precipitate ensures that the aqueous concentration remains at the solubility limit. The accumulated precipitate, which also decays, is effectively allowed to quantitatively dissolve back into solution as the aqueous element migrates away or decays, but only enough to maintain the aqueous concentration at the solubility limit. When the precipitate completely dissolves, the aqueous concentration falls below the solubility limit, as happens in Figure 3-16 for plutonium at ~5 Ma and for neptunium at ~30 Ma.

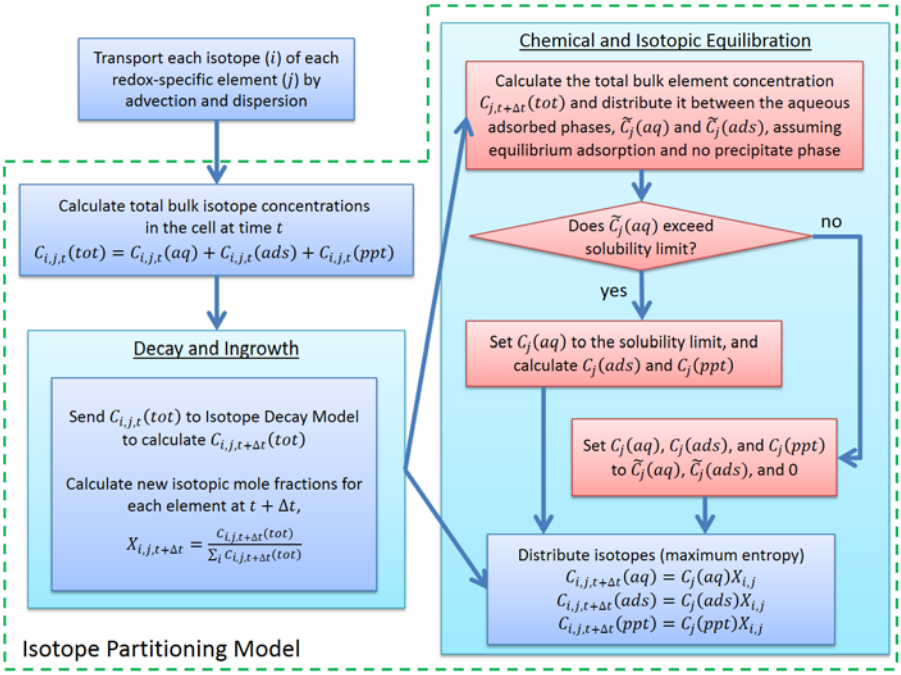

Figure 3-18. Flow diagram for the Isotope Partitioning Model.

4. CRYSTALLINE REPOSITORY REFERENCE CASE

The crystalline reference case for deep geologic disposal of commercial UNF builds upon previous work by Wang et al. (2014), Freeze et al. (2013c), and Mariner et al. (2011). The conceptual model includes a mined repository approximately half a kilometer below the surface in sparsely fractured crystalline host rock such as granite or metagranite in a stable cratonic terrain. Characteristics of the crystalline host rock that contribute to or impact post-closure safety include (Mariner et al. 2011; Freeze et al. 2013c):

- The high structural strength of the host rock, which stabilizes engineered barriers;
- The depth of burial, which isolates the repository from surface processes (such as erosion and glaciation);
- The low permeability of the host rock, which isolates the repository from surface waters;
- The reducing chemical environment, which limits waste package corrosion rates (contributing to waste containment), and limits radionuclide solubility and enhances radionuclide sorption (limiting and delaying radionuclide releases).
- The potential presence of a fracture network that creates a hydraulic connection between the repository and the biosphere, which if present could adversely impact the isolation of the repository and radionuclide releases.

This last characteristic is the primary feature that distinguishes the crystalline reference case from the salt and clay reference cases, in which the host rock is assumed to be a homogeneous medium of uniformly low permeability. Though the permeability of the crystalline matrix can be assumed to be uniformly low, the possibility of long-distance transport through fractures cannot be ignored.

The remainder of this section includes a description of the engineered (Section 4.1) and natural (Section 4.2) barriers (including characterization of the fractured host rock) followed by a quantitative post-closure performance assessment (PA) including simulation of fracture flow and transport (Sections 4.3 and 4.4).

4.1 Engineered Barriers

Specific post-closure basis information related to the engineered barriers includes:

- Characteristics of the repository (Section 4.1.1),
- Inventory characterization (Section 4.1.2),
- Waste form characterization (Section 4.1.3),
- Waste package characterization (Section 4.1.4), and
- Characteristics of the buffer, drifts, and access halls (Section 4.1.5).

4.1.1 Engineered Barrier Characteristics

The crystalline reference case calls for a mined repository located at 600 m below land surface in a fractured crystalline rock. It is assumed that a commercial repository would hold 70,000 MTHM of commercial UNF, which is the maximum allowed by the Nuclear Waste Policy Act of 1983 and about half of the total commercial UNF inventory predicted by 2055 in the “no replacement scenario” (Carter et al. 2013). This inventory could be accommodated in 168 disposal drifts, each 805 m in length, arranged in facing pairs on either side of a central access hallway (Wang et al. 2015). This layout (Table 4-1) is essentially the same as that assumed for the clay and salt reference cases (Mariner et al. 2015), with drift centers separated by 20 m, and waste packages emplaced lengthwise within the drifts with a spacing of 10 m center-to-center (5-m spacing, end-to-end). Repository access would be via vertical shafts and/or a

ramp. One quarter of the 70,000 MTHM inventory is included in simulations; dimensions used in the simulations ((Table 4-1) reflect the smaller inventory as well as adjustments needed to facilitate gridding.

Table 4-1. Dimensions for the crystalline reference case repository (modified from Wang et al. 2014).

Parameters	Reference Case Value	Simulated Value
Waste Package (WP)		
WP length (m)	5.00	5.00
WP outer diameter (m)	1.29	1.67 (on a side)
WP center-to-center spacing in-drift (m)	10.0	10.0
Inventory per 12-PWR WP (MTHM)	5.225	5.225
Number of WPs	13,398	3360
Emplacement Drift		
Drift diameter (m)	4.5	5.0 (on a side)
Drift center-to-center spacing (m)	20	20
Number of WPs per drift	80	80
Drift seal length (m)	10	5
Drift length, including seals (m)	805	805
Shaft access diameter (m)	5.4	NA
Access hall/ramp height (m)	5	5
Access hall/ramp width (m)	8	8.35
Number of drifts	168	42
Number of access halls	1	2
Repository		
Number of drift pairs (rounded up)	84	NA
Repository length (m)	1,618	822
Repository width (m)	1,665	825
Repository Depth (m)	600	585

4.1.2 Inventory

For simplicity, PA simulations assume that the inventory consists entirely of pressurized water reactor (PWR) UNF assemblies, each containing 0.435 MTHM. Radionuclide inventories (Table 4-2) and decay heat versus time curves (Figure 4-1) are taken from Carter et al. (2013) and assume an initial enrichment of 4.73 wt% ^{235}U, 60 GWd/MTHM burn-up, and 100-year out of the reactor (OoR) storage prior to deep geologic disposal. This inventory is identical to that assumed for the clay reference case (Mariner et al. 2015) and except for OoR time the same as that assumed for the salt reference case (Freeze et al. 2013b; Sevougian et al. 2014; Mariner et al. 2015). Because the average burn-up of UNF under the “no replacement scenario” is predicted to be only 54 GWd/MTHM (Carter et al. 2013), the assumption of 60 GWd/MTHM results in a conservatively high heat load.

Table 4-2. PWR UNF inventory of selected radionuclides for the crystalline reference case.

Isotope	Inventory (g/MTIHM)[1]	Inventory (g/g waste)[2]	Atomic weight (g/mol)[3]	Approximate Decay Constant (1/s)
^{241}Am	1.46E+03	1.01E-03	241.06	5.08E-11
^{243}Am	2.69E+02	1.87E-04	243.06	2.98E-12
^{238}Pu	2.84E+02	1.97E-04	238.05	2.56E-10
^{239}Pu	7.40E+03	5.14E-03	239.05	9.01E-13
^{240}Pu	4.11E+03	2.85E-03	240.05	3.34E-12
^{242}Pu	8.17E+02	5.67E-04	242.06	5.80E-14
^{237}Np	1.40E+03	9.72E-04	237.05	1.03E-14
^{233}U	4.33E-02	3.01E-08	233.04	1.38E-13
^{234}U	5.11E+02	3.55E-04	234.04	8.90E-14
^{236}U	6.27E+03	4.35E-03	236.05	9.20E-16
^{238}U	9.10E+05	6.32E-01	238.05	4.87E-18
^{229}Th	1.48E-05	1.03E-11	229.03	2.78E-12
^{230}Th	1.04E-01	7.22E-08	230.03	2.75E-13
^{36}Cl	5.01E-01	3.48E-07	35.97	7.30E-14
^{99}Tc	1.28E+03	8.89E-04	98.91	1.04E-13
^{129}I	3.13E+02	2.17E-04	128.9	1.29E-15
^{135}Cs	7.72E+02	5.36E-04	134.91	9.55E-15
All isotopes[4]	1.44E+06	1.00E+00	--	--

[1] from Carter et al. (2013, Table C-2)
[2](g isotope/g waste) = (g isotope/MTIHM)/(g waste/MTIHM), where g waste = g all isotopes
[3]Weast and Astle (1981)
[4]all isotopes are not listed here

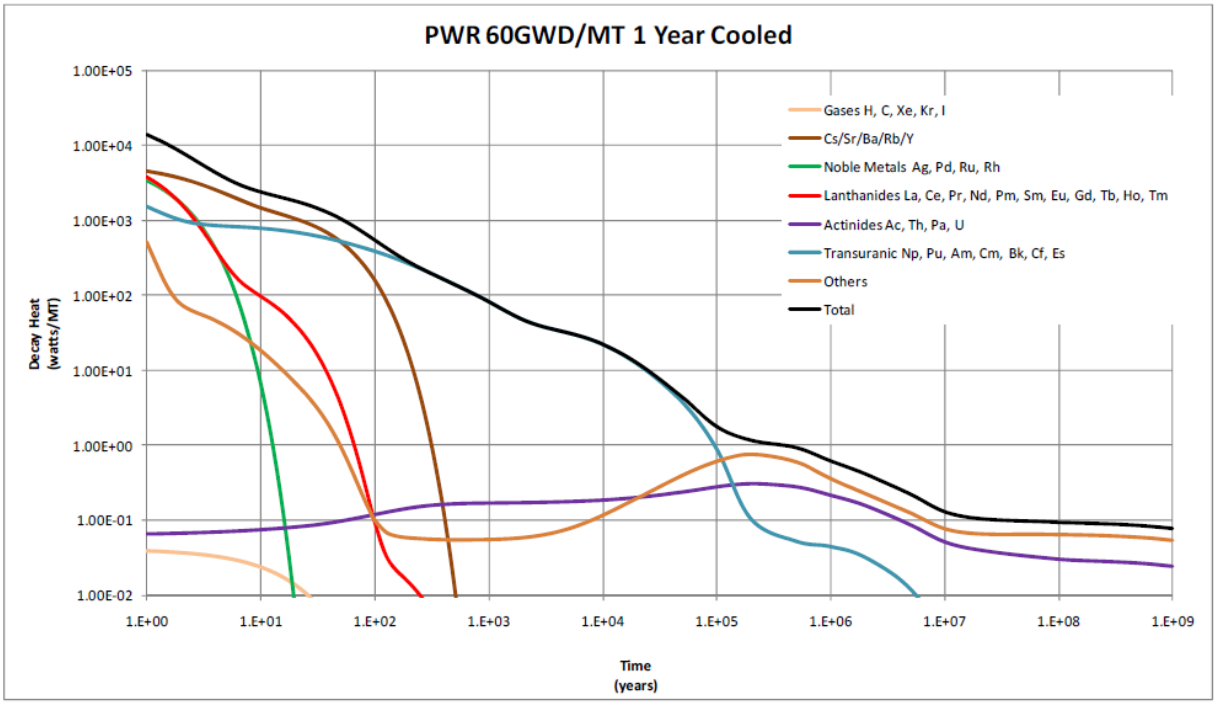

Figure 4-1. Heat of decay versus time for PWR UNF (60 GWd/MT burnup) from Carter et al. (2013). Crystalline reference case simulations assume 100-yr OoR storage and thus begin with the total wattage at 100 years.

4.1.3 Waste Form

Freeze et al. (2013c, Section 3.4.1.1) provided a description of commercial SNF, including the following characteristics. Spent uranium oxide (UO_2) fuel is a polycrystalline ceramic material with stable to high temperatures and the potential for slow degradation in the disposal environment. Cladding protects the fuel from degradation in the reactor, and can continue to protect the fuel from degradation in the repository. Cladding from commercial light-water reactors (i.e. boiling water reactors and pressurized water reactors) is generally made from Zircaloy, a zirconium alloy that is chemically stable and resistant to corrosion. In the reactor, fuel undergoes physical changes due to heating, radiation damage, and the build-up of fission products. Lighter elements (fission products) become concentrated in voids and the outer margins of the UO_2 matrix.

Concentration of fission products in voids of the waste form results in the waste form releasing radionuclides in two fractions: instant-release (upon waste package breach) and slow-release (according to the UO_2 matrix dissolution rate). See Section 3.2.2.3 for a description of the UO_2 waste form degradation model implemented in PFLOTRAN and Section 4.3.2.5 for parameter values used in PA.

4.1.4 Waste Package

The waste package is assumed to consist of a stainless steel canister containing 12 PWR UNF assemblies (5.22 MTHM) and a stainless steel overpack. The waste package is 5 meters in length and has a diameter of 1.29 m, consistent with the 12-PWR waste package described by Hardin et al. (2012). Due to gridding limitations, the size of simulated waste packages is 1.67 x 1.67 x 5 m^3, and is larger in volume than 12-PWR waste packages are expected to be.

Waste package porosity is set equal to the fraction of void space within a waste package, which is 50% (Freeze et al. 2013b). Permeability is set several orders of magnitude higher than that of the surrounding materials, so that flow through waste packages is uninhibited. The waste package is given the thermal properties of stainless steel (Shelton 1934). Probabilistic simulations sample on waste package tortuosity (which scales the effective diffusion coefficient; see Section 4.3.2.7) using a uniform uncertain distribution from 0.01 to 1.

The granite reference case is the first generic disposal system PA to take credit for waste package performance via calculation of canister vitality. See Section 3.2.1 for a description of the implementation in PFLOTRAN and Section 4.3.2.5 for parameter values used in PA.

4.1.5 Bentonite Buffer (Drifts and Access Halls)

The crystalline reference case assumes horizontal, in-drift emplacement with waste packages elevated on plinths of compacted bentonite and drifts buffered and filled with compacted bentonite pellets and/or bricks in one or two layers as shown in Figure 4-2 (Wang et al. 2014). Access halls may be filled with a mixture of crushed rock and bentonite or another geologic material rich in clay minerals (Mariner et al. 2011; Wang et al. 2014), but the present simulations assume the halls and drifts are both filled with a compacted bentonite buffer.

Compacted bentonite has low permeability, high sorption capacity (see Section 4.2.2.8), and may be engineered to achieve desirable thermal properties; for instance, quartz sand or graphite can be added to increase thermal conductivity (Choi and Choi 2008; Jobmann and Buntebarth 2009; Wang et al. 2015). The current set of simulations employs a single layer buffer with material properties appropriate for a compacted mixture of 70% bentonite and 30% quartz sand. The buffer is assigned a porosity of 0.35 (Liu et al. 2016), a permeability of 10^{-20} m^2 (Liu et al. 2016), and a water-saturated thermal conductivity of 1.5 W/m/K (Wang et al. 2014). Probabilistic simulations sample on porosity using a uniform uncertain distribution over the range 0.3 to 0.4.

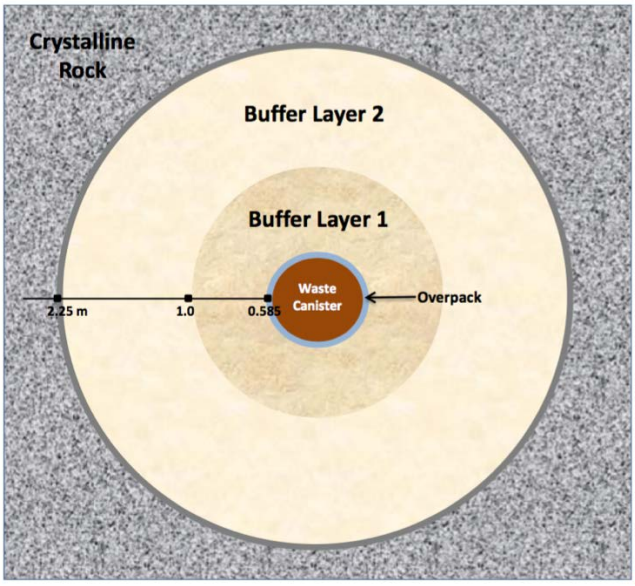

Figure 4-2. Schematic cross-section of a double-layer buffer in a disposal drift of a crystalline repository (Wang et al. 2014).

4.2 Geosphere/Natural Barriers

Specific post-closure basis information related to the geosphere and natural barriers include:

- Characteristics of the natural barriers (e.g., location, geologic setting) (Section 4.2.1),
- Host rock characterization (Section 4.2.2),
- Disturbed rock zone (DRZ) characterization (Section 4.2.3), and
- Overburden characterization (Section 4.2.4).

4.2.1 Natural Barrier Characteristics

The present concept for a mined repository in crystalline rock places the repository approximately half a kilometer below the land surface in a sparsely fractured crystalline rock (such as granite) that either outcrops or subcrops near surface. Regionally, the topographic slope is < 1°, and the water table is unconfined, a combination which would provide little driving force for deep fluid flow. The reference repository site has a stable cratonic terrain with low probabilities of seismicity, igneous activity, and human intrusion. The latter probability is reduced by avoiding regions with known geologic resources such as extensive fresh water aquifers, ore deposits, fossil fuels, or high geothermal heat flux (which offers the potential for geothermal development). This concept is consistent with international concepts of disposal in crystalline rock (e.g., SKB 2007).

Locations fitting this concept occur in the eastern half of the United States as shown in Figure 4-3 (Perry et al. 2014), where outcropping/subcropping crystalline basement is Precambrian to Archean in age (e.g., Barton et al. 2003) and measured heat flow is generally between 35 and 65 mW/m^2 (Blackwell et al. 2011). At repository depth, the host rock is saturated, likely with brackish water (see Section 4.2.2.6). The driving force for regional flow at depth is assumed to be similar to that in deep sedimentary basins, on the order of 0.001 m/m (e.g., Downey and Dinwiddie 1988).

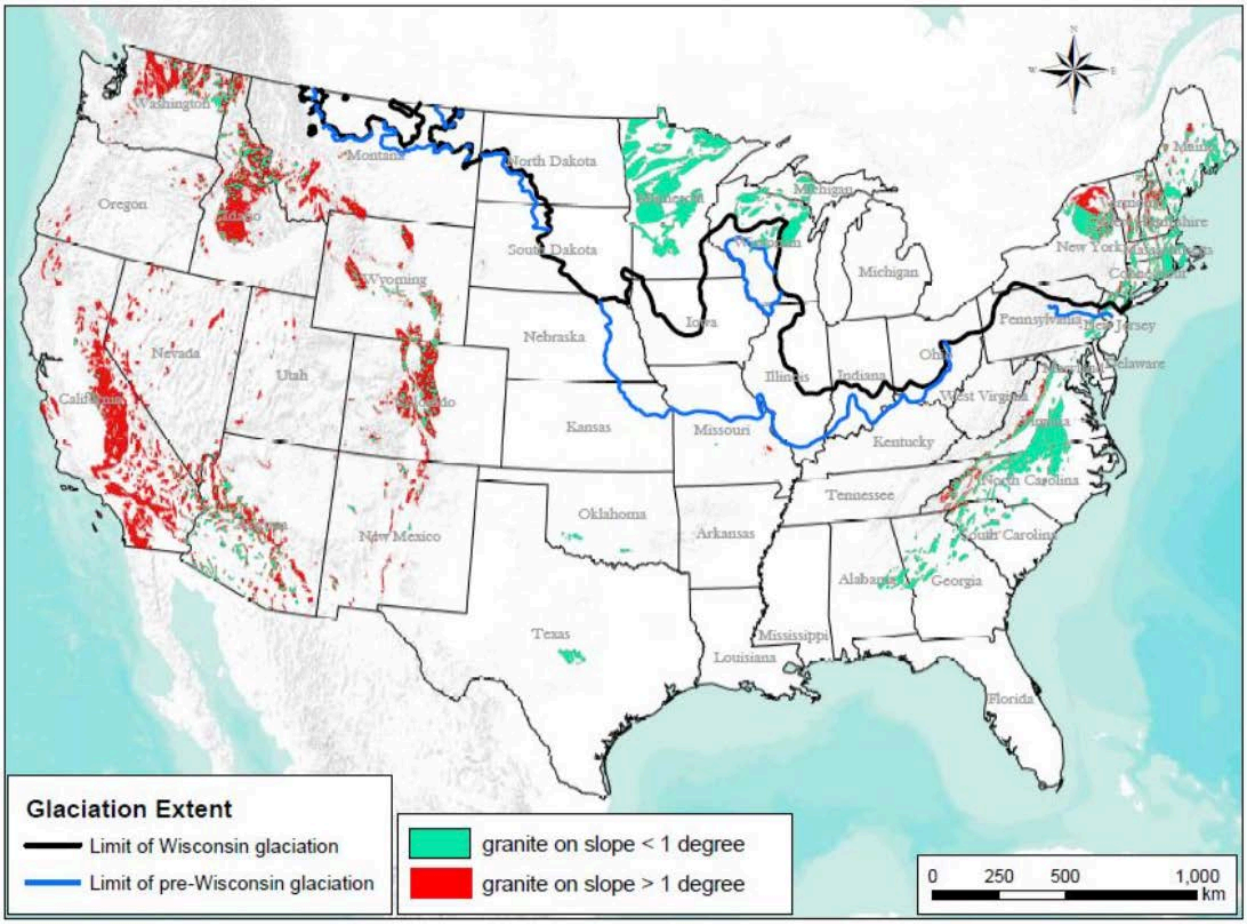

Figure 4-3. Locations of crystalline rock outcrop and near-surface subcrop in the U.S. Crystalline rock on a slope of <1° (green) occurs primarily in the eastern half of the U.S. Figure from Wang et al. (2014, Figure 2-13).

4.2.2 Crystalline Host Rock

The representation of fractured crystalline rock is based primarily on the well-characterized, sparsely fractured metagranite at Forsmark, Sweden (Follin et al. 2014; Joyce et al. 2014). The Forsmark site sits in the Fennoscandian Shield and consists of crystalline bedrock (primarily granite with lesser amounts of granodiorite, tonalite, and amphibolite) that formed between 1.89 and 1.85 Ga (1 Ga = 1 billion years), experienced ductile deformation and metamorphism, and cooled to the limit of brittle deformation between 1.8 and 1.7 Ga (SKB 2007). Subsequent brittle deformation occurred associated with later tectonic events (1.7 to 1.6 Ga and 1.1 to 0.9 Ga), and recent glaciation (< 1 Ma) has resulted in crystalline basement outcrops and thin (<25 m) Quaternary sedimentary deposits of variable thickness and extent (SKB 2008). Crystalline basement with similar history exists within the United States (for instance at the southern margin of the approximately 2-Ga-old Superior Craton in Minnesota and Wisconsin (e.g., Stone et al. 1989), and can be reasonably expected to have similar hydraulic properties.

Conceptually, the crystalline host rock is comprised of two entities: fractures and matrix. Numerically it is simulated with two types of grid cells: those containing a fracture or fractures and those without fractures (the matrix). Hydraulic parameters (permeability and porosity) describing fractured cells are derived from fracture parameters developed for the Forsmark metagranite (Follin et al. 2014; Joyce et al. 2014; Wang et al. 2014). Parameters describing matrix cells are derived from measurements made in tunnel walls of

underground research laboratories (URLs) in crystalline rock at the Grimsel Test Site, Switzerland (Schild et al. 2001; Soler et al. 2015), Lac du Bonnet batholith, Canada (Martino and Chandler 2004), and the Korean Underground Research Tunnel (Cho et al. 2013). All other parameters are identical in fracture and matrix cells.

4.2.2.1 Fracture Permeability and Porosity

Permeability due to fractures depends upon the distribution, orientation, and transmissivity of open, conductive fractures. Fracture porosity additionally depends on fracture aperture. Statistical descriptions of these fracture features are used to generate multiple realizations of fracture networks, which are mapped to an equivalent continuous porous medium domain (as explained in Section 3.1.3.1) in order to calculate the permeability and porosity of each grid cell intersected by a fracture or fractures. PA simulations use fracture parameters derived from parameters applicable to the sparsely fractured granite at Forsmark, Sweden.

At Forsmark, large-scale mappable features of concentrated brittle and/or ductile deformation (termed "deformation zones") bound volumes of relatively undeformed rock (Follin et al. 2014; Joyce et al. 2014). Each volume of relatively undeformed rock (termed a "fracture domain") is sparsely fractured, and the fractures within each can be described in terms of a number of "fracture sets," distinguished from each other on the basis of fracture orientation. At Forsmark six fracture domains are defined, each containing five fracture sets. As appropriate, three depth zones are defined (<200 m below sea level (mbsl), 200-400 mbsl, and >400 mbsl) in order to account for the decrease in fracture density and fracture transmissivity with depth. Each fracture set within a particular fracture domain and depth zone is described using a 3-dimensional Fisher distribution to describe the orientation of fracture poles in space, a truncated power-law distribution for fracture radii, and a fracture density, P_{32}, which is defined as the surface area of fractures per volume of rock (m^2/m^3). For each depth zone within a fracture domain, a relationship is given between fracture radius and fracture transmissivity. A schematic of how fracture domains and depth zones might apply to a volume of crystalline rock containing a mined repository is shown in Figure 4-4.

Table 2 Hydrogeological DFN parameters for each fracture domain, fracture set and depth zone

Fracture domain/elevation (m.a.s.l)[a]	Fracture set name	Orientation set pole: (trend, plunge), conc.	Size model, power-law (r_0, k_r) (m, −)	Intensity, (P_{32}), valid size interval: r_0 to 564 m (m^2/m^3)	Parameter values for the transmissivity models		
					Semi-correlated (a,b,σ)	Correlated (a,b)	Uncorrelated (μ,σ)
FFM01 and FFM06>−200	NS	(292, 1) 17.8	(0.038, 2.50)	0.073	$6.3 \cdot 10^{-9}$, 1.3, 1.0	$6.7 \cdot 10^{-9}$, 1.4	−6.7, 1.2
	NE	(326, 2) 14.3	(0.038, 2.70)	0.319			
	NW	(60, 6) 12.9	(0.038, 3.10)	0.107			
	EW	(15, 2) 14.0	(0.038, 3.10)	0.088			
	HZ	(5, 86) 15.2	(0.038, 2.38)	0.543			
FFM01 and FFM06 −200 to −400	NS	(292, 1) 17.8	(0.038, 2.50)	0.142	$1.3 \cdot 10^{-9}$, 0.5, 1.0	$1.6 \cdot 10^{-9}$, 0.8	−7.5, 0.8
	NE	(326, 2) 14.3	(0.038, 2.70)	0.345			
	NW	(60, 6) 12.9	(0.038, 3.10)	0.133			
	EW	(15, 2) 14.0	(0.038, 3.10)	0.081			
	HZ	(5, 86) 15.2	(0.038, 2.38)	0.316			
FFM01 and FFM06<−400	NS	(292, 1) 17.8	(0.038, 2.50)	0.094	$5.3 \cdot 10^{-11}$, 0.5, 1.0	$1.8 \cdot 10^{-10}$, 1.0	−8.8, 1.0
	NE	(326, 2) 14.3	(0.038, 2.70)	0.163			
	NW	(60, 6) 12.9	(0.038, 3.10)	0.098			
	EW	(15, 2) 14.0	(0.038, 3.10)	0.039			
	HZ	(5, 86) 15.2	(0.038, 2.38)	0.141			
FFM02>−200	NS	(83, 10) 16.9	(0.038, 2.75)	0.342	$9.0 \cdot 10^{-9}$, 0.7, 1.0	$5.0 \cdot 10^{-9}$, 1.2	−7.1, 1.1
	NE	(143, 9) 11.7	(0.038, 2.62)	0.752			
	NW	(51, 15) 12.1	(0.038, 3.20)	0.335			
	EW	(12, 0) 13.3	(0.038, 3.40)	0.156			
	HZ	(71, 87) 20.4	(0.038, 2.58)	1.582			
FFM03, FFM04 and FFM05>−400	NS	(292, 1) 17.8	(0.038, 2.60)	0.091	$1.3 \cdot 10^{-8}$, 0.4, 0.8	$1.4 \cdot 10^{-8}$, 0.6	−7.2, 0.8
	NE	(326, 2) 14.3	(0.038, 2.50)	0.253			
	NW	(60, 6) 12.9	(0.038, 2.55)	0.258			
	EW	(15, 2) 14.0	(0.038, 2.40)	0.097			
	HZ	(5, 86) 15.2	(0.038, 2.55)	0.397			
FFM03, FFM04 and FFM05<−400	NS	(292, 1) 17.8	(0.038, 2.60)	0.102	$1.8 \cdot 10^{-8}$, 0.3, 0.5	$7.1 \cdot 10^{-9}$, 0.6	−7.2, 0.8
	NE	(326, 2) 14.3	(0.038, 2.50)	0.247			
	NW	(60, 6) 12.9	(0.038, 2.55)	0.103			
	EW	(15, 2) 14.0	(0.038, 2.40)	0.068			
	HZ	(5, 86) 15.2	(0.038, 2.55)	0.250			

[a] Meters above sea level

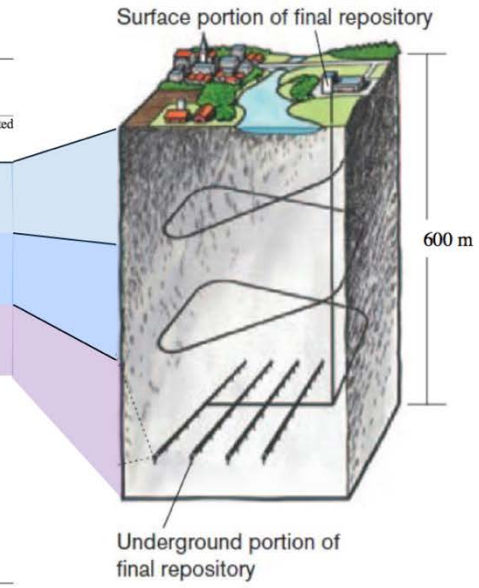

Figure 4-4. Schematic representation of how fracture domains and depth zones could be applied to a model domain containing a mined repository in crystalline rock. Highlighted fracture parameters apply to three depths below sea level (approximately coincident with the land surface at Forsmark). Fracture density decreases with depth and fracture transmissivity calculated from the given relationships decreases with depth. Table from Joyce et al. (2014). Image from Wang et al. (2014).

Parameters used to generate the fracture networks for use in PA simulations are listed in Table 4-3. Relative to the Forsmark fracture description, the current crystalline reference case makes several simplifying assumptions. These include:

- In the absence of a specific site with mapped features, the reference case domain contains a single deterministic deformation zone in order to acknowledge the need to map and model such features when a site is available.
- A single fracture domain (FFM01, 200-400 mbsl) is applied to the entire model domain.
- Only three fracture sets from the chosen domain are simulated, those with the largest number of open and flowing fractures (NS, NE, and HZ; Follin et al. 2014).
- For generality (joint sets tend to develop at right angles to each other; Twiss and Moores 1992), the NE trending set is rotated to an EW orientation.
- Although the Forsmark parameters are valid over the range of fracture radii from 0.038 m to 564 m (Follin et al. 2014; Joyce et al. 2014), the crystalline reference case uses a maximum fracture radius of 500 m and a minimum radius of 15 m.
- The fracture density is increased to ensure a percolating network.
- The crystalline reference case uses a direct correlation between fracture radius and fracture transmissivity.

Choices regarding fracture radii, density, and transmissivity are further discussed below.

Table 4-3. Parameters used to generate discrete fracture networks (modified from Wang et al. 2014).

Set	Orientation: Fisher Distribution for Poles			Size: Truncated Power Law for Radii			Fracture density (Requested)
	Mean Trend	Mean Plunge	κ	α	Max Radius r_x (m)	Min Radius r_0 (m)	Number of fractures in 1 km^3
NS	90°	0.0°	22	2.5	500	15	2100
EW	180°	0.0°	22	2.7	500	15	2000
HZ	360°	90.0°	10	2.4	500	15	2300

Fracture radii: Eliminating fractures with a radius smaller than 15 m is an acceptable simplification given the nature of the simulated fracture network, i.e., a sparse network with a large variation in fracture radius and direct correlation of fracture transmissivity to fracture radius. Hyman et al. (2015b) demonstrated that in this type of network, eliminating fractures with radii up to 25 m has essentially no effect on particle transport, because the largest fractures create a fracture backbone, through which the bulk of fluid flow occurs.

Fracture density: The fracture density necessary to ensure a percolating network (one that connects faces of a domain) is proportional to the length scale of the domain (Stauffer and Aharony 1994; Bour and Davy 1997). Forsmark fracture parameters (including density, P_{32}) were fit to borehole counts of open and flowing fractures assuming a percolation length scale of 200 m, the estimated distance between any given borehole and a deformation zone (Follin et al. 2014). Given P_{32} values, the number of fractures per unit volume ($n(r)$) associated with the radius interval 15 m to 500 m can be calculated according to (Hedin 2008):

$$n(r)dr = P_{32}\frac{(\alpha-2)r_0^{\alpha-2}}{\pi r^{\alpha+1}}dr \tag{4-1}$$

where α is the power law parameter, r_0 is the minimum fracture radius in the original distribution (0.038 m), and r is the base of the desired radius interval. Substituting in 15 m for r, the appropriate values for α (Table 4-3), and the P_{32} values of 0.142, 0.345, and 0.316 (Follin et al. 2014), we find that the number of fractures per cubic kilometer for the NS, EW, and HZ fracture sets is 337, 346, and 1091, respectively. The crystalline reference case uses larger fracture intensities in order to ensure a percolating fracture network within the multi-kilometer PA model domain.

Fracture transmissivity: The Forsmark parameter set includes three relationships between fracture radii and fracture transmissivity: direct correlation, partial correlation, and no correlation. The crystalline reference case implements direct correlation between fracture transmissivity and fracture radius according to (Follin et al. 2014):

$$\log(T_f) = \log(ar^b) \tag{4-2}$$

where T_f is fracture transmissivity (m^2/s), r is fracture radius (m) and a and b are constants with values of 1.6×10^{-9} and 0.8, respectively, for fracture domain FFM01 at a depth of 200-400 mbsl.

The simplifications discussed above bias the fracture networks generated for the crystalline reference case toward greater connectivity than what is likely to exist in a potential host rock. However, creating a simple, percolating network enabled us to develop the tools required to simulate a fractured medium.

4.2.2.2 Matrix Permeability

The matrix permeability of crystalline rock is low. In situ tests in the Lac du Bonnet URL and the Korean Underground Research Tunnel give matrix permeability values between 10^{-22} m^2 and 10^{-20} m^2 for granitic rock (Martino and Chandler 2004; Cho et al. 2013); laboratory tests on samples of the Grimsel granodiorite give values on the order of 10^{-20} m^2 to 10^{-19} m^2 (Schild et al. 2001). Laboratory permeability tests performed on gneisses and amphibolites from the KTB borehole indicate a decrease in matrix permeability with increasing effective stress, but in situ borehole tests demonstrate no dependence of matrix permeability on depth; instead mean values throughout the 9 km borehole are 7×10^{-20} m^2 with a log standard deviation of 1.2 (Huenges et al. 1997).

PA simulations use a matrix permeability of 10^{-20} m^2.

4.2.2.3 Matrix Porosity

Matrix porosity in deep crystalline rock is generally very small. Laboratory measurements of porosity in core samples of crystalline rock often give values of approximately 1% (Schild et al. 2001), but these values may be exaggerated due to formation and growth of microcracks during unloading and sample preparation. Using samples of the Grimsel (meta)granodiorite, Schild et al. (2001) found that when rock samples were impregnated with resin prior to being sampled from depth, the measured porosity was between 0.55% and 0.59%, while non-impregnated samples measured between 1% and 1.17% porosity. Had microcracks not been enhanced during sampling, the impregnated samples would have had 0% porosity. Schild et al. (2001) took the difference between values measured on impregnated and non-impregnated samples to be the in-situ porosity, approximately 0.4%; even this value may be high as they were unable to avoid sampling within the DRZ.

PA simulations use a matrix porosity of 0.5%.

4.2.2.4 Effective Diffusion Coefficient

Effective diffusion coefficients in crystalline rocks calculated from small scale experiments represent the ability of ions to diffuse through the unfractured rock matrix (e.g., Soler et al. 2015), while those calculated from large scale tracer tests in fractured rock represent strict matrix diffusion plus advective and dispersive processes that isolate fluids from the main flow path (e.g., Zhou et al. 2007). Soler et al. (2015) modeled in-situ diffusion of ^{3}H, $^{22}Na^{+}$, and $^{134}Cs^{+}$ and $^{137}Cs^{+}$ in granite at a maximum length scale of 20 cm; best-fit matrix diffusion coefficients ranged from 2×10^{-13} to 4×10^{-12} m^2/s. Zhou et al. (2007) reviewed matrix diffusion coefficients calculated from meter- to kilometer-scale tracer tests in fractured rock; in crystalline rocks they ranged from 3×10^{-12} to 3×10^{-8} m^2/s and were (with two exceptions) larger than matrix diffusion coefficients calculated for core-scale samples of the same rocks by a factor of 2 to 884. The largest of these values is larger than values for diffusion in free water, which though solute-specific and dependent on fluid properties, tend to be on the order of 1×10^{-9} m^2/s (Li and Gregory 1974).

PA simulations use an effective diffusion coefficient of 10^{-12} m^2/s throughout the crystalline host rock (in both fractured cells and matrix cells).

4.2.2.5 Thermal Properties and Thermal Environment

The thermal properties of rock depend strongly on temperature; thermal conductivity decreases and heat capacity increases with increasing temperature (Vosteen and Schellschmidt 2003). Vosteen and Schellschmidt (2003) measured thermal properties of a variety of igneous and metamorphic rocks at

temperatures from 0 °C to 500 °C, and compared their results to previous results in the literature. Their review indicates that for felsic rocks at temperatures up to approximately 25 °C thermal conductivity is between approximately 2.4 and 3.3 $Wm^{-1}K^{-1}$; at temperatures between 100 °C and 200 °C, thermal conductivity is between approximately 2.3 and 2.7 $Wm^{-1}K^{-1}$. Over the same range of temperature, heat capacity increase from 750 to over 900 $Jkg^{-1}K^{-1}$ (Vosteen and Schellschmidt 2003).

PA simulations assume a thermal conductivity of 2.5 $Wm^{-1}K^{-1}$ and a heat capacity of 830 $Jkg^{-1}K^{-1}$.

Temperature in the repository depends on the background geothermal heat flux and on the heat generated by radioactive decay of the waste. A geothermal heat flux of 60 mW/m^2, an annual mean surface temperature of 10 °C, and a thermal conductivity of 2.5 $Wm^{-1}K^{-1}$ result in a geothermal temperature gradient of approximately 25 °C/km and an ambient temperature at the depth of the repository (600 m) of approximately 25 °C. Peak repository temperatures are predicted to be just under 200 °C (Section 4.4.1). Though such a change in temperature will affect radionuclide diffusion rates, solubility, and sorption at this time, these processes are not modeled as a function of temperature.

4.2.2.6 Pore Fluid Chemistry

Pore fluid chemistry will influence waste package degradation rate, waste form dissolution rate, and solubility and transport (diffusion and sorption) of dissolved radionuclides. Pore fluid chemistry is site-dependent, but can be expected to be brackish, reducing, and about neutral pH, similar to pore fluids found in granite repository research sites in Finland, Sweden, and Canada (Table 4-4). Waste package degradation rate and waste form dissolution rate have been discussed above (Sections 4.1.4 and 4.1.3). Solubility, sorption, and diffusion are discussed elsewhere (Sections 4.2.2.7, 4.2.2.8, and 4.2.2.4).

Table 4-4. Groundwater compositions in granite at depths from 360 to 708 m (Mariner et al. 2011).

Parameter	Olkiluoto, Finland	Olkiluoto, Finland	Olkiluoto, Finland	Laxemar, Sweden	Forsmark, Sweden	Pinawa, Canada	East Bull Lake, Canada
Borehole	OL-KR20	OL-KR10	OL-KR12	KLX03	KFM02A	WN-4	EBL-2
Depth (m)	360	487	708	380	512	513	538
TDS (g L^{-1})	10.5	22.1	49.5	2.8	9.3	7.5	2.3
Ionic strength (eq L^{-1})	0.22	0.48	1.18	0.05	0.19	0.16	0.05
pH	7.4	8.0	8.2	7.9	7.2	8.1	7.4
Na (mol L^{-1})	0.11	0.21	0.36	0.03	0.09	0.07	0.03
Ca (mol L^{-1})	0.03	0.09	0.25	0.01	0.02	0.03	0.01
K (mol L^{-1})	2.8×10^{-4}	3.6×10^{-4}	4.9×10^{-4}	1.4×10^{-4}	9.0×10^{-4}	5.3×10^{-4}	5.4×10^{-5}
Mg (mol L^{-1})	2.6×10^{-3}	1.6×10^{-3}	1.5×10^{-3}	4.4×10^{-4}	9.3×10^{-3}	1.1×10^{-3}	7.0×10^{-5}
Sr (mol L^{-1})	1.6×10^{-4}	3.7×10^{-4}	1.1×10^{-3}	nr	nr	nr	3.3×10^{-5}
Mn (mol L^{-1})	5.8×10^{-6}	7.3×10^{-6}	9.3×10^{-6}	nr	nr	nr	nr
Cl (mol L^{-1})	0.18	0.38	0.86	0.04	0.15	0.11	0.04
SO_4 (mol L^{-1})	2.1×10^{-4}	1.0×10^{-5}	5.0×10^{-5}	1.3×10^{-3}	5.2×10^{-3}	6.6×10^{-3}	1.4×10^{-4}
CO_3 (mol L^{-1})	5.5×10^{-4}	1.1×10^{-4}	4.0×10^{-5}	3.1×10^{-3}	2.2×10^{-3}	3.5×10^{-3}	5.0×10^{-4}
SiO_2 (mol L^{-1})	3.6×10^{-4}	2.8×10^{-4}	2.1×10^{-4}	nr	nr	nr	5.4×10^{-5}
Fe (mol L^{-1})	2.5×10^{-6}	2.0×10^{-6}	3.8×10^{-7}	8.0×10^{-6}	3.3×10^{-5}	nr	nr
S(-II) (mol L^{-1})	5.6×10^{-6}	$<3.1 \times 10^{-7}$	1.3×10^{-6}	3.0×10^{-7}	0.0E+00	nr	nr
Reference	Posiva (2010), Table 6-6	Posiva (2010), Table 6-6	Posiva (2010), Table 6-6	SKB (2006b), p. 382	SKB (2006b), p. 382	Gascoyne et al. (1987), Table 3	Gascoyne et al. (1987), Table 3

nr = not reported

4.2.2.7 Solubility

PA simulations use the element solubility limits calculated by Mariner et al. (2011) throughout the model domain. Mariner et al. (2011) assumed a solution of 0.3 M NaCl, 0.05 M $CaCl_2$, and 0.001 M Na_2SO_4, a fixed partial pressure of H_2 of 10^{-7} atm, a pH of 7.5, and a temperature of 25°C. Additionally, it was assumed that element solubility is limited by relatively soluble hydroxide and hydrated phases, except in the case of U, for which UO_2 was assumed to be the solubility-controlling phase because of its presence in the waste form. The resulting solubility limits are listed in Table 4-5.

Assuming that no fractionation of isotopes occurs between the liquid and solid phases, the solubility limit of a given isotope (e.g., ^{238}Pu, ^{239}Pu, ^{240}Pu, or ^{242}Pu) in the transport domain of a cell can be calculated by multiplying the element solubility limit by the isotope's element mole fraction in the transport domain (e.g., $^{238}Pu/Pu_{TOTAL}$). See Section 3.2.4 for a more detailed description of the implementation in PFLOTRAN.

Table 4-5. Element solubility calculated at T = 25°C, pH 7.5 (Mariner et al. 2011).

Element	Solubility-Limiting Phase	Dissolved Concentration [a] (mol L^{-1})	Notes
Am (Ac, Cm)	$Am(OH)_3$	6×10^{-6}	Ac and Cm are assumed analogous to Am
Np (Pa)	$Np(OH)_4$	1×10^{-9}	Pa is assumed analogous to Np
Nb	$Nb(OH)_5$	4×10^{-5}	Posiva (2010, Table 1-9)
Pd	$Pd(OH)_2$	3×10^{-6}	Posiva (2010, Table 1-9)
Pu	$Pu(OH)_4$	2×10^{-7}	
Ra	$RaSO_4$	1×10^{-6}	(SO_4^{2-}) fixed at 10^{-3} mol L^{-1}
Sb	$Sb(OH)_3$	1×10^{-7}	
Se	$FeSe_2$	4×10^{-8}	
Sn	SnO_2	3×10^{-8}	
Tc	$TcO_2{:}2H_2O$(am)	3×10^{-8}	
Th	$Th(OH)_4$	4×10^{-7}	
U	UO_2	4×10^{-10}	
Zr	$Zr(OH)_4$	2×10^{-8}	Posiva (2010, Table 1-9)

[a] Calculated using the PHREEQC code version 2.14.2 and the thermo.com.V8.R6.230 database from Lawrence Livermore National Laboratories, except where noted. The solution assumed 0.3 M NaCl, 0.05 M $CaCl_2$, 10^{-3} m Na_2SO_4, and 10^{-7} atm H_2 (g).

4.2.2.8 Sorption

Many different models for the complex surface chemistry reactions included in sorption have been developed with varying levels of sophistication. The crystalline reference case assumes the simplest model: linear sorption characterized by a distribution coefficient K_d for each element. K_d values are material specific and depend heavily on pore fluid characteristics including temperature, pH, redox conditions, ionic strength, and concentrations of other solutes.

PA simulations assume no sorption within the waste packages. Within the bentonite buffer, K_d values are chosen appropriate for the brackish pore fluid compositions listed in Table 4-4 and reducing conditions (Table 4-6). Within the natural barrier (host rock, DRZ, and sediments), K_d values are set equal to those used for modeling sorption in the far-field granite at Olkiluoto (Table 4-7). Probabilistic simulations sample on Np K_d values in both the bentonite buffer and the natural barrier. Np K_d in the bentonite buffer is sampled between 0.1 m^3/kg (the value given by Mariner et al. 2011) and 702 m^3/kg (the upper limit recommended for "highly saline porewater" by SKB 2004). Np K_d in the natural barrier system is sampled between 0.047 m^3/kg and 20 m^3/kg as recommended for granite with saline pore water by SKB (2006a). Both distributions are log uniform.

Table 4-6. Bentonite K_d values for the chemical conditions of a granite repository (Mariner et al. 2011).

Element	K_d (m^3 kg^{-1})	Source/Notes
Ac [a]	10	Baston et al. (1999), see Am
Am	10	Ikeda and Amaya (1998) (high μ,[b] pH 5-10, Eh -220 mV)
C, Cl	0	Adsorption low, assumed non-sorbing
Cm	10	Baston et al. (1999)
Cs	0.1	Mucciardi et al. (1979) (montmorillonite, high μ, high Ca, pH 7-9.3)
I	0	Mucciardi et al. (1979) (montmorillonite, high μ, high Ca, pH 7.4-8.4)
Nb	3	Ikeda and Amaya (1998); Erdal (1977); Taki and Hata (1991)
Np, Pa [a]	0.1	Kitamura et al. (2002); Ashida et al. (1999) (pH 8-9, Eh -550 to -400 mV, μ =1M)
Pb	10	Ulrich and Degueldre (1993); Ikeda and Amaya (1998) (high μ, pH 5-8.5)
Pd	3	Tachi et al. (1999b)
Pu	1	Mucciardi et al. (1979); Ames et al. (1981) (high μ, pH 7-9)
Ra	1	Tachi and Shibutani (1999) for solution/solid ratio > 100; Ames et al. (1983)
Sb	0.1	Ikeda and Amaya (1998) (low Eh, high μ, bentonite)
Se	0.03	Tachi et al. (1999a)
Sn	30	Oda et al. (1999) (depends on pH)
Sr	0.01	Mucciardi et al. (1979) (bentonite, high μ, high Ca)
Tc	10	Baston et al. (1999) (high μ, high Na, high Ca, Eh ~ -400 mV, pH 8-10)
Th	3	Baston et al. (1991); Ueta (1998) (high μ)
U	10	Baston et al. (1999) (high μ, high Na, high Ca, Eh ~ -400 mV, pH 8-10)
Zr	30	Rancon and Rochon (1979) (depends on pH)

[a] K_d values for Ac are set equal to those of chemically similar Am. K_d values for Pa are set equal to those of chemically similar Np. [b] □= ionic strength

Table 4-7. Granite matrix K_d values used in Posiva (2010) for dilute/brackish groundwater (Mariner et al. 2011).

Element	K_d (m^3 kg^{-1})
C, Cl, I	0
Se	0.0005
Pd, Sn	0.001
Sr	0.005
Nb	0.02
Am, Cm, Ac [a]	0.04
Pa, Tc, Cs	0.05
U	0.1
Np, Th, Ra, Zr	0.2
Pu	0.5

[a] K_d values for Ac are set equal to those of chemically similar Am.

4.2.3 Disturbed Rock Zone (DRZ)

The DRZ is defined as the portion of the host rock adjacent to the engineered barrier system that experiences durable (but not necessarily permanent) changes due to the presence of the repository (Freeze et al. 2013b). The DRZ is expected to have elevated permeability with respect to the permeability of the host rock matrix due to the changes in stress induced by mining.

In-situ DRZ permeability has been measured in URLs in crystalline rock in Korea (Cho et al. 2013) and Canada (Martino and Chandler 2004). In both locations permeability was variable but generally decreased from disturbed to undisturbed values over a discrete distance from the tunnel wall. In the Korean Underground Research Tunnel gas permeability was as high as 10^{-17} m^2 for distance of 2 m from the tunnel wall; beyond that distance it was approximately 10^{-20} m^2 (fluid permeabilities are approximately an order of magnitude less than gas permeabilities; Cho et al. 2013). In the Lac du Bonnet URL, fluid permeability was between 10^{-16} and 10^{-19} m^2 for a distance of 0.3 to 0.5 m from the tunnel wall, beyond which is was between 10^{-22} and 10^{-20} m^2 (Martino and Chandler 2004).

PA simulations assume a 1.670 m thick DRZ on all sides of emplacement drifts and access halls. DRZ porosity is assumed to be 0.01, twice that of the undisturbed matrix; the effective diffusion coefficient is assumed to be 10^{-11} m^2, one order of magnitude higher than in the undisturbed host rock; and DRZ permeability is assumed to be 10^{-16} m^2, the highest value measured in the Canadian Lac du Bonnet URL (Martino and Chandler 2004). In probabilistic simulations, we sample on DRZ porosity using a uniform

distribution over the range 0.005 to 0.05, which also affects the value of the effective diffusion coefficient (see Section 4.3.2.7).

4.2.4 Sedimentary Overburden

The crystalline reference case assumes a 15-m-thick overburden of glacial sediments. Material properties including porosity (0.2) and permeability (10^{-15} m^2) are appropriate for a silty glacial till (Freeze and Cherry 1979). Probabilistic simulations sample on sediment permeability using a log uniform distribution over the range 10^{-16} m^2 to 10^{-13} m^2, effectively allowing the sedimentary overburden to represent anything from a clay-rich till to a silty sand (Freeze and Cherry 1979).

4.3 Post-Closure Performance Assessment

4.3.1 Conceptual Model

The conceptual framework for this preliminary generic post-closure PA focuses on the components of the engineered barrier (Section 4.1) and the natural barrier (Section 4.2) in the undisturbed scenario. Key characteristics of and processes occurring in each of the components of the engineered and natural barriers are summarized in Table 4-8. Because the PA does not consider the biosphere, the performance metric is maximum radionuclide concentration rather than dose.

Table 4-8. Conceptual representation of the engineered and natural barriers in PA.

Region	Component	Key characteristics	Key processes included in PA
Engineered Barrier	Waste Form	Commercial SNF (UO_2)	Radionuclide decay, instant release fraction, waste form dissolution
	Waste Package	Stainless steel	Degradation and breach
	Bentonite Buffer	Low permeability, high sorption capacity	Radionuclide advection, diffusion, sorption, decay
Natural Barrier	Crystalline Basement	Sparsely fractured, low permeability	Radionuclide advection, diffusion, sorption, decay
	DRZ	Enhanced permeability	Radionuclide advection, diffusion, sorption, decay
	Sediments	Thin, unconsolidated	Radionuclide advection, diffusion, sorption, decay

Simulations assume (1) a mined repository at 585 m depth in fractured crystalline rock; (2) 15 m of unconsolidated sedimentary overburden; (3) a head gradient of -0.0013 m/m from west to east (as in the salt and clay reference cases; Mariner et al. 2015); (4) a regional heat flux of 60 mW/m^2 and a mean annual surface temperature of 10 °C; and (5) a saturated domain.

4.3.2 Numerical Implementation

PA simulations, comprising 15 deterministic simulations and a suite of 50 probabilistic simulations for uncertainty and sensitivity analyses, were completed using the GDSA framework (Section 2.2). Probabilistic inputs for the simulations were prepared using Dakota's Latin Hypercube Sampling (LHS) capability.

The unstructured mesh was gridded with Cubit (Blacker et al. 2016). DFNs were generated with dfnWorks (Hyman et al. 2015a; Hyman et al. 2015b) and mapped to an equivalent continuous porous medium domain with mapDFN.py (Section 3.1.3.1).

4.3.2.1 Model Domain and Discretization

The model domain (Figure 4-5) is 3015 m in length (x), 2025 m in width (y), and 1260 m in height (z). Most of the domain is discretized into cells 15 m on a side. The repository and adjacent cells are discretized into cells 1.67 m (5/3 m) on a side. A narrow transitional zone of cells 5 m on a side exists between the repository cells and the remainder of the domain. Figure 4-6 shows an x-z slice through the repository at the y-midpoint of the repository. Figure 4-7 shows an x-y slice at the z-midpoint of the repository. The domain contains 4,848,260 cells; of these, approximately 2.5 million are the smaller cells in and around the repository.

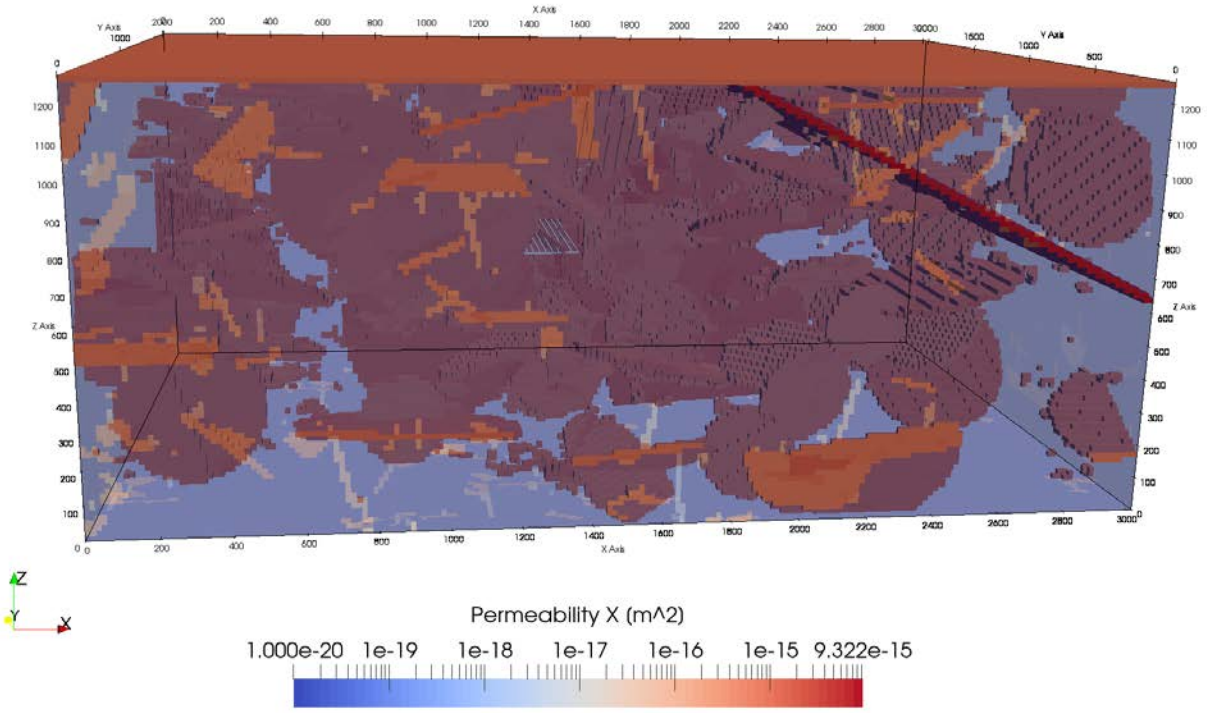

Figure 4-5. Transparent view of the model domain colored by permeability. The 3-dimensional structures inside the domain are the repository (colored gray rather than by permeability); the deterministic deformation zone, colored red due to its high permeability; and the largest fractures of a stochastically generated fracture network (Domain6 in Table 4-13). Small fractures do not appear in this image because grid cells with permeability less than 5×10^{-16} m^2 were not plotted.

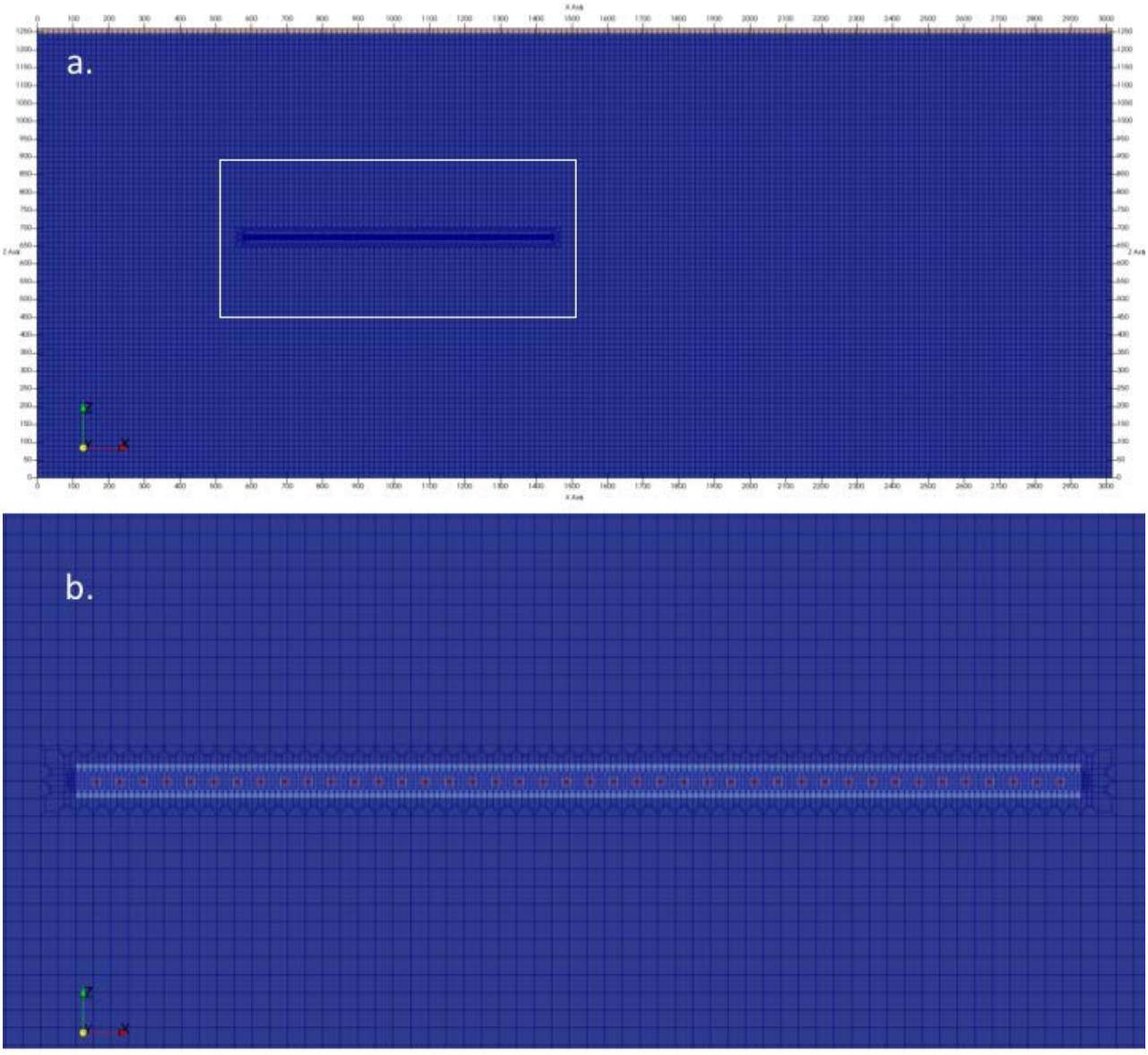

Figure 4-6. XZ slice of model domain (a). Most of the domain is discretized with cells 15-m on a side. Area of the repository is too finely-discretized to resolve at this scale. White box shows area of (b) in which discretization of repository (with cells 5/3 m on a side) can be seen. Colors represent materials: dark blue and medium blue, undisturbed host rock; light blue, DRZ; orange, buffer; red, waste packages; tan, sediment.

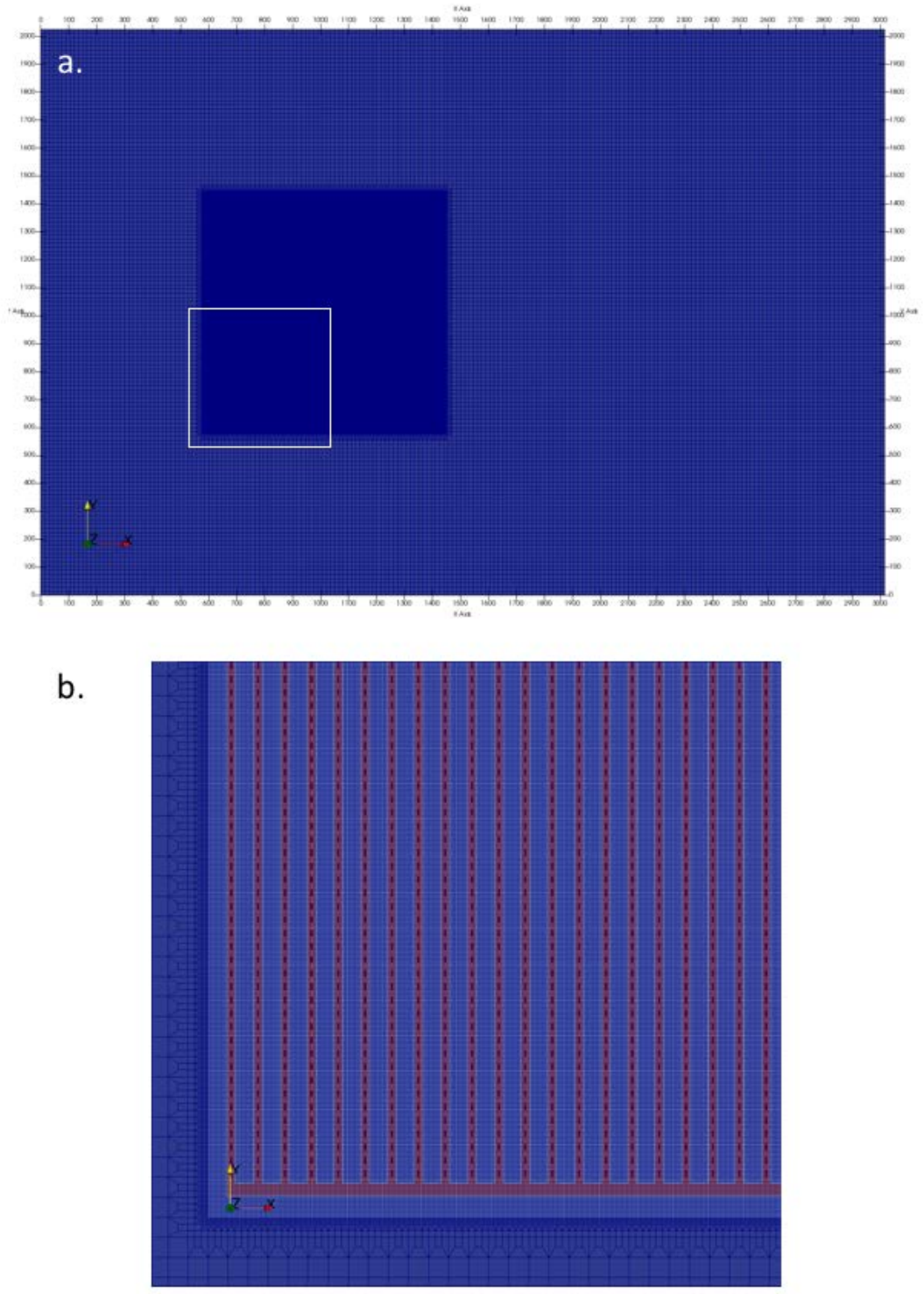

Figure 4-7. XY slice of model domain (a). Most of the domain is discretized with cells 15 m on a side. Area of the repository is too finely-discretized to resolve at this scale. White box shows area of (b) in which discretization of repository (with cells 5/3 m on a side) can be seen. Colors represent materials: dark blue and medium blue, undisturbed host rock; light blue, DRZ; orange, buffer; red, waste packages.

4.3.2.2 Initial Conditions

Initial conditions specified are pressure, temperature, and radionuclide concentrations. Initial pressures and temperatures throughout the model domain are calculated by applying a liquid flux of 0 m/s and an energy flux of 60 mW/m^2 to the base of the domain and holding temperature (10°C) and pressure (approximately atmospheric) constant at the top of the domain, and allowing the simulation to run to 10^6 years. Pressure at the top of the domain decreases from west (left) to east (right) with a head gradient of -0.0013 (m/m). This technique results in initial conditions that represent a geothermal temperature gradient and hydrostatic pressure gradient in the vertical direction, and a horizontal pressure gradient that drives flow from west to east. Simulations model include the 17 radionuclides listed in Table 4-2; initial concentrations of all radionuclides in all cells are 10^{-20} mol/L.

4.3.2.3 Boundary Conditions

Boundary conditions must be set for the six faces of the model domain. At all faces, initial pressures and temperatures are held constant. Radionuclide concentrations are held such that any fluid entering the model domain contains 10^{-20} mol/L of each radionuclide, while fluid exiting the model domain is allowed to carry with it ambient concentrations. Diffusive flux across boundaries is disallowed by specifying a zero concentration gradient.

4.3.2.4 Waste Package Heat Sources

Each waste package is modeled as a transient heat source. The energy (watts per waste package) entering the model domain is updated periodically according to values in a lookup table. The initial value is that for PWR UNF 100 yr OoR (calculated from the total decay heat at 100 years plotted in Figure 4-1). Between times specified in the lookup table, the energy input is linearly interpolated.

4.3.2.5 Waste Package Breach and Radionuclide Source Term

The waste package degradation model implemented in PFLOTRAN (Section 3.2.1) calculates canister vitality at each time step as a function of a base canister degradation rate, a canister material constant, and temperature. Waste package breach occurs when the canister vitality reaches zero. Deterministic simulations assign a base canister degradation rate for each waste package by sampling on a truncated log normal distribution with a mean of $10^{-4.5}$/yr, a standard deviation of 0.5 (log units) and an upper truncation of -3.5 (log units). Probabilistic simulations sample on the mean degradation rate using a log uniform distribution from $10^{-5.5}$/yr to $10^{-4.5}$/yr. The mean and standard deviation parameter values used in these simulations are placeholders used to approximate the conceptual timeline for waste package failure as presented in Wang et al. (2014, Figure 2-19) while also including heterogeneity across waste packages. Mechanistic models and appropriate data are needed for robust simulation of waste package degradation under predicted environmental conditions.

PFLOTRAN decays the radionuclide inventory in each waste package cell prior to waste package breach. From the time of waste package breach, the waste form releases radionuclides in two fractions: instant-release and slow-release. The instant-release fraction is due to the accumulation of certain fission products in void spaces of the waste form and occurs at the time of waste package breach. The crystalline reference case assumes a non-zero instant-release fraction for ^{135}Cs, ^{129}I, ^{99}Tc, and ^{36}Cl (Table 4-9), and zero for all other radionuclides in the simulations. The slow-release fraction is due to fuel matrix (UO_2) dissolution, which is modeled in this initial crystalline reference case using a fractional dissolution rate of 10^{-7}/yr starting from the time of waste package breach. This rate is the mode of a log triangular distribution (Table 4-10) appropriate for fuel 3,000-10,000 years OoR and strongly reducing conditions (SKB 2006a; Ollila 2008); for a complete discussion refer to Sassani et al. (2016, Section 3.2.1). Probabilistic simulations sample on the waste form dissolution rate over the range 10^{-8}/yr to 10^{-6}/yr, but simplify the distribution to log uniform rather than log triangular.

Table 4-9. Isotope instant release fractions recommended by Sassani et al. (2012) for PWR with 60 GWd/MTHM burn-up.

Isotope	Instant Release Fraction
^{135}Cs	.1
^{129}I	.1
^{99}Tc	.07
^{36}Cl	.05

Table 4-10. UNF dissolution rates; log triangular distribution from cited SKB (2006a) in Sassani et al. (2016, Section 3.2.1).

Parameter	Rate (yr^{-1})	Time to 50% dissolution (yr)	Time to 99% dissolution (yr)
Min	10^{-8}	6.93×10^{7}	4.61×10^{8}
Mode	10^{-7}	6.93×10^{6}	4.61×10^{7}
Max	10^{-6}	6.93×10^{5}	4.61×10^{6}

4.3.2.6 Material Properties

Material properties are discussed in Sections 4.1 and 4.2; values used in PA simulations are summarized in Table 4-11 (deterministic parameter values) and Table 4-12 (sampled parameter ranges). Additional information regarding the calculation of tortuosity and effective diffusion coefficient is given in Section 4.3.2.7.

Table 4-11. Parameter values used in deterministic simulations.

Model Region	Permeability (m^2)	Porosity ϕ	τ	Effective Diffusion Coefficient[2] (m^2/s)	Saturated Thermal Conductivity (W/m/K)	Heat Capacity (J/kg/K)	Grain Density (kg/m^3)
Waste Package	1×10^{-16}	0.50	1	5×10^{-10}	16.7	466	5000
Bentonite Buffer	1×10^{-20}	0.35	0.35	1.225×10^{-10}	1.5	830	2700
Crystalline Matrix	1×10^{-20}	0.005	0.2	1×10^{-12}	2.5	830	2700
Fractures	Calc'd[1]	Calc'd[1]	Calc'd[1]	1×10^{-12}	2.5	830	2700
DRZ	1×10^{-16}	0.01	1	1×10^{-11}	2.5	830	2700
Sediments	1×10^{-15}	0.20	0.2	4×10^{-11}	1.7	830	2700

[1] Calculated on a cell by cell basis for each fracture realization

[2] Effective diffusion coefficient = $D_w \tau \phi$, where the free water diffusion coefficient (D_w) = 1×10^{-9} m^2/s (Li and Gregory 1974)

Table 4-12. Sampled parameters and their distributions.

Parameter	Range	Units	Distribution
UNF Dissolution Rate	10^{-8} – 10^{-6}	yr^{-1}	log uniform
Mean Waste Package Degradation Rate	$10^{-5.5}$ – $10^{-4.5}$	yr^{-1}	log uniform
Waste Package τ	0.01 - 1.0		log uniform
Bentonite ϕ	0.3 - 0.5		uniform
DRZ ϕ	0.005 - 0.05		uniform
Np K_d bentonite	0.1 – 702	m^3kg^{-1}	log uniform
Np K_d natural barrier	1.26×10^5 – 5.37×10^7	m^3kg^{-1}	log uniform

4.3.2.7 Effective Diffusion Coefficient and Tortuosity

Diffusion coefficients in free water (D_w) depend on temperature and pressure, on the salinity and viscosity of the fluid, on the size (including hydration layer) of the ion in solution, and on charge balance constraints, which will generally slow anion and speed cation diffusion (Li and Gregory 1974). A description of diffusion in a porous medium must also account for pore volume, saturation, and tortuous diffusion paths (Li and Gregory 1974; Boudreau 1996). PFLOTRAN calculates the effective diffusion coefficient (D_e) as a function of tortuosity (θ), porosity (ϕ), and saturation (s) according to

$$D_e = \tau\phi s D_w, \tag{4-3}$$

where $\tau = 1/(\theta^2)$, and s is equal to 1 due to the assumption of a fully saturated model domain.

Tortuosity (θ), the ratio of diffusive path length to the length of a direct path, is always greater than unity. In unlithified sediments, it has been related to porosity by a number of authors (see review by Boudreau 1996). A commonly used relationship for natural sediments is derived from Archie's Law (Boudreau 1996)

$$\theta^2 = \phi^{1-n} \tag{4-4}$$

where n is an adjustable parameter with a value usually around 2 for a variety of rock types including unconsolidated sediment, consolidated sedimentary rock, and crystalline rock (Oelkers 1996). For natural materials of sedimentary origin and engineered materials of similar nature (bentonite buffer), post-closure PA simulations apply this relationship assuming $n = 2$, resulting in $\tau = \phi$. For other materials (waste package, DRZ, crystalline host rock), τ is chosen to achieve the desired value of D_e.

4.3.2.8 Fracture Realizations

Fifteen fracture realizations were generated for the crystalline reference case. Parameters used to generate the fracture realizations are listed in Table 4-3. Each realization contains a single deterministic deformation zone striking NS with a dip of 30° and a transmissivity of 1.5×10^{-6} m^2/s. Bulk permeability of the model domain for each realization was calculated for the equivalent porous medium representation in the west to east direction (left to right) by applying a known pressure gradient to the domain, finding the steady state fluid flux (q in m^3/m^2) across the east end of the domain, and calculating permeability (k) from (Freeze and Cherry 1979)

$$q = k\frac{\rho g}{\mu}\frac{dP}{dx} \quad (4\text{-}5)$$

where ρ is density, g is acceleration due to gravity, μ is viscosity, and dP/dx is the pressure gradient in the west to east direction. Characteristics of the fifteen realizations are listed in Table 4-13.

Table 4-13. Characteristics of 15 DFN realizations.

Realization	Requested number of fractures	Connected number of fractures	P32 of connected fractures (m^2/m^3)	Bulk permeability (m^2)
Domain1	49234	9112	0.0082	1.1×10^{-17}
Domain2	49234	9028	0.0083	7.1×10^{-18}
Domain3	49234	8380	0.0076	8.8×10^{-18}
Domain4	49234	9086	0.0083	1.7×10^{-17}
Domain5	49234	8787	0.0080	1.3×10^{-17}
Domain6	49234	8425	0.0076	7.5×10^{-17}
Domain7	49234	8522	0.0079	1.1×10^{-17}
Domain8	49234	8807	0.0081	9.6×10^{-18}
Domain9	49234	8915	0.0080	9.4×10^{-18}
Domain10	49234	8838	0.0079	7.6×10^{-18}
Domain11	49234	8622	0.0079	1.5×10^{-17}
Domain12	49234	8903	0.0080	1.3×10^{-17}
Domain13	49234	8412	0.0077	1.9×10^{-17}
Domain14	49234	8739	0.0079	1.1×10^{-17}
Domain15	49234	8332	0.0076	7.4×10^{-18}

4.4 Simulation Results

Deterministic and probabilistic results are discussed in terms of concentrations of the long-lived radionuclides ^{129}I ($t_{1/2} = 1.57\times10^7$ yr) and ^{237}Np ($t_{1/2} = 2.14\times10^6$ yr). ^{129}I is assumed to have unlimited solubility and to be non-sorbing; it thus behaves nearly conservatively. ^{237}Np is solubility-limited and sorbing. Temperature fields, flux vectors, and waste package breach times for a single deterministic simulation are also presented.

The current PA simulations are limited by their generic nature as well as the bias toward fracture connectivity discussed in Section 4.2.2.1, and should not be interpreted in terms of repository performance in a fractured crystalline host rock. Results can, however, contribute to prioritization of experimental efforts, improve understanding of site-specific data needs, inform optimization of repository design, and lead to improvements in modeling methods and analysis.

4.4.1 Deterministic Results

Temperature and fluid flow fields at various times for the fracture realization "Domain6" are shown in Figure 4-8 through Figure 4-13. By 10 years (Figure 4-9), the rising temperatures in the repository are driving fluid flow out of the repository. Temperatures peak just below 200 °C at approximately 200 years (Figure 4-10), although maximum fluid fluxes occurred earlier in response to repository warming (compare to Figure 4-9). The repository remains warmer than background at 1000 and 10,000 years (Figure 4-11 and Figure 4-12), and where fractures intersect the repository, fluid flow out of the repository is still occurring. By 100,000 years repository temperatures have returned to near background, and the thermal influence on the flow field is beginning to diminish (Figure 4-13).

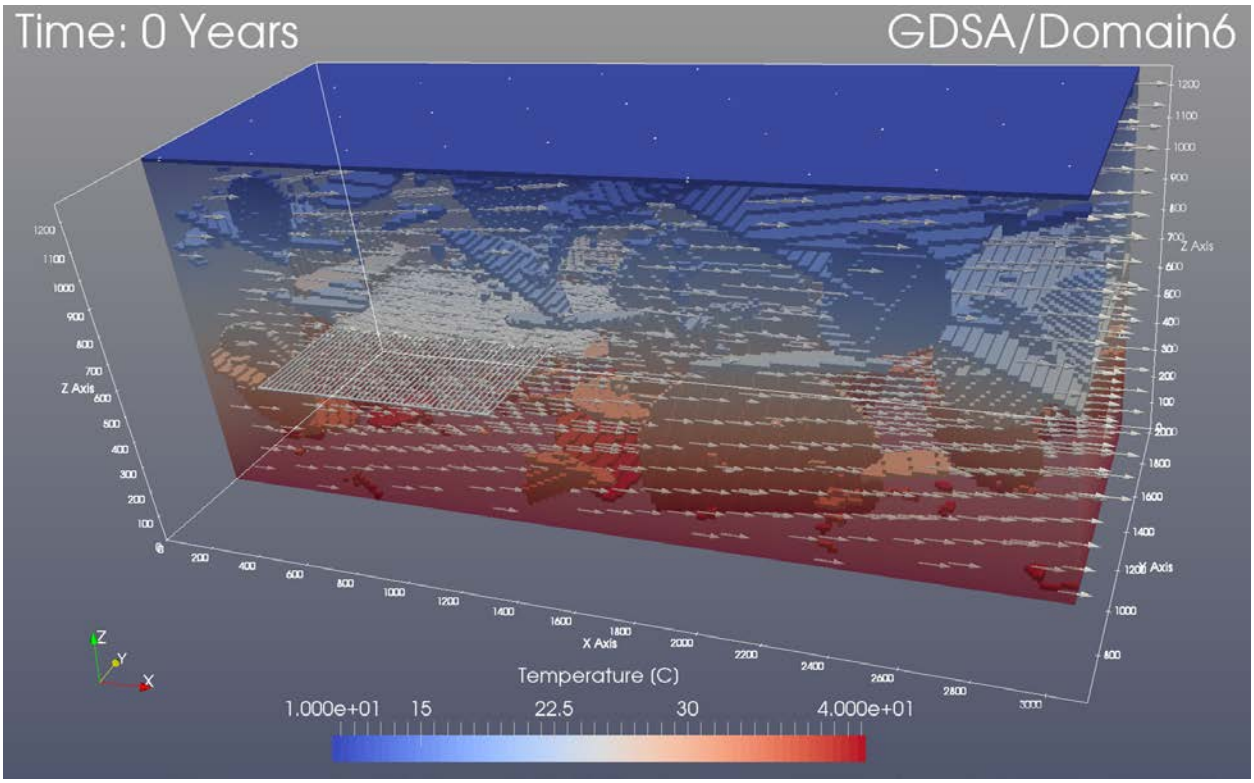

Figure 4-8. Background geothermal temperature gradient and regional flow field at 0 years (shown for the deterministic simulation of Domain6). The transparent model domain is truncated at y = 1012.5 m (the midpoint); the full repository and fractures with permeability greater than 5×10^{-16} m^2 (and y > 1012.5 m) are plotted. All elements are colored by temperature, except the flux vectors, which simply indicate the direction of flow. Notice that the maximum temperature on the color scale of 40 °C in this figure is less than the maximum of 197 °C in the figures that follow.

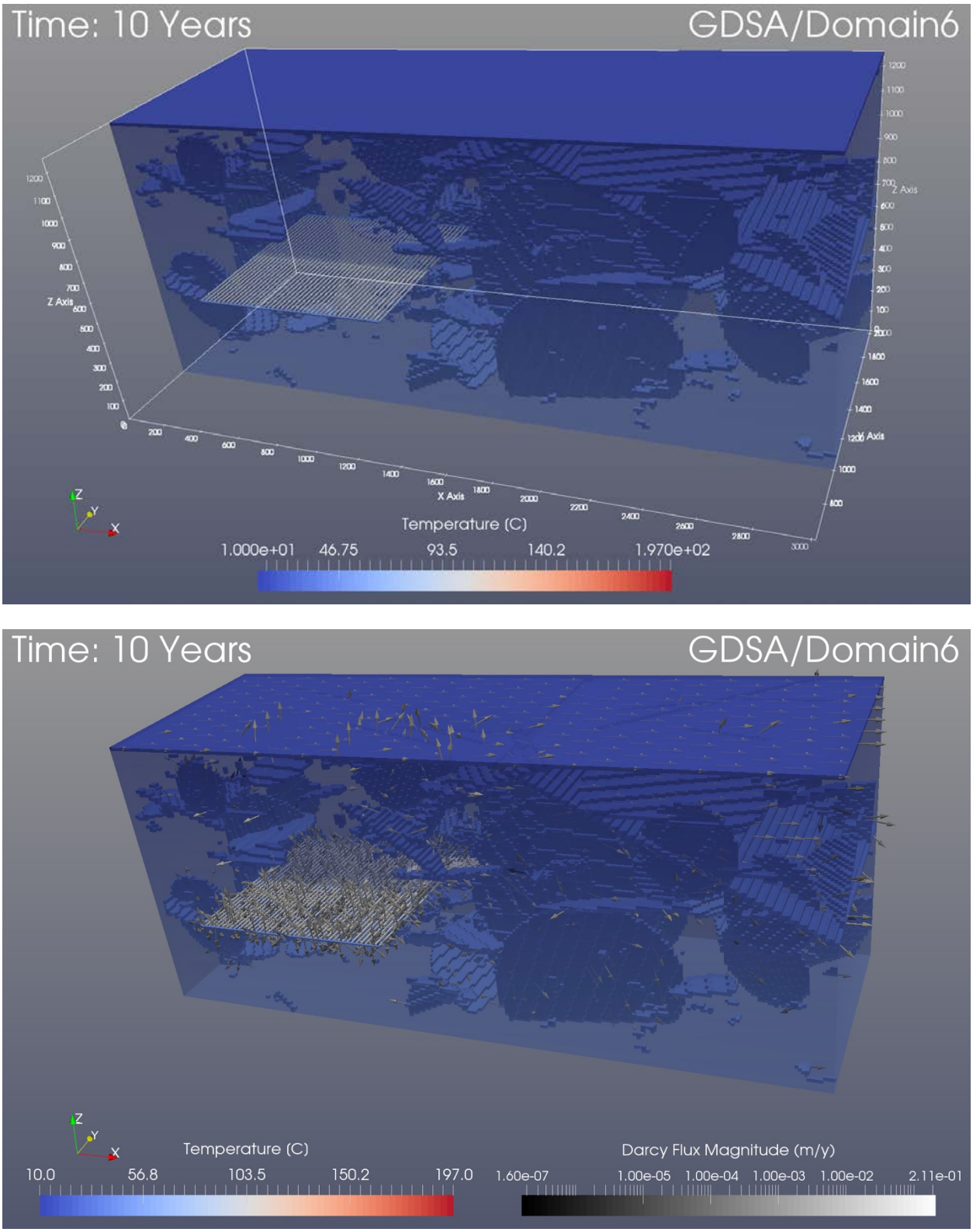

Figure 4-9. Temperature field at 10 years in the deterministic simulation of Domain6 (top). Plotted and colored as in Figure 4-8 except for difference in scale. Flux vectors at 10 years (bottom). Vectors are plotted for a subset of cells in fractures, sediments, and repository and colored by flux magnitude.

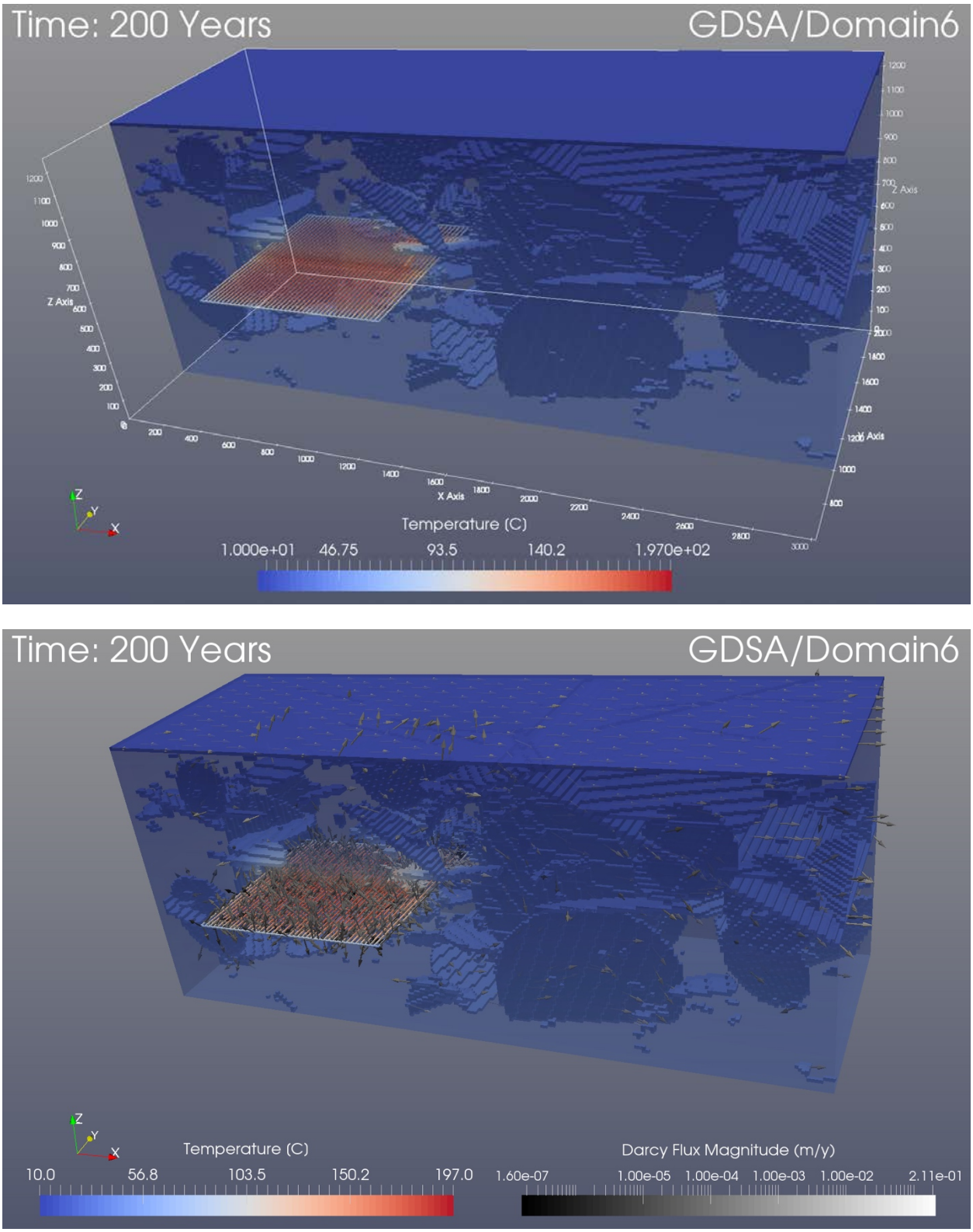

Figure 4-10. Temperature field (top) and Darcy flux vectors (bottom) at 200 years in the deterministic simulation of Domain6. Plotted and colored as in Figure 4-9.

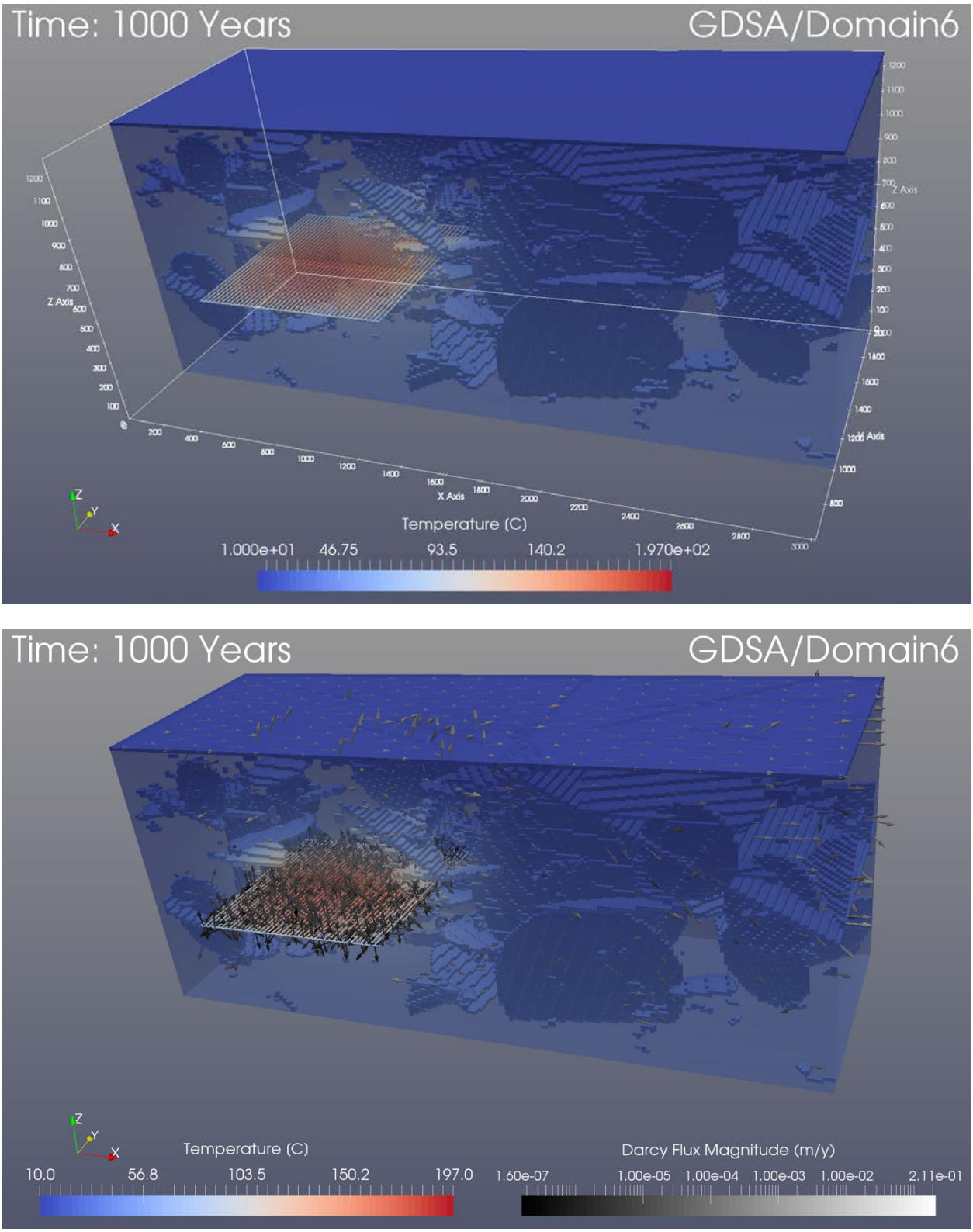

Figure 4-11. Temperature field (top) and Darcy flux vectors (bottom) at 1,000 years in the deterministic simulation of Domain6. Plotted and colored as in Figure 4-9.

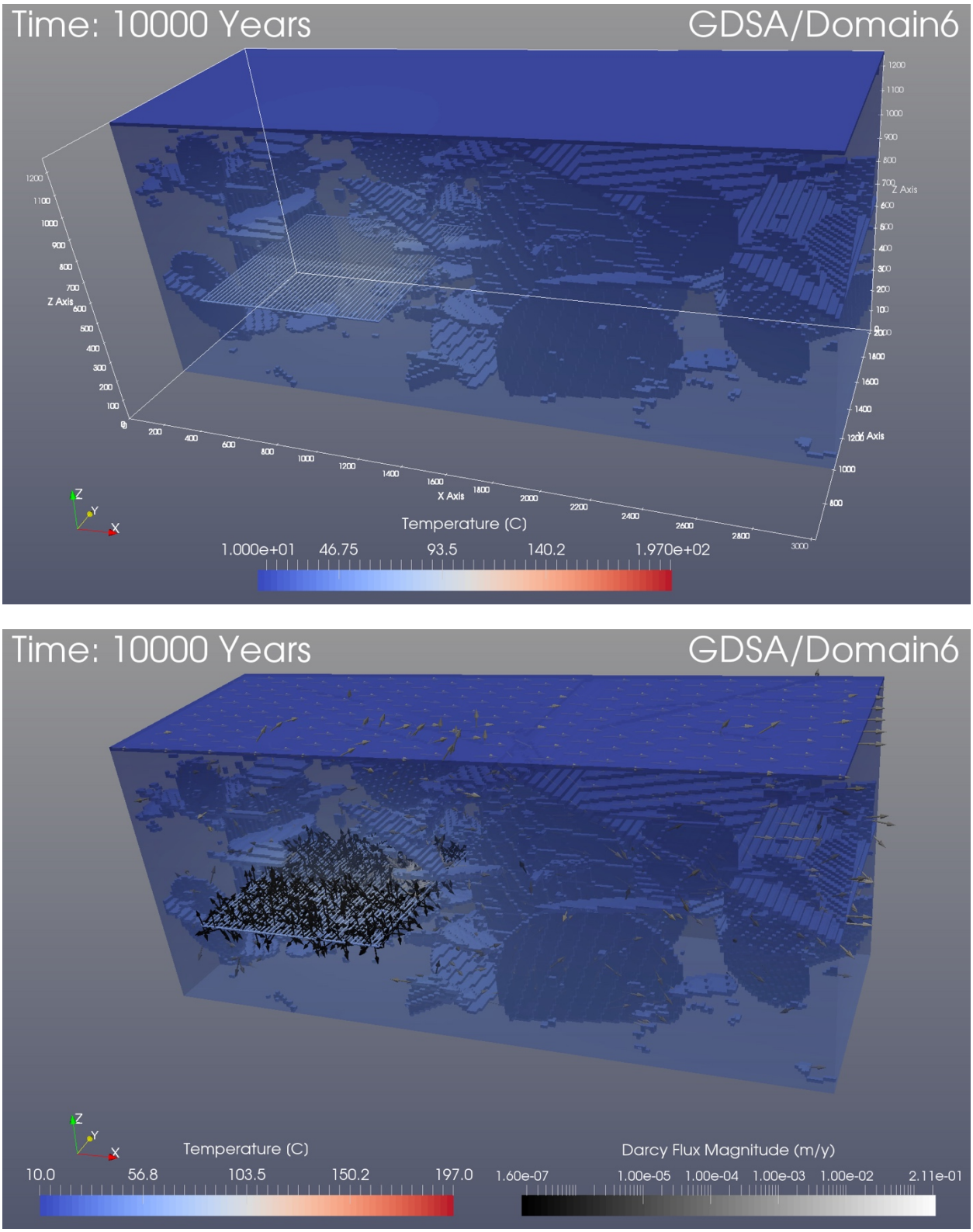

Figure 4-12. Temperature field (top) and Darcy flux vectors (bottom) at 10,000 years in the deterministic simulation of Domain6. Plotted and colored as in Figure 4-9.

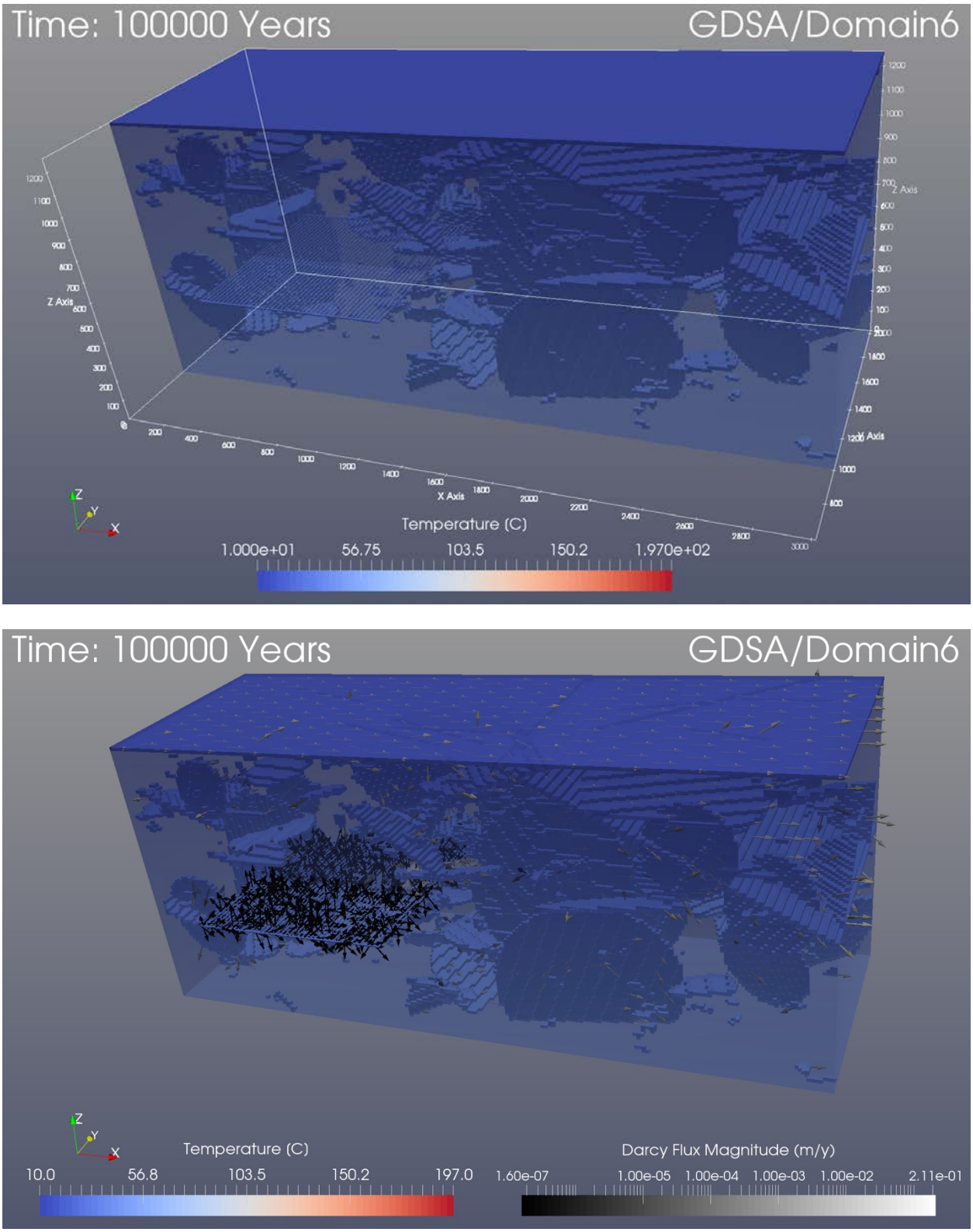

Figure 4-13. Temperature field (top) and Darcy flux vectors (bottom) at 100,000 years in the deterministic simulation of Domain6. Plotted and colored as in Figure 4-9.

Just over 100 (of 3360) waste packages breach by 400 years, and all waste packages breach by 405,000 years (Figure 4-14). Breach times do not vary from one fracture realization to another because the same spatial heterogeneity of canister degradation rates, based on a mean rate of $10^{-4.5}$ yr^{-1}, was used in all deterministic realizations, and though the degradation function is temperature-dependent, heat conduction is not affected by fracture distribution.

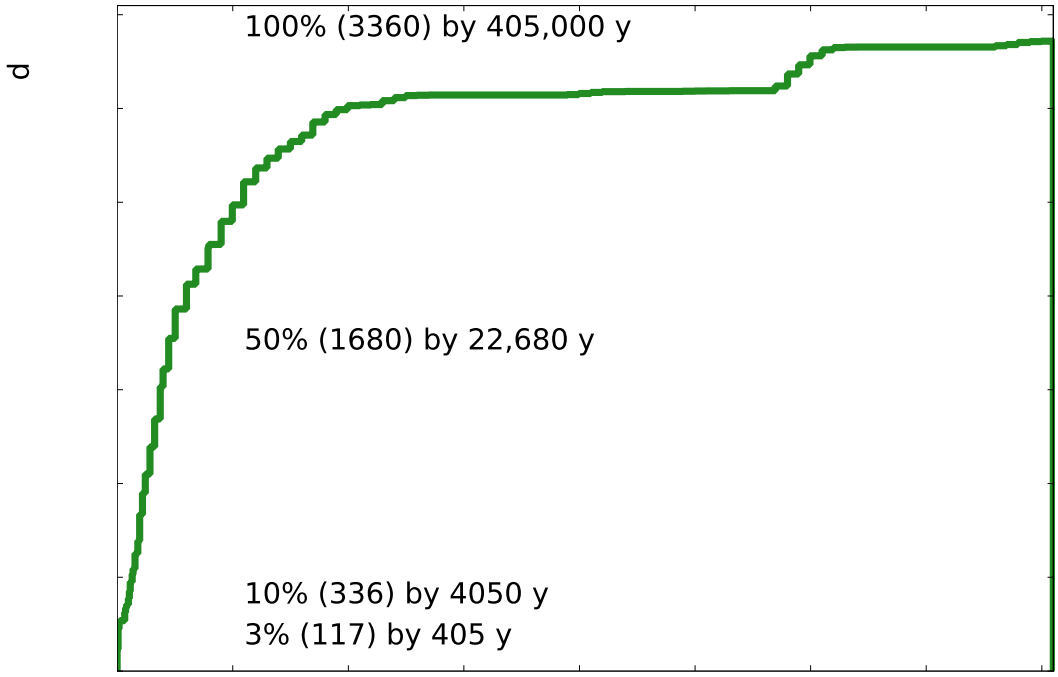

Figure 4-14. Cumulative number of waste packages breached versus time.

The spatial distribution of the nearly conservative ^{129}I at times up to 10^6 years is shown in Figure 4-15 through Figure 4-17. Between 300 and 400 years, transport in fractures carries ^{129}I to the east (right) face of the model domain over 1.5 km from the repository (Figure 4-15). With time, ^{129}I diffuses from the repository and from fractures into the crystalline rock matrix.

The spatial distribution of ^{237}Np, which both precipitates and sorbs, is shown in Figure 4-18. In 10^6 years, ^{237}Np has traveled less distance than ^{129}I traveled in 400 years.

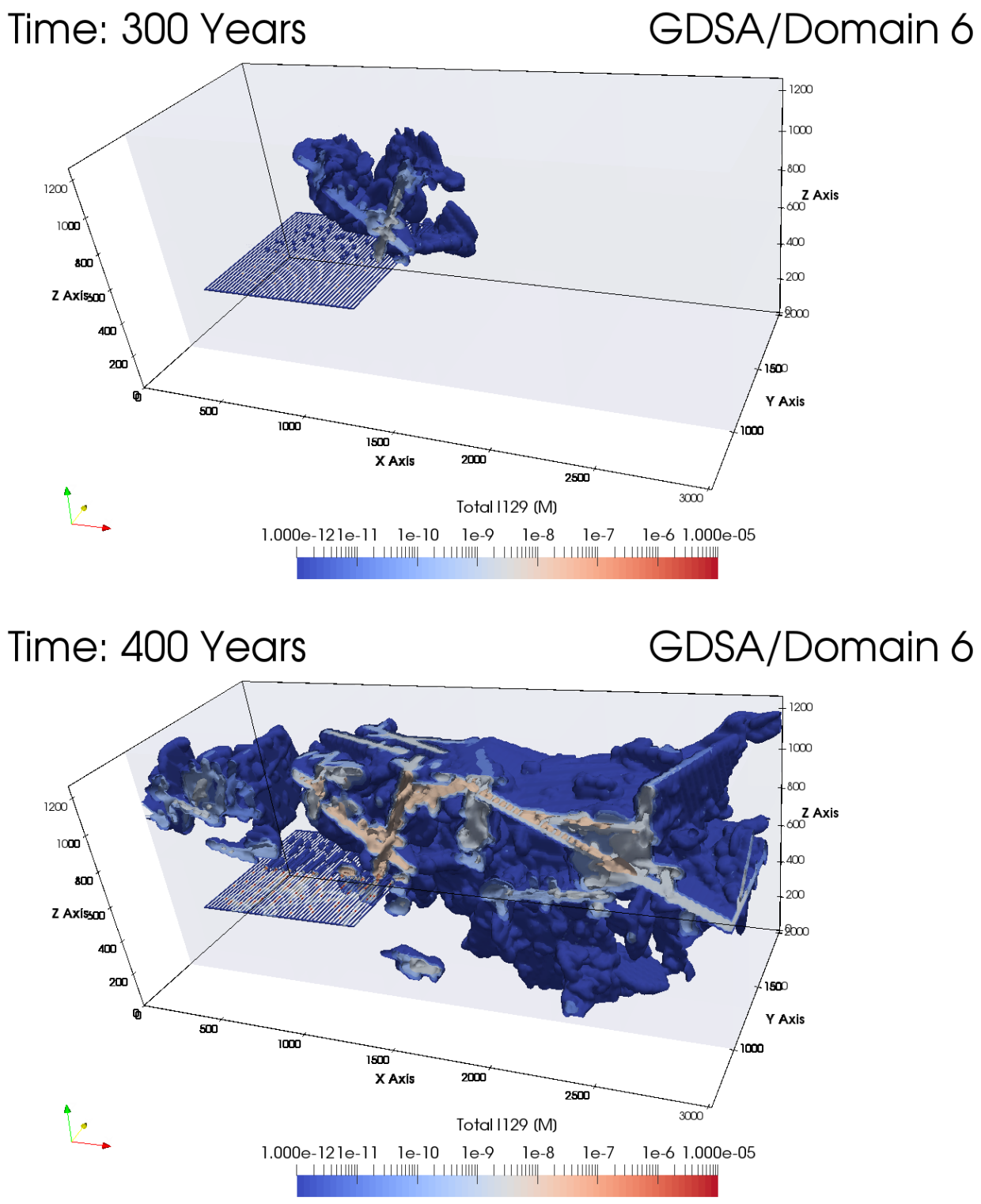

Figure 4-15. ^{129}I concentration at 300 years (top) and 400 years (bottom) in the deterministic simulation of Domain6. Concentration is contoured on a log scale at intervals of 10^{-12} mol/L to 10^{-5} mol/L; contours are colored by ^{129}I concentration.

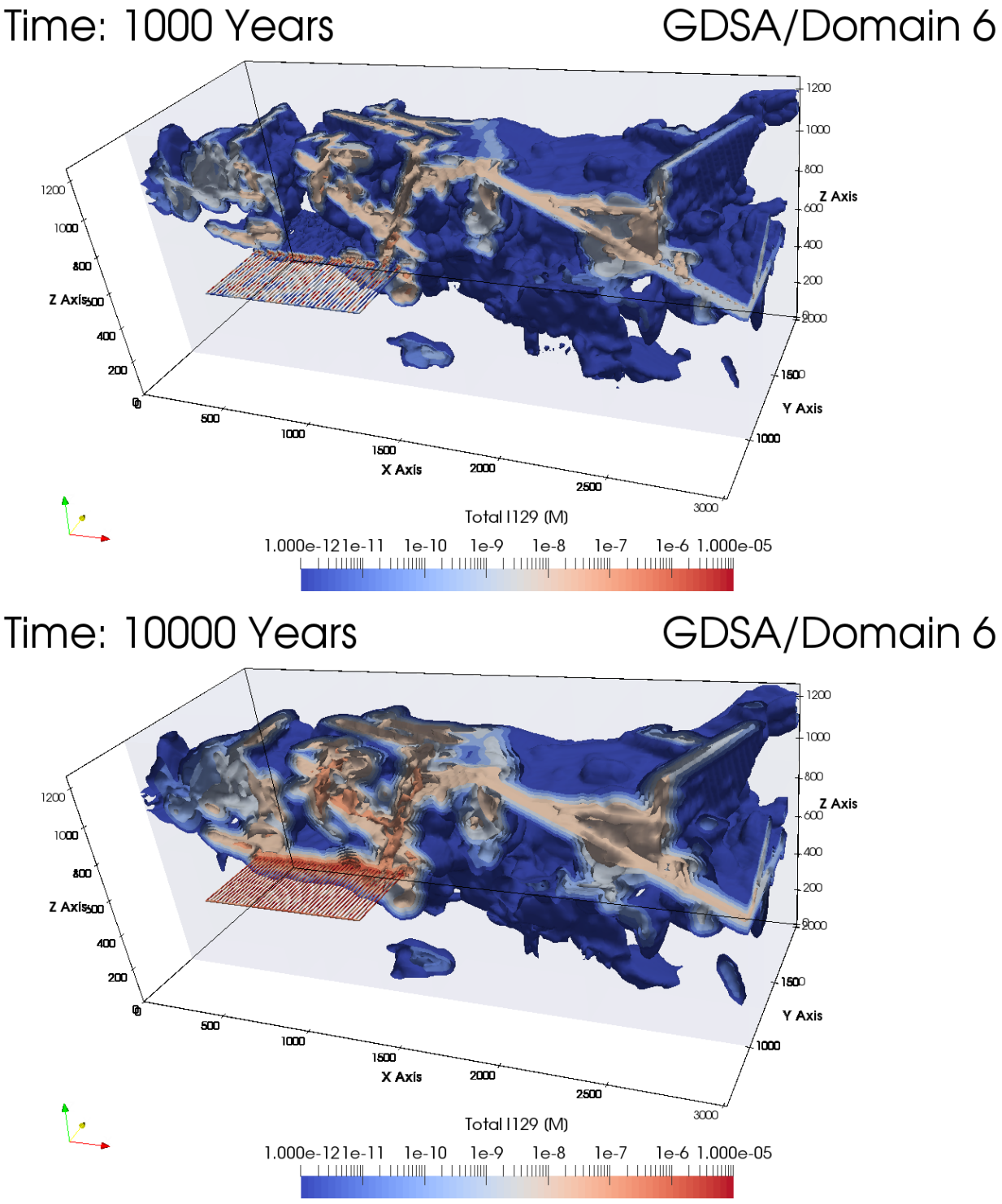

Figure 4-16. ^{129}I concentration at 1,000 years (top) and 10,000 years (bottom) in the deterministic simulation of Domain6. Contoured and colored as in Figure 4-15.

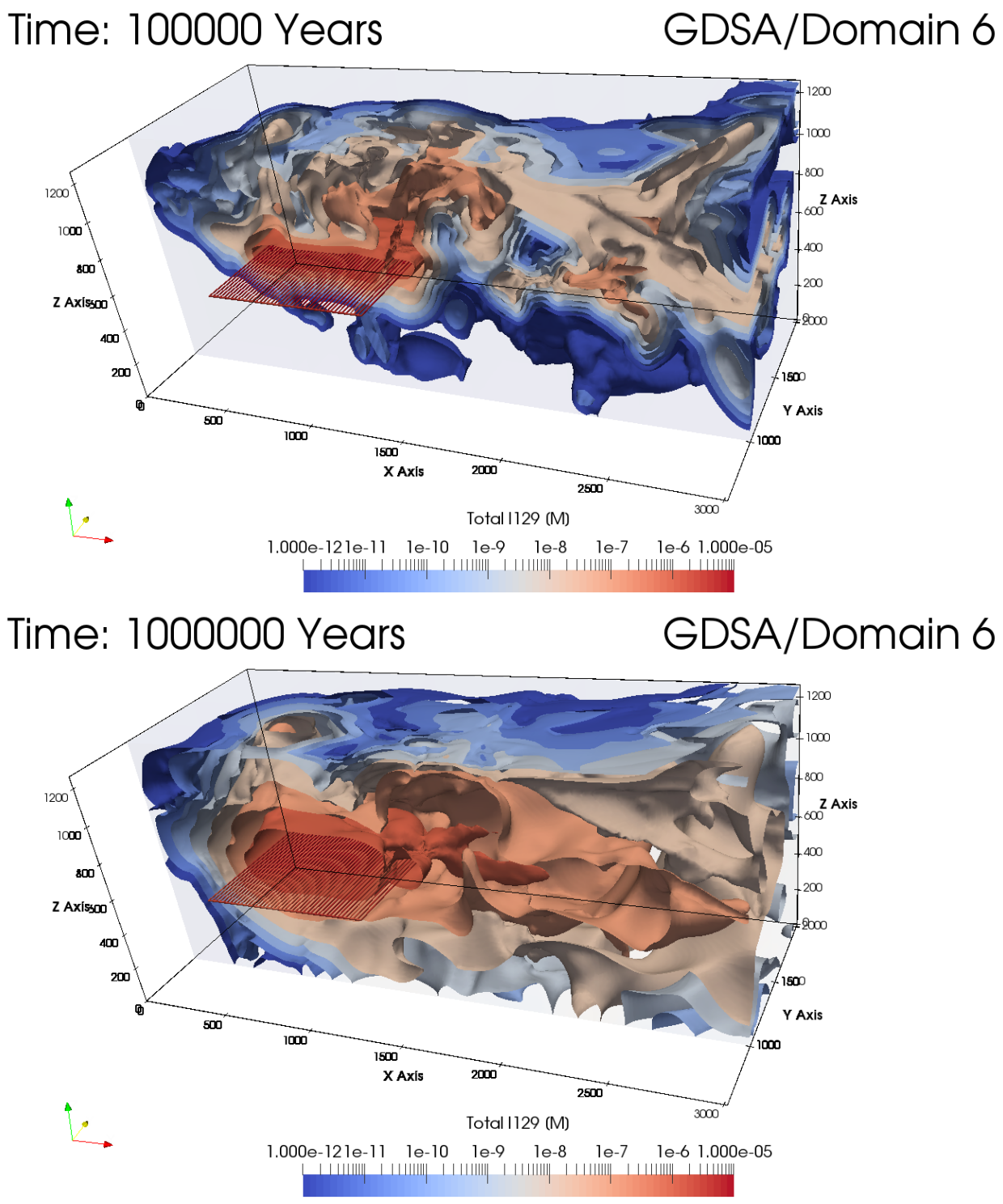

Figure 4-17. ^{129}I concentration at 10^5 years (top) and 10^6 years (bottom) in the deterministic simulation of Domain6. Contoured and colored as in Figure 4-15.

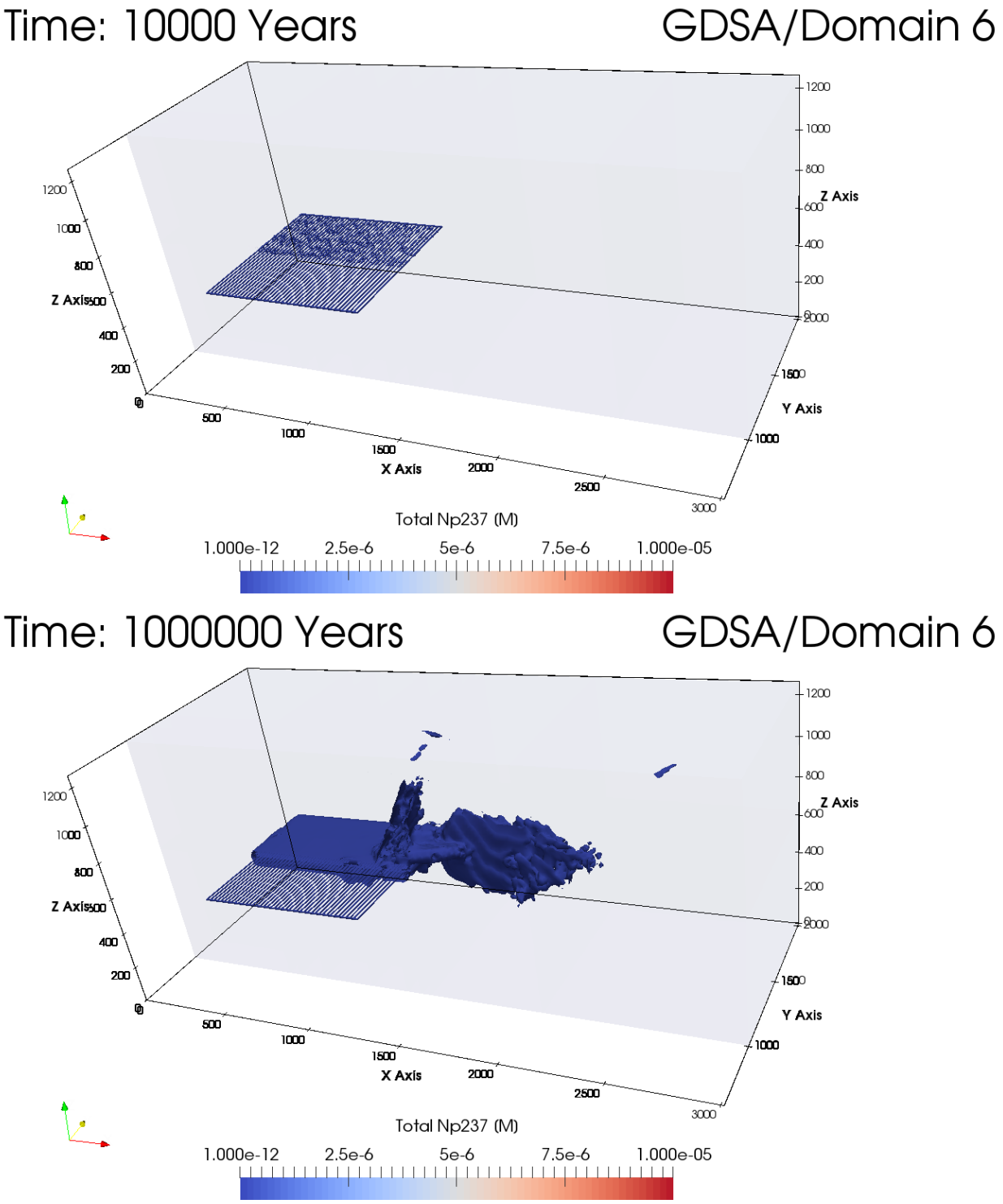

Figure 4-18. ^{237}Np concentration at 10,000 years (top) and 10^6 years (bottom) in the deterministic simulation of Domain6. Concentration is contoured and colored on the same scale as in figures of ^{129}I.

4.4.2 Comparing Fracture Domains

Break through curves for ^{129}I at three observation points in the sediment (glacial1, glacial2, and glacial3) and three observation points in the deformation zone (dz1, dz2, and dz3) (Figure 4-19) are compared in Figure 4-20 and Figure 4-21.

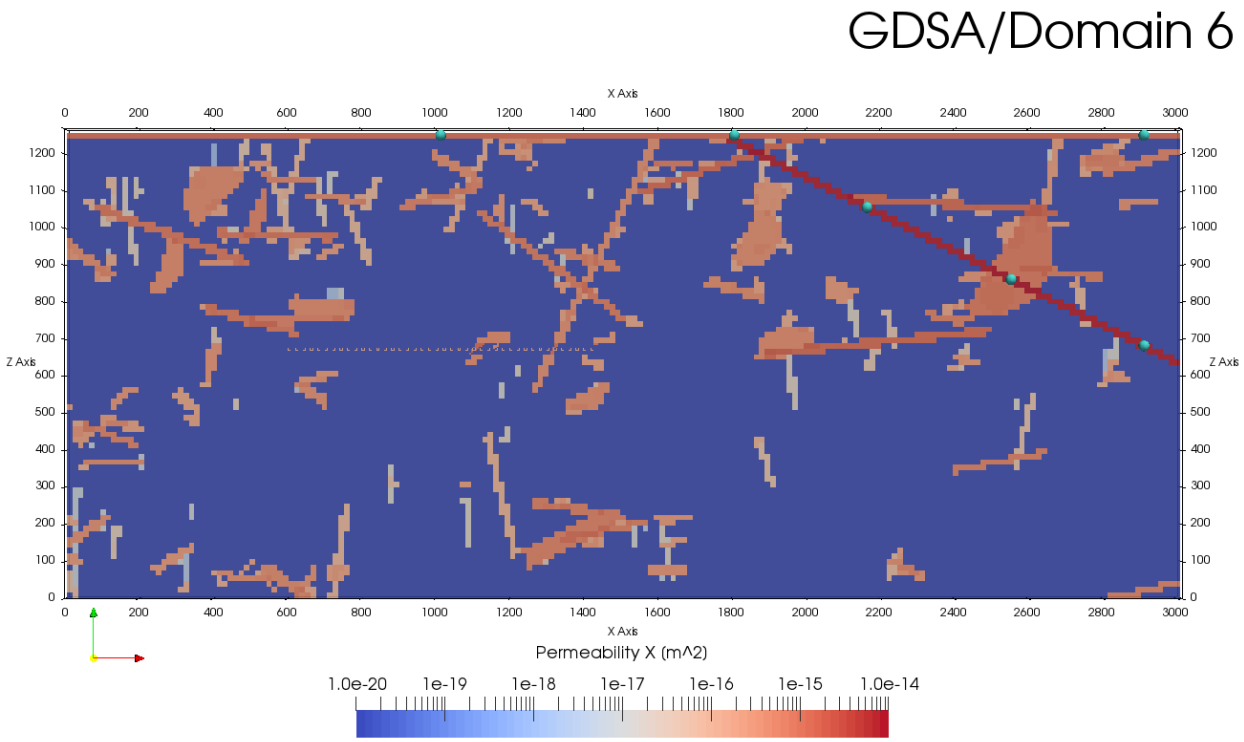

Figure 4-19. XZ cross section at the Y midpoint of the domain showing the locations of observation points (teal spheres) used in comparison of fracture realizations and in uncertainty and sensitivity analysis (Section 4.4.3). From left to right in uppermost layer (sediments): "glacial1," "glacial2," and "glacial3." From top to bottom in deformation zone: "dz1," "dz2", "dz3."

Among the sediment observation points, the spread in time of earliest arrival is almost three orders of magnitude, from a few hundred years to approximately 100,000 years. At which observation point ^{129}I first arrives depends on the fracture realization. In Figure 4-20, the two dashed lines indicate two simulations in which ^{129}I arrived at the furthest point from the repository first (approximately 300 years into the simulation) and at closer observation points thousands to tens of thousands of years later. Among the deformation zone observation points, the time of earliest arrival occurs almost uniformly at approximately 300 years. This timing is coincident with earliest waste package breach times and within the period of time when repository temperatures provide a driving force for flow away from the repository. These consistently early arrival times indicate rapid transport in fractures due to buoyancy-driven fluid fluxes. At all observation points, the spread in maximum concentration of ^{129}I is approximately four orders of magnitude. The timing of maximum concentration varies between approximately 10^4 and 10^6 years. The time of earliest arrival and the timing and magnitude of maximum concentration at any given point in the domain depend heavily on the connectivity (or lack thereof) between that point and the repository.

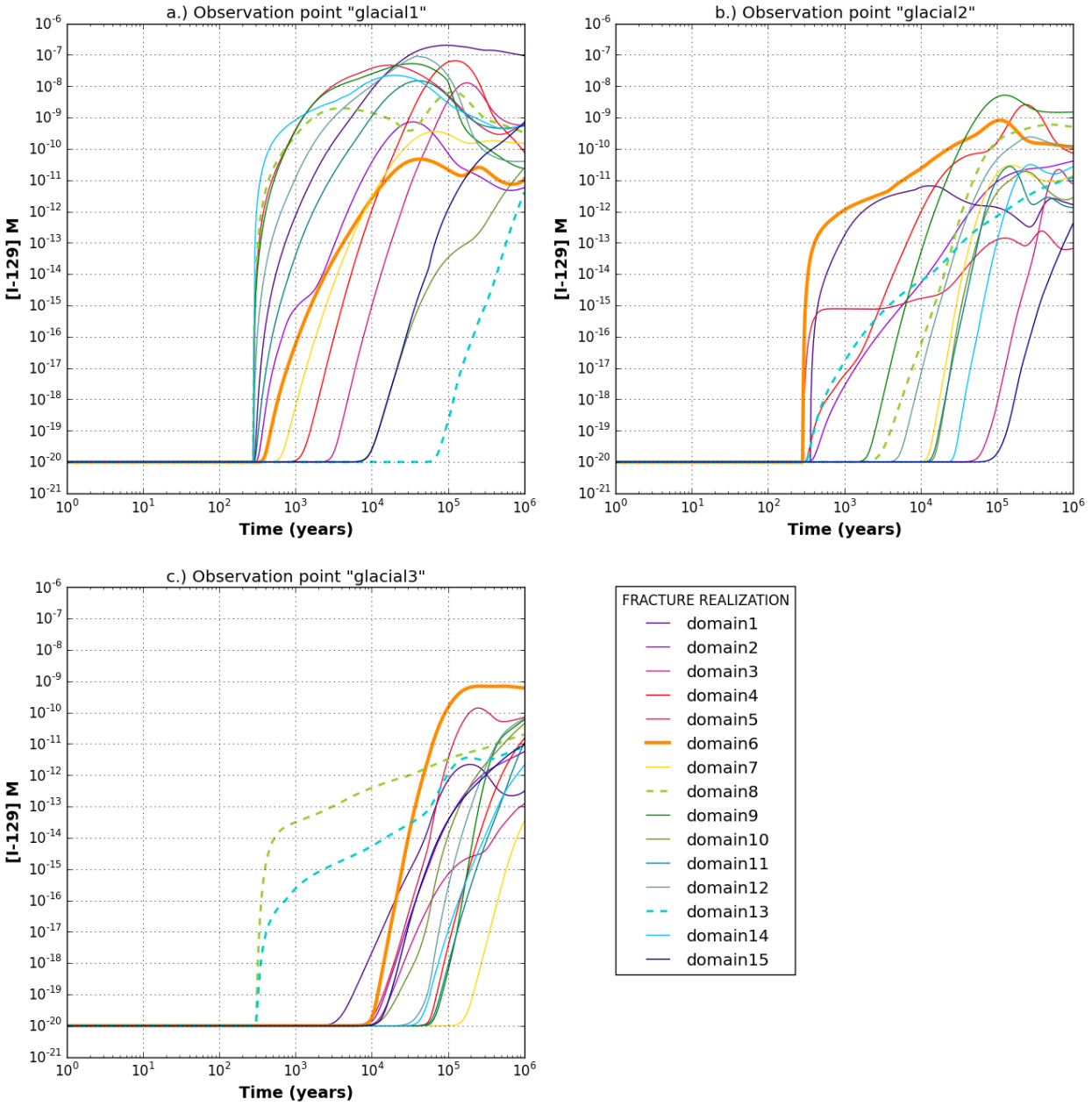

Figure 4-20. Predicted concentration of ^{129}I versus time for 15 fracture realizations at observation points a) glacial1, b) glacial2, and c) glacial3. The heavy orange line is Domain6, the fracture realization used in probabilistic simulations.

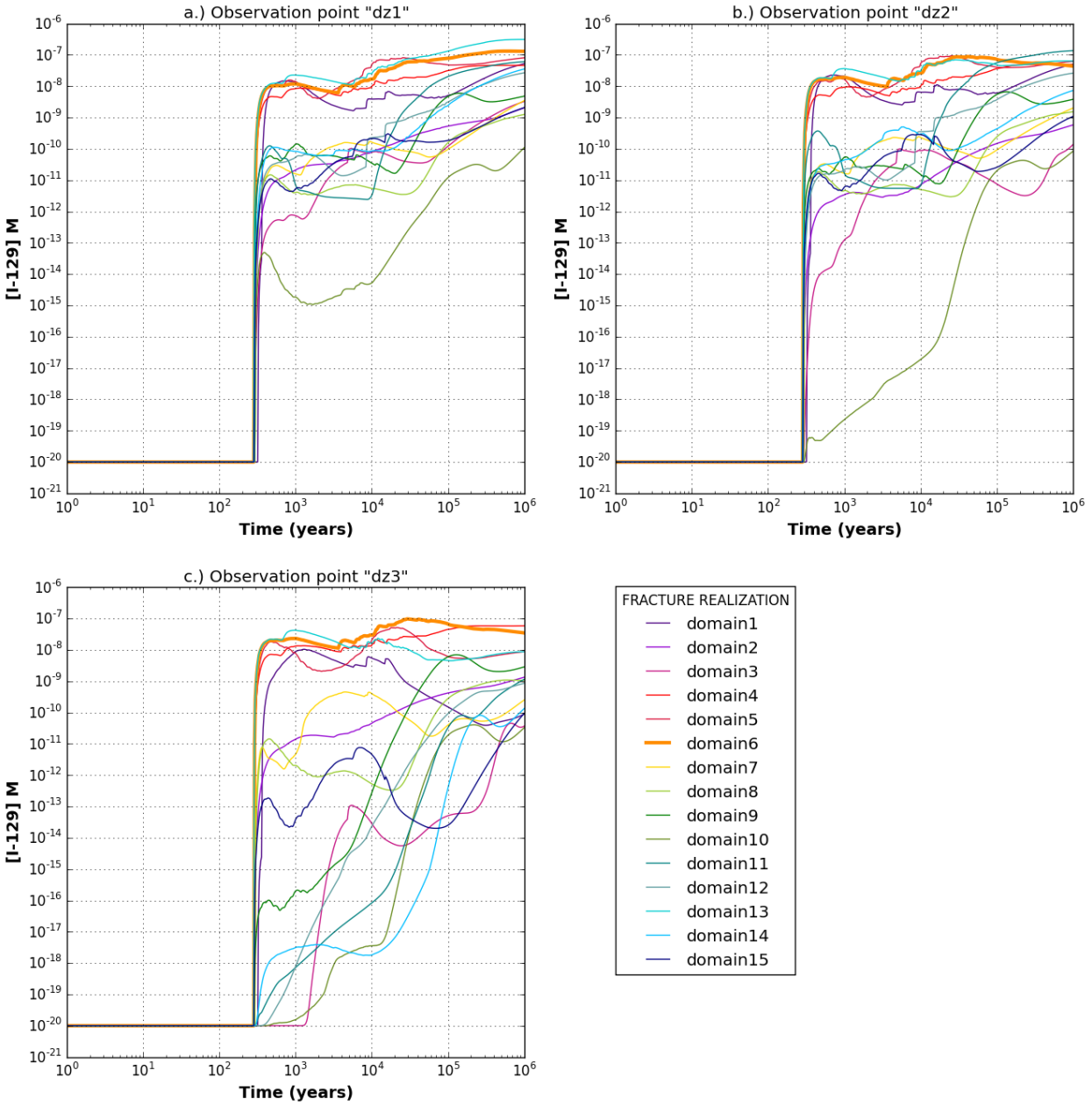

Figure 4-21. Predicted concentration of ^{129}I versus time for 15 fracture realizations at observation points a) dz1, b) dz2, and c) dz3. The heavy orange line is Domain6, the fracture realization used in probabilistic simulations.

4.4.3 Probabilistic Results

A suite of 50 probabilistic simulations was run using a single fracture realization (Domain6) and the parameter distributions listed in Table 4-12. Concentrations were observed at the same observation points used to compare fracture realizations (Figure 4-19). Breakthrough curves for ^{129}I are plotted in Figure 4-22 and Figure 4-23.

Predicted concentrations vary less due to sampled parameters than due to fracture realization. At all observation points except glacial3, the time of earliest arrival varies by less than a factor of two, falling

between approximately 300 and 500 years. At glacial3, the furthest observation point from the repository, the time of earliest arrival varies between approximately 400 and 10,000 years; this variation may indicate a travel path through the sediment and the influence of sediment properties (permeability, K_d) on travel time. At all observation points, the variation among simulations in maximum concentration of ^{129}I is less than the variation observed among fracture realizations. The largest variation, approximately three orders of magnitude, occurs at observation point glacial3, and probably reflects the influence of sediment properties on the travel path to this observation point.

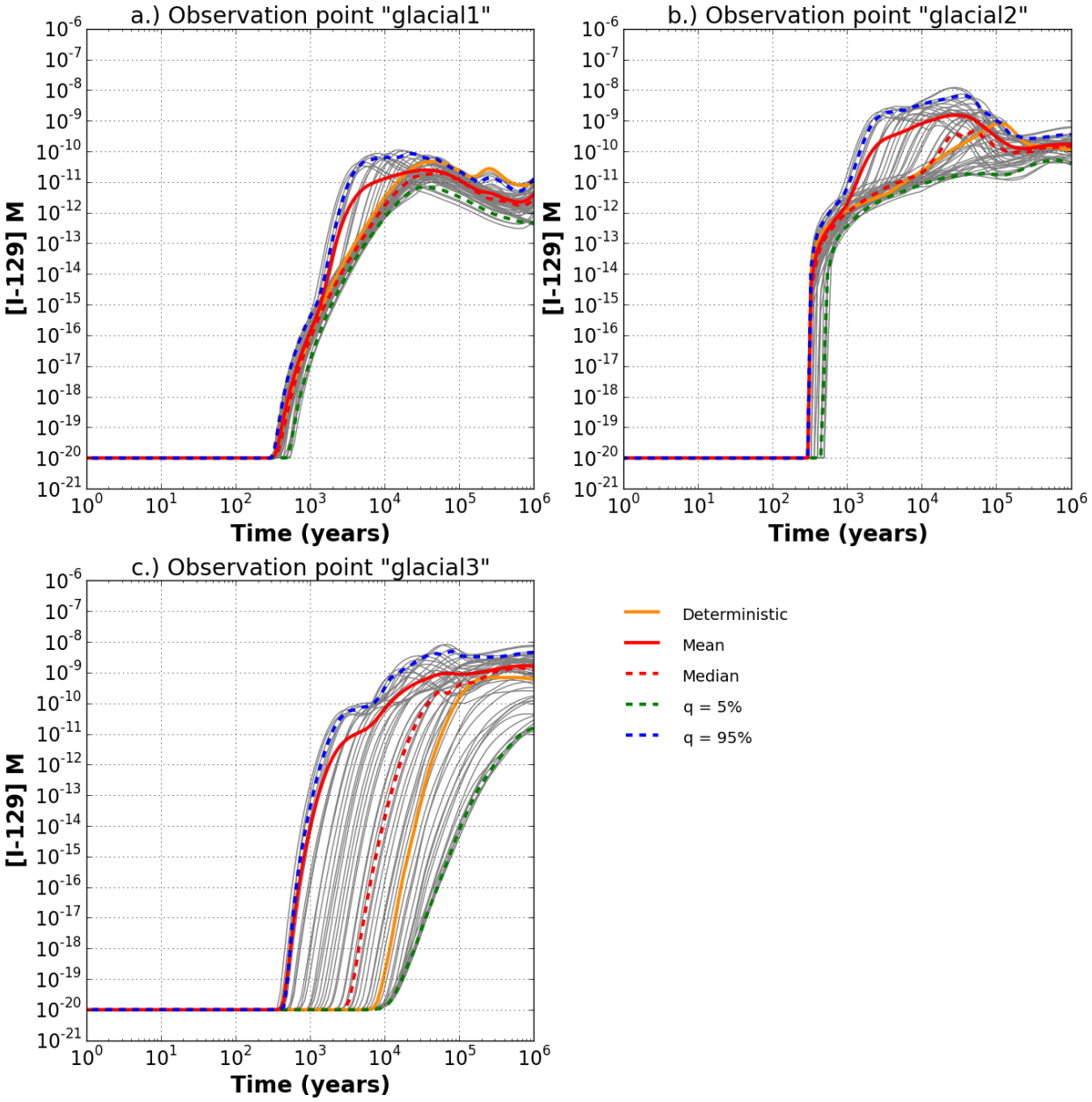

Figure 4-22. Predicted concentration of ^{129}I versus time for 50 sampled realizations at observation points a) glacial1, b) glacial2, and c) glacial3. The heavy orange line is the deterministic simulation of Domain6.

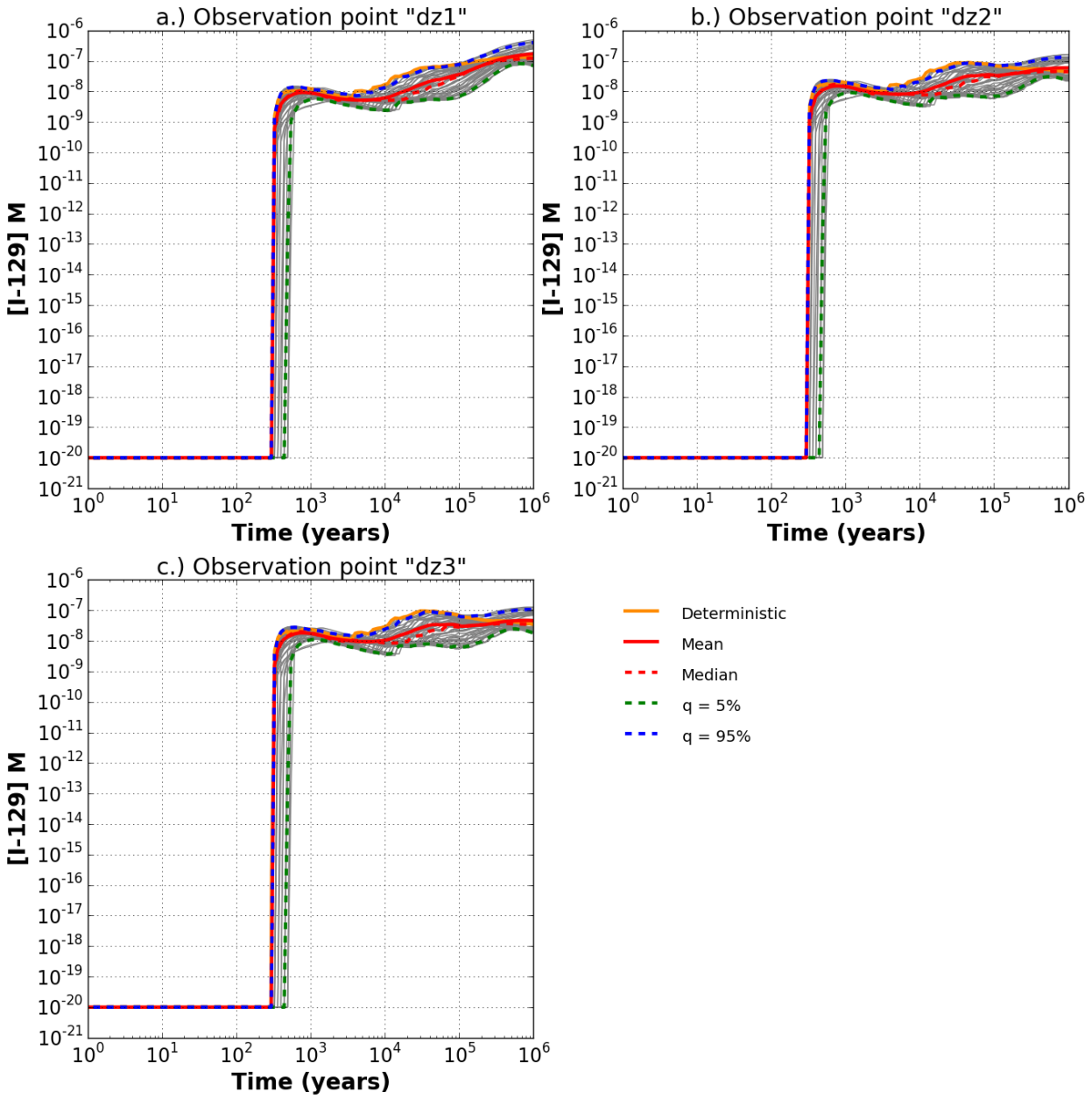

Figure 4-23. Predicted concentration of ^{129}I versus time for 50 sampled realizations at observation points a) dz1, b) dz2, and c) dz3. The heavy orange line is the deterministic simulation of Domain6.

Spearman rank correlation coefficients were calculated in order to assess the sensitivity of maximum concentration of ^{129}I and ^{237}Np to sampled parameters (Figure 4-24). Maximum concentration of ^{129}I at the sediment observation points exhibits the strongest positive correlation with sediment permeability and a smaller positive correlation with mean waste package degradation rate. Maximum concentration of ^{237}Np at the sediment observation points exhibits a strong negative correlation with the Np K_d in the natural barrier and positive correlations with UNF dissolution rate and sediment permeability. At the deformation zone observation points, maximum concentrations of both ^{129}I and ^{237}Np are positively correlated with UNF dissolution rate. As at the sediment observation points, maximum concentration of ^{129}I is positively correlated with waste package degradation rate, and maximum concentration of ^{237}Np is negatively correlated with its K_d in the natural barrier. These differences in behavior are related to characteristics of the radionuclides: simulations assume that ^{237}Np sorbs, while ^{129}I does not; ^{129}I has an instant release fraction, while ^{237}Np does not.

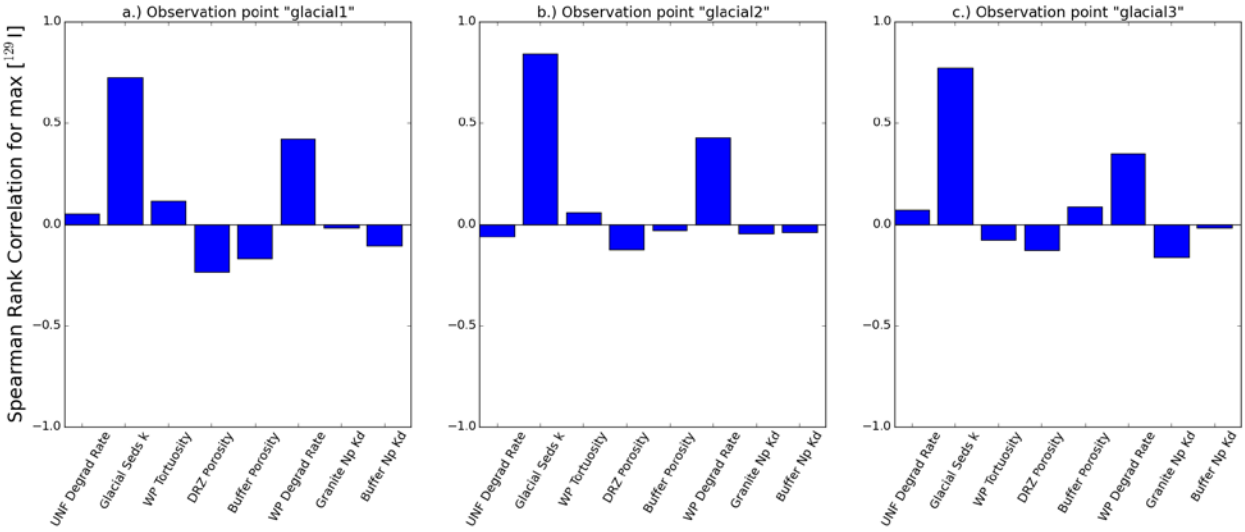

Figure 4-24. Spearman rank correlation coefficients for maximum concentration of ^{237}Np at sediment observation points.

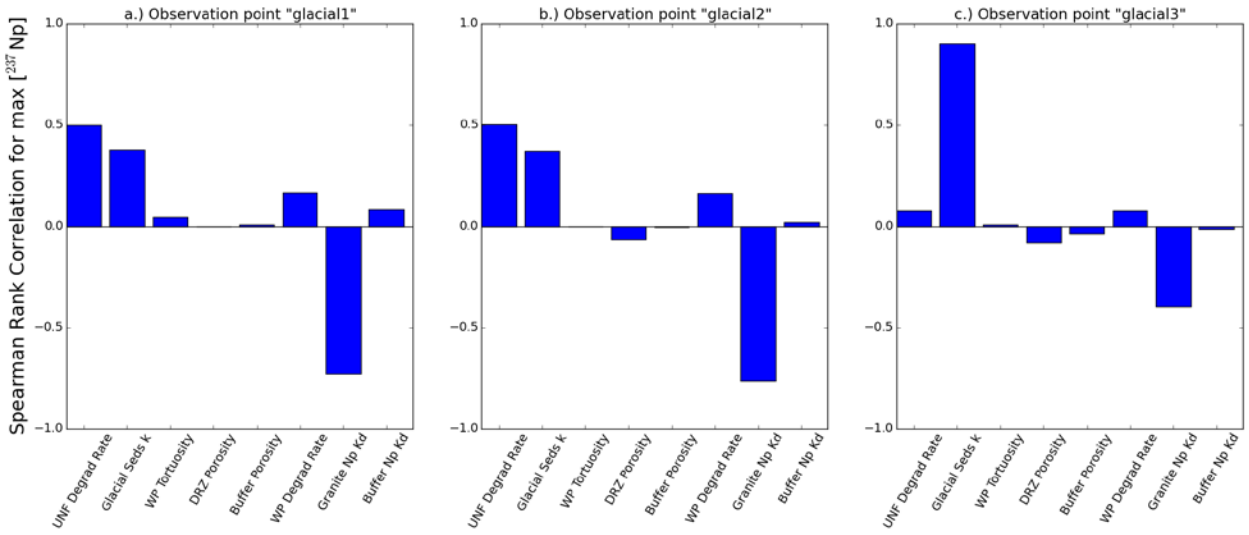

Figure 4-25. Spearman rank correlation coefficients for maximum concentration of ^{237}Np at sediment observation points.

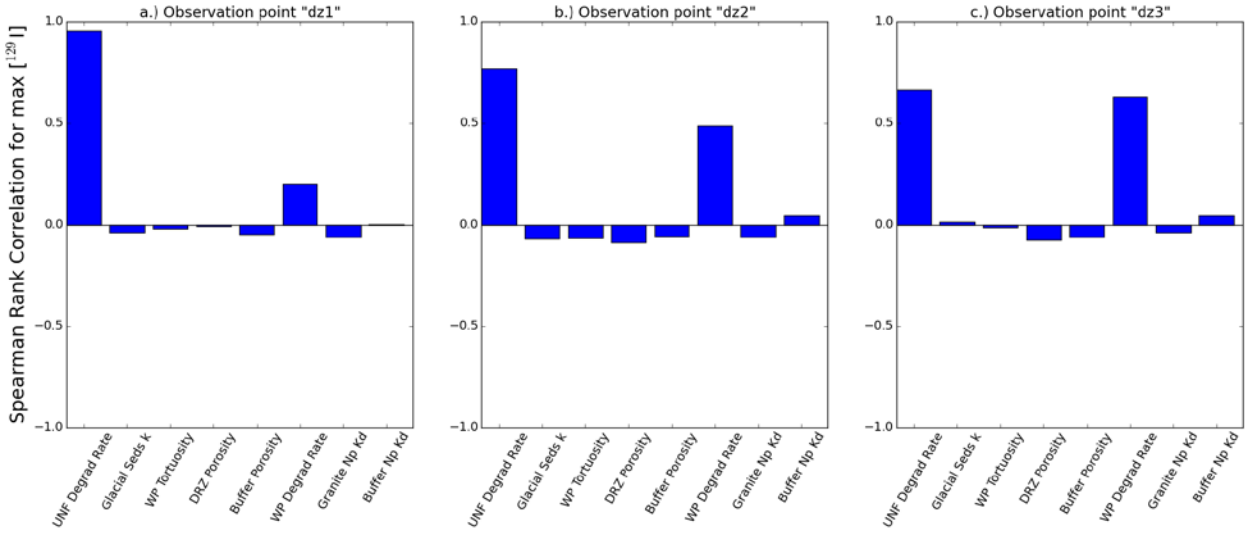

Figure 4-26. Spearman rank correlation coefficients for maximum concentration of ^{237}Np at sediment observation points.

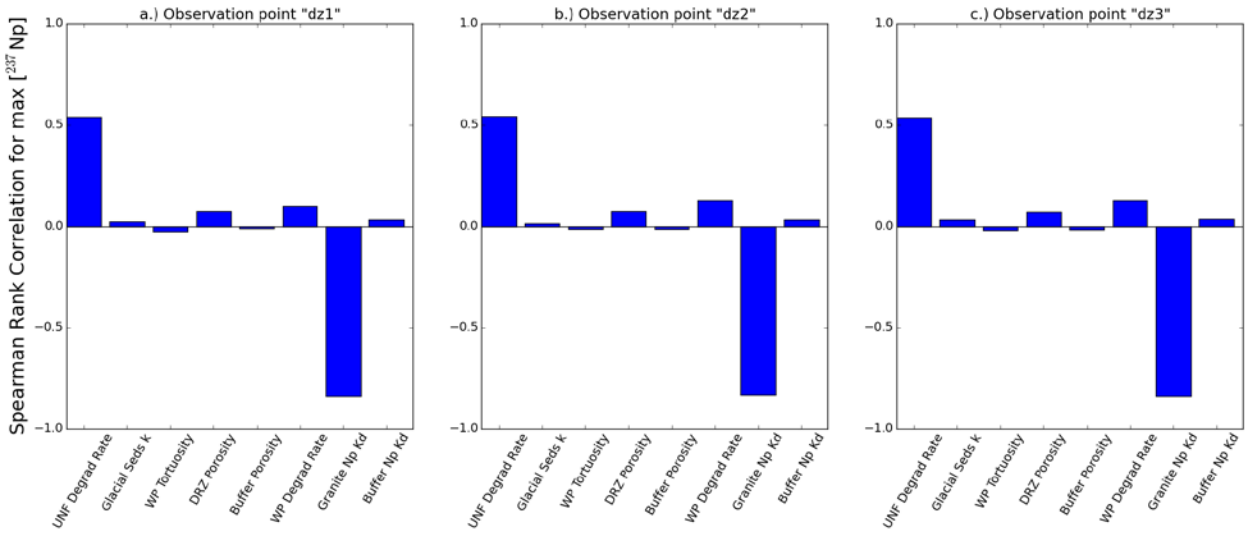

Figure 4-27. Spearman rank correlation coefficients for maximum concentration of ^{237}Np at sediment observation points.

4.5 Reference Case Conclusions

PA simulations for the crystalline reference case took advantage of process models newly integrated into PFLOTRAN including waste package degradation, a new waste form dissolution mechanism, isotope decay and ingrowth in all phases, and fracture flow and transport.

Comparison of breakthrough curves among fifteen fracture realizations and fifty simulations that sampled on other input parameters indicate that the uncertainty in magnitude and timing of predicted concentrations at any given location in the model domain is larger due to fracture distribution than to other sampled parameters. Maximum concentrations of ^{129}I and ^{237}Np are sensitive to properties of the engineered and natural barriers, including waste package degradation and waste form dissolution rates in the engineered barrier, and sorption coefficients and permeability of flow pathways in the natural barrier. Fractured media present new challenges in quantifying uncertainty and sensitivity, which might be addressed through introduction of a performance metric other than concentration (or dose) at a point location.

The current representation of the fractured host rock is biased toward greater connectivity than is likely to exist in a sparsely fractured rock selected for nuclear waste disposal. A large fracture density was necessary for this iteration of the crystalline reference case in order to create a system in which flow and transport occurs in the fractures. Having established the capability of simulating flow and transport in a fractured system, we can in the future 1) determine the influence of deterministic features on flow and transport pathways, and 2) determine the probability of a percolating network existing at various length scales given a realistic description of fractured crystalline rock. If a crystalline rock disposal site is selected, site-specific understanding of deterministic features and of the probability of a percolating network existing at the scales of interest will be necessary.

5. SUMMARY AND CONCLUSIONS

This report describes the FY 2016 activities of the Generic Disposal System Assessment (GDSA) group of the Used Fuel Disposition Campaign (UFDC). The primary mission of the GDSA group is to develop a geologic disposal system modeling capability for nuclear waste that can be used to probabilistically assess the performance of disposal options and proposed sites. The GDSA capability is a framework employing the HPC-capable codes PFLOTRAN and Dakota. In FY 2016 the GDSA group added a host of process modeling capabilities, expanded integration with other work packages for additional process models and data, and developed a new generic reference simulation for the disposal of spent fuel in crystalline rock.

Model development this year focused on the source term, isotope behavior, and fractured rock. Advances include (1) a new canister degradation model and model framework; (2) a fully-integrated waste form process model; (3) an expanded selection of waste form degradation models; (4) a new 3-generation analytical solution for decay and ingrowth; (5) a new isotope partitioning model incorporating element-specific precipitation, dissolution, and adsorption; and (6) a new discrete fracture network (DFN) simulation capability. The DFN capability resulted from close collaboration with members of the UFDC crystalline work package at Los Alamos National Laboratory and Sandia National Laboratories.

As in the previous year, a significant effort was made to further integrate with work packages across the UFDC. Like last year, the GDSA group requested input from the other work packages on process models and data that could be coupled or integrated with the GDSA PA model. Fifteen presentations on proposed new models and other enhancements were made by UFDC scientists at the annual meeting in Las Vegas. Slides of these presentations are included in the appendix of this report. A gap analysis was also performed to identify processes that need to be added to the model. The presentations and gap analysis were used to update the GDSA process model integration table. This table is developed and maintained by the GDSA group to help prioritize future integration and to track the progress and needs of the GDSA PA framework.

The new crystalline repository reference case makes use of the new capabilities added to the GDSA PA framework this year. Probabilistic simulation of radionuclide migration through discrete fracture networks in a multi-million cell, three-dimensional domain is an especially important advance. Realizations of the developed reference case indicate that maximum concentrations of ^{129}I and ^{237}Np at monitored locations in the model domain are sensitive to waste package degradation rates, waste form dissolution rates, and sorption coefficients and are particularly sensitive to fracture distribution. It should be noted that the fractured host rock simulated in this report is biased toward greater connectivity than is likely to exist in a sparsely fractured rock selected for nuclear waste disposal. A large fracture density was necessary for this iteration to create a system in which flow and transport occurs in the fractures. For applications to an actual site, it will be necessary to model identified fracture features and to quantify probabilities of percolating networks at the scales of interest.

Progress in the development of the GDSA framework continues to affirm that HPC-capable codes can be used to simulate important multi-physics couplings directly in a total system performance assessment of a geologic repository. The generic repository applications modeled to date indicate that the developing capability can simulate complex coupled processes in a multi-kilometer domain while simultaneously simulating the coupled behavior of meter-scale features, including every waste package within the domain.

Over the past several years the modeling capabilities of the GDSA framework have greatly advanced. Additional development is needed, however, for a mature PA framework. The challenge is to address the remaining needs using available resources. Meeting this challenge will require close integration with technical teams across the UFDC.

6. REFERENCES

Adams, B. M., K. R. Dalbey, M. S. Eldred, L. P. Swiler, W. J. Bohnhoff, J. P. Eddy, D. M. Vigil, P. D. Hough and S. Lefantzi (2012). DAKOTA, A Multilevel Parallel Object-Oriented Framework for Design Optimization, Parameter Estimation, Uncertainty Quantification, and Sensitivity Analysis: Version 5.2+ User's Manual. SAND2010-2183. Sandia National Laboratories, Albuquerque, New Mexico.

Adams, B. M., M. S. Ebeida, M. S. Eldred, J. D. Jakeman, L. P. Swiler, W. J. Bohnhoff, K. R. Dalbey, J. P. Eddy, K. T. Hu, D. M. Vigil, L. E. Baumann and P. D. Hough (2013). Dakota, a Multilevel Parallel Object-Oriented Framework for Design Optimization, Parameter Estimation, Uncertainty Quantification, and Sensitivity Analysis, Version 5.3.1+ Theory Manual. SAND2011-9106, Updated May 22, 2013, http://dakota.sandia.gov/. Sandia National Laboratories, Albuquerque, New Mexico.

Ames, L. L., J. E. McGarrah and B. A. Walker (1981). Basalt-radionuclide reactions: FY-1981. Annual report. RHO-BW-CR-127-P; PNL-3992; Other: ON: DE83005224 United StatesOther: ON: DE83005224Fri Feb 08 01:12:48 EST 2008NTIS, PC A07/MF A01.HNF; EDB-83-040979English. Pacific Northwest Laboratories, Richland, Washington. OSTI ID: 6553197; Legacy ID: DE83005224.

Ames, L. L., J. E. McGarrah and B. A. Walker (1983). "Sorption of trace constituents from aqueous-solutions onto secondary minerals 2. Radium." Clays and Clay Minerals **31**(5): 335-342.

Anttila, M. (2005). Radioactive Characteristics of the Spent Fuel of the Finnish Nuclear Power Plants. Working Report 2005-71. Posiva Oy, Olkiluoto, Finland.

Arnold, B. W., P. V. Brady, S. J. Bauer, C. Herrick, S. Pye and J. Finger (2011). Reference Design and Operations for Deep Borehole Disposal of High-Level Radioactive Waste. SAND2011-6749. Sandia National Laboratories, Albuquerque, New Mexico.

Ashida, T., T. Shibutani, H. Sato, Y. Tachi, A. Kitamura and K. Kawamura. (1999). "Nuclide Migration Study in the QUALITY-Data Acquisitions for the Second Progress Report." JAEA Sorption Database System, Version 3 Retrieved Sept., 2010, from http://migrationdb.jaea.go.jp/english.html.

Balay, S., J. Brown, K. Buschelman, V. Eijkhout, W. D. Gropp, D. Kaushik, M. G. Knepley, L. Curfman McInnes, B. F. Smith and H. Zhang (2013). PETSc Users Manual. ANL-95/11 – Revision 3.4. Argonne National Laboratory, Argonne, Illinois.

Barton, K. E., D. G. Howell, J. F. Vigil, J. C. Reed and J. O. Wheeler (2003). The North America Tapestry of Time and Terrain. Geologic Investigations Series I-2781. Denver, CO, United States Geological Survey.

Baston, G. M. N., J. A. Berry, K. A. Bond, M. Brownsword and C. M. Linklater. (1991). "Studies of the Effects of Organic Materials on the Sorption of Uranium(IV) and Thorium(IV) on London Clay and Caithness Flagstones." JAEA Sorption Database System, Version 3 Retrieved Sept., 2010, from http://migrationdb.jaea.go.jp/english.html.

Baston, G. M. N., J. A. Berry, M. Brownsword, T. G. Heath, D. J. Ilett, R. McCrohon, C. J. Tweed and M. Yui (1999). The sorption of polonium, actinium and protactinium onto geological materials. Scientific Basis for Nuclear Waste Management Xxii. D. J. Wronkiewicz and J. H. Lee. Warrendale, Materials Research Society. **556:** 1107-1114.

Blacker, T., S. J. Owen, M. L. Staten, R. W. Quador, B. Hanks, B. Clark, R. J. Meyers, C. Ernst, K. Merkley, R. Morris, C. McBride, C. Stimpson, M. Plooster and S. Showman (2016). CUBIT

Geometry and Mesh Generation Toolkit 15.2 User Documentation. SAND2016-1649 R. Sandia National Laboratories, Albuquerque, NM.

Blackwell, D. D., M. C. Richards, Z. S. Frone, J. F. Batir, M. A. Williams, A. A. Ruzo and R. K. Dingwall. (2011). "SMU Geothermal Laboratory Heat Flow Map of the Conterminous United States, 2011." from Supported by Google.org. Available at http://www.smu.edu/geothermal. Retrieved August 21, 2015.

Boudreau, B. P. (1996). "The diffusive tortuosity of fine-grained unlithified sediments." Geochimica Et Cosmochimica Acta **60**(16): 3139-3142.

Bour, O. and P. Davy (1997). "Connectivity of random fault networks following a power law fault length distribution." Water Resources Research **33**(7): 1567-1583.

Carter, J. T., A. J. Luptak, J. Gastelum, C. Stockman and A. Miller (2013). Fuel Cycle Potential Waste Inventory for Disposition. FCRD-USED-2010-000031 Rev 6. Savannah River National Laboratory, Aiken, South Carolina.

Chen, X., G. Hammond, C. Murray, M. Rockhold, V. Vermeul and J. Zachara (2013). "Applications of Ensemble-based Data Assimilation Techniques for Aquifer Characterization using Tracer Data at Hanford 300 Area." Water Resources Research **49**: 7064-7076.

Chen, X., H. Murakami, M. Hahn, G. E. Hammond, M. L. Rockhold, J. M. Zachara and Y. Rubin (2012). "Three-Dimensional Bayesian Geostatistical Aquifer Characterization at the Hanford 300 Area using Tracer Test Data." Water Resources Research **48**.

Cho, W. J., J. S. Kim, C. Lee and H. J. Choi (2013). "Gas permeability in the excavation damaged zone at KURT." Engineering Geology **164**: 222-229.

Choi, H. J. and J. Choi (2008). "Double-layered buffer to enhance the thermal performance in a high-level radioactive waste disposal system." Nuclear Engineering and Design **238**(10): 2815-2820.

Clayton, D., G. Freeze, T. Hadgu, E. Hardin, L. Lee, J. Prouty, R. Rogers, W. M. Nutt, J. Birkholzer, H. H. Liu, L. Zheng and S. Chu (2011). Generic Disposal System Modeling - Fiscal Year 2011 Progress Report. SAND 2011-5828P, FCRD-USED-2011-000184. Sandia National Laboratories, Albuquerque, New Mexico.

DOE (2011). Used Fuel Disposition Campaign Disposal Research and Development Roadmap. F. C. T. Office of Nuclear Energy. FCRD-USED-2011-000065 REV 0. US Department of Energy, Washington, DC.

Downey, J. S. and G. A. Dinwiddie (1988). The Regional Aquifer System Underlying the Northern Great Plains in Parts of Montana, North Dakota, South Dakota, and Wyoming - Summary. Professional Paper 1402-A. United States Geological Survey, Washington, DC.

Erdal, B. R., K. Wolfsberg, R. Vidale, C. Duffy and D. C. Hoffman. (1977). "Laboratory Measurements of Radionuclide Distribution between Selected Ground Waters and Geologic Media." JAEA Sorption Database System, Version 3 Retrieved Sept., 2010, from http://migrationdb.jaea.go.jp/english.html.

Follin, S., L. Hartley, I. Rhen, P. Jackson, S. Joyce, D. Roberts and B. Swift (2014). "A methodology to constrain the parameters of a hydrogeological discrete fracture network model for sparsely fractured crystalline rock, exemplified by data from the proposed high-level nuclear waste repository site at Forsmark, Sweden." Hydrogeology Journal **22**(2): 313-331.

Freeze, G., P. Gardner, P. Vaughn, S. D. Sevougian, P. E. Mariner and V. Mousseau (2013a). Evaluation of Advanced Performance Assessment Modeling Frameworks: Annotated Outline. FCRD-UFD-2013-000218, SAND2013-6913P. Sandia National Laboratories, Albuquerque, New Mexico.

Freeze, G., W. P. Gardner, P. Vaughn, S. D. Sevougian, P. Mariner, V. Mousseau and G. Hammond (2013b). Enhancements to the Generic Disposal System Modeling Capabilities. SAND2013-10532P, FCRD-UFD-2014-000062. Sandia National Laboratories, Albuquerque, New Mexico.

Freeze, G., P. E. Mariner, J. A. Blink, F. A. Caporuscio, J. E. Houseworth and J. C. Cunnane (2011). Disposal System Features, Events, and Processes (FEPs): FY11 Progress Report. FCRD-USED-2011-000254. SAND2011-6059P. Sandia National Laboratories, Albuquerque, New Mexico.

Freeze, G. and P. Vaughn (2012). Development of an Advanced Performance Assessment Modeling Capability for Geologic Disposal of Nuclear Waste: Methodology and Requirements. SAND2012-10208. Sandia National Laboratories, Albuquerque, New Mexico.

Freeze, G., M. Voegele, P. Vaughn, J. Prouty, W. M. Nutt, E. Hardin and S. D. Sevougian (2013c). Generic Deep Geologic Disposal Safety Case. FCRD-UFD-2012-000146 Rev. 1, SAND2013-0974P. Sandia National Laboratories, Albuquerque, New Mexico.

Freeze, R. A. and J. A. Cherry (1979). Groundwater. Englewood Cliffs, New Jersey, Prentice-Hall, Inc.

Gascoyne, M., C. C. Davison, J. D. Ross and R. Pearson (1987). Saline groundwaters and brines in plutons in the Canadian Shield, Special Paper 33. Saline Water and Gases in Crystalline Rocks. P. Fritz and S. K. Frape. Waterloo, Ontario, Geological Association of Canada**:** 53-68.

Hammond, G., P. Lichtner and C. Lu (2007). "Subsurface multiphase flow and multicomponent reactive transport modeling using high performance computing." Journal of Physics: Conference Series 78: 1-10.

Hammond, G. E. and P. Lichtner (2010). "Field-Scale Modeling for the Natural Attenuation of Uranium at the Hanford 300 Area using High Performance Computing." Water Resources Research **46**.

Hammond, G. E., P. C. Lichtner, C. Lu and R. T. Mills (2011a). PFLOTRAN: Reactive Flow and Transport Code for Use on Laptops to Leadership-Class Supercomputers. Groundwater Reactive Transport Models. F. Zhang, G. T. Yeh and J. Parker, Bentham Science Publishers.

Hammond, G. E., P. C. Lichtner, R. T. Mills and C. Lu (2008). "Toward petascale computing in geosciences: application to the Hanford 300 Area." Journal of Physics Conference Series **125**: 12051-12051.

Hammond, G. E., P. C. Lichtner and M. L. Rockhold (2011b). "Stochastic Simulation of Uranium Migration at the Hanford 300 Area." Journal of Contaminant Hydrology **120-121**: 115-128.

Hardin, E., J. Blink, H. Greenberg, M. Sutton, M. Fratoni, J. Carter, M. Dupont and R. Howard (2011). Generic Repository Design Concepts and Thermal Analysis (FY11). FCRD-USED-2011-000143 Rev. 2. Sandia National Laboratories, Albuquerque, New Mexico.

Hardin, E., T. Hadgu, D. Clayton, R. Howard, H. Greenberg, J. Blink, M. Sharma, M. Sutton, J. Carter, M. Dupont and P. Rodwell (2012). Repository Reference Disposal Concepts and Thermal Load Management Analysis. O. o. U. N. F. Disposition. FCRD-UFD-2012-000219 Rev. 2. US Department of Energy, Washington, DC.

Hartley, L. and S. Joyce (2013). "Approaches and algorithms for groundwater flow modeling in support of site investigations and safety assessment of the Forsmark site, Sweden." Journal of Hydrology **500**: 200-216.

Hedin, A. (2008). "Semi-analytic stereological analysis of waste package/fracture intersections in a granitic rock nuclear waste repository." Mathematical Geosciences **40**(6): 619-637.

Huenges, E., J. Erzinger, J. Kuck, B. Engeser and W. Kessels (1997). "The permeable crust: Geohydraulic properties down to 9101 m depth." Journal of Geophysical Research-Solid Earth **102**(B8): 18255-18265.

Hyman, J. D., S. Karra, N. Makedonska, C. W. Gable, S. L. Painter and H. S. Viswanathan (2015a). "dfnWorks: A discrete fracture network framework for modeling subsurface flow and transport." Computers & Geoscience **84**: 10-19.

Hyman, J. D., S. L. Painter, H. Viswanathan, N. Makedonska and S. Karra (2015b). "Influence of injection mode on transport properties in kilometer-scale three-dimensional discrete fracture networks." Water Resources Research **51**(9): 7289-7308.

Ikeda, T. and T. Amaya. (1998). "Model Development of Chemical Evolution in Repository Vol.II Acquisition of Nuclide Migration Data in Near-Field." JAEA Sorption Database System, Version 3 Retrieved Sept., 2010, from http://migrationdb.jaea.go.jp/english.html.

Jerden, J., G. Hammond, J. M. Copple, T. Cruse and W. Ebert (2015). Fuel Matrix Degradation Model: Integration with Performance Assessment and Canister Corrosion Model Development. O. o. U. N. F. Disposition. FCRD-UFD-2015- 000550. US Department of Energy, Washington, DC.

Jobmann, M. and G. Buntebarth (2009). "Influence of graphite and quartz addition on the thermo-physical properties of bentonite for sealing heat-generating radioactive waste." Applied Clay Science **44**(3-4): 206-210.

Joyce, S., L. Hartley, D. Applegate, J. Hoek and P. Jackson (2014). "Multi-scale groundwater flow modeling during temperate climate conditions for the safety assessment of the proposed high-level nuclear waste repository site at Forsmark, Sweden." Hydrogeology Journal **22**(6): 1233-1249.

Kienzler, B., M. Altmaier, C. Bube and V. Metz (2012). Radionuclide Source Term for HLW Glass, Spent Nuclear Fuel, and Compacted Hulls and End Pieces (CSD-C Waste). KIT Scientific Reports 7624. Karlsruhe Institute of Technology, Baden-Württemberg, Germany.

Kitamura, A., T. Tomura and T. Shibutani. (2002). "Sorption Behavior of Neptunium onto Smectite under Reducing Conditions in Carbonate Media." JAEA Sorption Database System, Version 3 Retrieved Sept., 2010, from http://migrationdb.jaea.go.jp/english.html.

Li, Y. H. and S. Gregory (1974). "Diffusion of ions in sea-water and in deep-sea sediments." Geochimica et Cosmochimica Acta **38**(5): 703-714.

Lichtner, P. C. and G. E. Hammond (2012). Quick Reference Guide: PFLOTRAN 2.0 (LA-CC-09-047) Multiphase-Multicomponent-Multiscale Massively Parallel Reactive Transport Code. DRAFT LA-UR-06-7048. December 8, 2012. Los Alamos National Laboratory, Los Alamos, New Mexico.

Lichtner, P. C., G. E. Hammond, C. Lu, S. Karra, G. Bisht, B. Andre, R. Mills and J. Kumar (2015). PFLOTRAN User Manual: A Massively Parallel Reactive Flow and Transport Model for Describing Surface and Subsurface Processes. http://www.pflotran.org/docs/user_manual.pdf.

Liu, J. F., Y. Song, F. Skoczylas and J. Liu (2016). "Gas migration through water-saturated bentonite-sand mixtures, COx argillite, and their interfaces." Canadian Geotechnical Journal **53**(1): 60-71.

Lu, C. and P. C. Lichtner (2007). "High resolution numerical investigation on the effect of convective instability on long term CO2 storage in saline aquifers." Journal of Physics Conference Series **78**: U320-U325.

Mariner, P. E., W. P. Gardner, G. E. Hammond, S. D. Sevougian and E. R. Stein (2015). Application of Generic Disposal System Models. FCRD-UFD-2015-000126, SAND2015- 10037 R. Sandia National Laboratories, Albuquerque, New Mexico.

Mariner, P. E., J. H. Lee, E. L. Hardin, F. D. Hansen, G. A. Freeze, A. S. Lord, B. Goldstein and R. H. Price (2011). Granite Disposal of U.S. High-Level Radioactive Waste. SAND2011-6203. Sandia National Laboratories, Albuquerque, New Mexico

Martino, J. B. and N. A. Chandler (2004). "Excavation-induced damage studies at the Underground Research Laboratory." International Journal of Rock Mechanics and Mining Sciences **41**(8): 1413-1426.

Meacham, P. G., D. R. Anderson, E. J. Bonano and M. G. Marietta (2011). Sandia National Laboratories Performance Assessment Methodology for Long-Term Environmental Programs: The History of Nuclear Waste Management. SAND2011-8270. Sandia National Laboratories, Albuquerque, New Mexico.

Mills, R., C. Lu, P. C. Lichtner and G. Hammond (2007). "Simulating Subsurface Flow and Transport on Ultrascale Computers using PFLOTRAN." Journal of Physics Conference Series **78**: 012051.

Mucciardi, A. N., T. C. Johnson and J. Saunier. (1979). "Statistical Investigation of the Mechanics Controlling Radionuclide Sorption." JAEA Sorption Database System, Version 3 Retrieved Sept., 2010, from http://migrationdb.jaea.go.jp/english.html.

Navarre-Sitchler, A., R. M. Maxwell, E. R. Siirila, G. E. Hammond and P. C. Lichtner (2013). "Elucidating geochemical response of shallow heterogeneous aquifers to CO2 leakage using high-performance computing: implications for monitoring CO2 sequestration." Advances in Water Resources **53**: 44-55.

Noseck, U., J. Flugge, P. Reimus, B. Lanyon, T. Schafer, V. Cvetkovic and I. Blechschmidt (2016). GTS Phase VI – CFM Phase 2: Modelling of Tracer, Colloid, and Radionuclide/Homologue Transport for Dipole 06.002 – Pinkel surface packer. NTB 16-06. NAGRA, Switzerland.

Oda, C., T. Ikeda and M. Shibata. (1999). "Experimental Studies for Sorption Behavior of Tin on Bentonite and Rocks and Diffusion Behavior of Tin in Compacted Bentonite." JAEA Sorption Database System, Version 3 Retrieved Sept., 2010, from http://migrationdb.jaea.go.jp/english.html.

Oelkers, E. H. (1996). Properties of Rocks and Fluids for Mass Transport Calculations. Reactive Transport in Porous Media. P. C. Lichtner, C. I. Steefel and E. H. Oelkers. Washington, D. C., Mineralogical Society of America**:** 131-191.

Ollila, K. (2008). Dissolution of unirradiated UO2 and UO2 doped with 233U in low- and high-ionic strength NaCl under anoxic and reducing conditions. Working Report 2008-50. Posiva Oy, Eurajoki, Finland.

Perry, F. V., R. E. Kelley, P. F. Dobson and J. E. Houseworth (2014). Regional Geology: A GIS Database for Alternative Host Rocks and Potential Siting Guidelines. FCRD-UFD-2014-000068, Unlimited Release Report LA-UR-14-20368. Los Alamos National Laboratory, Los Alamos, New Mexico.

Posiva (2010). Models and Data Report 2010. Posiva Oy, Olkiluoto, Finland.

Rancon, D. and J. Rochon. (1979). "Retention of long-lived radionuclides in different neutral materials." JAEA Sorption Database System, Version 3 Retrieved Sept., 2010, from http://migrationdb.jaea.go.jp/english.html.

Rechard R.P., e. (1995). Performance assessment of the direct disposal in unsaturated tuff of spent nuclear fuel and high-level waste owned by US Department of Energy. SAND94-2563/1,2,3. Sandia National Laboratories, Albuquerque, New Mexico.

Rechard, R. P. (2002). General approach used in the performance assessment for the Waste Isolation Pilot Plant. Scientific Basis for Nuclear Waste Management XXV. Boston, Massachussetts, Materials Research Society.

Rechard, R. P. and C. T. Stockman (2014). "Waste degradation and mobilization in performance assessments of the Yucca Mountain disposal system for spent nuclear fuel and high-level radioactive waste." Reliability Engineering and System Safety **122**(2): 165-188.

Rechard, R. P. and M. S. Tierney (2005). "Assignment of probability distributions for parameters in the 1996 performance assessment for the Waste Isolation Pilot Plant, Part 1: Description of process." Reliability Engineering and System Safety **88**(1): 1-32.

Reimus, P. W., M. Zavarin and Y. Wang (2016). Colloid-Facilitated Radionuclide Transport: Current State of Knowledge from a Nuclear Waste Repository Risk Assessment Perspective. FCRD-UFD-2016-000446. Los Alamos National Laboratory, Los Alamos, New Mexico.

Sassani, D., J. Jang, P. Mariner, L. Price, R. Rechard, M. Rigali, R. Rogers, E. Stein, W. Walkow and P. Weck (2016). The On-line Waste Library (OWL): Usage and Inventory Status Report. FCRD-UFD-2016-000080. Sandia National Laboratories, Albuquerque, New Mexico.

Sassani, D. C., C. F. Jové Colón, P. Weck, J. L. Jerden, K. E. Frey, T. Cruse, W. L. Ebert, E. C. Buck, R. S. Wittman, F. N. Skomurski, K. J. Cantrell, B. K. McNamara and Z. Soderquist (2012). Integration of EBS Models with Generic Disposal System Models. FCRD-UFD-2012-000277, SAND2012-7762P. Sandia National Laboratories, Albuquerque, New Mexico.

Schild, M., S. Siegesmund, A. Vollbrecht and M. Mazurek (2001). "Characterization of granite matrix porosity and pore-space geometry by in situ and laboratory methods." Geophysical Journal International **146**(1): 111-125.

Selroos, J. O., D. D. Walker, A. Strom, B. Gylling and S. Follin (2002). "Comparison of alternative modelling approaches for groundwater flow in fractured rock." Journal of Hydrology **257**(1-4): 174-188.

Sevougian, S. D., G. A. Freeze, W. P. Gardner, G. E. Hammond and P. E. Mariner (2014). Performance assessment modeling and sensitivity analyses of generic disposal system concepts. SAND2014-17658. Sandia National Laboratories, Albuquerque, New Mexico.

Sevougian, S. D., G. A. Freeze, P. Vaughn, P. Mariner and W. P. Gardner (2013). Update to the Salt R&D Reference Case. FCRD-UFD-2013-000368, SAND2013-8255P. Sandia National Laboratories, Albuquerque, New Mexico.

Shelton, S. M. (1934). "Thermal conductivity of some irons and steels over the temperature range 100 to 500 C." Bureau of Standards Journal of Research **12**(4/6): 441-450.

SKB (2004). SR-Can Data and uncertainty assessment: Migration parameters for the bentonite buffer in the KBS-3 concept. TR-04-18. Svensk Karnbranslehantering AB, Stockholm, Sweden.

SKB (2006a). Data report for the safety assessment SR-Can. SKB TR-06-25. Svensk Kärnbränslehantering AB, Stockholm, Sweden.

SKB (2006b). Long-term safety for KBS-3 repositories at Forsmark and Laxemar – a first evaluation. SKB TR-06-09. Svensk Kärnbränslehantering AB, Stockholm, Sweden.

SKB (2007). Geology Forsmark. R-07-45. Svensk Karnbranslehantering AB, Stockholm, Sweden.

SKB (2008). Bedrock hydrogeology Forsmark. R-08-45. Svensk Karnbranslehantering AB, Stockholm, Sweden.

Soler, J. M., J. Landa, V. Havlova, Y. Tachi, T. Ebina, P. Sardini, M. Siitari-Kauppi, J. Eikenberg and A. J. Martin (2015). "Comparative modeling of an in situ diffusion experiment in granite at the Grimsel Test Site." Journal of Contaminant Hydrology **179**: 89-101.

Stauffer, D. and A. Aharony (1994). Introduction to Percolation Theory. Boca Raton, FL, CRC Press.

Stone, D., D. C. Kamineni, A. Brown and R. Everitt (1989). "A Comparison of Fracture Styles in 2 Granite Bodies of the Superior Province." Canadian Journal of Earth Sciences **26**(2): 387-403.

Tachi, Y. and T. Shibutani. (1999). "Sorption and Diffusion Behavior of Radium on Bentonite and Rocks." JAEA Sorption Database System, Version 3 Retrieved Sept., 2010, from http://migrationdb.jaea.go.jp/english.html.

Tachi, Y., T. Shibutani, Y. Nishikawa and T. Shinozaki. (1999a). "Sorption Behavior of Selenium on Bentonite and Granodiorite under Reducing Conditions." JAEA Sorption Database System, Version 3 Retrieved Sept., 2010, from http://migrationdb.jaea.go.jp/english.html.

Tachi, Y., T. Shibutani, H. Sato and M. Shibata. (1999b). "Sorption and Diffusion Behavior of Palladium in Bentonite, Granodiorite and Tuff." JAEA Sorption Database System, Version 3 Retrieved Sept., 2010, from http://migrationdb.jaea.go.jp/english.html.

Taki, H. and K. Hata. (1991). "Measurement Study on Distribution Coefficient and Effective Diffusion Coefficient for Some Rocks and Bentonite." JAEA Sorption Database System, Version 3 Retrieved Sept., 2010, from http://migrationdb.jaea.go.jp/english.html.

Twiss, R. J. and E. M. Moores (1992). Structural Geology. New York, W. H. Freeman and Company.

Ueta, S. (1998). "Development of Database System for Performance Assessment(III)." JAEA Sorption Database System, Version 3 Retrieved Sept., 2010, from http://migrationdb.jaea.go.jp/english.html.

Ulrich, H. J. and C. Degueldre (1993). "The sorption of Pb-210, Bi-210 and Po-210 on montmorillonite - A study with emphasis on reversibility aspects and on the effect of the radioactive decay of adsorbed nuclides." Radiochimica Acta **62**(1-2): 81-90.

Vaughn, P., G. Freeze, J. Lee, S. Chu, K. D. Huff, W. M. Nutt, T. Hadgu, R. Rogers, J. Prouty, E. Hardin, B. Arnold, E. Kalinina, W. P. Gardner, M. Bianchi, H. H. Liu and J. Birkholzer (2013). Generic Disposal System Model: Architecture, Implementation, and Demonstration. FCRD-UFD-2012-000430 Rev. 1, SAND2013-1539P. Sandia National Laboratories, Albuquerque, New Mexico.

Vosteen, H. D. and R. Schellschmidt (2003). "Influence of temperature on thermal conductivity, thermal capacity and thermal diffusivity for different types of rock." Physics and Chemistry of the Earth **28**(9-11): 499-509.

Wang, Y., P. Gardner, P. Reimus, S. L. Painter, N. Makedonska, A. Pollack, J. Houseworth, J. Rutqvist, D. Asahina, F. Chen, V. Vilarrasa, H. H. Liu, J. Birkholzer, J. D. Begg, M. Zavarin, A. Kersting and G. Y. Kim (2013). Natural System Evaluation and Tool Development – International Collaborations: FY13 Progress Report. FCRD-UFD-2013-000628. Sandia National Laboratories, Albuquerque, New Mexico.

Wang, Y., T. Hadgu, E. A. Kalinina, J. Jerden, J. M. Copple, T. Cruse, W. Ebert, E. Buck, R. Eittman, R. Tinnacher, C. Tournassat, J. Davis, H. Viswanathan, S. Chu, T. Dittrich, F. Hyman, S. Karra, N. Makedonska, P. Reimus, M. Zavarin and C. Joseph (2016). Used Fuel Disposition in Crystalline Rocks: FY16 Progress Report. FCRD-UFD-2016-000076, SAND2015-9297 R. Sandia National Laboratories, Albuquerque, New Mexico.

Wang, Y., T. Hadgu, E. Matteo, J. N. Kruichak, M. M. Mills, R. Tinnacher, J. Davis, H. S. Viswanathan, S. Chu, T. Dittrich, F. Hyman, S. Karra, N. Makedonska, P. Reimus, M. Zavarin, P. Zhao, C.

Joseph, J. B. Begg, Z. Dai, A. B. Kersting, J. Jerden, J. M. Copple, T. Cruse and W. Ebert (2015). Used Fuel Disposal in Crystalline Rocks: FY15 Progress Report. FCRD-UFD-2015-000125. Sandia National Laboratories, Albuquerque, New Mexico.

Wang, Y., E. Matteo, J. Rutqvist, J. Davis, L. Zheng, J. Houseworth, J. Birkholzer, T. Dittrich, C. W. Gable, S. Karra, N. Makedonska, S. Chu, D. Harp, S. L. Painter, P. Reimus, F. V. Perry, P. Zhao, J. B. Begg, M. Zavarin, S. J. Tumey, Z. R. Dai, A. B. Kersting, J. Jerden, K. E. Frey, J. M. Copple and W. Ebert (2014). Used Fuel Disposal in Crystalline Rocks: Status and FY14 Progress. FCRD-UFD-2014-000060, SAND2014-17992 R. Sandia National Laboratories, Albuquerque, New Mexico.

Weast, R. C. and M. J. Astle, Eds. (1981). CRC Handbook of Chemistry and Physics. Boca Raton, Florida, CRC Press, Inc.

Zhou, Q. L., H. H. Liu, F. J. Molz, Y. Q. Zhang and G. S. Bodvarsson (2007). "Field-scale effective matrix diffusion coefficient for fractured rock: Results from literature survey." Journal of Contaminant Hydrology **93**(1-4): 161-187.

APPENDIX A: MODEL INTEGRATION PRESENTATIONS

Table A-1. Model integration presentations from the 2016 UFDC Working Group Meeting.

Used Fuel Disposition Campaign

Introduction and Objectives for GDSA ⇔ Process Model Integration

S. David Sevougian
Sandia National Laboratories

2016 UFDC Annual Working Group Meeting
Process Model Integration Session, June 8, 2016
Las Vegas, NV

Sandia National Laboratories is a multi-program laboratory managed and operated by Sandia Corporation, a wholly owned subsidiary of Lockheed Martin Corporation, for the United States Department of Energy's National Nuclear Security Administration under contract DE-AC04-94AL85000. *SAND2016-5295PE*.

Used Fuel Disposition

Outline

- Timeline and context
- PA model philosophy
- Linkages: PA model ⇔ process models
- Model integration template
- Goals of this session
- Agenda

Used Fuel Disposition

Timeline and Context

You are here

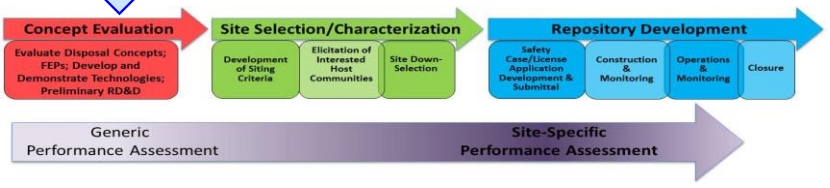

Performance Assessment Functions

1. **Evaluate potential disposal concepts/sites in various host rock media throughout the timeline**
2. **Help prioritize modeling and testing RD&D activities:**

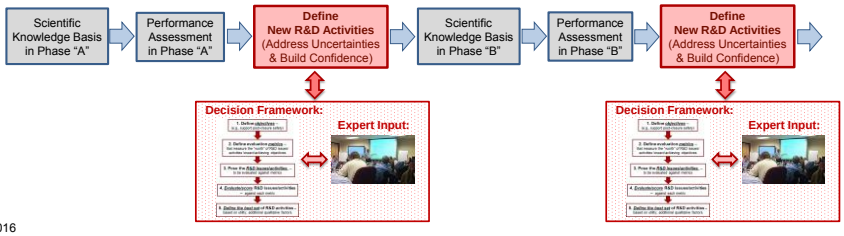

Used Fuel Disposition

GDSA-PA Philosophy

- **Direct representation in PA model of significant coupled multi-physics processes in three dimensions (3-D), over a large heterogeneous domain**
  - *Lessening reliance on assumptions, simplifications, and process abstractions*
- **Realistic spatial resolution of features and processes**
  - *Explicit representation of all waste packages*
- **Appropriate quantification and propagation of uncertainties, based on model form and data availability at various spatial scales**

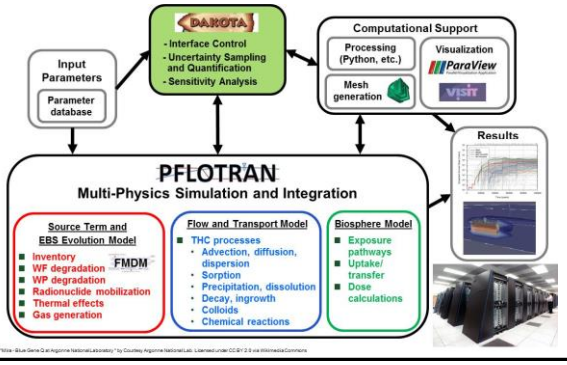

Used Fuel Disposition

Linkages: GDSA ⇔ Process Models

- **Crystalline workscope structure (based on FEPs):**
  - Generally applicable to other concepts/media: clay, salt, DBH

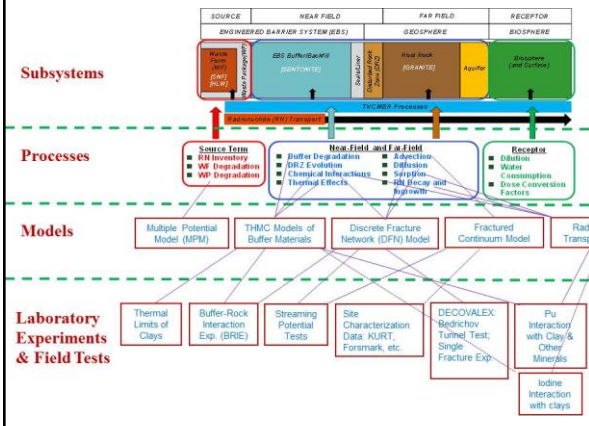

- **GDSA workscope/ model/code structure:**

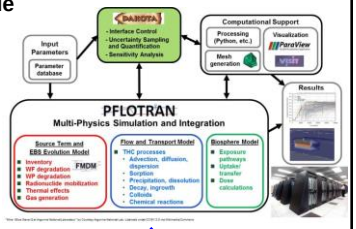

Used Fuel Disposition

Process Model Integration Template

Model Integration Template – Integration with PA

1.	**Name of Model:**
2.	**Principal Investigator(s) and Affiliation:**
3.	**Brief Model Description:** • Describe the processes and/or events considered in the model, as well as the applicable feature (e.g., waste form, DRZ, etc.), i.e., include a description of the FEP or FEPs addressed by this model.
4.	**R&D Issue(s) and Safety Case Objectives Addressed by This Model:** • How will the modeled FEP(s) affect repository performance (especially biosphere dose) in a meaningful way? • Why is it important from a regulatory perspective? • Describe the current "state of the art" knowledge regarding the issue(s) addressed and why this particular model advances the state of the art in an important way.
5.	**Proposed method for coupling this model to the PA model**[1] • Direct coupling or abstraction? • Time scale of transient modeled processes (10 years, 100 years…. 1,000,000 years?). • Degree of abstraction: reduced dimensionality; simplified representation; response surface. • Key environmental inputs required from the PA model (and its coupled submodels) and key outputs delivered by this model. • Are there other models you are aware of that are not being developed, which are needed for your model or for PA?
6.	**Real time integration horizon: estimate how long before the proposed model is ready for integration with PA and how long the integration activities might take?** • Are there intermediate steps or degrees of coupling with PA, e.g., can you couple a certain version of your model in an expedited fashion and then go to the next more detailed version—please describe how

[1] The PA simulation framework is based on PFLOTRAN, which is a parallel Fortran 2003/2008 code running in an HPC environment. A desired goal is to reduce the level of "abstraction" required, relative to previous PAs, like Yucca Mtn. However, your model must have reasonable run times in relation to all other parts of the PA model.

In 2015 (last FY):

- **17 templates received from process modelers**
- **4 additional templates internal to GDSA**
- **10 chosen for additional information**

Thank you! But please update, as the model evolves!

Used Fuel Disposition

Objective and Goal: This Session

- **OBJECTIVE: Facilitate the integration of UFD process modeling with GDSA by addressing:**
  - (1) *Integration progress* made during FY 2016, and
  - (2) *How* the process model can be coupled to the GDSA-PA Framework in FY17 and beyond.
- **GOAL: The outcome of this session is envisioned to be a rough scope/timeline for integration of process models with GDSA-PA, with an emphasis on FY17 workscope.**
- **METHODS: Response surfaces are NOT the preferred coupling method. Direct coupling or reduced-order mechanistic models (ROMs) are preferred.**

June 8, 2016 7

Used Fuel Disposition

Agenda

3:50 – 3:55 Introduction and Objectives (Sevougian)

3:55 – 4:15 LIGHTNING Talks on Ongoing FY2015-16 Integration (5 min per talk)

1. Density dependence on salinity – **crystalline (deep borehole)** (**Hammond**)
2. DFN Model – **crystalline** (**Stein/Makedonska**)
3. Colloid-facilitated transport model (progress and future work) – **all media** (**Reimus**)
4. CSNF degradation model (FMDM) – **all media** (**Jerden**)

4:15 – 5:20 LIGHTNING Talks on Possible New FY17 Integration Workscope (5 min/talk)

5. Salt coupled THM processes (TOUGH-FLAC) – **salt** (**Rutqvist**)
6. THC Processes in salt – **salt** (**Stauffer**)
7. TOUGH-FLAC/BBM/RBSN models – **argillite and/or crystalline (deep borehole)** (**Rutqvist**)
8. THMC model (illitization) and THM model (TPHM Hooke's) – **argillite** (**Zheng**)
9. DFN enhancements – **granite** (**Viswanathan**)
10. Waste package degradation – **argillite and/or crystalline** (**Jove-Colon**)
11. Waste package and waste form degradation – **all media** (**Frederick**)
12. Glass degradation – **all media** (**Rieke**)
13. Grid refinement – **all media** (**Alzraiee/Hammond**)
14. THM processes in salt (PFLOTRAN-Adagio) – **salt** (**Park/Hammond**)
15. A control variate method for performance assessment – **all media** (**MacKinnon**)
16. Remaining process model gaps – **all media** (**Mariner**)

Herr Hammond

5:20 – 5:40 Integration discussion (All)

June 8, 2016 8

Used Fuel Disposition Campaign

PFLOTRAN Process Modeling: Density Dependence on Salinity

Glenn Hammond
Sandia National Laboratories

2016 UFDC Annual Working Group Meeting
Integration Session, June 8, 2016
Las Vegas, NV

Sandia National Laboratories is a multi-program laboratory managed and operated by Sandia Corporation, a wholly owned subsidiary of Lockheed Martin Corporation, for the United States Department of Energy's National Nuclear Security Administration under contract DE-AC04-94AL85000. SAND2016-5319 PE

Used Fuel Disposition

Motivation

- Brine density is heavily dependent upon solute concentrations in saline aquifers.
- How to implement a salinity-dependent brine density for all flow process models within PFLOTRAN without doubling the number of flow process models?

Used Fuel Disposition

PFLOTRAN Process Model Coupler (PMC)

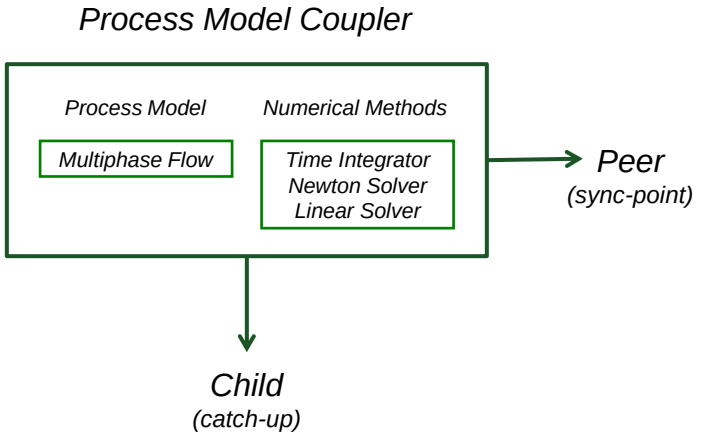

3

Used Fuel Disposition

Hypothetical PFLOTRAN PMC Hierarchy

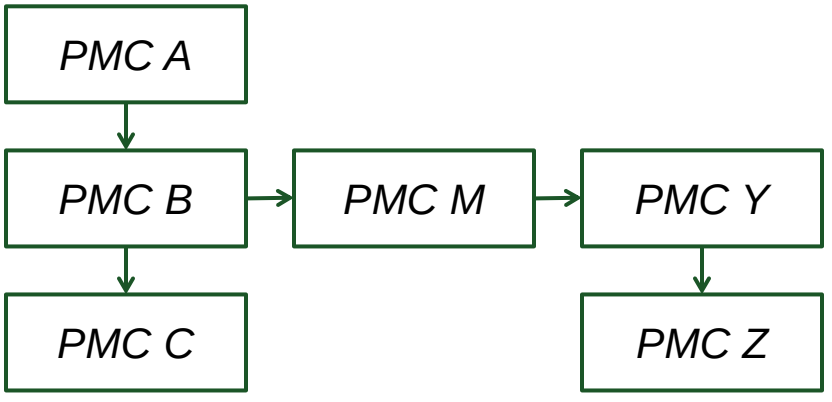

4

Used Fuel Disposition

Salinity Update Process Model

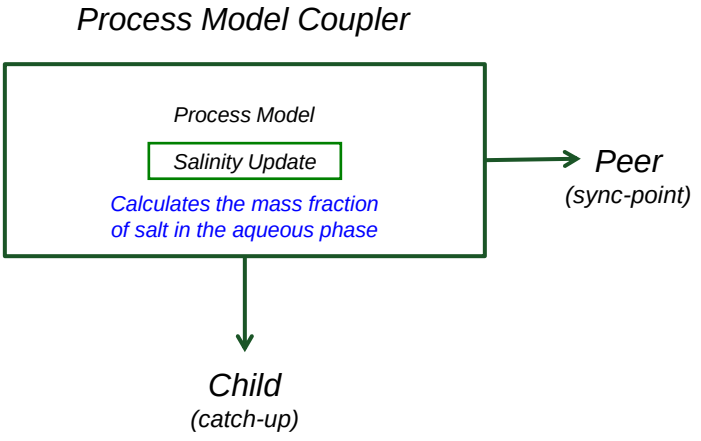

5

Used Fuel Disposition

PFLOTRAN Salinity Update

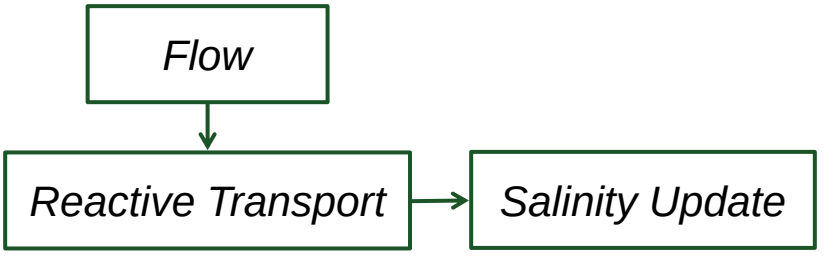

6

Used Fuel Disposition

PFLOTRAN::EOS::EOS_Water:: EOSXXXBatzleAndWang()

Batzle, M and Z. Wang, (1992) Seismic properties of pore fluids, Geophysics, V57, N11, P 1396-1408.

Water Density [g/cm^3]

$$\rho_W = 1 + 1 \times 10^{-6}(-80T - 3.3T^2 + 0.00175T^3 + 489P - 2TP + 0.016T^2P - 1.3 \times 10^{-5}T^3P - 0.333P^2 - 0.002TP^2) \quad (27a)$$

Brine Density [g/cm^3]

$$\rho_B = \rho_W + S\{0.668 + 0.44S + 1 \times 10^{-6}[300P - 2400PS + T(80 + 3T - 3300S - 13P + 47PS)]\}, \quad (27b)$$

Brine Viscosity [mPa-s]

$$\eta = 0.1 + 0.333S + (1.65 + 91.9S^3) \exp\{-[0.42(S^{0.8} - 0.17)^2 + 0.045]T^{0.8}\}. \quad (32)$$

P = pressure [Pa], T = temperature [C], S = mass fraction [-]

7

Used Fuel Disposition

Modifications to the PFLOTRAN Input Deck

```
SIMULATION
  SIMULATION_TYPE SUBSURFACE
  PROCESS_MODELS
    SUBSURFACE_FLOW flow
      MODE RICHARDS
    /
    SUBSURFACE_TRANSPORT transport
      GLOBAL_IMPLICIT
    /
    AUXILIARY SALINITY
      SPECIES Na+ 22.9898
      SPECIES Cl- 35.4527
    /
  /
/

...

EOS WATER
  DENSITY BATZLE_AND_WANG
  VISCOSITY BATZLE_AND_WANG
/
```

8

Used Fuel Disposition

PFLOTRAN Workflow

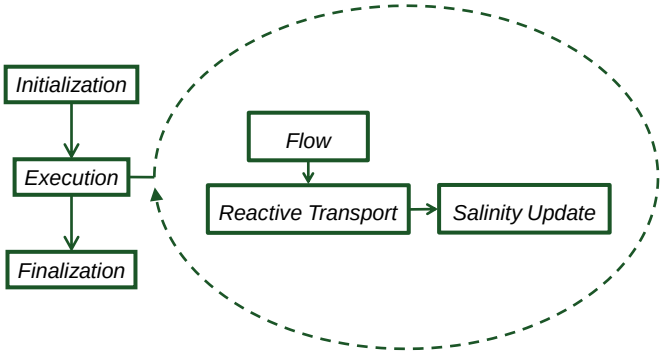

9

Used Fuel Disposition

Density Driven Flow from Salt Layer

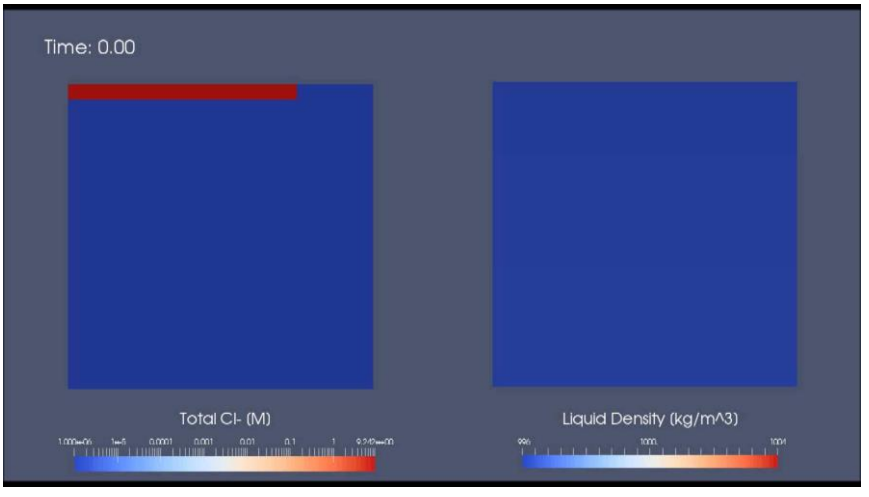

Kuhlman, 2016

10

Used Fuel Disposition Campaign

Integrating Discrete Fracture Networks with Performance Assessment

Emily Stein, Kris Kuhlman
Sandia National Laboratories
Nataliia Makedonska, Satish Karra, Jeffrey Hyman
Los Alamos National Laboratory

2016 UFDC Annual Working Group Meeting
GDSA Integration Session, June 8, 2016
Las Vegas, NV

Sandia National Laboratories is a multi-program laboratory managed and operated by Sandia Corporation, a wholly owned subsidiary of Lockheed Martin Corporation, for the United States Department of Energy's National Nuclear Security Administration under contract DE-AC04-94AL85000. SAND2016-5225P

Used Fuel Disposition

Motivation

- **Crystalline Reference Case requires:**

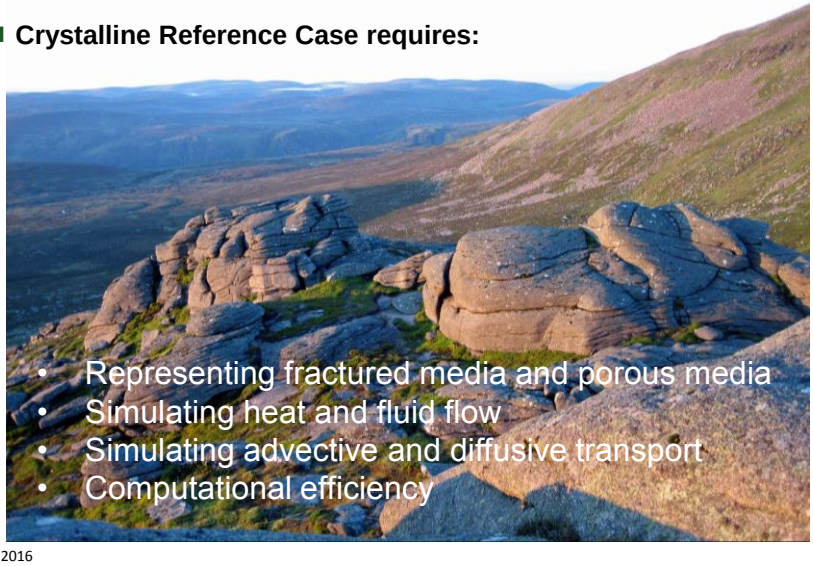

Used Fuel Disposition

Options

- Couple Discrete Fracture Network with Continuous Porous Medium

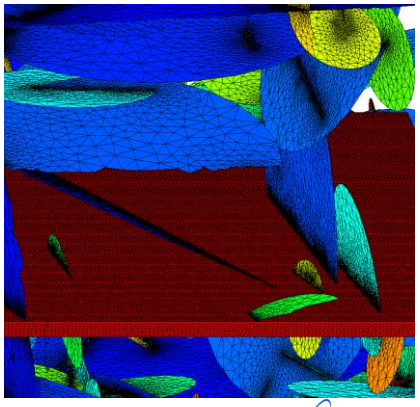

OR

- Map *DFN* to *CPM*

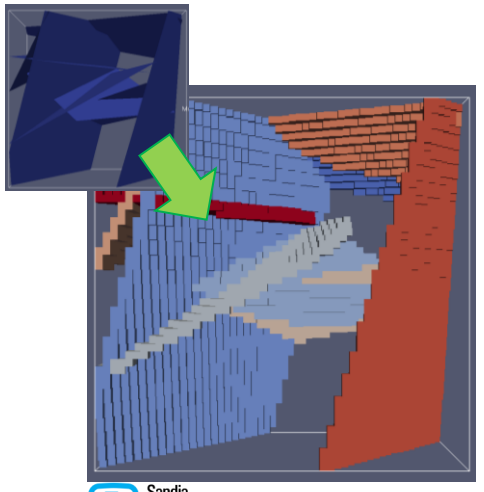

Los Alamos NATIONAL LABORATORY EST. 1943

Sandia National Laboratories

Used Fuel Disposition

Method

Los Alamos NATIONAL LABORATORY EST. 1943

DFNWorks

1. Generate DFN
2. Assign aperture and transmissivity to each fracture

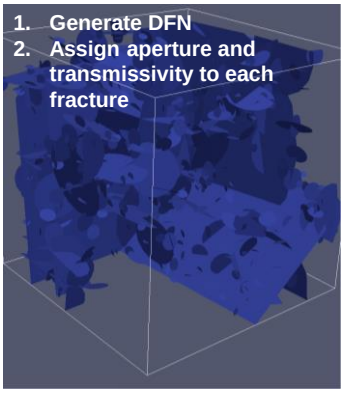

$b=(12T\mu/\rho g)^{1/3}$

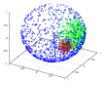

$T=\log(1.6*10^{-9}*r^{0.8})$

$k = T\rho g/\mu b$

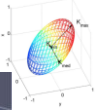

$\phi = V_f/V_{cell}$

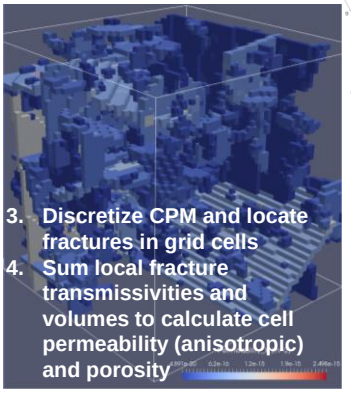

3. Discretize CPM and locate fractures in grid cells
4. Sum local fracture transmissivities and volumes to calculate cell permeability (anisotropic) and porosity

mapDFN

Sandia National Laboratories

Used Fuel Disposition

Compare:

	DFN	CPM
Number of cells	~1.7 million	287,496
Time to 1 My	103 minutes	1.9 minutes
Path length	the standard	longer
Connectivity	the standard	greater

3.

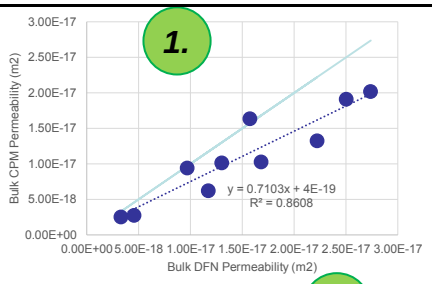

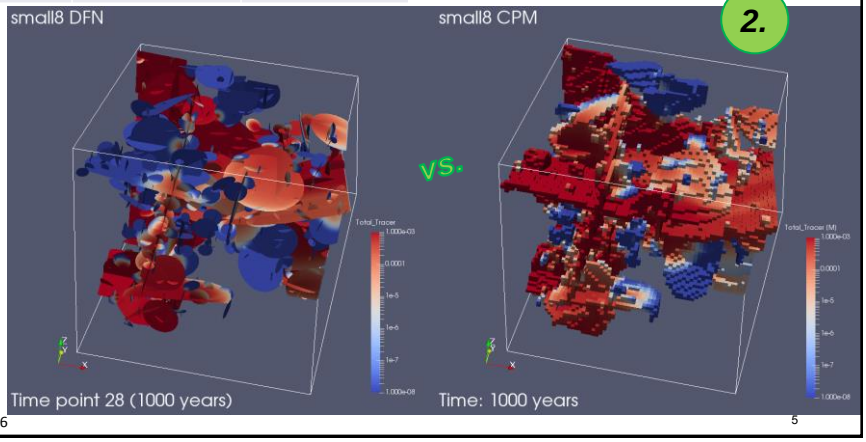

Used Fuel Disposition

Success!

- **DFN mapped to CPM:**

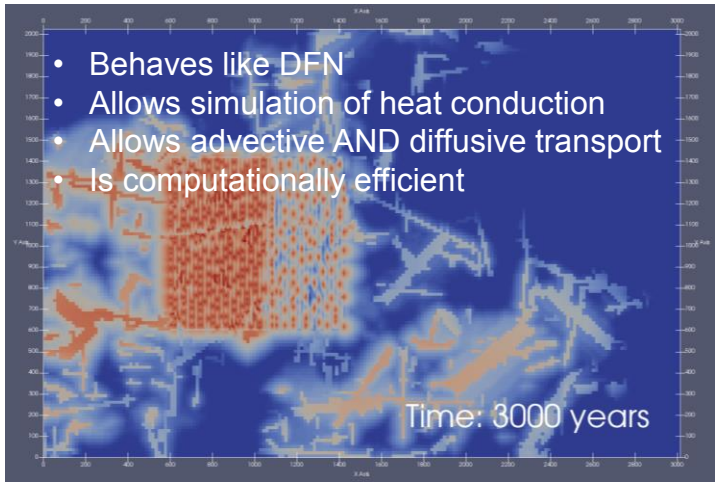

Used Fuel Disposition Campaign

Next-Gen PA Model: Approach for Colloid-Facilitated Transport

Paul Reimus and Mavrik Zavarin

Model Integration Session
UFD Working Group Meeting
June 8, 2016

Used Fuel Disposition

Two Transport Regimes – Easy to Model, Difficult to Mechanistically Parameterize

$$R_{eff} = \frac{1+\frac{\rho_B}{\phi}K_d + K_{d,col}C_{col}}{1 + K_{d,col}C_{col}} \approx \frac{1+\frac{\rho_B}{\phi}K_d}{1 + K_{d,col}C_{col}}$$

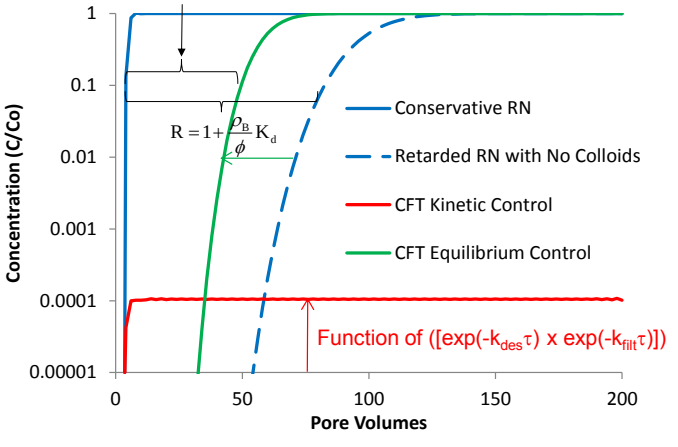

Used Fuel Disposition

Colloid Transport Equations

- **Colloid Transport (General):**

$$\frac{\partial C_c}{\partial t} + div(v_c C_c + D_c \nabla C_c) =$$

$$\underbrace{-k_{fc}\frac{SA}{V}C_c\left(1-\frac{S_c}{S_{c,max}}\right)+k_{rc}\frac{SA}{V}S_c}_{\text{Reversible Filtration}} \underbrace{-k_{fc,ir}\frac{SA}{V}C_c\left(1-\frac{S_{c,ir}}{S_{c,ir,max}}\right)}_{\text{Irreversible Filtration}} + \underbrace{\frac{SA}{V}P_c}_{\text{Production}}$$

Mobile Colloids

$$\frac{\partial S_c}{\partial t} = k_{fc}C_c\left(1-\frac{S_c}{S_{c,max}}\right) - k_{rc}S_c$$

Reversibly Immobilized Colloids

$$\frac{\partial S_{c,ir}}{\partial t} = k_{fc,ir}C_c\left(1-\frac{S_{c,ir}}{S_{c,ir,max}}\right)$$

Irreversibly Immobilized Colloids

- **At a true steady state,** $\frac{\partial S_c}{\partial t} = 0$, **and** $P_c \cong k_{fc,ir}C_c\left(1-\frac{S_{c,ir}}{S_{c,ir,max}}\right)$

Assume colloids limited to flowing domain

Used Fuel Disposition

Solute Transport Equations

- **Mobile Solute Transport Equation:**

$$\frac{\partial C_a}{\partial t} + div(v_a C_a + D_a \nabla C_a) =$$

$$\sum_{i=1}^{nsites}\left[-k_{as,i}\frac{\rho_B}{\emptyset}C_a\left(1-\frac{S_{a,i}}{S_{a,max,i}}\right)+k_{sa,i}\frac{\rho_B}{\emptyset}S_{a,i}\right] +$$

$$\sum_{i=1}^{ncolsites}\left[-k_{ac,i}C_aC_c\left(1-\frac{C_{ac,i}C_c}{C_{ac,max,i}C_c}\right)+k_{ca,i}C_{ac,i}C_c\right] +$$

$$\sum_{i=1}^{ncolsites}\frac{SA}{V}\left[-k_{ac,i}C_aS_c\left(1-\frac{C_{ac,i}S_c}{C_{ac,max,i}S_c}\right)+k_{ca,i}C_{ac,i}S_c - k_{ac,i}C_aS_{c,ir}\left(1-\frac{C_{ac,i}S_{c,ir}}{C_{ac,max,i}S_{c,ir}}\right)\right]$$

\+ *terms accounting for matrix diffusion or diffusion into secondary porosity*

- **Solute Sorbed onto Immobile Surfaces (*nsites* equations):**

$$\frac{\partial S_{a,i}}{\partial t} = k_{as,i}C_a\left(1-\frac{S_{a,i}}{S_{a,max,i}}\right) - k_{sa,i}S_{a,i}$$

(Flowing domain only; more terms needed if secondary porosity)

Used Fuel Disposition

Solute Associated with Colloids Equations

- **Solute Sorbed to Mobile Colloids (*ncolsites* equations):**

$$\frac{\partial C_{ac,i}C_c}{\partial t} + div\left(v_a C_{ac,i}C_c + D_c \nabla C_{ac,i}C_c\right) = k_{ac,i}C_{ac,i}C_c\left(1 - \frac{C_{ac,i}C_c}{C_{ac,max,i}C_c}\right) - k_{ca,i}C_{ac,i}C_c$$
$$-k_{fc}\frac{SA}{V}C_{ac,i}C_c\left(1 - \frac{S_c}{S_{c,max}}\right) + k_{rc}\frac{SA}{V}C_{ac,i}S_c - k_{fc,ir}\frac{SA}{V}C_{ac,i}C_c\left(1 - \frac{S_{c,ir}}{S_{c,ir,max}}\right)$$

- **Solute Sorbed to Immobile Colloids (*ncolsites* equations):**

$$\frac{\partial C_{ac,i}S_c}{\partial t} = k_{ac,i}C_a S_c\left(1 - \frac{C_{ac,i}S_c}{C_{ac,max,i}S_c}\right) - k_{ca,i}C_{ac,i}S_c +$$
$$k_{ac,i}C_a S_{c,ir}\left(1 - \frac{C_{ac,i}S_{c,ir}}{C_{ac,max,i}S_{c,ir}}\right) - k_{ca,i}C_{ac,i}S_{c,ir}$$
$$-k_{fc}C_{ac,i}C_c\left(1 - \frac{C_{ac,i}S_c}{C_{ac,max,i}S_c}\right) + k_{rc}C_{ac,i}S_c - k_{fc,ir}C_{ac,i}S_c\left(1 - \frac{C_{ac,i}S_{c,ir}}{C_{ac,max,i}S_{c,ir}}\right)$$

Used Fuel Disposition

Additional Solute Detail on Colloid or Immobile Media Surfaces

- **Transformations on Surfaces (from Mavrik, with extensions/generalizations from Paul):**

Surface Mediated-Reduction With 'Aging' of Reduced Surface Species

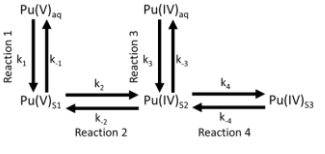

Aging Process Only

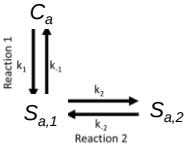

Two Sorption Sites with Surface Transformation

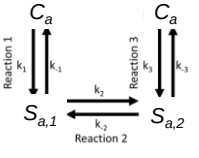

Surfaces could be Colloids or Immobile Media

Used Fuel Disposition

Total Conservative Mass Fraction – A Simplification

- **'Convolution' of fraction of nonfiltering colloids with fraction of nondesorbing solutes**
- **That is, 'fraction of solute not desorbing from fraction of colloids not filtering over transport time τ', given by:**

$$= \int_0^{k_{fc,max}} Exp\left[-\left(\frac{SA}{V}\right)k_{fc}\tau\right]\left\{\int_0^{k_{ca,max}} \{Exp[-k_{ca}\tau]\, P[k_{ca}]\}\, dk_{ca}\right\}_{k_{fc}} P[k_{fc}]\, dk_{fc}$$

Used Fuel Disposition

Other Simplifications

- **If the time scale of transport is long relative to both forward and reverse rates of any given reaction, that reaction can be assumed to be at equilibrium**
  - Good rule of thumb is if $(SA/V)k_f\tau >$ 5-10 and $k_f\tau >$ 5-10, then equilibrium assumption is good
  - Also, if sorption/filtration site density (S_{max}) is very large, then linear K_d-type approach works
- **Every linear equilibrium assumption reduces number of equations by one (sorbed or filtered species equation is eliminated)**
- **Special case of all reactions being at equilibrium and having a steady-state colloid concentration, C_{col}:**

Solute Transport Eq.: $$\frac{\partial C}{\partial t} + v_f\frac{\partial C}{\partial x} - D_c\frac{\partial^2 C}{\partial x^2} + \frac{\rho_B}{\phi}K_d\frac{\partial C}{\partial t} + K_cC_{col}\frac{\partial C}{\partial t} + v_fK_cC_{col}\frac{\partial C}{\partial x} = 0$$

Rearranged: $$\left(1+\frac{\rho_B}{\phi}K_d + K_cC_{col}\right)\frac{\partial C}{\partial t} + (1+K_cC_{col})v_f\frac{\partial C}{\partial x} - D_c\frac{\partial^2 C}{\partial x^2} = 0$$

Effective Solute Retardation Factor: $$R_C = \frac{1+\frac{\rho_B}{\phi}K_d + K_cC_{col}}{1+K_cC_{col}}$$

Note $K_d = k_{as}/k_{sa}$, $K_c = k_{ac}/k_{ca}$

Used Fuel Disposition

Fuel Matrix Degradation Model

James Jerden, Kurt Frey, Bill Ebert
Argonne National Laboratory

ACKNOWLEDGMENT: This work is supported by the U.S. Department of Energy, Office of Nuclear Energy, Used Fuel Disposition Campaign

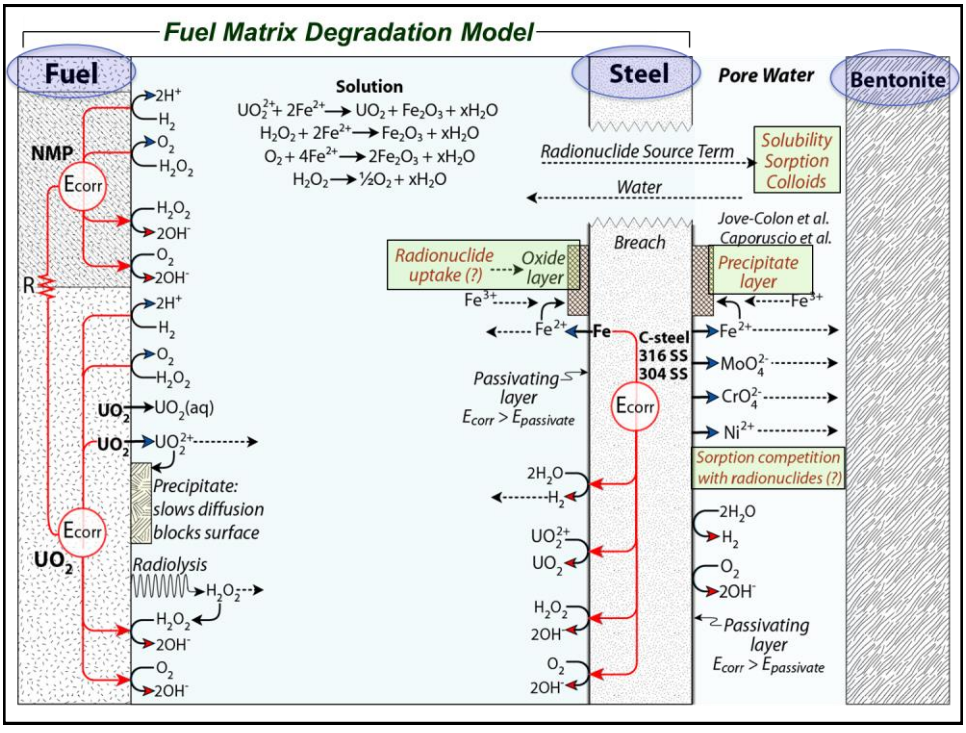

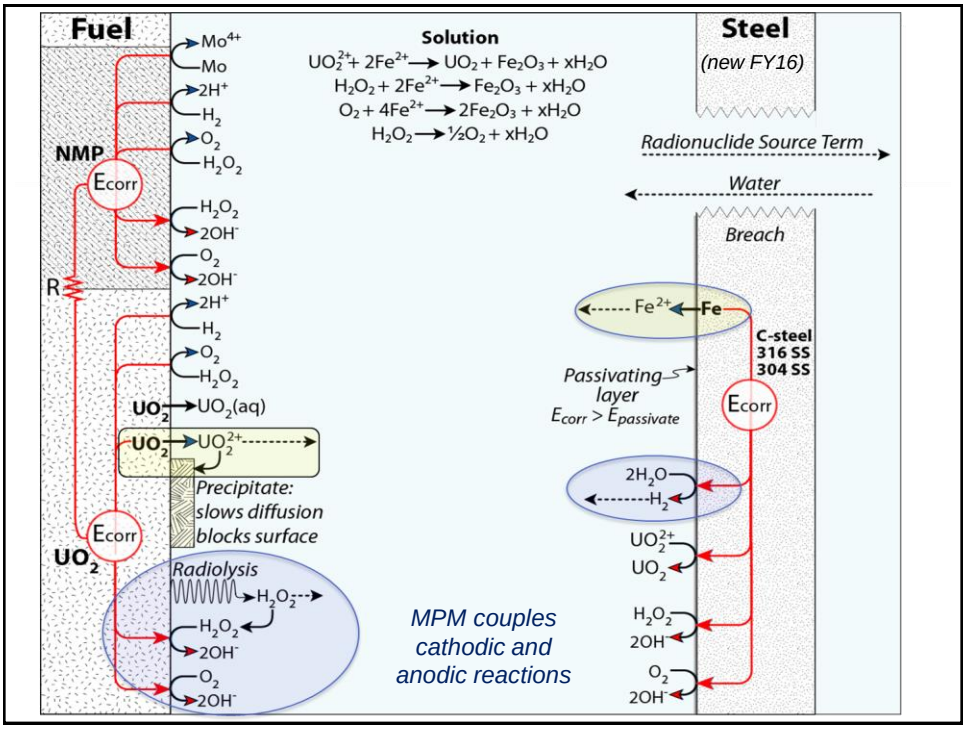
Fuel
Steel
(new FY16)
Solution
$UO_2^{2+} + 2Fe^{2+} \rightarrow UO_2 + Fe_2O_3 + xH_2O$
$H_2O_2 + 2Fe^{2+} \rightarrow Fe_2O_3 + xH_2O$
$O_2 + 4Fe^{2+} \rightarrow 2Fe_2O_3 + xH_2O$
$H_2O_2 \rightarrow ½O_2 + xH_2O$
NMP
Ecorr
R
UO_2
Mo^{4+}
Mo
$2H^+$
H_2
O_2
H_2O_2
$2OH^-$
$UO_2(aq)$
UO_2^{2+}
Precipitate:
slows diffusion
blocks surface
Radiolysis
Radionuclide Source Term
Water
Breach
Fe^{2+}
Fe
C-steel
316 SS
304 SS
Passivating layer
$E_{corr} > E_{passivate}$
$2H_2O$
MPM couples cathodic and anodic reactions

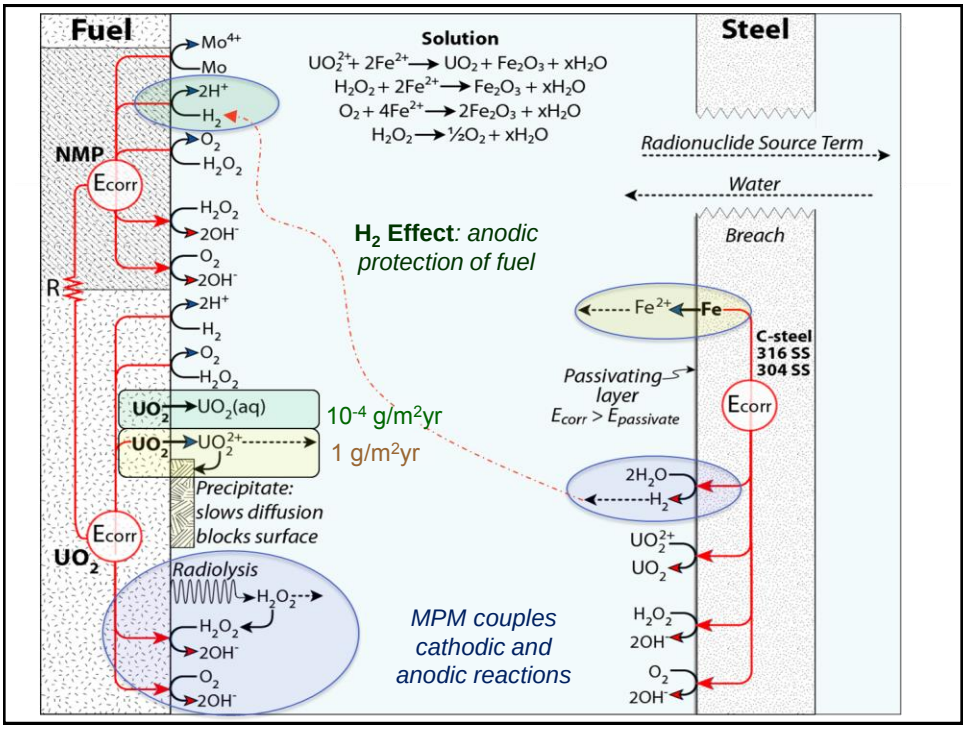
Fuel
Steel
Solution
$UO_2^{2+} + 2Fe^{2+} \rightarrow UO_2 + Fe_2O_3 + xH_2O$
$H_2O_2 + 2Fe^{2+} \rightarrow Fe_2O_3 + xH_2O$
$O_2 + 4Fe^{2+} \rightarrow 2Fe_2O_3 + xH_2O$
$H_2O_2 \rightarrow ½O_2 + xH_2O$
NMP
Ecorr
R
UO_2
Mo^{4+}
Mo
$2H^+$
H_2
O_2
H_2O_2
$2OH^-$
$UO_2(aq)$
UO_2^{2+}
Precipitate:
slows diffusion
blocks surface
Radiolysis
Radionuclide Source Term
Water
Breach
Fe^{2+}
Fe
C-steel
316 SS
304 SS
Passivating layer
$E_{corr} > E_{passivate}$
$2H_2O$
H_2 Effect: anodic protection of fuel
10^{-4} g/m²yr
1 g/m²yr
MPM couples cathodic and anodic reactions

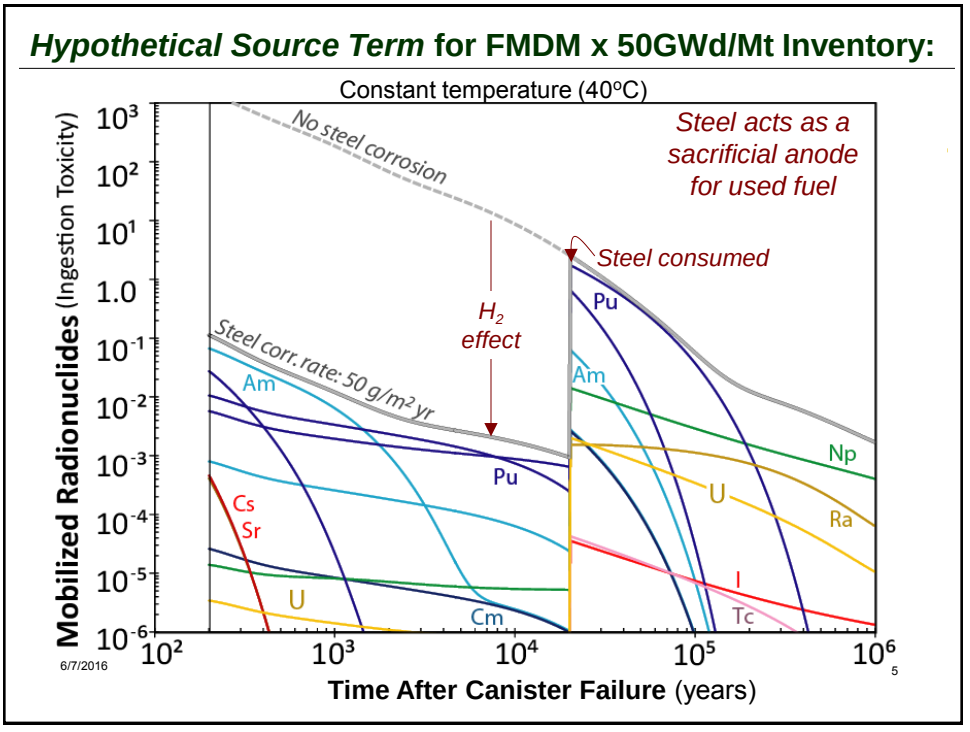
Hypothetical Source Term for FMDM x 50GWd/Mt Inventory:
Constant temperature (40°C)
Mobilized Radionuclides (Ingestion Toxicity)
No steel corrosion
Steel acts as a sacrificial anode for used fuel
Steel consumed
H2 effect
Steel corr. rate: 50 g/m2 yr
Am
Pu
Cs
Sr
U
Cm
Np
Ra
I
Tc
6/7/2016
Time After Canister Failure (years)

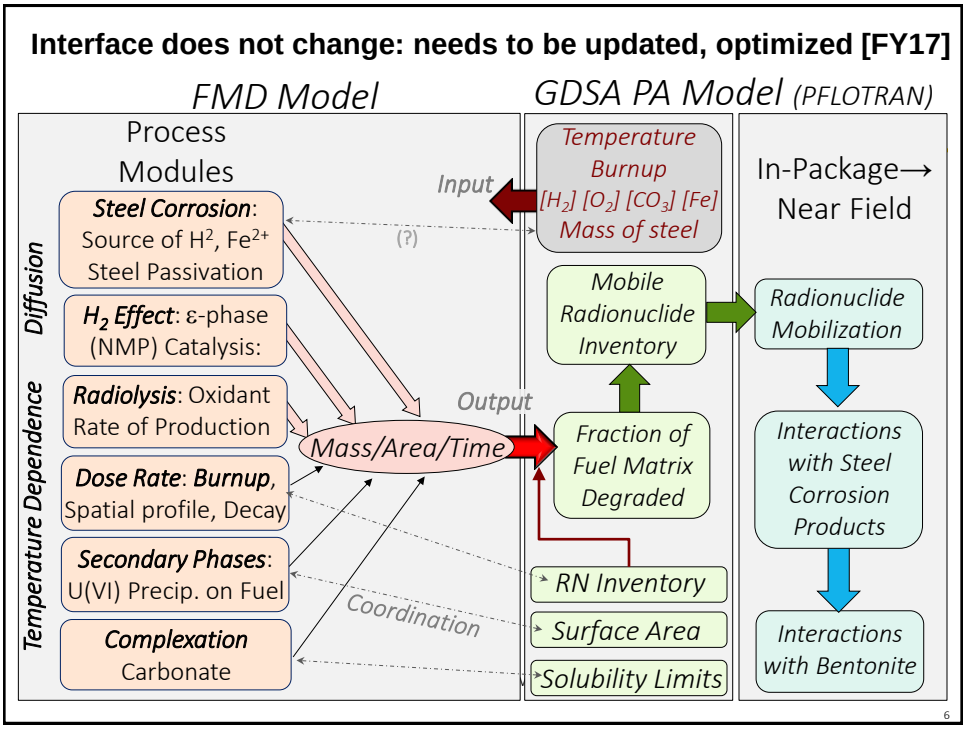
Interface does not change: needs to be updated, optimized [FY17]
FMD Model
GDSA PA Model (PFLOTRAN)
Process Modules
Steel Corrosion: Source of H2, Fe2+ Steel Passivation
H2 Effect: ε-phase (NMP) Catalysis:
Radiolysis: Oxidant Rate of Production
Dose Rate: Burnup, Spatial profile, Decay
Secondary Phases: U(VI) Precip. on Fuel
Complexation Carbonate
Diffusion
Temperature Dependence
Input
(?)
Output
Mass/Area/Time
Coordination
Temperature Burnup [H2] [O2] [CO3] [Fe] Mass of steel
Mobile Radionuclide Inventory
Fraction of Fuel Matrix Degraded
RN Inventory
Surface Area
Solubility Limits
In-Package→ Near Field
Radionuclide Mobilization
Interactions with Steel Corrosion Products
Interactions with Bentonite

Used Fuel Disposition

Fuel Matrix Degradation Model: Development and Integration

- **FY16 Integration Accomplishments**
  - As part of the addition of steel corrosion to FMDM we optimized the code:
    - *Improved math for flux calculations to improve stability and avoiding recursion*
    - *Code profiling to identify computing bottlenecks and approaches to addressing these: sparse functions, clean up how U oxidation/reduction in bulk reactions, etc.*
- **FY17 Needs**
  - Update & optimize FMDM – PA interface code *(FMDM Fortran):*
    - *Build on successful integration runs by GDSA in FY16*
  - Validation of FMDM rates
  - Investigate processes that could counteract H_2 effect: *Br, S, others?*
  - *Communicate with canister design/selection group - inform decisions where there is flexibility in design*

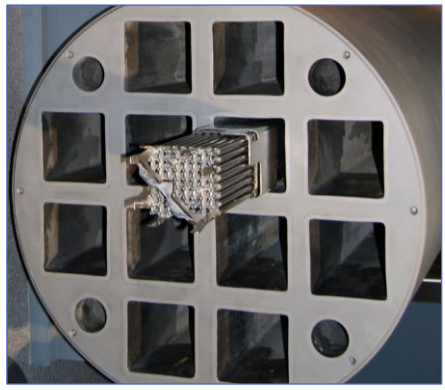

Used Fuel Disposition

Discussion Slides

Used Fuel Disposition

Fuel Matrix Degradation Model V.3

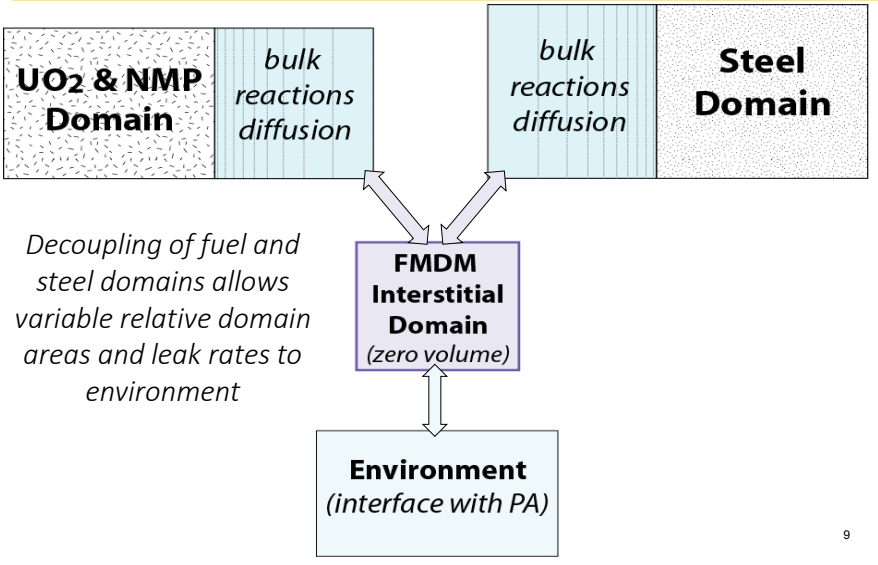

9

Used Fuel Disposition

Ideas for optimization

- Use **sparse functions**: The overall FMDM system is very sparse (>99.5% of matrix have values of zero). Sparse matrix implementation would probably speed things up considerably – *not done originally because we didn't want to complicate building the code with the need for external libraries.*
- More than half of the total simulation time for a 100ka run is spent on getting the very **first time step** to converge. Later time steps use the solutions from previous time steps and finish much more rapidly. Need to store FMDM step results rather than re-initializing (*already done?*).
- Getting rid of **recursion** in the surface reaction function wouldn't speed things up too much because it doesn't branch out with multiple self-calls; it's really two completely different functions that were lumped together. The motivation for that lumping was to avoid duplicating the surface reactions in multiple places.

Used Fuel Disposition Campaign

Salt Coupled THM Processes – TOUGH-FLAC

TOUGH-FLAC *provides a model framework for modeling* ***coupled THM processes in the EBS and host rock and their interactions*** *using state-of-the-art macroscopic constitutive models for bentonite, crushed rock salt backfill, clay, salt and crystalline host rocks*

Jonny Rutqvist
Lawrence Berkeley National Laboratory

UFD WG Meeting in Las Vegas
Model Integration Session
June 9, 2016

Used Fuel Disposition

Salt Coupled THM Processes – TOUGH-FLAC

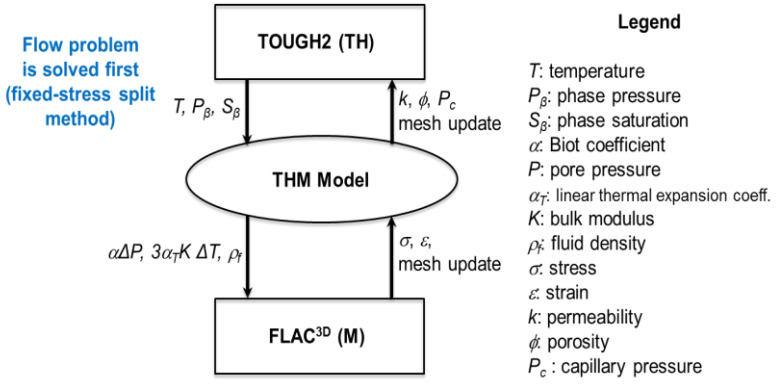

- *Lux/Wolters solid salt constitutive model (creep, TM damage-induced permeability (DZ), high pressure fluid filtration, sealing, heating)*
- *Crushed salt constitutive model (THM properties as a function of compaction and solidification)*
- *Large-strain and deformable mesh*
- *Brine migration, evaporation, condensation, salt precipitation etc. (THMC)*

Used Fuel Disposition

Salt Coupled THM Processes – TOUGH-FLAC

Associated FEPS:

The most closely associated FEP is 2.1.01.01 (see below – from the UFD Roadmap spreadsheet/tables). Related FEPs are Flow Through the EBS (2.1.08.01), 2.1.08.03 (Flow through Backfill), 2.1.08.06 (Alteration and Evolution of EBS Flow Pathways), 2.1.08.09 (Influx/Seepage Into the EBS), Open Boreholes (1.1.01.01), Thermal Effects on Flow in EBS (2.1.11.10), 2.2.01.01 (Evolution of EDZ) , Flow Through Host Rock (2.2.08.01), Effects of Excavation on Flow (2.2.08.04), Mechanical Effects from Preclosure Operations (1.01.02.02), Heat Generation in EBS (2.1.11.01), Effects of Backfill on EBS Thermal Environment (2.1.11.03), Effects of Drift Collapse on EBS Thermal Environment (2.1.11.04), Effects of Influx (Seepage) on Thermal Environment (2.1.11.05), Thermal-Mechanical Effects on Backfill (2.1.11.08), Thermally-Driven Buoyant Flow / Heat Pipes in EBS (2.1.11.12), Effects of Gas on Flow Through the EBS (2.1.12.02), Gas Transport in EBS (2.1.12.03), Thermal-Mechanical Effects on Geosphere (2.2.11.06)

Objective	Feature	Process (Issue)		
		UFD FEP ID	UFD FEP Title	Process/Issue Description
Limited Release – Natural Barriers	Natural System - Geosphere	2.2.01.01	Evolution of EDZ	- Lateral extent, heterogeneities - Physical properties - Flow pathways - Chemical characteristics of groundwater in EDZ - Radionuclide speciation and solubility in EDZ - Thermal-mechanical effects - Thermal-chemical alteration

Used Fuel Disposition

Salt Coupled THM Processes – TOUGH-FLAC

Affect on repository performance:

Coupled THM processes are relatively short-lived from safety assessment perspective, but could potentially give rise to permanent changes, such as formation of a damaged zone around excavations that could provide a path for transport of radionuclides if released from a waste package.

As for the natural salt, it is well known that its initial tightness could be affected by processes that take place at different stages during the lifetime of a repository.

1) *Development of an excavation damaged zone (EDZ) around the mined openings represents a potential risk because preferential flow pathways could be created.*

1) *A pore pressure-driven percolation process (fluid infiltration) can take place if the pore pressure locally exceeds the minimum compressive principal stress.*

These perturbations, however, are generally not persistent in a plastic medium such as rock salt. Once the stress regime becomes favorable, healing takes place. Healing processes consist in the development of cohesion between former crack planes (in extension of pore space closure).

Used Fuel Disposition

Salt Coupled THM Processes – TOUGH-FLAC

Example THM induced flow in the near field:

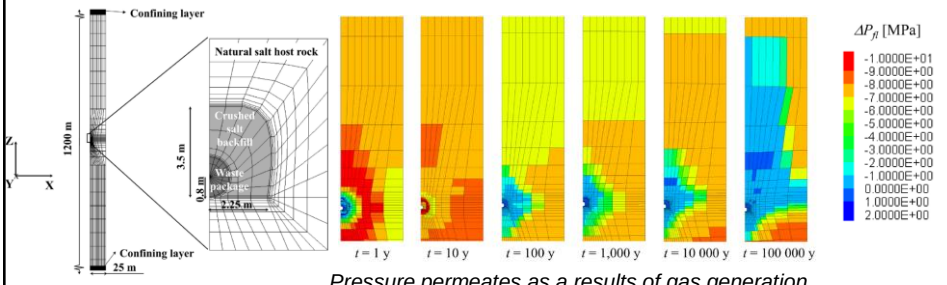

Pressure permeates as a results of gas generation

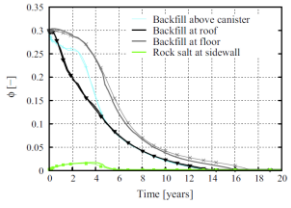

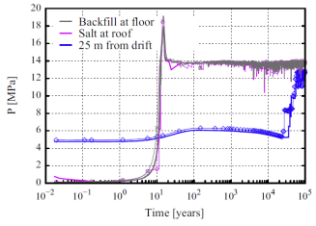

Used Fuel Disposition

Salt Coupled THM Processes – TOUGH-FLAC

State of the art:

- *Damage, healing and percolation processes within natural salt have been thoroughly studied at the laboratory scale and have been included in advanced, validated constitutive relationships. Damage and healing have also been observed in various field studies.*
- *The Lux-Wolters constitutive model, is the most comprehensive model for salt THM behavior, including damage, sealing and healing, although similar constitutive models have been developed at other academic institutions is Germany.*
- *For modeling salt and consolidation of the EBS, coupling under large strain has been developed and tested for TOUGH-FLAC, and creep is also included and linked through the Lux-Wolters model.*
- *In a salt repository, the analysis of EDZ evolution must be conducted using a model that includes both the EBS and host rock and their interactions, meaning that the evolution of the host rock or the evolution of the EBS cannot be analyzed independently.*

Used Fuel Disposition

Salt Coupled THM Processes – TOUGH-FLAC

Coupling to the PA model:

- *The TOUGH-FLAC with salt constitutive THM models provides a tool for calculating the evolution of the crushed salt backfill and the host rock, including the disturbed rock zone (DRZ) from just after emplacement to over 100,000 years.*
- *The analysis for coupling to the PA model might be conducted in a 2D cross-section of one emplacement drift or alternative a 3D model focused on the near field of an emplacement tunnel or a few emplacement tunnels in different parts of a repository and for different FEPs such as nominal case or such as for cases of extensive gas generation.*
- *The **input** required is the geometry, heat source, THM properties of buffer and host rock, initial THM conditions (such as in situ stress).*
- *The **output** to the PA model would be the changes in flow properties (e.g. permeability and porosity) in the EBS and near-field including the buffer and DRZ and also to inform PA related to local flow created by coupled THM processes.*

Used Fuel Disposition

Salt Coupled THM Processes – TOUGH-FLAC

When ready for integration?

- *2D analysis over 100,000 year has been demonstrated and could provide output to PA today for currently implemented constitutive models*
- *3D has also been demonstrated associated with modeling of large-scale field tests over tens of years and could potentially be extended to thousands of years if considering multiple tunnels in parts of a repository*
- *For larger models including 3D of multiple emplacement tunnels and shafts to be included in this kind of model, more efficient calculations would be necessary, which could be solved with future porting of TOUGH-FLAC for high performance computing. Such porting of the FLAC3D code is planned to be conducted within the next few years.*

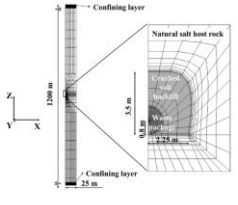

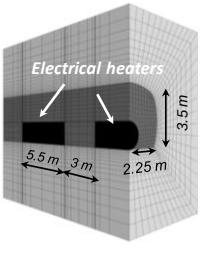

U.S. DEPARTMENT OF ENERGY | Nuclear Energy

Thermo-Hydro-Chemical Coupling in Salt

(0) **WHY** the given process model is important to PA

(1) **Integration progress** made during FY16

(2) **HOW** the process model can be coupled to the GDSA-PA framework in FY17 and beyond.

Phil Stauffer
Los Alamos National Laboratory

Los Alamos NATIONAL LABORATORY EST. 1943

U.S. DEPARTMENT OF ENERGY
Nuclear Energy

Thermo-Hydro-Chemical Coupling in Salt

- (0) *WHY* the given process model is important to PA

Short term evolution of water in backfill

Strong feedback of water on consolidation

Dehydration of ubiquitous impurities

Generation of acid vapors (HCl)

Los Alamos NATIONAL LABORATORY EST. 1943

U.S. DEPARTMENT OF ENERGY
Nuclear Energy

Thermo-Hydro-Chemical Coupling in Salt

■(1) **Integration progress** made during FY16

LANL and SNL working to add capability to PFLOTRAN based on FEHM experience with code validation tests

- Given a constant flow rate we compared the FEHM solution to an analytical solution for water removal using the holding capacity of 20°C air and the air-flow rate
- FEHM and PFLOTRAN successfully dry out the matrix water and remove the water in vapor form

Los Alamos NATIONAL LABORATORY EST. 1943

Sandia National Laboratories

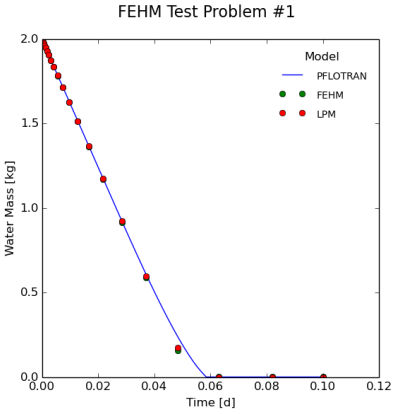

3

U.S. DEPARTMENT OF ENERGY
Nuclear Energy

Thermo-Hydro-Chemical Coupling in Salt

■(2) **HOW** the process model can be coupled to the GDSA-PA framework in FY17 and beyond.

A) We envision that the current coupled processes could be added to PFLOTRAN in the next years to allow our numerical techniques to be performed in massive parallel on a UFD standard code.

B) Possibility to reduce the total number of process calculations based on results of planned field testing.

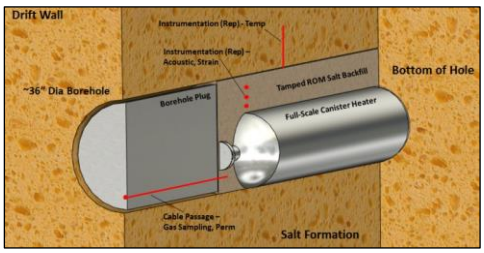

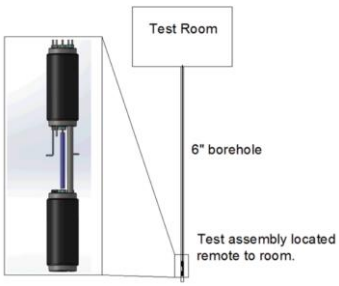

4

U.S. DEPARTMENT OF ENERGY
Nuclear Energy

Thermo-Hydro-Chemical Coupling in Salt

Thanks

5

U.S. DEPARTMENT OF ENERGY
Nuclear Energy

Lightning Goals

3:50 – 5:40 pm, Wednesday, June 8 – Rm. 1243

OBJECTIVE: Facilitate the integration of UFD process modeling with the GDSA Performance Assessment Model. During this session we will review information about 14 process models, to be given in a series of five-minute "lightning" talks that encompass:

(1) Integration progress made during FY16

(2) How the process model can be coupled to the GDSA-PA framework in FY17 and beyond. (Response surfaces are NOT the preferred coupling method. Direct coupling or reduced-order mechanistic models (ROMs) are preferred.)

GOAL: The outcome of this session is envisioned to be a tentative scope/timeline for integration of process models with GDSA-PA, with an emphasis on FY17 workscope.

6

U.S. DEPARTMENT OF ENERGY

Nuclear Energy

- **Hi All,**
- **The Integration Session at the 2015 UFD June Working Group meeting was quite successful, and we've made good progress through the year (which we will report upon at this year's meeting). The five-minute LIGHTNING talks were a particular favorite of the DOE customer and various managers! (See attached presentation excerpt for a list of last year's talks.)**
- **Based on our ongoing success and the importance of this effort to our DOE customer, we wish to hold another such session this June to help formulate plans for ongoing and new integration during FY2017. We already have some Lightning talks in mind but in order to choose the best candidates for further integration between Performance Assessment (PA) and Process Modeling, we (Dave Sevougian, Yifeng Wang, Carlos Jove-Colon, Kevin McMahon, Bob MacKinnon) are again requesting your input. Our request goes beyond just Crystalline and Argillite, as we would like to include all repository concepts in the modeling integration, including Salt, Deep Borehole, and Defense Repository.**
- **Specifically, we request that by April 29th you revise your old Model Integration Templates in Track Changes to indicate progress, changes, and new ideas for integrating with PA (email back to me). Also, if you'd like to provide a completely new template/new idea, we welcome that. (WIPP folks may want to contact Glenn Hammond in this regard.)**
- **I've attached all the pertinent info from the GDSA Deliverable of FY2015. This attached file has a blank model template, as well as all the filled-out model templates provided by you last year. In addition, it includes the current version of the Model Integration Table (current as of the deliverable date)---feel free to comment on it as you see fit.**
- **Thanks for your help in this matter and once we receive the updated templates (or your indication that nothing has changed), we will finalize the schedule for the Lightning Talks and let you know if you've been picked to "come on down". I've attached the latest draft of the June Working Group Meeting schedule. Note that the Integration Session is the same time/day as last year, so mark your calendars (Wednesday, 3:50 pm)! It should be fun. J**
- **If you have any questions, please feel free to contact me. Or, if I've forgotten to cc someone, please feel free to forward this e-mail.**
-

March 2016 7

Used Fuel Disposition Campaign

TOUGH-FLAC/BBM/RBSN models – clay and/or crystalline (deep borehole)

TOUGH-FLAC *provides a model framework for modeling* ***coupled THM processes in the EBS and host rock and their interactions*** *using state-of-the-art macroscopic constitutive models for bentonite, crushed rock salt backfill, clay, salt and crystalline host rocks*

Jonny Rutqvist
Lawrence Berkeley National Laboratory

UFD WG Meeting in Las Vegas
Model Integration Session
June 9, 2016

Used Fuel Disposition

TOUGH-FLAC with BBM and BExM

TOUGH-FLAC

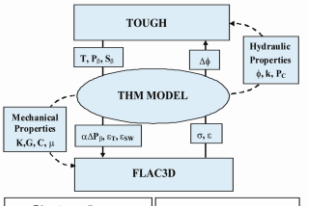

—— Direct couplings
– – Indirect coupling

C = Cohesion
G = Shear modulus
K = Bulk modulus
k = Intrinsic permeability
P_β = Pressure of phase β
P_c = Capillary pressure
S_β = Saturation of phase β

T = Temperature
ε = Strain
ε_T = Thermal strain
ε_{SW} = Swelling strain
α = Biot's parameter
ϕ = Porosity
μ = Coefficient of friction
σ = Stress

1) Barcelona Basic Model (BBM)

A constitutive model for thermo-elasto-plastic behavior of unsaturated soils (bentonite)

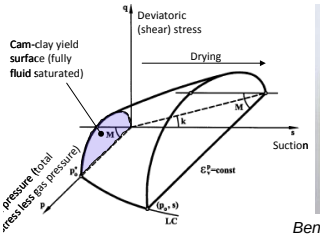

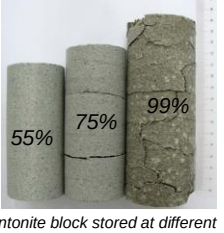

Bentonite block stored at different relative humidity (Teodori et al 2011)

- Shear strength and stiffness depends on saturation (or suction)
- Wetting-induced swelling or collapse strains

2) Barcelona Expansive Model (BExM)

- Micro- and macro-structure
- Proper modeling of fluid flow through macro pores and their changes with stress and saturation
- Provides a link for coupling mechanics with chemistry

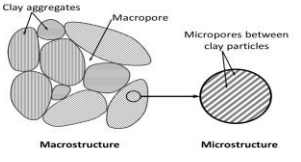

Used Fuel Disposition

TOUGH-FLAC with BBM and BExM

Affect on repository performance:

*Coupled **THM processes are relatively short-lived** from safety assessment perspective, but could potentially give rise to **permanent changes**, such as formation of a damaged zone around excavations that could provide a path for transport of radionuclides if released from a waste package.*

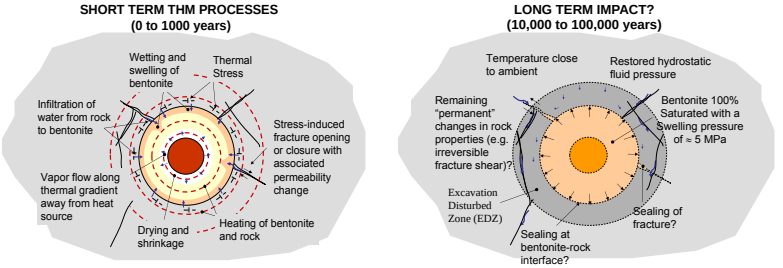

*The **mechanical evolution and swelling of the protective buffer are imperative to its functions**, such as to provide long-term mechanical support to seal the excavation damage zone and to prevent further damage during the thermal peak.*

*At the same time, the mechanical evolution of the buffer is governed **by complex coupled interactions** with temperature and hydraulics, between micro and macro clay structures, as well as with the host rock*

Used Fuel Disposition

TOUGH-FLAC/BBM/RBSN Models

Associated FEPS:

The most closely associated FEP is 2.1.04.01 (see below – from the UFD Roadmap spreadsheet/tables). Related FEPs are Flow Through the EBS (2.1.08.01), 2.1.08.03 (Flow through Backfill), 2.1.08.06 (Alteration and Evolution of EBS Flow Pathways), 2.1.08.09 (Influx/Seepage Into the EBS), Open Boreholes (1.1.01.01), Thermal Effects on Flow in EBS (2.1.11.10),), 2.2.01.01 (Evolution of EDZ) , Flow Through Host Rock (2.2.08.01), Effects of Excavation on Flow (2.2.08.04), Mechanical Effects from Preclosure Operations (1.01.02.02), Degradation of Liner/Rock Reinforcement Materials in EBS (2.1.06.01), Heat Generation in EBS (2.1.11.01), Effects of Backfill on EBS Thermal Environment (2.1.11.03), Effects of Drift Collapse on EBS Thermal Environment (2.1.11.04), Effects of Influx (Seepage) on Thermal Environment (2.1.11.05), Thermal-Mechanical Effects on Backfill (2.1.11.08), Thermally-Driven Buoyant Flow / Heat Pipes in EBS (2.1.11.12), Effects of Gas on Flow Through the EBS (2.1.12.02), Gas Transport in EBS (2.1.12.03), Thermal-Mechanical Effects on Geosphere (2.2.11.06),

Objective	Feature	Process (Issue)		
		UFD FEP ID	UFD FEP Title	Process/Issue Description
Containment Limited Release – Engineered Barriers	Backfill/Buffer	2.1.04.01	Evolution and degradation of backfill/buffer	- Alteration - Thermal expansion / Degradation - Swelling/Compaction - Erosion/Dissolution - Evolution of backfill flow pathways

Used Fuel Disposition

TOUGH-FLAC with BBM and BExM

Example of calculated permeability evolution in the buffer:

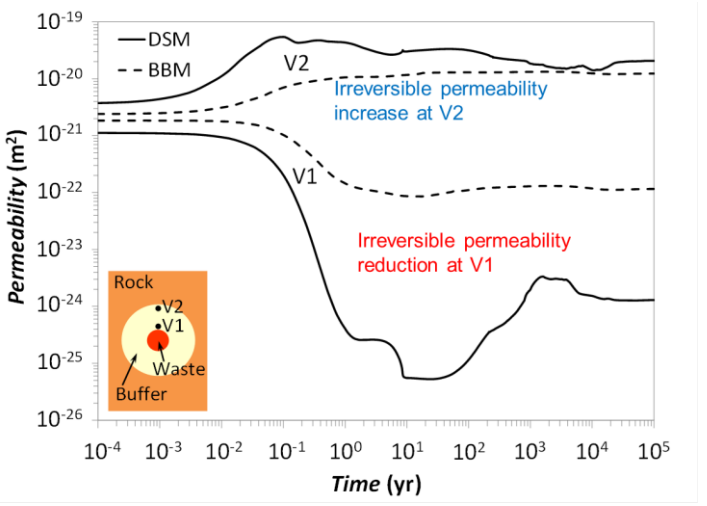

Used Fuel Disposition

TOUGH-FLAC with BBM and BExM

State of the art:

- ***BBM is well established and tested*** *for the modeling of unsaturated-saturated soils, including bentonite*
- *The input parameters for different types of bentonite (e.g. compacted bentonite blocks, pellets, sand-bentonite mixtures) are being established through laboratory experiments and large scale field experiments.*
- *BExM can in addition to BBM be used for modeling the underlying dual-structural behavior, which is important to consider in swelling clay for accurate and mechanistically correct modeling of the resaturation, swelling, and permeability evolution of the buffer.*
- ***BExM and dual-structural models is at the forefront of research*** *and further testing, validations against experiments and applications are needed to gain experience and confidence in using such advanced model (only one other code (CodeBright, has such a model)*
- *The dual-structure model (BExM) can also provide the necessary link between mechanical and chemical processes (See Liange Zhen, TOUGHREACT-FLAC)*

Used Fuel Disposition

TOUGH-FLAC with BBM and BExM

Coupling to the PA model:

- *The TOUGH-FLAC with BBM and BExM constitutive THM models provides a tool for calculating the evolution of the EBS and the host rock, including the disturbed rock zone (DRZ) from just after emplacement to over 100,000 years.*
- *The analysis for coupling to the PA model might be conducted in a **2D cross-section** of one emplacement drift or alternative a **3D model** focused on the **near field of an emplacement tunnel or a few emplacement tunnels in different parts of a repository** and for different FEPs such as nominal case or such as for cases of extensive gas generation.*
- *The **input r**equired is the geometry, heat source, THM properties of buffer and host rock, initial THM conditions (such as in situ stress).*
- *The **output** to the PA model would be the changes in flow properties (e.g. permeability and porosity) in the EBS and near-field including the buffer and DRZ and also to inform PA related to local flow created by coupled THM processes.*

Used Fuel Disposition

Input to PA via TOUGH-FLAC-RBSN

Model discrete fracture developments as seen in nature mechanistically:

:

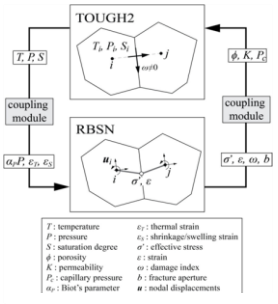

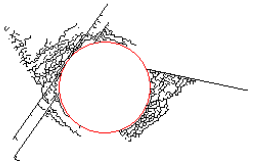

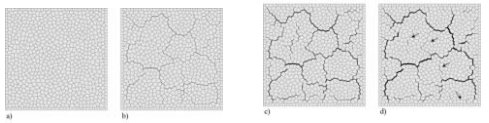

Fracture development → Patch isolation → Enlarged patches

The development of fractures in the RBSN model could be translated into effective fracture properties for use in TOUGH-FLAC as a continuum fracture field.

A coarse coupling (in time) of TOUGH-FLAC with RBSN to periodically to account for fracture generation/attenuation.

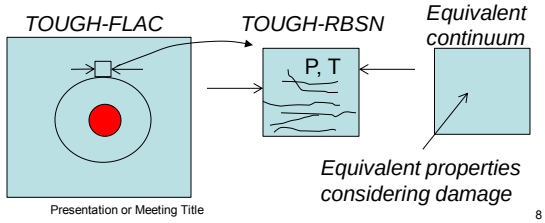

Equivalent properties considering damage

Used Fuel Disposition

TOUGH-FLAC/BBM/RBSN

When ready for integration?

- *TOUGH-FLAC 2D analysis over 100,000 year has been demonstrated and could provide output to PA today for currently implemented constitutive models*
- *TOUGH-FLAC 3D has also been demonstrated associated with modeling of large-scale field tests over tens of years and could be extended to 100,000 years if considering multiple tunnels in parts of a repository*
- *For any site, there will be a need to develop and study rock behavior in situ, such as the evolution of DRZ which will **depend on the rock type and site specific properties**. An appropriate model for the evolution of the DRZ properties should be developed, calibrated, and validated against such in situ experiments (i.e. drift scale test and niche excavation experiments at Yucca Mountain)*
- *For larger models including 3D of multiple emplacement tunnels and shafts to be included in this kind of THM model, more efficient calculations would be necessary, which could be solved with future porting of TOUGH-FLAC for high performance computing. Such porting of the FLAC3D code planned to be conducted within the next few years. RBSN is also being modified for high performance computing.*

Used Fuel Disposition

TOUGH-FLAC/BBM/RBSN

Example: A repository in welded tuff (Rutqvist and Tsang, 2003)

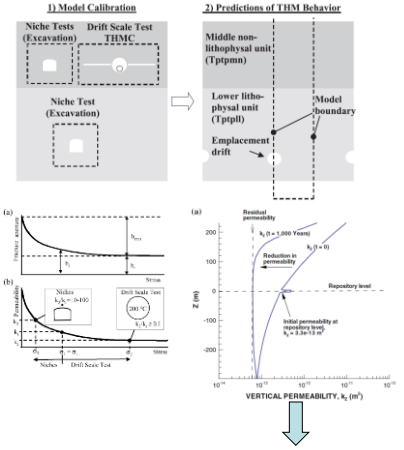

Evolution of permeability to PA model

Example Granitic Rock using URL (Canada) data (Rutqvist et al. 2009)

1 Model Calibration

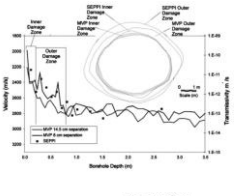

2 Predict long term THM

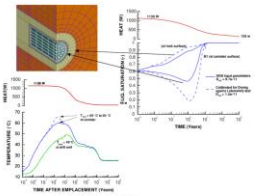

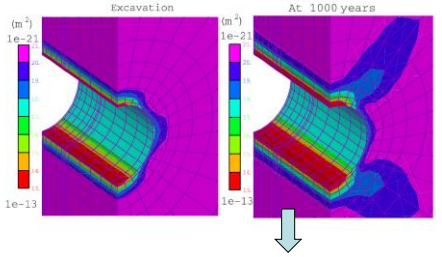

Evolution of permeability to PA model

Used Fuel Disposition Campaign

Integrating Coupled Processes into PA model

Liange Zheng, Jonny Rutqvist, Jens Birkholzer

Lawrence Berkeley National Laboratory

UFD Annual Meeting, June 6-9, 2016

Used Fuel Disposition

Features and Focuses of the coupled THMC Model

- **Focuses of the model**
  - ✓ *Illitization, i.e. the transformation of smectite to illite*
  - ✓ *Geochemically induced swelling stress change*
  - ✓ *Long term evolution of hydrological (e.g. permeability) and chemical (e.g sorption capacity) changes as a results of coupled THMC evolution..*
- **Major features of the model**
  - ✓ *Coupled THMC processes, especially MC coupling*
  - ✓ *Interactions between EBS bentonite and host rock, canister and EBS bentonite*
  - ✓ *High temperature*
- **Current status**
  - ✓ *Coupled THMC model had been developed for a generic clay rock repository with bentonite backfilled EBS.*
  - ✓ *FY16 model incorporate canister-bentonite interaction, but chemical model needs to be fine-tuned*
  - ✓ *Two chemical-mechanical coupling schemes for bentonite have been tested: extended linear swelling and dual structure BExM*

Used Fuel Disposition

Snapshot of the Model

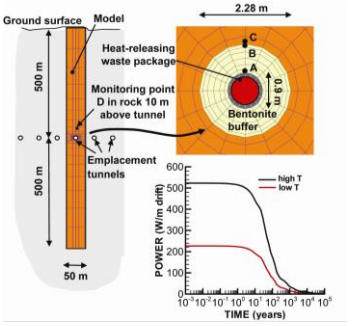

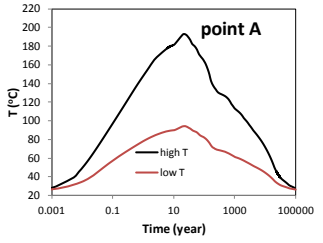

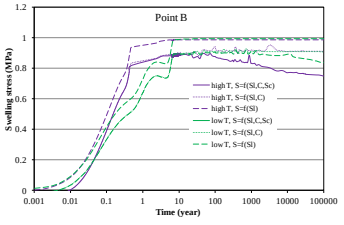

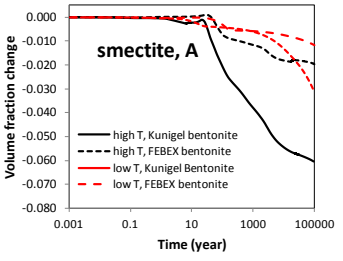

Used Fuel Disposition

Integration with PA Model

- *Significant R&D is needed to improve and validate the model*
- *Difficulties for direct coupling with PA model:*
  - *PA model needs to be able to simulating THMC process simultaneously and consider the couplings between different processes*
  - *Detailed coupling between THMC process might be too expensive to run in PA model*
- *Abstraction is more doable. Response surface, for example, illitization as a function of key flow, chemical parameters and time, can be established based on coupled THMC model and integrated to the PA model.*

Used Fuel Disposition

Non-Darcian Flow:
Background and Proposed model

- Non-Darcian flow is evidenced in laboratory experiments and nanoscale flow simulation.
- *It is* critical for the advection in Excavation Damaged Zone (EDZ) and water flow from host rock to EBS for buffer to function (swelling) properly.

Proposed model (Liu and Birkholzer, 2013) :

$$q = K[i - \frac{I}{\gamma(\frac{1}{\alpha})}\gamma(\frac{1}{\alpha}, \left(\frac{i}{I*}\right)^{\alpha})]$$

$$I = \frac{I*}{\alpha}\gamma\left(\frac{1}{\alpha}\right) \quad \gamma(a,x) = \int_0^x t^{a-1}e^{-t}dt \quad \gamma(a) = \int_0^\infty t^{a-1}e^{-t}dt$$

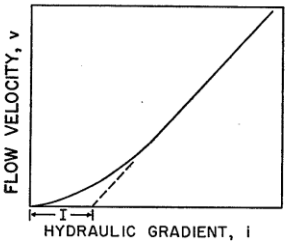

5

Used Fuel Disposition

Non-Darcian Flow:
Proposed Model

Relationship between permeability and threshold hydraulic gradient

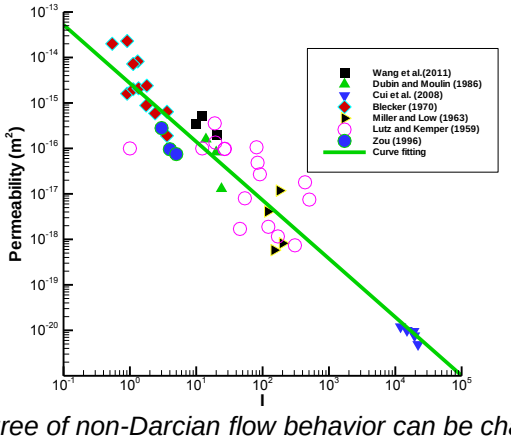

$$I = Ak^B$$

A= 4.0 E-12 and B =-0.78

Liu and Birkholzer, 2013

The degree of non-Darcian flow behavior can be characterized by permeability (k) (or pore size) and threshold gradient (I), respectively.

6

Used Fuel Disposition

Non-Darcian Flow: Implementation and Testing

Non-Darcian flow model was implemented in TOUGH2 and had been used to model the FEBEX in situ test

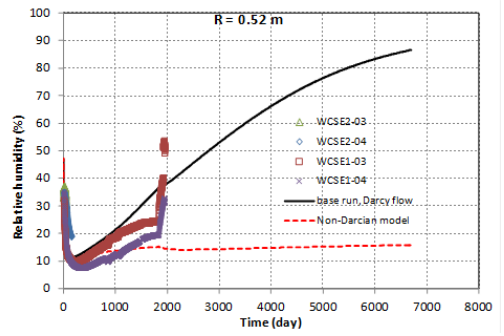

***Observations**: TH model with Non-Darcian flow significantly underestimates RH data. Plausible reasons:*
- ❑*Non-Darcian flow VS relative permeability*
- ❑*Threshold gradient is affected by capillary pressure*

***Lessons learned:** processes uncertainties VS parameters uncertainties*

7

Used Fuel Disposition

Integration with PA Model

- ➢*Hydrological parameters needs to be established for Non-Darcian flow*
- ➢*Coefficients for the permeability-threshold gradient needs to be calibrated*
- ➢*The effect of temperature, salinity and capillary pressure on Non-Darcian flow need to be better understood*
- ➢*Direct integration can be done: integration might be easy but parameters calibration is challenging*

Used Fuel Disposition Campaign

Discrete Fracture Network Approach for GDSA modeling

Hari Viswanathan, Nataliia Makedonska, Satish Karra, Jeffrey Hyman
Los Alamos National Laboratory
Emily Stein
Sandia National Laboratories

2016 UFDC Annual Working Group Meeting
GDSA Integration Session, June 8, 2016
Las Vegas, NV

Sandia National Laboratories is a multi-program laboratory managed and operated by Sandia Corporation, a wholly owned subsidiary of Lockheed Martin Corporation, for the U.S. Department of Energy's National Nuclear Security Administration under contract DE-AC04-94AL85000. SAND2016-nnnnn

Used Fuel Disposition

Conceptual Model

- *Repository site is represented by continuous porous media*
- *Surrounding fractured rock is simulated using DFN approach by DFNWorks*
- *Fractures in DFN are generated using fracture characteristics of Forsmark repository site.*
- *Simulation domain: 3015 m x 2025 m x 1260 m*

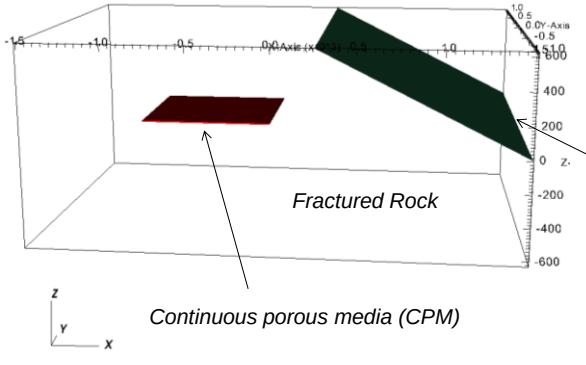

Used Fuel Disposition

Coupled DFN with continuum porous media

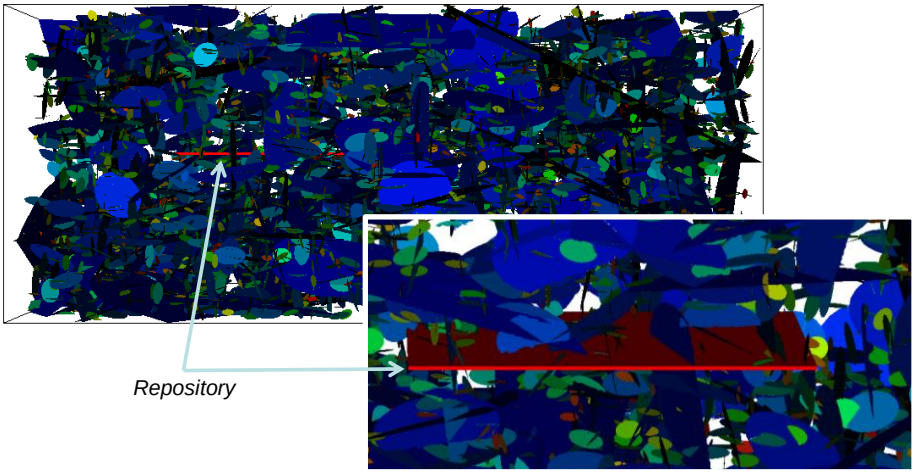

3

Used Fuel Disposition

Two dimensional fracture grid is coupled with three dimensional volume mesh

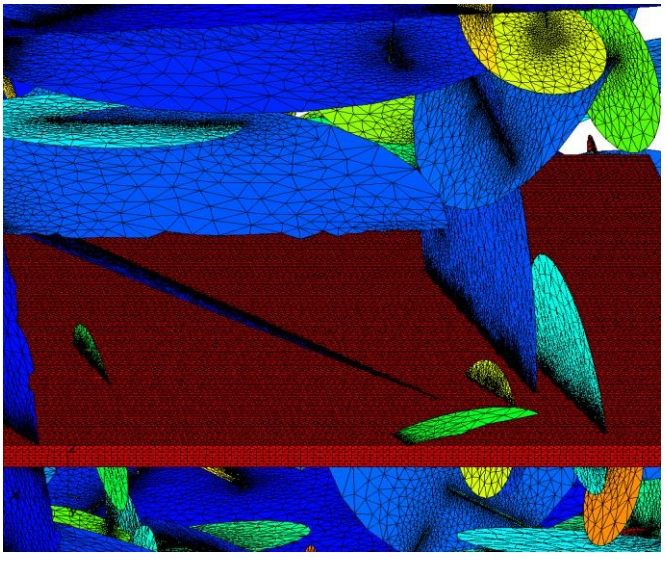

4

Used Fuel Disposition

Transport calculation on simple example

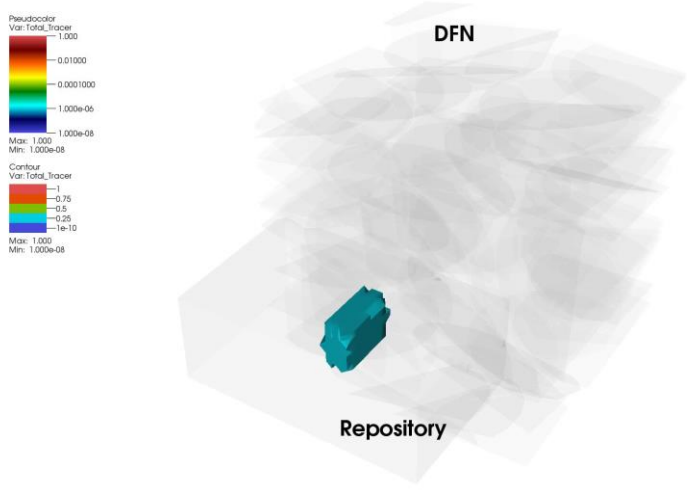

Used Fuel Disposition

Future plans

- **Model flow and transport on DFN with realistic parameters on a large scale**
- **Increase a modeling realism by applying proper boundary conditions and realistic flow rates**
- **Compare DFN results, where advective transport is dominating, to GDSA modeling of Sandia lab., where diffusion component present.**

Used Fuel Disposition Campaign

Waste package degradation: Clay – Metal Interactions

Carlos F. Jové Colón
Sandia National Laboratories

Florie A. Caporuscio
Los Alamos National Laboratory

Las Vegas, Nevada – June 7 – 9, 2016

SAND2016-5247 PE

Sandia National Laboratories is a multi-program laboratory managed and operated by Sandia Corporation, a wholly owned subsidiary of Lockheed Martin Corporation, for the U.S. Department of Energy's National Nuclear Security Administration under contract DE-AC04-94AL85000. SAND2016-nnnnn

Used Fuel Disposition

Reactive-Transport Modeling of the Near- and Field with PFLOTRAN

- Reactive transport modeling base case scenario(s):
  - Interaction with EBS components gauged by anoxic hydrothermal experiments (e.g., Steel/copper corrosion in the presence of clay)
  - Backfill/buffer composition, secondary phases (e.g., pyrite) influencing metal corrosion reactions (e.g., copper):
  - Evaluate geochemical feedbacks (e.g., redox zones) and U transport and concentration profiles

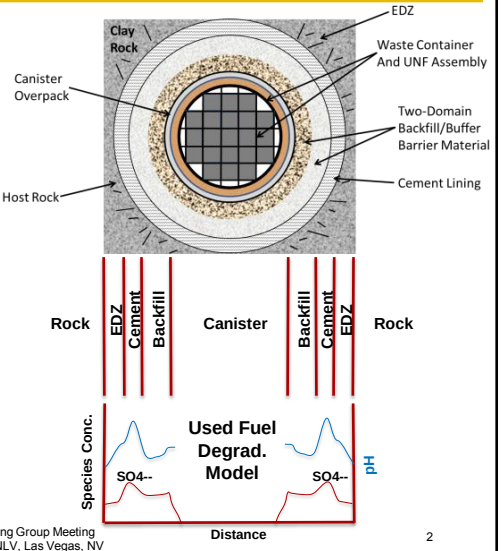

Used Fuel Disposition

Waste Canister Degradation: 304 & 316L Stainless Steel – Clay Interactions

- **Uniform corrosion – no pitting:**
  - $2.97Fe_{1.22}Cr_{0.35}Ni_{0.23} + 4H_2O \rightarrow (Cr_{1.04},Fe_{0.96})(Fe_{0.69},Ni_{0.31})O_4 + 1.97Fe^{2+} + 0.37Ni^{2+} + 8H^+ + 12.68e^-$
- **Corrosion products:**
  - **Chromite passivation layer**
  - **Fe-rich smectite**
  - **Chlorite**
  - **Pentlandite $(Fe,Ni)_9S_8$ (early)**
  - **Millerite (NiS)**
- **5 µm corrosion layer.**
  - 43 µm/year corrosion rate
- **316SS more extensive passive layer**

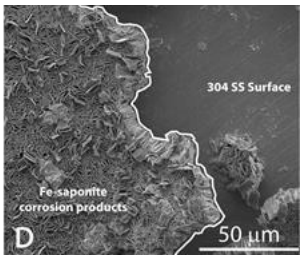

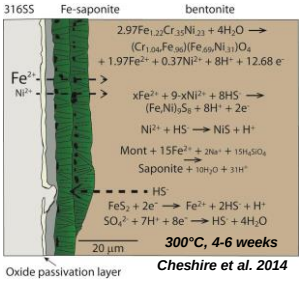

Cheshire et al. 2014

Used Fuel Disposition

Waste Canister Degradation: Low Carbon Steel – Clay Interactions

- **Corrosion Products:**
  - **Fe-smectites (Fe-saponite)**
  - **Pyrrhotite ($Fe_{1-x}S$)**
- 13 to 56 µm thick 'corrosion-product' layer.
- ~20 µm corrosion pitting
  - 214 µm/year corrosion rate
- No passivation layer → corrosion expected to continue
- Extensive Fe_3O_4 layers develops

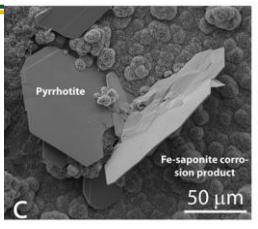

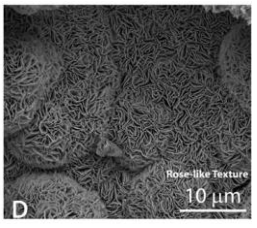

Cheshire et al. 2014

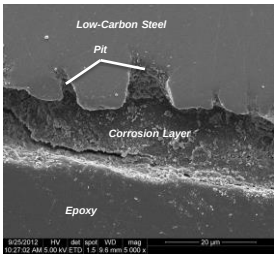

Ramped-up exp's:
- ***T = 25/100/200/300/25°C,***
- ***5 weeks***

Sources: Cheshire et al. 2014; Jové Colón et al. 2015

Used Fuel Disposition

Waste Canister Degradation: Copper – Clay Interactions

- Sulfide-induced corrosion (anoxic):
  - Pyrite (FeS_2) decomposition
- Primary corrosion product → Chalcocite (Cu_2S):
  - $Cu^\circ + H_2S + CuCl_2^- = Cu_2S_{(s)} + 2Cl^- + H_2$
- 13 µm thick chalcocite layer
- Appears as pitting corrosion

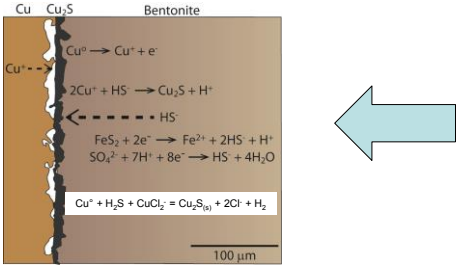

Cheshire et al. 2014

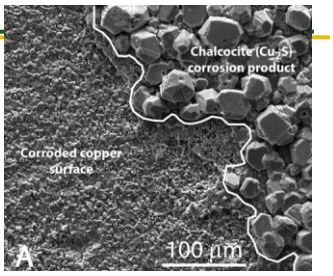

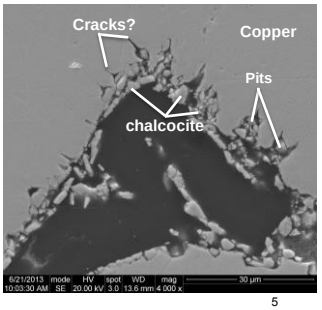

Used Fuel Disposition

Geochemical and Reactive-Transport Model Implementation

- **Waste package degradation based on clay – metal interactions:**
  - **Fe-rich clay parageneses**
  - **Corrosion products**
  - **Aqueous-Solid Equilibria**
  - **Sulfide effects (e.g., pyrite decomposition)**
- **Implementation within a reactive transport model:**
  - **PFLOTRAN**
  - **Model Conceptualization (BC's, transport-limited)**

Copper Corrosion Example

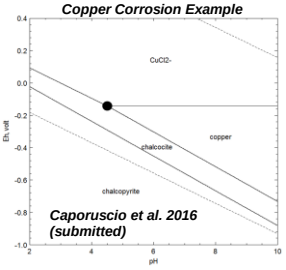

Caporuscio et al. 2016 (submitted)

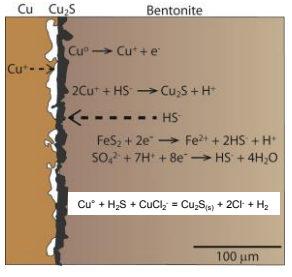

Used Fuel Disposition

ACKNOWLEDGMENTS

- Dr. Michael C. Cheshire (currently at ORNL) conducted the experimental and characterization work presented here.
- Discussions with Charles R. Bryan (SNL) on steel corrosion are greatly appreciated.
- This work supported by the DOE-NE Used Fuel Disposition Campaign Fuel Cycle Technologies R&D program.

Used Fuel Disposition

BACKUP SLIDES

Used Fuel Disposition

Reactive-Transport Modeling of the Near- and Field with PFLOTRAN

- Reactive-transport simulations of base-case scenarios on the near- and far-field domains
- 1D or 2D **scoping** model representation for a single canister
- Coupled processes (THC):
  - Solute transport
  - Fluid-rock-canister interactions (solution-mineral equilibria, dissolution/ precipitation, sorption)
  - Heat load according to waste type
  - Variable backfill saturation(?)
- Evaluate U transport from wasteform source to the EBS / host-rock interface
- Evaluate changes in mineral volume fractions and porosity

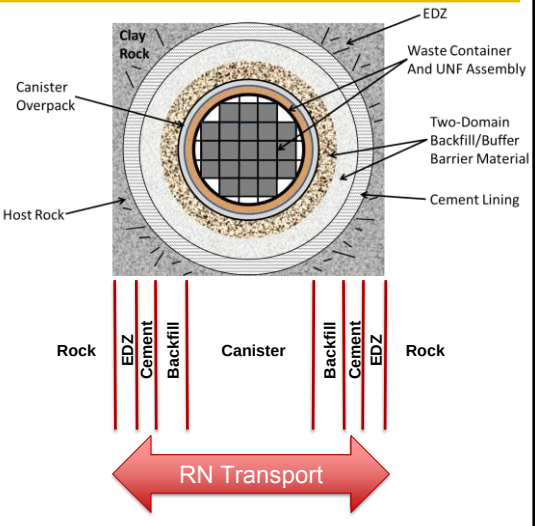

June 8th. 2016 UFD Working Group Meeting June 7-9, UNLV, Las Vegas, NV 9

Used Fuel Disposition Campaign

Waste Package and Waste Form Degradation and Implementation in PFLOTRAN

Jennifer M. Frederick
Glenn E. Hammond and Paul Mariner
Sandia National Laboratories

2016 UFDC Annual Working Group Meeting
GDSA Session, June 8, 2016
Las Vegas, NV

Sandia National Laboratories is a multi-program laboratory managed and operated by Sandia Corporation, a wholly owned subsidiary of Lockheed Martin Corporation, for the United States Department of Energy's National Nuclear Security Administration under contract DE-AC04-94AL85000. *SAND2016-5216 PE*

PFLOTRAN's Waste Form Process Model

PFLOTRAN's implementation of waste package and waste form degradation.

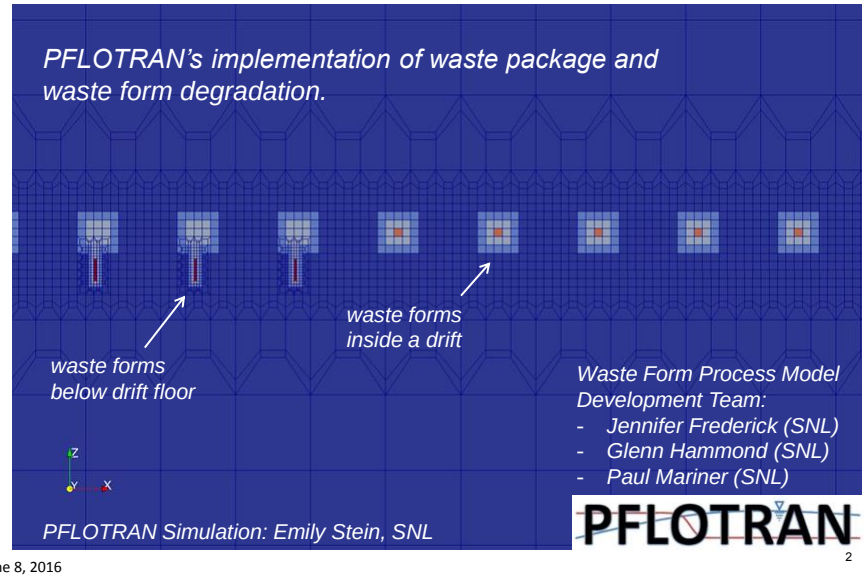

PFLOTRAN Simulation: Emily Stein, SNL

Waste Form Process Model Development Team:
- *Jennifer Frederick (SNL)*
- *Glenn Hammond (SNL)*
- *Paul Mariner (SNL)*

PFLOTRAN

Used Fuel Disposition

PFLOTRAN's Waste Form Process Model

Consists of 3 Main Components:

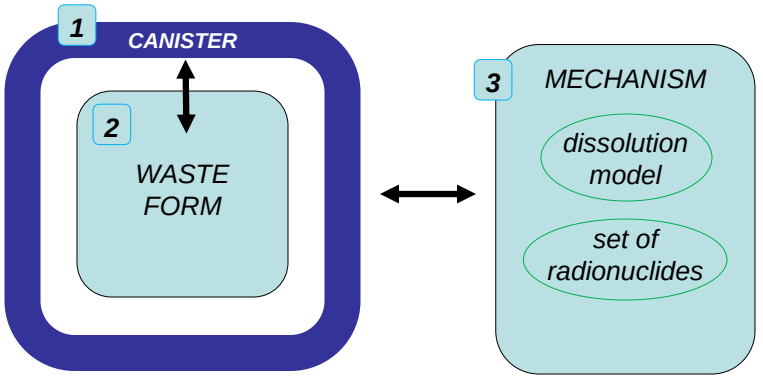

"waste form object"
"fruit"

"waste form type"
"banana, apple, orange, etc."

June 8, 2016 3

Used Fuel Disposition

PFLOTRAN's Waste Form Process Model

Major restructuring in FY16 improves modularity.

canister vitality (0-100%)

canister degradation rate

waste form 1
- *coordinate point*
- *RN concentrations*
- *eff. dissolution rate*
- *volume*
- *mech. pointer*

Mechanism **GLASS**
- *radionuclide set*
- *bulk density*
- *specific surface area*
- *dissolution function*
- *base dissolution rate*

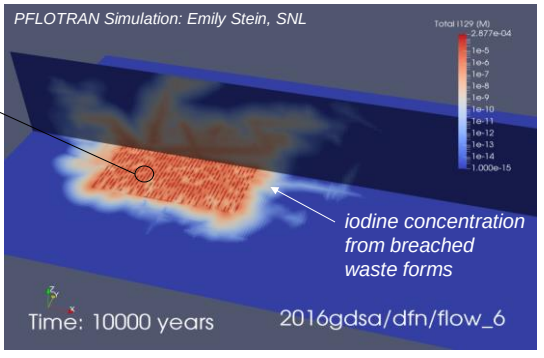

- *Each canister & waste form is independent and can fetch the local conditions*
- *Canister breach times and dissolution rates now vary*
- *Multiple waste form types in a single simulation (mechanism pointer)*

June 8, 2016 4

Used Fuel Disposition

PFLOTRAN's Waste Form Process Model

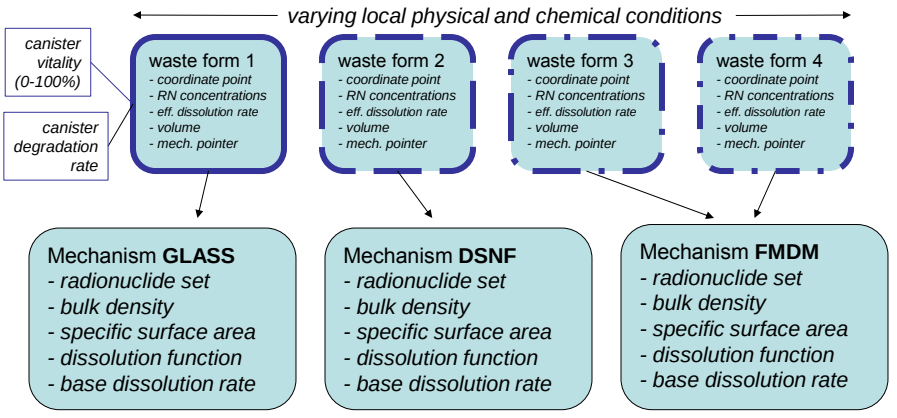

Benefits of modular design:

- *Modularity increases the numerical efficiency (lots of waste forms, few mechanisms)*

June 8, 2016 5

Used Fuel Disposition

PFLOTRAN's Waste Form Process Model

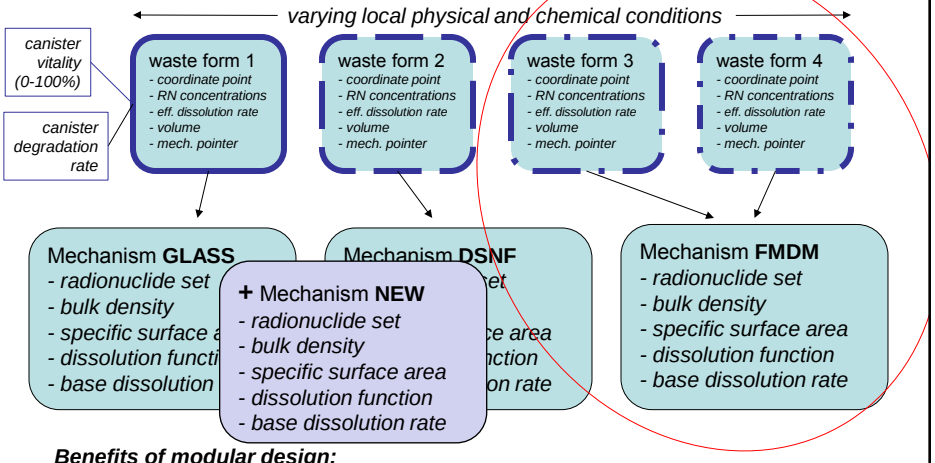

Benefits of modular design:

- *Modularity increases the numerical efficiency (lots of waste forms, few mechanisms)*
- *New functionality can be easily integrated (without messing with existing infrastructure)*

June 8, 2016 6

Used Fuel Disposition

PFLOTRAN's Waste Form Process Model

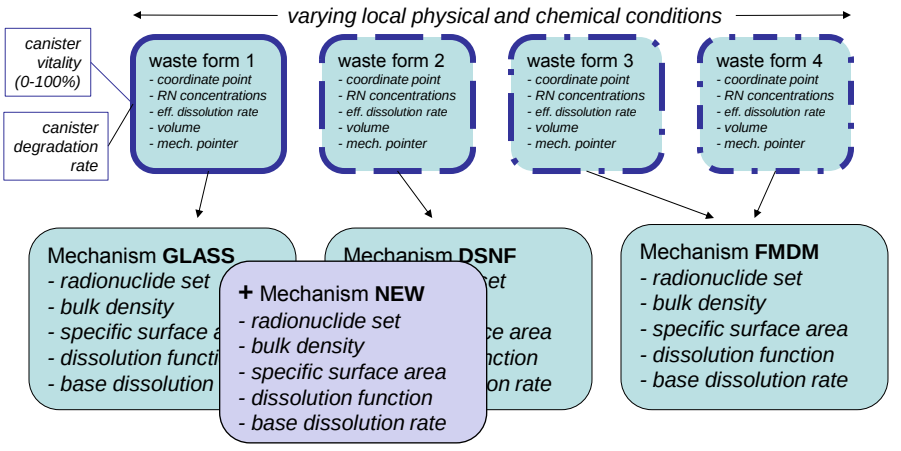

We invite you to collaborate on this process model
We can help you implement the new waste form you envision

Used Fuel Disposition Campaign

Integration of Glass Degradation Model into the PA Model

Peter C. Rieke, Sebastian Kerisit, Joe Ryan
Pacific Northwest National Laboratory

UFD Annual Meeting
June 8th, 2016

THE PACIFIC NORTHWEST NATIONAL LABORATORY, operated by BATTELLE for the UNITED STATES DEPARTMENT OF ENERGY under contract DE-AC05-76RL01830

Used Fuel Disposition

Glass Models Developed in Glass Corrosion Modeling Tool

- **Aagaard-Helgeson (Transition State Theory)**
  - Simple Algebraic Formulation

$$R_{gls} = k_0 a_{H^+}{}^{\eta} \exp\left(\frac{E_a}{RT}\right)\left(1-\left(\frac{C_{SiO_2(aq)}}{K_g}\right)^{1/\nu}\right)$$

- **GRAAL Model**
  - Time Stepping Solver

$$dL_c/dt = r_c\left(1-\left(Q/K_g\right)^{\alpha}\right) \qquad dL_g/dt = \left(\frac{1}{\frac{1}{r_h}+\frac{L_g}{D}}\right) - dL_c/dt \quad (L_g \geq 0)$$

- **Grambow-Mueller Model**
  - 1D, Time Stepping Solver

Used Fuel Disposition

Glass Models Developed in Glass Corrosion Modeling Tool

- **New Gel End Member (GEM) Model**
  - Thermodynamic Model of Gel Composition from Glass Hydrolysis
  - Kinetic Model of Gel Phase(s) Dissolution
  - Still Under Development.
- **Stage III Glass Dissolution Driven by Mineral Precipitation**
  - Include in Glass Alteration Models Given Above
  - Include as Separate Process in Pflotran

$$\frac{dC_i}{dt} = \left\{\frac{S}{V} J_i - f_i^{\min} \frac{dC_{\min}}{dt}\right\} - \frac{Q_f}{V}\left(C_i - C_i^0\right)$$

Used Fuel Disposition

Work Progress

- **Pflotran Installed and Tested on 'Cascade'**
- **FMDM Model Installed and Tested for 40 Waste Form**
- **Waste Form Module Underwent Extensive Revision**
- **New Waste Form Mechanism Cloned using the FMDM, Custom, and Glass Mechanisms as Templates**
  - New Chemistry Specific to Glass Model Mapped to Pflotran Chemistry
  - Input File Read Routine Modified to Read New Mechanism
  - Simple AH/TST Model Place Holder

$$R_{gls} = k_0 a_{H^+}{}^{\eta} \exp\left(\frac{E_a}{RT}\right)\left(1 - \frac{C_{SiO_2(aq)}}{K_g}\right)$$

- **Glass Degradation Model Interface is Operational**
- **Tested on a 11x11x5 Structured Grid with One Waste Form**

Used Fuel Disposition

Future Work

- Validate Model Unit Conversion
- Isolate Model as Separate Subroutine
- Develop Model Using PETSC Tools
- Run with Multiple and/or Mixed Type Waste Forms
- Run with Canister Breaching Option
- Create an Interface to Glass Composition Data

Used Fuel Disposition Campaign

Advances in PFLOTRAN Gridding: Octree Refinement and Ghost Node Correction

Ayman Alzraiee and Glenn Hammond
Sandia National Laboratories

2016 UFDC Annual Working Group Meeting
Integration Session, June 8, 2016
Las Vegas, NV

Sandia National Laboratories is a multi-program laboratory managed and operated by Sandia Corporation, a wholly owned subsidiary of Lockheed Martin Corporation, for the United States Department of Energy's National Nuclear Security Administration under contract DE-AC04-94AL85000. SAND2016-5326 PE

Used Fuel Disposition

Motivation

- **Why vary grid resolution in space (and/or time)?**
  - Improve accuracy
  - Keep runtimes manageable
- **Why octree grid refinement?**
  - Flexibility
  - Maximize accuracy with a fixed number of degrees of freedom
  - Works within PFLOTRAN's existing unstructured gridding infrastructure
- **Challenges**
  - Data distribution and management
  - Potential load imbalance
  - Development of robust solvers

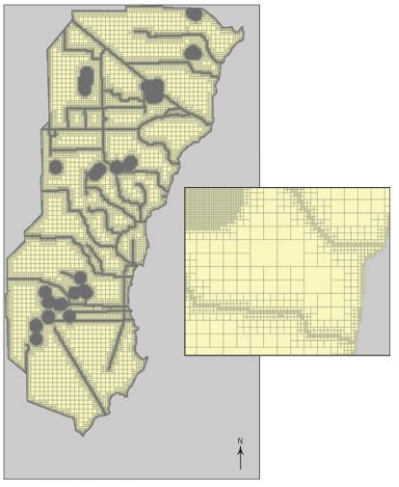

MODFLOW-USG Manual, Figure 7

Used Fuel Disposition

Approaches to Gridding in PFLOTRAN

- **Structured**
  - Cartesian
  - Radial
- **Unstructured**
  - Implicit - traditional finite element mesh defined by nodes/elements
  - Explicit - finite volume mesh defined by volumes, areas, distances and connectivity

3

Used Fuel Disposition

Approaches to Gridding in PFLOTRAN

- **Structured**
  - Cartesian
  - Radial
- **Unstructured**
  - Implicit - traditional finite element mesh defined by nodes/elements
  - **Explicit - finite volume mesh defined by volumes, areas, distances and connectivity**

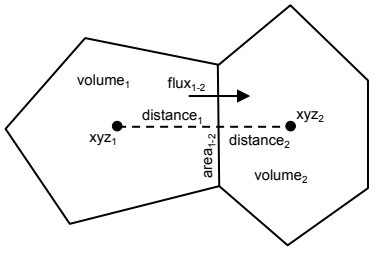

4

Used Fuel Disposition

Explicit Unstructured Grid File Format

```
CELLS 15
1 4.0625 4.0625 4.0625 5.20833
2 4.375 4.375 3.125 2.60417
3 3.3333 3.3333 3.75 7.8125
4 3.3333 1.6667 3.75 7.8125
5 3.3333 1.6667 1.25 7.8125
6 1.25 3.75 3.75 15.625
7 2.1875 4.0625 0.9375 1.30208
8 2.1875 3.4375 1.5625 1.30208
...
CONNECTIONS 24
1 2 4.16667 4.16667 3.3333 6.25
1 3 3.75 3.75 3.75 8.8388
3 4 3.75 2.5 3.75 6.25
3 6 2.5 3.75 3.75 6.25
4 5 3.3333 1.6667 2.5 3.125
4 11 2.5 1.25 3.75 6.25
5 12 2.5 1.25 1.25 6.25
6 9 1.25 3.75 2.5 6.25
6 11 1.25 2.5 3.75 6.25
7 8 2.08333 3.75 1.25 2.2097
7 10 2.08333 4.5833 1.25 2.2097
7 15 2.08333 3.75 0.41667 2.2097
...
```

Cell Center
Cell ID
Cell Volume
Cell IDs
Face Center
Face Area

5

Used Fuel Disposition

Proofs of Concept Using Explicit Unstructured Grids

- **Explicit unstructured grids provide flexibility for defining many grid configurations in a single format**

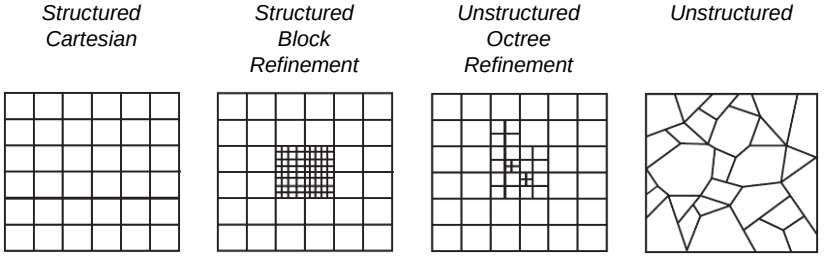

6

Used Fuel Disposition

Examples of Octree Grid Refinement

- Each cubic finite volume cell is divided into 8 cells.
- Each rectangular face is divided into 4 faces.
- Levels of refinement can be implemented in PFLOTRAN through the REGION card which is capable of delineating zones based on a point, line, rectangle, polygon, or custom list of points.

Refine a region defined by a polygon

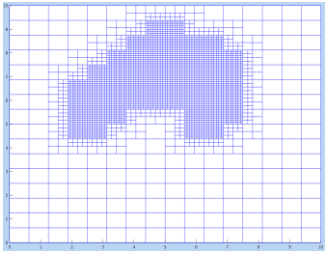

Refine a region defined by a line

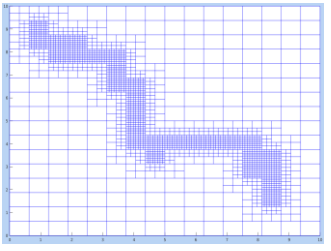

7

Used Fuel Disposition

Pseudo Porous Media Approach to Fracture Flow (Capilla et al., 2002)

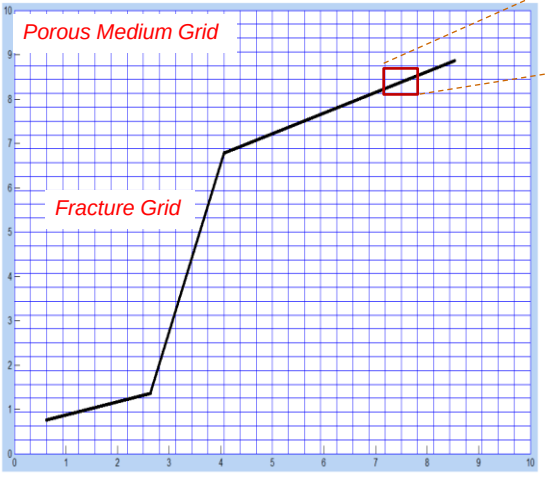

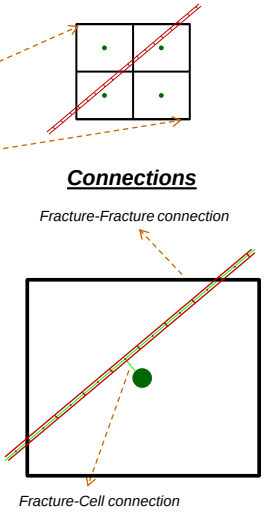

8

Used Fuel Disposition

Fracture Flow with Octree Refinement

- Octree grid is used to refine the finite volume grid around the fractures.
- Darcy flow is assumed in fractures.

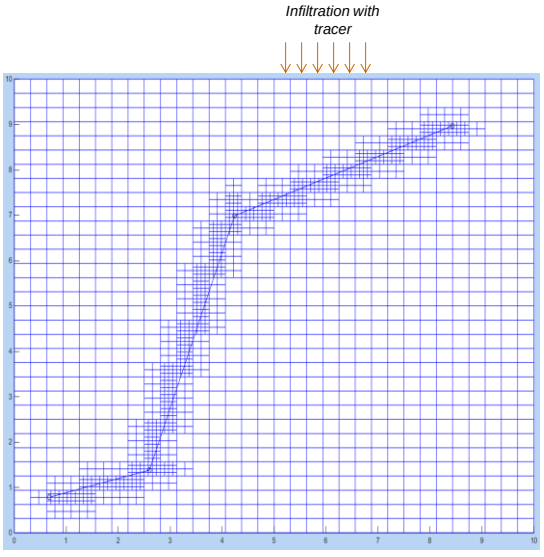

9

Used Fuel Disposition

Fracture Flow with Octree Refinement

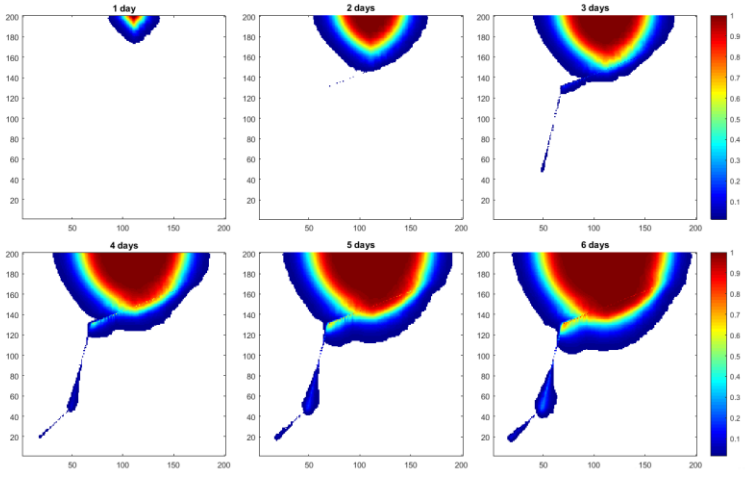

10

Used Fuel Disposition

Network of Fracture on Cartesian Grid

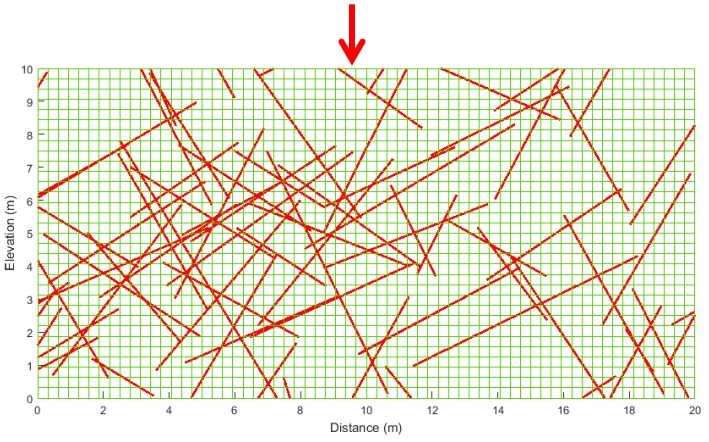

11

Used Fuel Disposition

Network of Fracture on Cartesian Grid

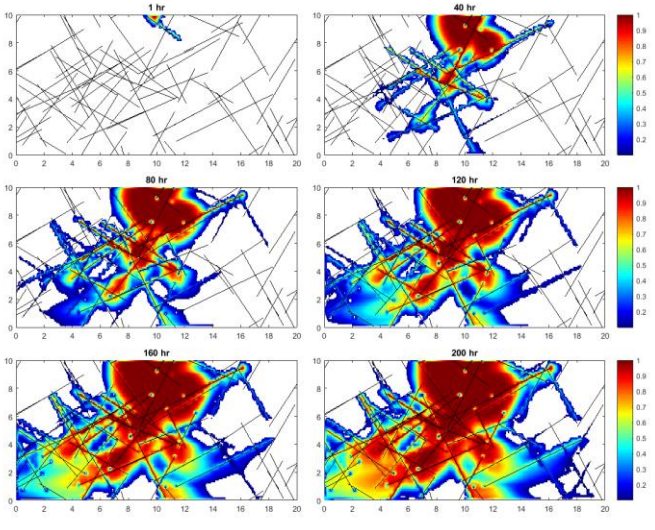

12

Used Fuel Disposition

Increasing Accuracy through Ghosting Nodes

- Fluxes within the finite volume method are more accurate when they are orthogonal to cell interfaces
- Ghost node correction can be used to reduce numerical error.
- Ghost node approximations are linear interpolations of ordinary cell-centered (non-ghosted) state variables.
- Ghost node correction is currently under development in PFLOTRAN.

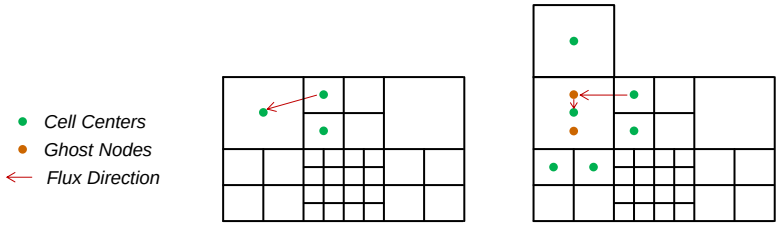

13

Used Fuel Disposition

14

Used Fuel Disposition

Proposed Implementation of Ghost Node Correction in PFLOTRAN

Modified GRID card

```
GRID
   TYPE unstructured_explicit ./usgfile.usg
   GRAVITY 0. 0 -9.81
   GHOST_NODE_CORRECTION ./gncorrection.gnc
END
```

Ghost nodes correction file

```
1  4
2  35 61 3.125 0.5 5.312
3  28 61 4.0625 0.5 4.375
4  41 71 3.125 0.5 7.1875
5  48 71 4.0625 0.5 8.125
```

Number of ghost nodes

Coordinates of the ghost nodes

Child cell id

Parent cell id

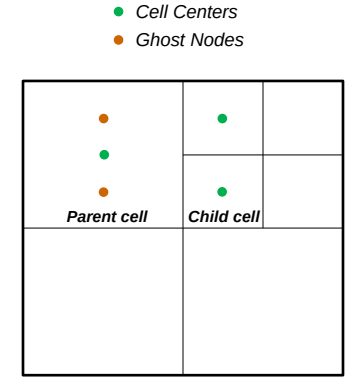

15

Used Fuel Disposition

Discrete Fractures Using Unstructured Grids

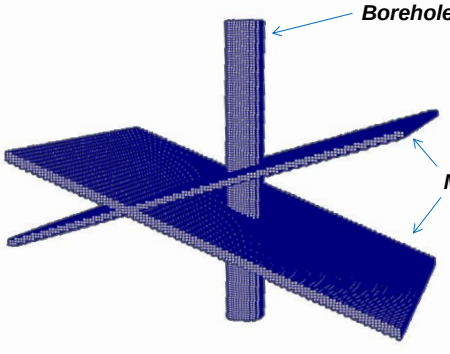

16

Used Fuel Disposition Campaign

THM processes in Salt (PFLOTRAN-Sierra/Solid Mechanics)

Heeho Park, Ayman Alzraiee, Glenn Hammond
Sandia National Laboratories

2016 UFDC Annual Working Group Meeting
Integration Session, June 8, 2016
Las Vegas, NV

Sandia National Laboratories is a multi-program laboratory managed and operated by Sandia Corporation, a wholly owned subsidiary of Lockheed Martin Corporation, for the United States Department of Energy's National Nuclear Security Administration under contract DE-AC04-94AL85000. SAND2015-XXXXP

Used Fuel Disposition

WIPP Creep Closure

- **The excavation of the WIPP will result in a plastic deformation of the salt material (creep) and resultant closure of excavated areas.**
- **The creep closure causes the reduction of void volume. It increases repository pressure over time with gas generation from waste decomposition and microbial activity.**
- **Values of porosity are calculated as a function of time and gas pressure from a look-up table**
  - It was obtained by modeling deformation of a waste-filled room using a finite element structural mechanics code, SANTOS.
- **The waste-filled room in PFLOTRAN is modeled as homogeneous high porosity media.**

Used Fuel Disposition

Creep Closure in PFLOTRAN

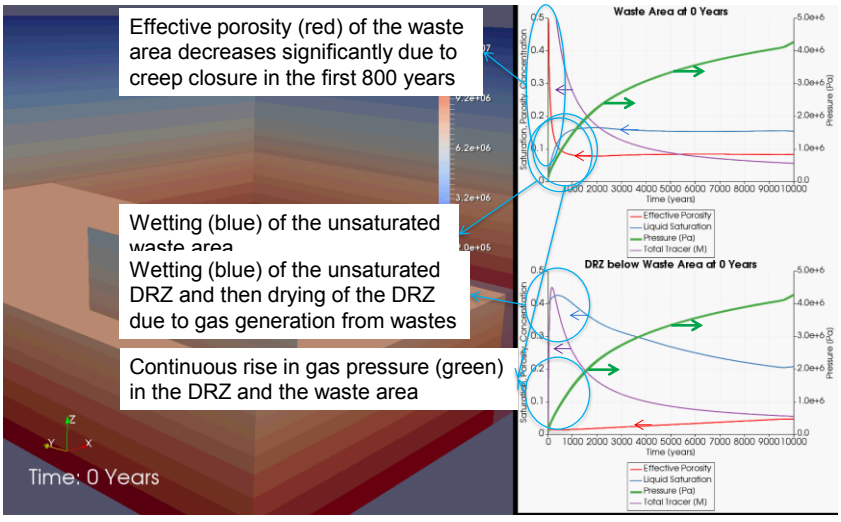

Used Fuel Disposition

PFLOTRAN-Sierra/Solid Mechanics (SM)

- **Increasingly mechanistic representations of salt creep closure are needed.**
- **TOUGH-FLAC simulations of THM processes have shown promise.**
  - Rutqvist, 2011
  - Blanco-Martin et al., 2016
- **For massively-parallel simulation of THM within the GDSA PA framework, we propose coupling:**
  - PFLOTRAN - reactive multiphase flow
  - Sierra/SM - solid mechanics
- **PFLOTRAN-Sierra/SM will be benchmarked against TOUGH-FLAC.**

Used Fuel Disposition

Converting Finite Element Grid to Finite Volume Grid

- Finite element nodes are treated as centers of finite volume cells
- Interfaces are generated to be perpendicular to flowlines.

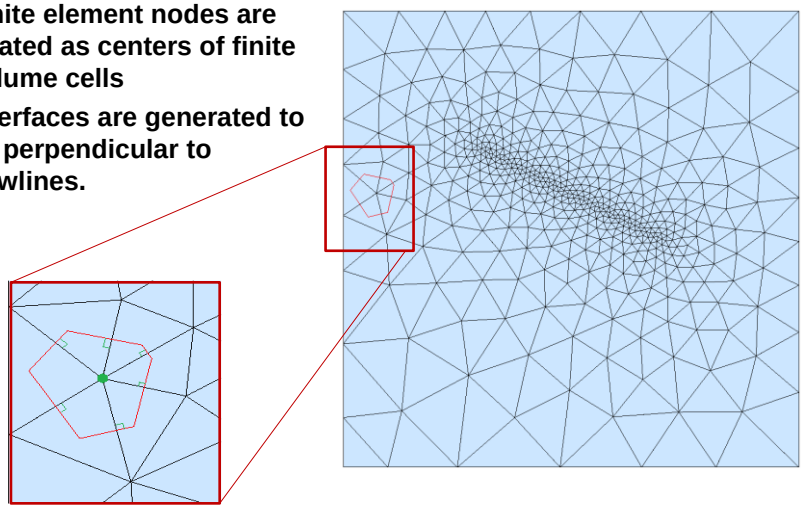

5

Used Fuel Disposition

Discussion/Questions

- This procedure can be automated within PFLOTRAN to allow PFLOTRAN to read either FE or FV grids

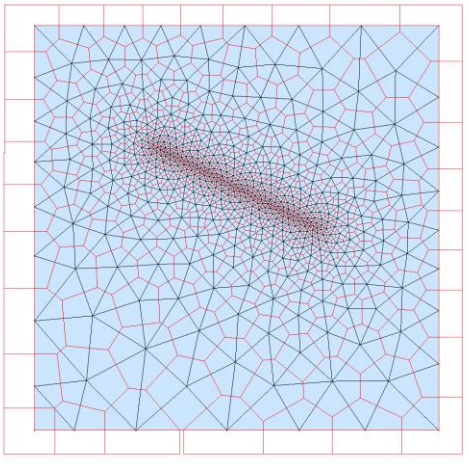

6

Used Fuel Disposition Campaign

Statistical Outputs of Probabilistic Performance Assessment

Robert J. MacKinnon
Sandia National Laboratories

Used Fuel Disposition Working Group Meeting
June 2016

Sandia National Laboratories is a multi-program laboratory managed and operated by Sandia Corporation, a wholly owned subsidiary of Lockheed Martin Corporation, for the U.S. Department of Energy's National Nuclear Security Administration under contract DE-AC04-94AL85000. SAND2016-5123 PE

Used Fuel Disposition

Performance Assessment Modeling and Predictions

- **PA is the required regulatory approach for assessing DGR compliance with quantitative radiological safety criteria**
- **Overall error and uncertainty arise from the following major modeling activities:**
  - Selection of the mathematical models providing an abstraction of the physical processes and events of interest;
  - Identification of appropriate parameters and data defining the models;
  - Use of physical observations and measurements, including data from the literature, laboratory, and field to validate and calibrate the models;
  - Development of a computational model through discretization of the mathematical model and its implementation on a computer;
  - Identification of specific goals of PA simulations and the performance quantities of interest; and
  - Quantification of uncertainties in the predictions, including sensitivity analysis.

Used Fuel Disposition

Regulation requests "mean" and "median" values of dose to a reasonably maximally exposed individual

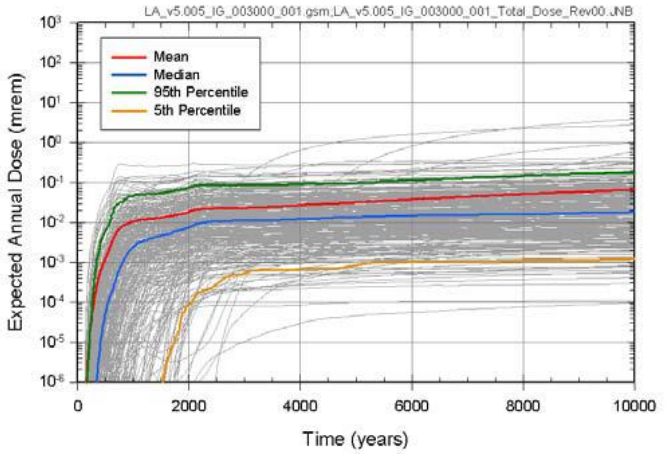

Used Fuel Disposition

Expected Value of Performance Quantity of Interest: Precision and Reliability

$$|e_{MC}(S)| \leq e^{*}_{MC} = z_{1-\frac{\alpha}{2}}\frac{|S|}{\sqrt{N_R}},$$

95%

50%

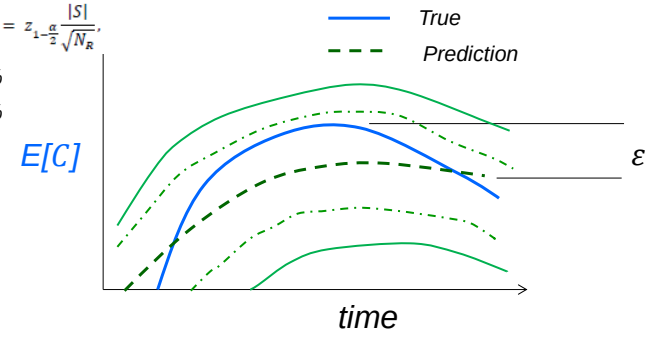

$$\varepsilon = Statistical\ Error + Spatial\ Discretization\ Error + Temporal\ Discretization\ Error$$

with +/- Confidence levels

Used Fuel Disposition

Numerical Errors

Tolerance = maximum allowable ε

Statistical Error $e_{MC} \sim \frac{S}{\sqrt{N_R}}$

Spatial Error $e_h \sim C_h h^{\,k}$

Temporal Error $e_t \sim C_t \Delta t^{\,l}$

Computational Work $W \sim O(N_R \times N_e \times N_t)$

1: Mackinnon and Kuhlman, 2016. A Control Variate Method for Probabilistic Performance Assessment: Improved Estimates for Mean Performance Quantities of Interest

2: Currently analyzing e_{MC} and e_h for elliptic model problem, including W

3: Parabolic Model Problem e_{MC}, e_h, e_t, W

Goal is to meet the tolerance with $\frac{dW}{d\varepsilon} = 0$

Used Fuel Disposition

Control Variate Technique

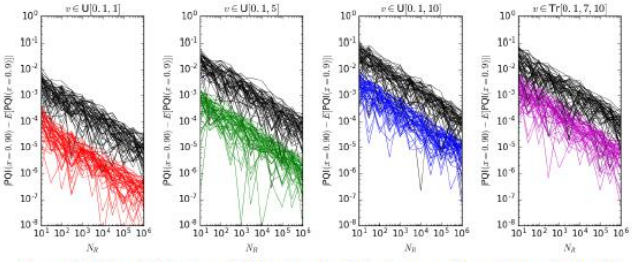

Figure 2. PQI(x=0.9) for Four Distributions in Table 1 across Sample Sizes N_R for 50 different random seeds.